OFFICIAL JOURNAL OF THE SCIENTIFIC SOCIETY OF ANATOMISTS, HISTOLOGISTS, EMBRYOLOGISTS AND TOPOGRAPHIC ANATOMISTS OF UKRAINE

DOI: 10.31393
ISSN 1818-1295
eISSN 2616-6194

ВІСНИК МОРФОЛОГІЇ
REPORTS OF MORPHOLOGY

Vol. 30, №1, 2024

Scientific peer-reviewed journal in the fields of normal and pathological anatomy, histology, cytology and embryology, topographical anatomy and operative surgery, biomedical anthropology, ecology, molecular biology, biology of development

Published since 1993
Periodicity: 4 times a year

Vinnytsya · 2023

ВІСНИК МОРФОЛОГІЇ - REPORTS OF MORPHOLOGY

Founded by the "Scientific Society of Anatomists, Histologists, Embryologists, and Topographic Anatomists of Ukraine" and National Pyrogov Memorial Medical University, Vinnytsya in 1993

Certificate of state registration КВ №9310 from 02.11.2004

Professional scientific publication of Ukraine in the field of medical sciences in specialties 221, 222, 228, 229
According to the list of professional scientific publications of Ukraine, approved by the order of the Ministry of Education and Science of Ukraine No. 1188 of 24.09.2020
Professional scientific publication of Ukraine in the field of biological sciences in specialty 091
According to the list of professional scientific publications of Ukraine, approved by the order of the Ministry of Education and Science of Ukraine No. 1471 of 26.11.2020

Approved by the Academic Council of National Pyrogov Memorial Medical University, Vinnytsya, protocol №8 from 29.02.2024.

Indexation: Scopus, CrossRef, Index Copernicus, Google Schoolar Metrics, National Library of Ukraine Vernadsky

Address editors and publisher:
Pyrogov Str. 56,
Vinnytsya, Ukraine - 21018
Tel.: +38 (0432) 553959
E-mail: nila@vnmu.edu.ua

Computer page-proofs - Klopotovska L.O.
Translator - Gunas V.I.
Technical support - Levenchuk S.S.
Scientific editing - editorship

The site of the magazine - https://morphology-journal.com

CONTENT

DOI: 10.31393/morphology-journal-2024-30(1)-01 Reports of Morphology, Vol. 30, №1, Pages 5-15

ISSN 1818-1295 eISSN 2616-6194

REPORTS OF MORPHOLOGY

Official Journal of the Scientific Society of Anatomists, Histologists, Embryologists and Topographic Anatomists of Ukraine

journal homepage: https://morphology-journal.com

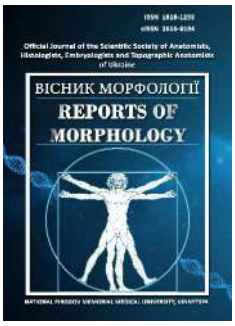

Comparative assessment of tissue response to a mesh implant made of polypropylene modified with carbon nanotubes and silver nanoparticles

Viltsaniuk O. A., Kravchenco V. M., Viltsaniuk O. O., Dereziuk A. V., Sheremeta R. O.
National Pirogov Memorial Medical University, Vinnytsya, Ukraine

ARTICLE INFO
Received: 15 November 2023
Accepted: 03 January 2024

UDC: 616.34-007.43-089:581.41:599.323.4:612.08

CORRESPONDING AUTHOR
e-mail: viltsanyuk@gmail.com
Viltsaniuk O. A.

CONFLICT OF INTEREST
The authors have no conflicts of interest to declare.

FUNDING
Not applicable.

DATA SHARING
Data are available upon reasonable request to corresponding author.

Treatment of abdominal hernias remains one of the most urgent problems of modern surgery. A large number of complications after hernia operations require the development of new types of implants for tissue plastic surgery. The purpose of the study is to carry out an experimental comparative assessment of tissue reaction to the implantation of the developed polypropylene mesh implant modified with carbon nanotubes and silver nanoparticles. Research was conducted on 105 sexually mature laboratory rats in three series of experiments (35 rats each). In the first series, polypropylene mesh implants were implanted in the tissues of the anterior abdominal wall, in the second - polypropylene implants coated with an antiseptic, and in the third - polypropylene implants modified with carbon nanotubes and silver nanoparticles. Animals were removed from the experiment after preliminary anesthesia 3, 5, 7, 14, 21, 30 and 90 days after the operation. The tissues of the abdominal wall were taken together with the implants, histological preparations were made, which were stained with hematoxylin and eosin and according to Van Gieson. We studied the composition and ratio of elements of cell infiltration in tissues with further statistical processing of the obtained data. It was established that during the implantation of mesh edoprostheses, regardless of their type, necrotic changes with reactive inflammation, the presence of inflammatory cell infiltrate, tissue swelling and microcirculation disorders were detected in the tissues 3-5 days after the operation. Under the condition of implantation of the developed mesh, a less pronounced exudative phase of inflammation and an earlier onset of the reparation phase were detected. Depending on the type of implant used, the subsequent reaction differed between the groups of experimental animals, which was evidenced by the regression of inflammatory phenomena in the tissues and the processes of formation of the fibrous capsule around the implants. During the implantation of nanomodified mesh implants by the 7th day of the experiment, the exudative phase of inflammation ended and the formation of a thin connective tissue capsule began, the formation of which was completed by the 21st day of observation, while when the mesh was implanted with polypropylene and polypropylene with an antimicrobial coating, the formation of the capsule lasted up to 30 days. Thus, it was established that the exudative phase of inflammation continues in the tissues around the implantation of classic polypropylene and polypropylene meshes with an antimicrobial coating up to the 14th day of the experiment, and the connective tissue capsule is formed up to the 30th day. At the same time, in the tissues around the mesh implants made of polypropylene modified with carbon nanotubes and silver nanoparticles, the exudative phase of inflammation ended by the 7th day of the experiment. This ensured the intensity of reparative regeneration processes and the separation of the implant from the surrounding tissues by a thin connective tissue capsule for up to 21 days of observation.

Keywords: *polypropylene mesh implants, carbon nanotubes, silver nanoparticles, morphological changes, biological compatibility.*

Introduction

The problems of treating abdominal hernias remain one of the most urgent problems of modern surgery [8, 10, 15].

Today, polypropylene mesh implants are widely used in hernia repair [4, 5, 18, 28]. But the results of the treatment

of this pathology and complications in the postoperative period are not entirely satisfactory, among which purulent-inflammatory ones remain the most severe, lead to recurrence of hernias, require repeated surgical interventions and significantly worsen the quality of life of patients [17, 32]. To eliminate the shortcomings inherent in classic implants, a number of implants with various types of polymer coatings with antimicrobial properties, substances that improve reparative processes and other properties have been developed. But they do not completely satisfy surgeons, since they are used in limited quantities and do not always meet generally accepted requirements.

Therefore, the development of new types of mesh implants of high strength with antimicrobial and other properties remains an urgent problem. The solution of which is possible only by developing implants using materials with new properties.

A modern scientific direction that allows obtaining new materials with given or new properties is nanotechnology, which involves the introduction of nanoparticles into the composition of matrix substances, which give materials new properties [9, 21].

Today, carbon nanotubes and nanoparticles of various metals are widely used as polymer and metal nanofillers [20, 30, 31], which are introduced into matrix substances to obtain new materials or give known materials new properties [6, 7, 11]. The use of nanotechnology made it possible to obtain fundamentally new types of materials with new or specified properties that are widely used in industry, but information on the use of nanocomposite or nanomodified materials in medicine is limited.

Today, polypropylene threads have been created that contain carbon nanotubes and silver nanoparticles, which have high strength and antimicrobial activity and can be used as surgical suture material. On the basis of the obtained threads, which were used as raw materials for the manufacture of mesh implants, we developed a new type of nanocomposite mesh implants with antimicrobial properties. But for the introduction of the developed endoprostheses into clinical practice, it is necessary to study the reaction of tissues to their implantation, which will allow to substantiate their biocompatibility with tissues and develop indications for use in the clinic.

The purpose of the research is to carry out an experimental comparative evaluation of the reaction of tissues to the implantation of the developed polypropylene mesh implant modified with carbon nanotubes and silver nanoparticles.

Material and methods

Experimental studies were performed in compliance with the requirements of international law (the Helsinki Declaration of Human Rights of 1975 and the Vancouver Convention of 1974, 1994 on biomedical experiments), as well as in accordance with the laws and documents on bioethics of Ukraine (protocol of the Bioethics Committee of the National Pirogov Memorial Medical University, Vinnytsya No. 9 dated November 19, 2019).

The experimental part of the work was performed on 105 sexually mature laboratory rats with a body weight of 200 to 250 g in the vivarium of the National Pirogov Memorial Medical University, Vinnytsya, which were maintained in accordance with generally accepted norms. Rats were divided into three series of experiments (35 animals in each series). In the first series of experiments, polypropylene mesh implants were implanted, in the second - polypropylene mesh implants with antimicrobial properties, on which the antiseptic polyhexamethylene guanidine chloride was applied as an antimicrobial agent by spraying. In the third series, developed polypropylene mesh implants made of polypropylene threads were implanted into which carbon nanotubes and silver nanoparticles were introduced at the formation stage.

Operative interventions were performed after premedication with diphenhydramine at the rate of 1.5 mg/kg of body weight and aminazine (0.02 mg/kg), under ketamine anesthesia (by intramuscular injection of ketamine at the rate of 10 mg/kg of rat body weight). After anesthetizing the animals, they were fixed on the table, the operating field was treated with Betadine and alcohol three times, after which a middle laparotomy was performed. The peritoneum, muscles, and aponeurosis of the anterior abdominal wall were sutured, and mesh implants measuring 1.0 x 0.5 cm were placed on the junction line and fixed with separate nodal sutures to the anterior abdominal wall along the junction line, in the first series of experiments, with atraumatic suture material with polypropylene, and in the second - polypropylene suture material covered with an antiseptic, and in the third - polypropylene suture material modified with carbon nanotubes and silver nanoparticles. After that, the skin and subcutaneous tissue were sutured with knotted sutures with the appropriate suture material and the postoperative wound was treated with Betadine. In the postoperative period, the general condition of the animals and the condition of the postoperative wound were monitored. The animals were removed from the experiment by decapitation after preliminary anesthesia with sodium thiopental at the rate of 50 mg/kg of body weight 3, 5, 7, 14, 21, 30 and 90 days after the surgical intervention. In the animals removed from the experiment, body weight was measured, visible skin and mesh implantation sites were evaluated, and tissues of the anterior abdominal wall were excised together with the implants for morphological studies. The tissues taken for the study were fixed in a 10 % solution of neutral formalin, dehydrated, embedded in paraffin, and 3-5 μm thick sections were prepared on a microtome. The prepared histological preparations were stained with hematoxylin-eosin and according to Van Gieson [22]. Microscopy of histological preparations was carried out using an OLIMPUS BX 41 light microscope (certificate of the Ministry of Health of Ukraine on state registration

No. 8120/2008, code 9011800000). Image visualization was performed using the cellSens Entry program (xv Image Processing), morphometry was performed using the Quickphoto micro 3.2 program (license agreement No. 925113924). The composition and ratio of elements of inflammatory cell infiltration was studied using immersion microscopy. In the obtained histological preparations, the density of the cellular infiltrate in the tissues around the implanted meshes, its cellular composition, and the counting of cells of the fibroplastic series (from young fibroblasts to fibrocytes) were evaluated [3].

Identified changes in the examined tissues were documented by micro photography and processed using the Quick PHOTO MICRO 2.3 program.

Statistical data analysis was performed using Statistica 6.4 v12 software, Stat Soft. Inc. and Microsoft Office Excel 2016. Determination of the nature of data distribution was carried out using the Shapiro-Wilk test. Taking into account the assessment of the normality of the data distribution of quantitative parameters, the comparison of groups was carried out using the t-test. For data that had a non-normal distribution, the calculation was performed using the Mann-Whitney (U) test. The marginal level of error of the first kind (α) is accepted at a level of no more than 5 % ($p<0.05$) [1].

Results

The study of morphological changes in the tissues three days after the implantation of endoprostheses showed that there was swelling and inflammatory cell infiltration in the tissues, which was the least when the developed mesh was implanted. In the tissues around the implanted polypropylene mesh, moderately expressed, diffuse, relatively uniform, inflammatory infiltration was determined, which formed a demarcation shaft. The infiltrate was mainly located within the subcutaneous adipose tissue, spread between the contracted elements of the mesh, capturing at the same time the large subcutaneous muscle, the dermis, and the rectus abdominis muscle adjacent to the mesh. Small areas of necrosis, signs of tissue swelling and the formation of micro-abscesses were noted at the level of the grid location. The vessels of the microcirculatory channel were unevenly expanded, full of blood. Focal diapedesis hemorrhages were determined, the destruction of collagen fibers was observed (they were fragmented, in some places in the form of structureless bands and deep masses that unevenly and insufficiently perceived picrofuchsin) and small accumulations of fibrinoid substance were detected.

A similar microscopic picture was found in the location of the polypropylene implant covered with an antiseptic. On histological preparations, areas of necrosis and significant swelling were revealed. Inflammatory cellular infiltration, which formed a demarcation shaft, was located mainly within the subcutaneous fat tissue, not involving the dermis, but spread to the rectus abdominis muscle. A productive reaction in the form of a thin (in 1-3 layers of cells) epithelioid cell wall was observed directly around the mesh elements, and in places, on the contrary, an exudative reaction with the formation of microabscesses.

In the tissues around the implants, there was an expansion of the lumen and a moderate fullness of the vessels of the microcirculatory channel and large accumulations of fibrinoid substance (Fig. 1).

During this period of observation, the tissues around the polypropylene mesh modified with carbon nanotubes and silver nanoparticles showed slight signs of edema, dilated blood vessels, focal diapedesis hemorrhages, and unevenly expressed cellular infiltration.

The infiltrate was mainly located around part of the mesh threads and within the subcutaneous fat tissue, and unlike previous series of experiments, it did not invade the dermis and the rectus abdominis muscle to which the implant was attached. The cellular composition of the infiltrate did not differ from its composition in previous series of experiments and was also represented by neutrophilic

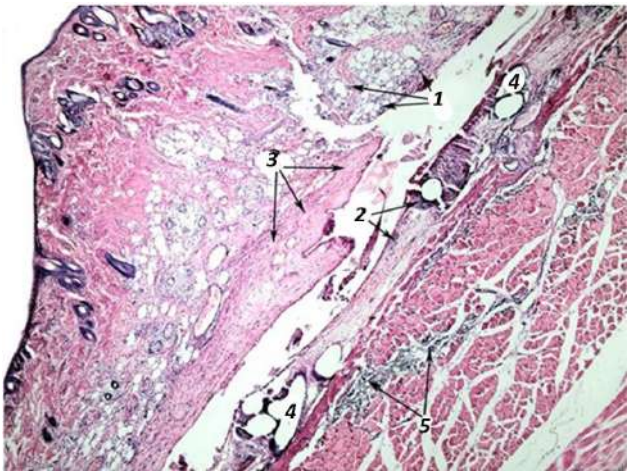

Fig. 1. Inflammatory leukocyte infiltration in the hypodermis (1), in the tissues and rectus abdominis muscle (2, 5), fibrinoid substance (3) around the implanted polypropylene mesh with an antimicrobial coating (4) on the 3rd day of the experiment. Staining with hematoxylin and eosin. x40.

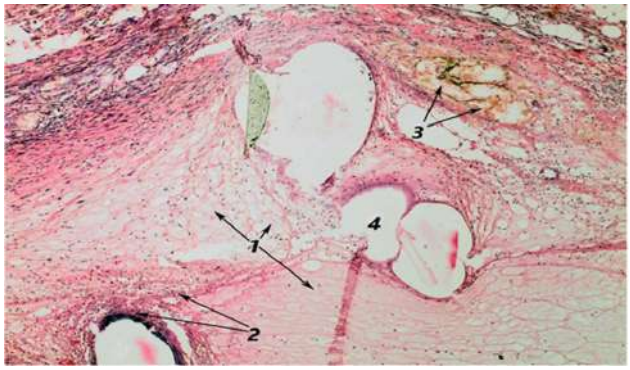

Fig. 2. Tissue swelling (1), inflammatory leukocyte infiltration (2), dilated blood vessels (3) around the implanted polypropylene mesh modified with silver nanoparticles and carbon nanotubes (4) on the 3rd day of the experiment. Staining with hematoxylin and eosin. x100.

leukocytes, plasma cells, lymphocytes and macrophage-monocytic elements. Small areas of fibrinoid substance deposition were found at the level of the mesh location (Fig. 2).

During the morphometric study of changes in cellular composition after 3 days of the experiment, the density of the cellular infiltrate around the implanted meshes was as follows. The infiltrate density around the polypropylene mesh was 812.0±66.5 cells/mm^2. Around the polypropylene mesh coated with an antiseptic, its density was 934.0± 71.0 cells/mm^2 and 622.0±60.3 cells/mm^2 around the developed mesh, which was significantly less ($p<0.005$) than around the meshes implanted in the first and second series of experiments. The study of the composition of the cellular infiltrate showed that the infiltrate in all experiments was dominated by segmented neutrophilic leukocytes, the number of which around the polypropylene mesh was at the level of 714.6±58.6 cells/mm^2, around the polypropylene mesh with an antimicrobial coating - 756.5±57.6 cells/mm^2 and the lowest number of neutrophils of leukocytes ($p<0.05$) was in the composition of the infiltrate around the developed meshes - 485.2±47.0 cells/mm^2. The number of plasma cells in the infiltrate was: around the polypropylene mesh - 18.71±4.03 cells/mm^2, around the polypropylene mesh covered with an antiseptic up to 74.70±5.69 cells/mm^2 and around the designed meshes 62.20±6.05 cells/mm^2; lymphocytes - 32.48±2.60 cells/mm^2 around polypropylene mesh, 56.02±4.30 cells/mm^2 around mesh covered with an antiseptic and 43.51±4.24 cells/mm^2 around developed mesh. Macrophage-monocytic elements were detected around polypropylene meshes in the amount of 16.23± 1.32 cells/mm^2, around meshes covered with antiseptic 46.74±3.52 cells/mm^2 and 31.11±3.00 cells/mm^2 around developed meshes. In the tissues, cells of the fibroblastic series were also detected, which were represented mainly by young fibroblasts, the number of which was significantly higher around the elements of the developed mesh - 209.9±12.3 cells/mm^2, while around the polypropylene meshes their number was at the level of 114.0± 7.6 cells/mm^2 and around of polypropylene nets covered with an antiseptic, cells of the fibroblastic series were found in a small amount - 94.40±5.20 cells/mm^2.

On the seventh day after implantation of polypropylene endoprostheses, inflammatory cell infiltration in tissues became more pronounced. At the same time, the infiltrate was located not only within the subcutaneous adipose tissue and between the structural elements of the mesh, but also spread to the rectus abdominis muscle. Young granulation tissue was found in the tissues in the central parts of the implanted mesh. A granulation shaft of epithelioid cells was located directly around part of the mesh elements, among which there were multinucleated giant foreign body cells of various types (Fig. 3).

At the location of the polypropylene implant covered with an antiseptic, during this period of observation, moderate swelling of the tissues was determined, the mesh itself had a slightly pronounced deformation. Inflammatory cellular infiltration remained in the tissues, which had a diffuse character. At the same time, its expressiveness has significantly decreased compared to the previous period of observation. Inflammatory infiltration persisted in the hypodermis, in the area of connected tissues, in the area after the surgical wound, and in the form of small foci in the rectus abdominis muscle. Granulation tissue of various degrees of maturity was located around the mesh itself and its individual elements, among which cells of the fibroplastic series and multinucleated giant foreign body cells of various types were determined (Fig. 4).

On the seventh day, there was no tissue swelling around the implanted mesh made of polypropylene modified with carbon nanotubes and silver nanoparticles. Inflammatory cell infiltration became diffuse, its density was significantly

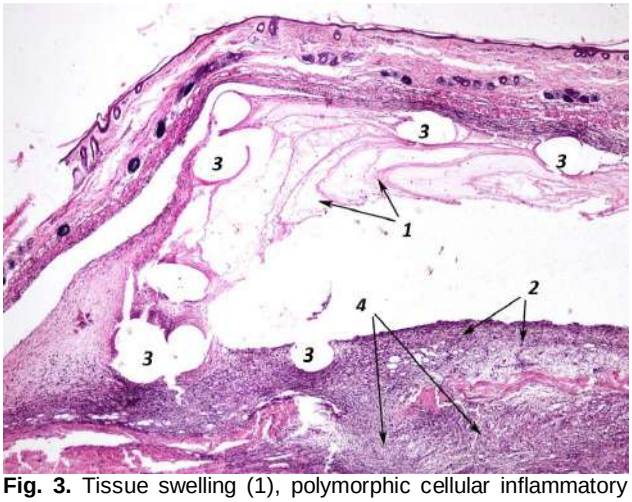

Fig. 3. Tissue swelling (1), polymorphic cellular inflammatory infiltration (2) in tissues (3) and rectus abdominis muscle (4) around the implanted polypropylene mesh on the 7th day of the experiment. Staining with hematoxylin and eosin. x40.

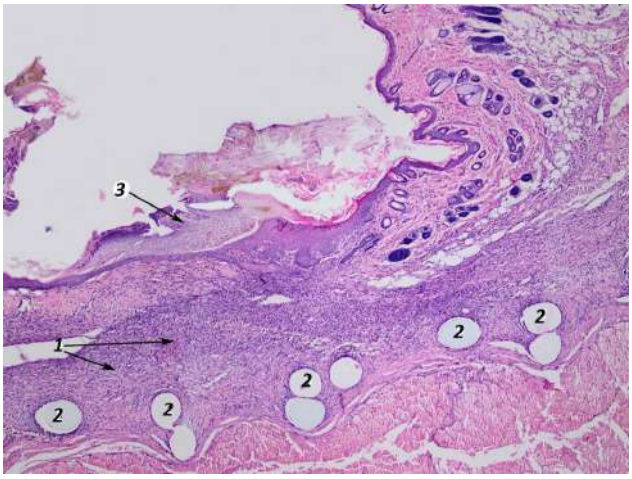

Fig. 4. Granulation tissue with polymorphic cellular inflammatory infiltration (1) in the tissues around the implanted polypropylene mesh covered with an antiseptic (2), scab on the surface of the postoperative wound (3) on the 7th day of the experiment. Staining with hematoxylin and eosin. x40.

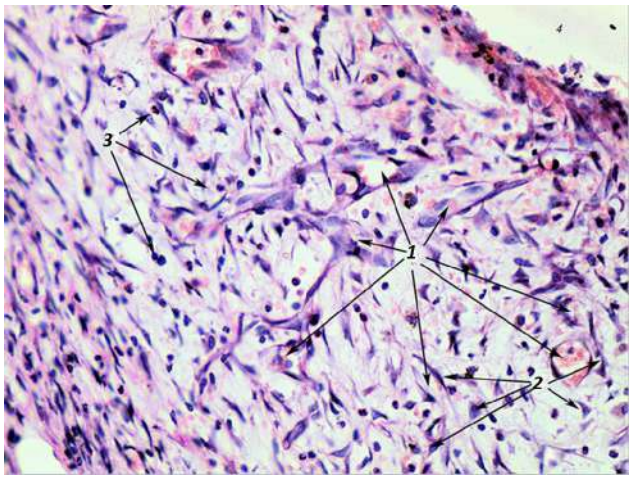

Fig. 5. Vessels of young granulation tissue (1), active fibroblasts (2), eosinophilic granulocytes (3) in the tissues around the implanted polypropylene mesh modified with silver nanoparticles and carbon nanotubes on the 7th day of the experiment. Staining with hematoxylin and eosin. x400.

lower ($p<0.05$) than in the experiments of the comparison groups. The inflammatory infiltrate in the form of cells occupied only the hypodermis, it did not spread to the rectus abdominis muscle. At the same time, abundant masses of fibrinoid substance were deposited at the site of mesh implantation. Granulation tissue of various degrees of maturity with an intercellular matrix and a large number of active fibroblasts was determined around the mesh and its individual elements (Fig. 5).

On the 7th day of observation, the density of the cellular infiltrate around the implanted meshes around the polypropylene meshes increased to 1032±74 cells/mm^2, around the polypropylene mesh with an antimicrobial coating to 810.0±40.1 cells/mm^2, and around the implanted polypropylene mesh modified with carbon nanotubes and silver nanoparticles - 843.0±47.9 cells/mm^2. At the same time, there was a change in the composition of the cells that were found in the infiltrate.

The number of neutrophil leukocytes compared to the previous period of observation decreased significantly ($p<0.05$) and was 608.9±44.0 cells/mm^2 around polypropylene meshes, 354.1±20.1 cells/mm^2 around polypropylene meshes with an antimicrobial coating and 299.7±14.8 cells/mm^2 around developed nets During this period of observation, a significant ($p<0.05$) increase in the number of plasma cells was noted: around polypropylene meshes, their number was 206.4±14.9 cells/mm^2, around polypropylene meshes with an antimicrobial coating - 178.2±8.8 cells/mm^2 and 143.3±8.1 cells/mm^2 around developed grids. A similar pattern was observed with the number of lymphocytes. Thus, the number of lymphocytes in the cellular infiltrate around polypropylene implants was 123.8±8.9 cells/mm^2, around polypropylene meshes with an antimicrobial coating - 129.6±6.4 cells/mm^2, and around engineered meshes - 151.7±8.6 cells/mm^2. A similar picture was observed with macrophage-monocytic elements, the number of which also increased significantly compared to the previous period of observation and amounted to 92.88±6.70 cells/mm^2 around polypropylene meshes, around polypropylene meshes with an antimicrobial coating - 202.5±10.0 cells/mm^2, and around developed meshes - 193.9±11.0 cells/mm^2. The intensification of the phenomena of reparative regeneration processes and the formation of a connective tissue capsule around the implants during this period of observation was evidenced by an increase in the number of fibroplastic cells in the cellular infiltrate around the implants. It should be noted that the number of these cells was different depending on the type of implant. Thus, the number of fibroblastic cells around polypropylene meshes was 2411±162 cells/mm^2, around polypropylene meshes coated with an antiseptic - 2093±121 cells/mm^2, and around developed meshes - 3904±279 cells/mm^2. In addition to the cells of the regenerative row, multinucleated giant foreign body cells were found in the infiltrate around the meshes. The largest number of them was in the tissues around the implanted mesh covered with an antiseptic - 14.02±1.57 cells/mm^2, around polypropylene meshes - 6.021±2.503 cells/mm^2, and the smallest number was found around the developed mesh - 4.011±1.053 cells/mm^2.

On the 14th day of the experiment, inflammatory changes were detected around the elements of the polypropylene mesh in the surrounding tissues, the granulomatous epithelioid cell mass with plasma cells, fibroblasts and multinucleated giant foreign body cells remained and became more pronounced. Fibrous tissue was determined in the area of polypropylene mesh implantation, which was represented by thin bundles and dissociated collagen fibers. Fibrous tissue, along with collagen fibers, contained a significant number of differentiated fibroblasts. At the same time, in the deep sections, between the elements of the mesh, areas of granulation tissue were preserved. Among the collagen fibers, separate areas of dense infiltration by plasma cells and multinucleated giant cells of foreign bodies were determined.

On the 14th day of the experiment, a slight deformation of the polypropylene mesh covered with an antiseptic was determined. Around it, instead of granulation tissue, fibrous tissue was found, represented by thin bundles of mature and immature collagen fibers, and cellular inflammatory infiltration of tissues remained. An unevenly expressed, vascularized granulomatous shaft of epithelioid cells and neutrophilic granulocytes was located around the mesh elements, which also contained fibroblasts, eosinophils, and multinucleated giant cells of foreign bodies. As in the previous series of experiments, areas of dense cellular infiltration and areas of granulation tissue located between mesh elements were found.

In the tissues around the developed meshes, during this period of observation, fibrous tissue, represented by bundles of different thicknesses and dissociated collagen

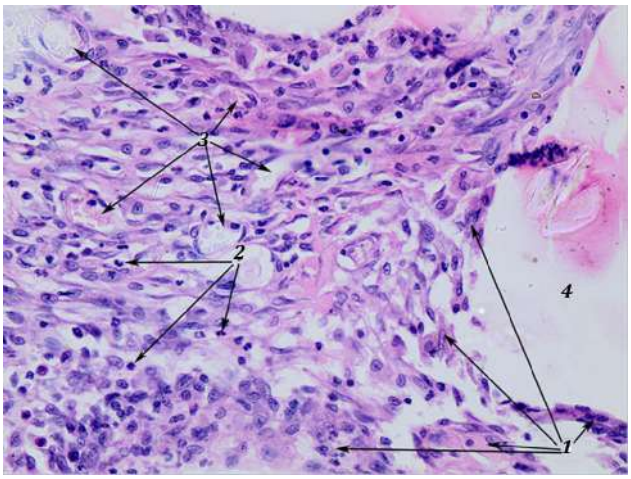

Fig. 6. Granulomatous epithelioid cell shaft (1) with eosinophilic granulocytes (2), microcirculatory vessels (3) in the tissues around the implanted polypropylene mesh modified with silver nanoparticles and carbon nanotubes (4) on the 14th day of the experiment. Staining with hematoxylin and eosin. x400.

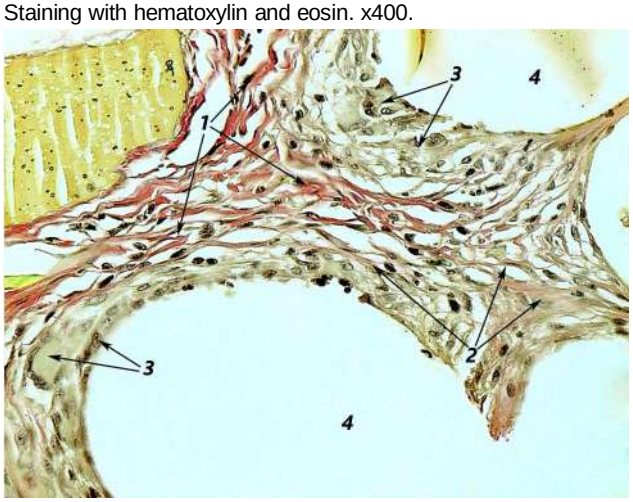

Fig. 7. Mature collagen fibers (1), collagen-producing active fibroblasts (2), granulomatous cell shaft with giant multinucleated cells (3) in the tissues around the implanted polypropylene mesh modified with silver nanoparticles and carbon nanotubes (4) on the 14th day of the experiment. Van Gieson staining. x400.

fibers, was determined on the periphery of the implanted mesh. Collagen bundles and individual fibers of fibrous tissue were ordered, directed parallel to the plane of the mesh, capturing and surrounding its elements. Weakly expressed, scattered inflammatory cellular infiltration was noted in the tissues. Directly around the mesh elements, a thin granulomatous epithelioid cell shaft with the presence of multinucleated giant cells of foreign bodies was preserved (Fig. 6, 7). Inflammatory cell infiltration in the tissues was not determined outside the mesh implantation zone.

The calculation of the composition of cells around the implanted meshes showed that the inflammatory phenomena around the implanted meshes continued to decrease. The density of the cellular infiltrate, during this period of observation, was 413.0±43.5 cells/mm^2 around polypropylene meshes, meshes with an antimicrobial coating - 301.0±22.2 cells/mm^2 and around the developed mesh - 297.0±27.2 cells/mm^2. A decrease in inflammation was also evidenced by a decrease in the number of neutrophil leukocytes in the tissues around the implanted polypropylene mesh to 82.60±8.70 cells/mm^2, around polypropylene meshes with an antimicrobial coating to 24.08±1.82 cells/mm^2, and around the developed mesh - 14.85±1.40 cells/mm^2. Regardless of the type of mesh, during this period of observation, a change in cellular composition was noted, which characterized the predominance of alteration processes over exudation processes and activation of reparative regeneration processes with the formation of a connective tissue capsule around the implants. Thus, the number of plasma cells in the cellular infiltrate around the polypropylene mesh increased to 202.4±21.3 cells/mm^2, to 35.64±3.31 cells/mm^2 around polypropylene meshes with an antimicrobial coating, and to 27.09±2.00 cells/mm^2 around the designed mesh. The number of lymphocytes also increased to 49.56± 5.22 cells/mm^2 around polypropylene mesh, 154.4± 14.1 cells/mm^2 around polypropylene mesh with antimicrobial coating, and 90.32±6.73 cells/mm^2 around designed meshes. The number of macrophage-monocytic elements also increased to 78.47±8.26 cells/mm^2 around the polypropylene mesh, to 92.07±8.45 cells/mm^2 around the polypropylene meshes with an antimicrobial coating, and around the designed mesh to 159.5±11.8 cells/mm^2. Also, the number of cells of the fibroblastic series increased in the tissues around the implanted meshes, the number of which in the infiltrate around the polypropylene meshes was 1852±85 cells/mm^2, around the meshes coated with an antiseptic - 1608±111 cells/mm^2, and around the designed meshes - 2552±138 cells/mm^2. The number of multinucleated giant cells of foreign bodies also increased.

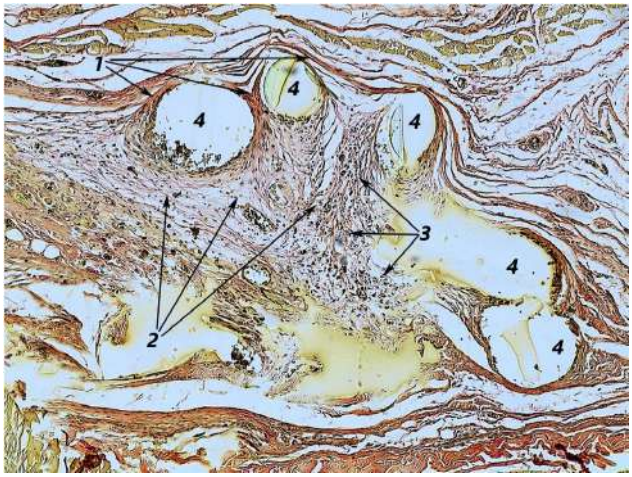

Fig. 8. Areas of mature (1) and immature (2) connective tissue in the fibrous capsule with foci of inflammatory cell infiltration (3) around the implanted polypropylene mesh (4) on the 21st day of the experiment. Van Gieson staining. x100.

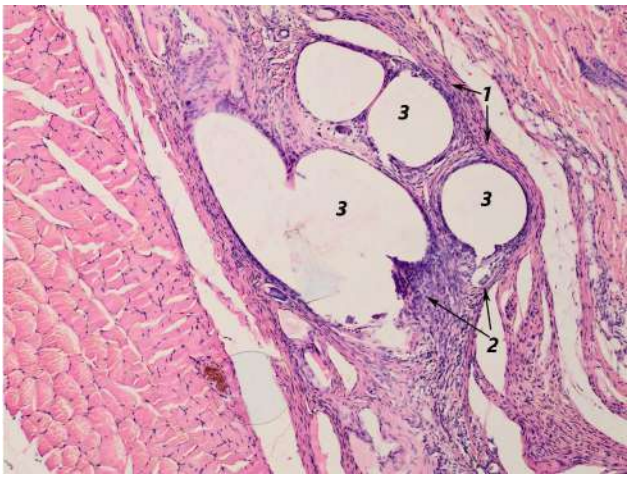

Fig. 9. Connective tissue capsule (1) with foci of inflammatory cell infiltration (2) in the tissues around the implanted polypropylene mesh covered with an antiseptic (3) on the 21st day of the experiment. Staining with hematoxylin and eosin. x100.

In the tissues around the polypropylene mesh up to 7.004±2.750 cells/mm^2, around the meshes with antimicrobial coating - 12.04±2.60 cells/mm^2 and up to 9.027±3.410 cells/mm^2 around the designed mesh.

On the 21st day of the experiment, fibrous tissue of heterogeneous structure and maturity was determined in the area of polypropylene mesh implantation. Along the surface of the grid, the fibrous tissue was represented by a thin layer of densely arranged collagen fibers oriented parallel to the plane of the grid. At the same time, the latter simultaneously penetrated between the mesh elements and incompletely covered them. Between the mesh cells, fibrous tissue was formed by immature thin bundles of collagen fibers. Tissues were unevenly infiltrated with cellular elements. The granulomatous epithelioid cell shaft around the mesh elements, which contained fibroblasts and single multinucleated giant cells of foreign bodies, remained, but became less pronounced (Fig. 8).

On the 21st day of observation, in the area of implantation of a polypropylene mesh covered with an antiseptic, fibrous tissue of a heterogeneous degree of maturity was determined on the surface of the mesh: mature collagen fibers partially enveloped the mesh elements themselves. Along with this, mainly between the mesh elements, areas of fibrous tissue formed by loose thin bundles of immature collagen fibers were determined. In the fibrous tissue, unevenly expressed inflammatory cell infiltration took place. A thin granulomatous, epithelioid-cell shaft, which was preserved around the mesh elements, with individual multinucleated giant cells of foreign bodies was found along the periphery of the mesh in separate places (Fig. 9).

Whereas in the zone of implantation of the nanocomposite mesh, mature fibrous tissue was determined. On the surface of the mesh and around its threads, fibrous tissue was represented by bundles of thickened mature, mostly compactly arranged, collagen fibers. Inflammatory cell infiltration at the mesh implantation site was absent. Single multinucleated giant foreign body cells were found in the tissues directly adjacent to the meshes. Inflammatory phenomena and structural disorders in the tissues beyond the location of the mesh were not detected, which indicated the completion of the processes of formation of the connective tissue capsule around the implanted mesh (Fig. 10).

During the morphometric examination during this period of observation, a slight cellular infiltrate was detected around the meshes, the density of which was 194.0± 12.8 cells/mm^2 around the polypropylene meshes, 206.0±11.5 cells/mm^2 around the polypropylene meshes with an antimicrobial coating, and 173.0±11.8 cells/mm^2 around the developed mesh. Neutrophil leukocytes in the composition of the infiltrate were in small numbers: around the polypropylene nets, their number was 3.461± 0.240 cells/mm^2, around the polypropylene nets with an antimicrobial coating - 2.063±0.127 cells/mm^2, and around the developed net, neutrophil leukocytes were found in the form of single cells. The number of plasma cells also decreased. Their number around polypropylene meshes was 13.84±0.94 cells/mm^2, around polypropylene meshes with an antimicrobial coating - 8.247±0.462 cells/mm^2, and plasma cells were found around the developed mesh in the form of single cells. The number of lymphocytes in the infiltrate remained elevated: around polypropylene meshes up to 76.12±5.19 cells/mm^2, around polypropylene meshes with an antimicrobial coating - 76.22±4.20 cells/mm^2, and around the developed meshes their number was significantly reduced in comparison with control experiments and the previous observation period up to 3.882±0.265 cells/mm^2. However, the number of macrophage-monocytic elements in the cellular infiltrate was not significantly different from the previous period of observation and amounted to 79.58±5.43 cells/mm^2 around polypropylene meshes, 119.5±6.7 cells/mm^2 around

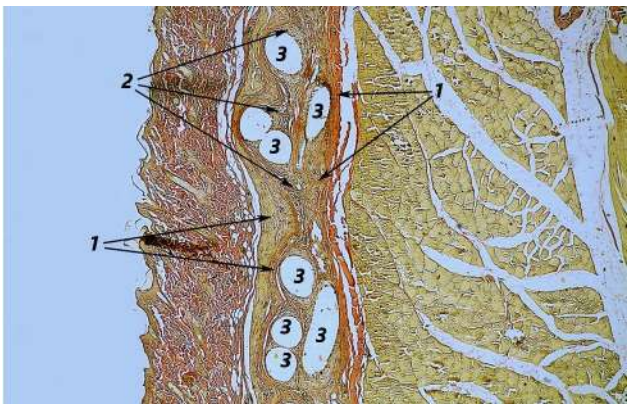

Fig. 10. Fibrous capsule with ordered bundles of collagen fibers (1), granulomatous cellular reaction (2), around the tissues around the implanted polypropylene mesh modified with silver nanoparticles and carbon nanotubes (3) on the 21st day of the experiment. Van Gieson staining. x40.

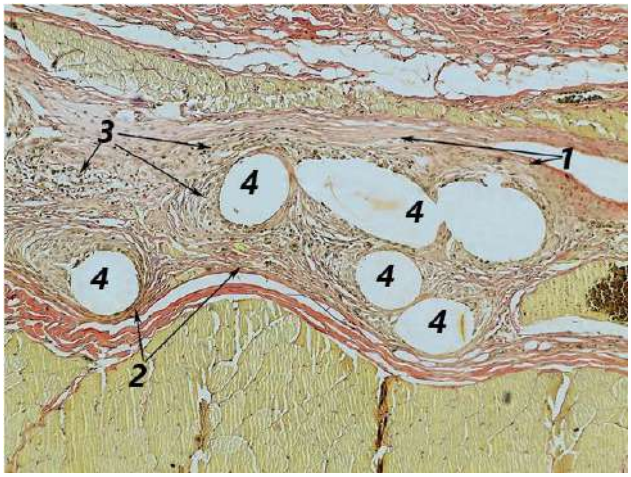

Fig. 11. Areas of immature (1) and mature with ordered bundles of collagen fibers (2) fibrous capsule, granulomatous cellular reaction with an admixture of granulocytes (3) in the tissues around the implanted (4) polypropylene mesh with an antimicrobial coating on the 30th day of the experiment. Van Gieson staining. x100.

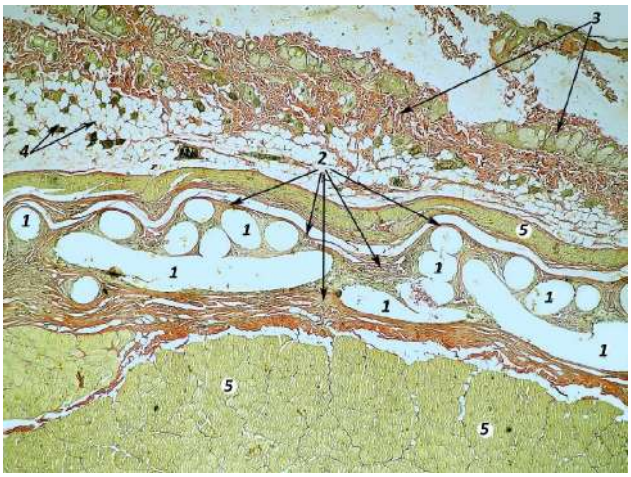

Fig. 12. Implanted polypropylene mesh modified with silver nanoparticles and carbon nanotubes (1), fibrous capsule (2), preserved structure of skin (3), hypodermis (4) and muscles of the anterior abdominal wall (5) on the 90th day of the experiment. Van Gieson staining. x40.

polypropylene meshes with an antimicrobial coating and 190.1±12.6 cells/mm^2 around developed nets During this period of observation, the bulk of the cells in the cellular infiltrate consisted of fibroplastic cells. Thus, their number was 1207±71 cells/mm^2 around polypropylene nets, 1593±100 cells/mm^2 around polypropylene nets with an antimicrobial coating, and 943.0±68.7 cells/mm^2 around developed nets. In addition, the number of foreign body multinucleated giant cells increased: 12.05±5.42 cells/mm^2 around polypropylene mesh, 8.002±3.165 cells/mm^2 around polypropylene meshes with antimicrobial coating, and 7.002±3.235 cells/mm^2 around developed mesh.

On the 30th day, a well-formed capsule of fibrous tissue was found around the implanted polypropylene mesh, represented by uniformly densely arranged bundles of collagen (picrinophilic) fibers oriented along the mesh, covering its individual elements and abdominal muscles in a sleeve-like fashion. Fibrous areas of fibrous tissue sclerosis were determined between the mesh elements. A small number of differentiated fibroblasts were found on the periphery of areas of sclerosis. An uneven epithelioid-cellular granulation shaft with the presence of multinucleated giant cells of foreign bodies and fibroblasts was also preserved around the mesh elements. The structure of the intact dermis and underlying muscle was not altered.

Around the nets with an antimicrobial coating, the histological picture, similar to the previous term, was mostly preserved for a day. A capsule was located around the implanted mesh and its elements, formed by bundles of collagen fibers of various degrees of maturity, associated with collagen fibers of the aponeurosis of the rectus abdominis muscle and the perimysium of the large subcutaneous muscle. An uneven shaft of epithelioid cells with multinucleated giant cells of foreign bodies and active fibroblasts was located around the mesh elements (Fig. 11).

On the 30th day, the fibrous tissue around the implanted developed mesh, the mesh modified with silver nanoparticles and carbon nanotubes, contained bundles of collagen fibers homogeneous in structure and maturity. The latter were located along the plane of the grid and around its elements, forming a clear fibrous capsule intimately connected with the connective tissue formations of the muscles. Inflammatory cell infiltration in the surrounding tissues was not determined. The normal histological structure of the surrounding tissues was also preserved, and the restoration of the spatial structure of the implanted mesh itself was noted.

On the 30th day, a slight cellular infiltrate was detected around the polypropylene implants and around the polypropylene mesh with an antimicrobial coating. The density of the infiltrate was 97.00±6.67 cells/mm^2 around polypropylene meshes and 111.0±14.1 cells/mm^2 around polypropylene meshes with an antimicrobial coating. Whereas no foci of infiltration were detected in the tissues around the developed meshes.

On the 90th day, the processes of formation of the fibrous capsule around the implants were completed and the implants were separated from the surrounding tissues (Fig. 12). During histological examination, foci of inflammatory infiltration and pathological changes were not detected. The cellular composition in the tissues around the implants did not differ from its composition in the tissues before the operation.

Discussion

According to the literature, morphological changes in the tissues around mesh implants in the early days after surgery are characterized by the presence of inflammatory processes with alteration phenomena followed by a transition to reparative processes aimed at delimiting the

implants from the surrounding tissues by a fibrous capsule [2, 13, 23, 25, 26, 29].

The analysis of the obtained data of our research made it possible to establish that during the implantation of mesh endoprostheses in the tissues of the anterior abdominal wall of rats, regardless of their species, in the first days after the operation, the same changes were detected, which are associated with the body's reaction to traumatic damage due to surgical trauma. Intraoperative damage to the tissues of the abdominal wall in experimental animals on the 3-5th day after surgery was manifested by necrotic changes with reactive inflammation, which was evidenced by the presence of an inflammatory infiltrate dominated by neutrophilic leukocytes, tissue infiltration by cellular elements, tissue swelling and marked microcirculation disorders. At the same time, the maximum manifestations of alteration phenomena were observed during the implantation of a classic polypropylene mesh and a polypropylene mesh covered with an antiseptic, and the minimum during the implantation of a developed mesh modified with carbon nanotubes and silver nanoparticles, where a less pronounced exudative phase of inflammation and an earlier onset of the repair phase were detected. But this reaction differed between groups of experimental animals depending on the type of implant used, as evidenced by the regression of inflammatory phenomena in the tissues around the implants and the processes and terms of the formation of the fibrous capsule around the meshes. During the implantation of nanocomposite mesh implants, by the 7th day of the experiment, the exudative phase of inflammation ended and the formation of a thin connective tissue capsule began. The connective tissue capsule around the developed implants was fully formed on the 21st day of the experiment, while when implanting a classic polypropylene mesh and polypropylene with an antimicrobial coating, the formation of the capsule around the implants lasted until the 30th day of the experiment.

According to many researchers [12, 19, 24, 27], surgical trauma and the presence of an implant in the tissues lead to the occurrence of an inflammatory process, which prevents the delimitation of the implant, and contributes to the occurrence of postoperative complications. Long periods of alteration processes around implanted mesh endoprostheses lead to the development of complications in the early postoperative period. At the same time, long periods of reparative processes aimed at the formation of a connective tissue capsule around implants lead to the formation of a predominantly immature, rough, thick fibrous capsule, which in turn leads to the emergence of so-called late postoperative complications, which worsen the quality of life of patients, contribute to the recurrence of hernias and require repeated surgical interventions [7, 14, 16].

A comparative morphometric and morphological analysis of the reaction of the tissues of the anterior abdominal wall in rats to the implantation of the developed mesh showed that the reaction of the tissues to the developed mesh implant is less pronounced than to the polypropylene mesh and the polypropylene implant coated with an antiseptic and indicates the high biocompatibility of the developed mesh implants and the possibility of their use for surgical treatment of abdominal hernias, which will prevent the occurrence of both early and late postoperative complications.

The data we obtained showed a high biocompatibility of the developed implant with the tissues of experimental animals, which requires further study in the clinic during surgical treatment of abdominal hernias.

Conclusions

1. During the implantation of classic meshes made of polypropylene and polypropylene with an antimicrobial coating, the exudative phase of inflammation in the tissues around the implants was detected up to 14 days of observation, and the formation of a connective tissue capsule around the implants lasted up to 30 days of observation.

2. The exudative phase of inflammation in the tissues around the mesh implants made of polypropylene modified with carbon nanotubes and silver nanoparticles was completed by the 7th day of the experiment, which ensured a greater intensity of the reparative regeneration processes and the separation of the implant from the surrounding tissues by a thin connective tissue capsule up to the 21st day of observation.

References

[1] Altman, D. G. (1990). *Practical statistics for medical research.* CRC press. ISBN 978-0-412-27630-9. doi: 10.1201/9780429258589

[2] Ávila, O. R., Parizzi, N. G., Souza, A. P. M., Botini, D. S., Alves, J. Y., & Almeida, S. H. M. (2016). Histological response to platelet-rich plasma added to polypropylene mesh implemented in rabbits. *International braz j urol*, 42(5), 993-998. doi: 10.1590/S1677-5538.IBJU.2015.0319

[3] Avtandilov, H. H. (1990). *Медицинская морфометрия [Medical morphometry].* M.: Медицина=M.: Medicine.

[4] Babiy, I. V., Vlasov, V. V., Pidmurniak, O. O., & Hurnitskyi, A. E. (2019). Результати хірургічного лікування пахвинної грижі за методикою IL LICHTENSTEIN з використанням різних типів імплантатів [Results of surgical treatment of inguinal hernia using the method of IL LICHTENSTEIN using different types of implants]. *Клінічна анатомія та оперативна хірургія=Clinical anatomy and operative surgery,* 18(1), 57-61. doi: 10.24061/1727-0847.18.1.2019.9

[5] Basile, F., Biondi, A., & Donati, M. (2013). Surgical approach to abdominal wall defects: history and new trends. *International journal of surgery,* 11(1), S20-S23. doi: 10.1016/S1743-9191(13)60008-4

[6] Bhandari, V., Jose, S., Badanayak, P., Sankaran, A., & Anandan, V. (2022). Antimicrobial finishing of metals, metal oxides, and metal composites on textiles: a systematic review. *Industrial & Engineering Chemistry Research,* 61(1), 86-101. doi: 10.1021/acs.iecr.1c04203

[7] Fakoori, E., & Karami, H. (2018). Preparation and characterization

of ZnO-PP nanocomposite fibers and non-woven fabrics. *The Journal of The Textile Institute,* 109(9), 1152-1158. doi: 10.1080/00405000.2017.1417681

[8] Gherghinescu, M. C., Copotoiu, C., Lazar, A. E., Popa, D., Mogoanta, S. S., & Molnar, C. (2017). Continuous local analgesia is effective in postoperative pain treatment after medium and large incisional hernia repair. *Hernia,* 21, 677-685. doi: 10.1007/s10029-017-1625-8

[9] Hassan, T., Salam, A., Khan, A., Khan, S. U., Khanzada, H., Wasim, M., ... & Kim, I. S. (2021). Functional nanocomposites and their potential applications: A review. *Journal of Polymer Research,* 28, 1-22. doi: 10.1007/s10965-021-02408-1

[10] International guidelines for groin hernia management (2018). *Hernia,* 22(1), 1-165. doi: 10.1007/s10029-017-1668-x

[11] Jin, K., Eyer, S., Dean, W., Kitto, D., Bates, F. S., & Ellison, C. J. (2019). Bimodal nanofiber and microfiber nonwovens by melt-blowing immiscible ternary polymer blends. *Industrial & Engineering Chemistry Research,* 59(12), 5238-5246. doi: 10.1021/acs.iecr.9b04887

[12] Kallinowski, F., Fortelny, R. H., Köckerling, F., Mayer, F., Morales-Conde, S., & Sandblom, G. (2022). *Editorial: mesh complications in hernia surgery.* Front Surg 9: 841672. doi: 10.3389/fsurg.2022.841672

[13] Kelly, M., Macdougall, K., Olabisi, O., & McGuire, N. (2017). In vivo response to polypropylene following implantation in animal models: a review of biocompatibility. *International urogynecology journal,* 28, 171-180. doi: 10.1007/s00192-016-3029-1

[14] Köckerling, F., Hoffmann, H., Adolf, D., Weyhe, D., Reinpold, W., Koch, A., & Kirchhoff, P. (2020). Female sex as independent risk factor for chronic pain following elective incisional hernia repair: registry-based, propensity score-matched comparison. *Hernia,* 24, 567-576. doi: 10.1007/s10029-019-02089-2

[15] Köckerling, F., & Simons, M. P. (2018). Current concepts of inguinal hernia repair. *Visceral medicine,* 34(2), 145-150. doi: 10.1159/000487278

[16] Kroese, L. F., Kleinrensink, G. J., Lange, J. F., Gillion, J. F., Ain, J. F., Beck, M., ... & Zaranis, C. (2018). External validation of the European hernia society classification for postoperative complications after incisional hernia repair: a cohort study of 2,191 patients. *Journal of the American College of Surgeons,* 226(3), 223-229. doi: 10.1016/j.jamcollsurg.2017.11.018

[17] Lermite, E., & Arnaud, J. P. (2012). Prospective randomized study comparing quality of life after shoudice or mesh plug repair for inguinal hernia: short-term results. *Surgical technology international,* 22, 101-106. PMID: 23023573

[18] Lockhart, K., Dunn, D., Teo, S., Ng, J. Y., Dhillon, M., Teo, E., & van Driel, M. L. (2018). Mesh versus non-mesh for inguinal and femoral hernia repair. *Cochrane Database of Systematic Reviews,* 9(9), CD011517. doi: 10.1002/14651858.CD011517.pub2

[19] Lopez-Cano, M., Martin-Dominguez, L. A., Pereira, J. A., Armengol-Carrasco, M., & Garcia-Alamino, J. M. (2018). Balancing mesh-related complications and benefits in primary ventral and incisional hernia surgery. A meta-analysis and trial sequential analysis. *PLoS One*, 13(6), e0197813. doi: 10.1371/journal.pone.0197813

[20] Mohd Nurazzi, N., Asyraf, M. M., Khalina, A., Abdullah, N., Sabaruddin, F. A., Kamarudin, S. H., ... & Sapuan, S. M. (2021). Fabrication, functionalization, and application of carbon nanotube-reinforced polymer composite: An overview. *Polymers,* 13(7), 1047. doi: 10.3390/polym13071047

[21] New functional substances and materials for chemical engineering (2021). PH "Akademperiodyka", Kyiv, 2021. doi: 10.15407/akademperiodyka.444.332

[22] Sarkysov, D. S. & Perov, Yu. L. (1996). *Микроскопическая техника [Microscopic technique].* M: Медицина=M: Medicine.

[23] Plencner, M., Prosecká, E., Rampichová, M., East, B., Buzgo, M., Vysloužilová, L., ... & Amler, E. (2015). Significant improvement of biocompatibility of polypropylene mesh for incisional hernia repair by using poly-e-caprolactone nanofibers functionalized with thrombocyte-rich solution. *International journal of nanomedicine,* 10, 2635-2646. doi: 10.2147/IJN.S77816

[24] Plymale, M. A., Davenport, D. L., Walsh-Blackmore, S., Hess, J., Griffiths, W. S., Plymale, M. C., ... & Roth, J. S. (2020). Costs and complications associated with infected mesh for ventral hernia repair. *Surgical Infections,* 21(4), 344-349. doi: 10.1089/sur.2019.183

[25] Ponce Leon, F., Manso, J. E. F., Abud, V. L., Nogueira, W., Silva, P. C., & Martinez, R. (2018). Sublay repair results in superior mesh incorporation and histological fibrogenesis in comparison to onlay and primary suture in an experimental rat model. *Hernia*, 22(6), 1089-1100. doi: 10.1007/s10029-018-1808-y

[26] Qiu, W., Zhong, C., Xu, R., Zou, T., Wang, F., Fan, Y., ... & Yang, Z. (2018). Novel large-pore lightweight polypropylene mesh has better biocompatibility for rat model of hernia. *Journal of Biomedical Materials Research Part A,* 106(5), 1269-1275. doi: 10.1002/jbm.a.36326

[27] Stoikes, N., Roan, E., Webb, D., & Voeller, G. R. (2018). The Problem of Seroma After Ventral Hernia Repair. *Surgical technology international,* 32, 93-98. PMID: 29791714

[28] Tanasescu, C., Moisin, A., Mihetiu, A., Serban, D., Costache, A., & Bratu, D. G. (2021). The use of polypropylene mesh in inguinal hernia surgery: A retrospective study. *Experimental and Therapeutic Medicine,* 22(4), 1-6. doi: 10.3892/etm.2021.10627

[29] Taylor, D. (2018). The failure of polypropylene surgical mesh in vivo. *Journal of the mechanical behavior of biomedical materials*, 88, 370-376. doi: 10.1016/j.jmbbm.2018.08.041

[30] Thomas, S., Mishra, R., & Kalarikkal, N. (Eds.). (2017). *Micro and nano fibrillar composites (MFCs and NFCs) from polymer blends.* Woodhead Publishing. ISBN: 9780081019917. doi: 10.1016/B978-0-08-101991-7.09989-1

[31] Vimbela, G. V., Ngo, S. M., Fraze, C., Yang, L., & Stout, D. A. (2017). Antibacterial properties and toxicity from metallic nanomaterials. *International journal of nanomedicine*, 12, 3941-3965. doi: 10.2147/IJN.S134526

[32] Wilson, R. B., & Farooque, Y. (2022). Risks and prevention of surgical site infection after hernia mesh repair and the predictive utility of ACS-NSQIP. *Journal of Gastrointestinal Surgery,* 26(4), 950-964. doi: 10.1007/s11605-022-05248-6

ПОРІВНЯЛЬНА ОЦІНКА РЕАКЦІЇ ТКАНИН НА СІТЧАСТИЙ ІМПЛАНТАТ З ПОЛІПРОПІЛЕНУ, МОДИФІКОВАНОГО ВУГЛЕЦЕВИМИ НАНОТРУБКАМИ ТА НАНОЧАСТИНКАМИ СРІБЛА

Вільцанюк О. А., Кравченко В. М., Вільцанюк О. О., Дерезюк А. В., Шеремета Р. О.

Лікування гриж живота залишається однією з найбільш актуальних проблем сучасної хірургії. Велика кількість ускладнень після операцій з приводу гриж потребує розробки нових видів імплантатів для проведення пластики тканин. Мета дослідження - провести в експерименті порівняльну оцінку реакції тканин на імплантацію розробленого сітчастого імплантату з поліпропілену, модифікованого вуглецевими нанотрубками та наночастинками срібла. Дослідження проведені на 105

статевозрілих лабораторних щурах в трьох серіях дослідів (по 35 щурів у кожній). У першій серії в тканини передньої черевної стінки були імплантовані поліпропіленові сітчасті імплантати, в другій - поліпропіленові імплантати з покриттям антисептиком, а в третій - поліпропіленові імплантати, модифіковані вуглецевими нанотрубками та наночастинками срібла. Тварин виводили з досліду після попереднього знеболення через 3, 5, 7, 14, 21, 30 та 90 діб після операції. Вилучали тканини черевної стінки разом з імплантатами, виготовляли гістологічні препарати, які забарвлювали гематоксиліном і еозином та за Ван-Гізон. Вивчили склад і співвідношення елементів клітинної інфільтрації в тканинах з подальшою статистичною обробкою отриманих даних. Встановлено, що при імплантації сітчастих ендопротезів незалежно від їх виду на 3-5 доби після операції в тканинах виявлялися некротичні зміни з реактивним запаленням, наявність запального клітинного інфільтрату, набряк тканин та порушення мікроциркуляції. За умови імплантації розробленої сітки виявляли менш виражену ексудативну фазу запалення і більш ранній початок фази репарації. В залежності від виду використаного імплантату подальша реакція відрізнялась між групами експериментальних тварин, про що свідчили регрес явищ запалення в тканинах та процеси формування фіброзної капсули навколо імплантатів. При імплантації наномодифікованих сітчастих імплантатів до 7 доби експерименту ексудативна фаза запалення завершувалась і починалось формування тонкої сполучнотканинної капсули, формування якої завершувалось до 21 доби спостереження, тоді як при імплантації сітки з поліпропіленом та поліпропіленом з антимікробним покриттям формування капсули тривало до 30 доби. Таким чином, встановлено, що в тканинах навколо імплантації класичних сіток з поліпропілену та поліпропілену з антимікробним покриттям до 14 доби експерименту триває ексудативна фаза запалення, а сполучнотканинна капсула формується до 30 доби. В той же час, в тканинах навколо сітчастих імплантатів з поліпропілену, модифікованого вуглецевими нанотрубками та наночастинками срібла, ексудативна фаза запалення завершувалась до 7 доби експерименту. Це забезпечувало інтенсивність процесів репаративної регенерації та відмежування імплантату від навколишніх тканин тонкою сполучнотканинною капсулою до 21 доби спостереження.

Ключові слова: *поліпропіленові сітчасті імплантати, вуглецеві нанотрубки, наночастинки срібла, морфологічні зміни, біологічна сумісність.*

Author's contribution

Viltsaniuk O. A. - conceptualization, research, review writing and editing.
Kravchenco V. M. - research, methodology and writing of the original draft, formal analysis and validation.
Viltsaniuk O. O. - project administration.
Dereziuk A. V. - software, resources.
Sheremeta R. O. - data visualization.

DOI: 10.31393/morphology-journal-2024-30(1)-02 Reports of Morphology, Vol. 30, №1, Pages 16-24

ISSN 1818-1295 eISSN 2616-6194

REPORTS OF MORPHOLOGY

Official Journal of the Scientific Society of Anatomists, Histologists, Embryologists and Topographic Anatomists of Ukraine

journal homepage: https://morphology-journal.com

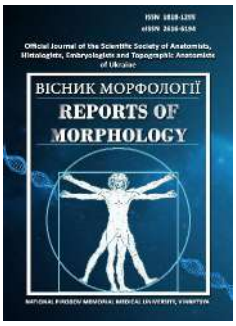

Diagnostic and prognostic markers of morphofunctional heart state impairment and long-term persistence of heart failure in patients with myocarditis

Cherniuk S. V., Marchenko K. S.

State institution "National Scientific Center "The M. D. Strazhesko Institute of Cardiology, Clinical and Regenerative Medicine of the National Academy of Medical Sciences of Ukraine", Kyiv, Ukraine

ARTICLE INFO

Received: 11 October 2023

Accepted: 05 January 2024

UDC: 616.127-002-036.12:355.11

CORRESPONDING AUTHOR

e-mail: cerniuk.sergey@gmail.com

Cherniuk S. V.

CONFLICT OF INTEREST

The authors have no conflicts of interest to declare.

FUNDING

The study was carried out from named scholarship of the Verkhovna Rada of Ukraine for young scientists - doctors of sciences for 2023. Resolution of the Verkhovna Rada of Ukraine No. 3297-IX dated August 9, 2023.

DATA SHARING

Data are available upon reasonable request to corresponding author.

The problem of myocarditis has gained special relevance in recent years, therefore, the search for new diagnostic and prognostic markers of the disease unfavorable course is expedient for the timely appointment of optimal drug therapy, strengthening of regimen measures and adequate monitoring of the patient's clinical condition. The purpose of the study: to establish laboratory and instrumental markers of morphofunctional heart state impairment and to develop a mathematical model for early prediction of long-term heart failure persistence in patients with myocarditis. We included 80 patients with acute myocarditis with a severe course and reduced left ventricular ejection fraction (LVEF) - ≤40 %. Assessment of laboratory and instrumental indicators was carried out in the 1st month from the onset of symptoms, after 6 and after 12 months of observation. All patients underwent for immunological studies, 24-hour ECG monitoring, echocardiography with speckle-tracking and cardiac magnetic resonance imaging. After 12 months of follow-up frequency of adverse cardiovascular events (ACE) was assessed. Statistical processing included Student's t-test for comparison of mean values, binary logistic regression and ROC analysis, discriminant analysis. A set of morphofunctional instrumental indicators determined during the 1st month from the onset of myocarditis, which can serve as predictors of cardiovascular events during the next 12 months, was established: left ventricular ejection fraction ≤30 %; indicator of longitudinal global strain ≤7.0 %; the presence of paroxysms of non-sustained ventricular tachycardia; the presence of inflammatory changes in ≥6 segments and delayed contrast enhancement in ≥5 segments of the left ventricle. A mathematical model has been created, with the help of which it is possible to predict the adverse course of the disease with long-term (at least 12 months) persistence of heart failure already within the 1st month from the onset of myocarditis.

Keywords: *myocarditis, diagnosis, prognosis, morphofunctional heart state, immune state, echocardiography, cardiac magnetic resonance imaging.*

Introduction

Myocarditis is an inflammatory lesion of the heart muscle of various etiology and is characterized by a wide spectrum of nonspecific clinical symptoms with an unpredictable course. The disease most often has a viral etiology and can be associated with both the direct cytotoxic effect of viruses on the myocardium and the activation of immunopathological reactions, that leads to autoimmune heart damage and long-term persistence of the inflammatory process [2, 4, 11, 29]. In recent years, the problem of myocarditis has become especially relevant in connection with the COVID-19 pandemic and its consequences. By itself, the coronavirus infection can rarely become the direct cause of inflammatory heart damage - its specific weight in the structure of etiological factors among other viruses is up to 5 % [6, 20]. However, it has been proven that COVID-19 is able to stimulate the replication of other viruses in the myocardium, or activate immunopathological reactions from the hypersecretion of pro-inflammatory cytokines with the development of the well-known phenomenon called "cytokine storm" [20, 25,

30]. Another problem, which is relevant primarily for our country, is the active hostilities that continue on the territory of Ukraine as a result of Russian aggression, which lead to an increase in the incidence of myocarditis in the most vulnerable category of people - young and middle-aged men [3, 20]. So, to date, according to the received data, myocarditis occurs more often in men (about 2/3 of cases) and has a more severe course [18, 20, 31]. Moreover, the disease is most often observed in the age range of 30-45 years [22, 31]. Factors contributing to an increase in the likelihood of developing myocarditis in conditions of war, in particular in military personnel, internally displaced persons and persons injured as a result of hostilities, are the deterioration of living conditions and the quality of food, hypothermia, the influence of acute and chronic stress, the need for a long-term stay in stable team, which leads to activation of viral infections. In view of the above, the problem of myocarditis, in particular in Ukraine, has gained special relevance in recent years, therefore, the search for new diagnostic and prognostic markers of the adverse course of the disease is expedient for the timely appointment of optimal drug therapy, strengthening of regimen measures and adequate monitoring of the patient's clinical condition.

The purpose of the study - to establish laboratory and instrumental markers of morphofunctional heart state impairment and to develop a mathematical model for early prediction of long-term heart failure persistence in patients with myocarditis.

Material and methods

The study included 80 patients with acute myocarditis of a severe course, who at the time of inclusion had a reduced ejection fraction (EF) of the left ventricle - ?40 % according to the recommendations of the European Society of Cardiology and II-IV functional class of heart failure according to the classification of the New York Heart Association [23]. The diagnosis of myocarditis and the determination of the criteria for the severe course of the disease were established on the basis of the Recommendations for the diagnosis and treatment of myocarditis and on the basis of the Standards for the diagnosis and treatment of cardiovascular diseases of the All-Ukrainian association of cardiologists of Ukraine for the year 2021 [16].

The study was conducted in accordance with the principles of bioethics set forth in the Helsinki Declaration "Ethical Principles of Medical Research Involving Human Subjects" and the "Universal Declaration of Bioethics and Human Rights (UNESCO)", on the basis of the department of non-coronary heart diseases, rheumatology and therapy from June 2022 to March 2023. The research was approved by the ethics commission of the State institution "National Scientific Center "The M. D. Strazhesko Institute of Cardiology, Clinical and Regenerative Medicine of the National Academy of Medical Sciences of Ukraine" (Protocol of the meeting No. 1-27 dated June 13, 2022). All patients signed an informed consent to the processing of personal data before the start of the research in accordance with the Order of the Ministry of Health of Ukraine No. 110 dated 14.02.2012 "On the approval of forms of primary accounting documentation and Instructions for filling them which are used in health care institutions independently from the form of ownership and subordination". Information processing was carried out in accordance with the requirements of the Law of Ukraine "On the Protection of Personal Data".

Assessment of the clinical condition of patients, laboratory and instrumental indicators was carried out in the 1st month from the onset of symptoms before the appointment of optimal medical therapy, after 6 and after 12 months of observation. Dynamic monitoring during 12 months allowed us to assess the frequency of cardiovascular events, which included: death, development of a stroke, and the need for hospitalization due to decompensation of heart failure.

Patients who were included in the study, during dynamic monitoring, received optimal drug therapy for heart failure according to the latest recommendations of the European Society of Cardiology for 2021 year, which included: angiotensin-converting enzyme inhibitors, beta-blockers, mineralocorticoid receptor antagonists, sodium-glucose cotransporter-2 inhibitors [23]. Immunosupressive therapy with corticosteroids was administrated according to All-Ukrainian association of cardiologists of Ukraine algorithm [16]. If indicated, diuretics, antiarrhythmic drugs, and anticoagulants were prescribed.

Immunological studies were carried out in peripheral blood in the Department of Immunology and Biochemistry of the State institution "National Scientific Center "The M. D. Strazhesko Institute of Cardiology, Clinical and Regenerative Medicine of the National Academy of Medical Sciences of Ukraine", in order to determine:

- levels of pro-inflammatory cytokines - interleukin-1β (IL-1β), interleukin-6 (IL-6), tumor necrosis factor α (TNF-α) and anti-inflammatory interleukin-10 (IL-10) in blood serum by enzyme immunoassay;
- cardiospecific antibodies (CA) to cardiac L-myosin (CM) and beta1-adrenoceptors (β_1-AR) by calculation of optical plane units (OPU) using the ELI-Viscerotest test system;
- expression of Toll-like receptors of the 2nd and 4th types on the surface of monocytes by the method of flow cytofluorimetry based on the study of the average fluorescence intensity (AFI).

24-hour (Holter) ECG monitoring was performed on a Philips Digitrack TM-plus 3100A device. The percentage of ventricular extrasystoles (VE) relative to the number of normal ventricular complexes, and the presence of paroxysms of non-sustained ventricular tachycardia (NSVT) were assessed. The presence of tachycardia with 3 or more ventricular complexes lasting up to 30 seconds according to the Standards for the diagnosis and treatment of cardiovascular diseases of the All-Ukrainian association

of cardiologists of Ukraine was considered as a criterion for NSVT [16].

Transthoracic echocardiography (EchoCG) was performed on an Aplio Artida SSH - 880 CV ultrasonic diagnostic device, Toshiba Medical System Corporation (Japan). In the two-dimensional mode, during systole and diastole, the end-diastolic volume (EDV) of the left ventricle was calculated, which was related to the body surface area and an indexed indicator was obtained - left ventricular EDVi. Left ventricular EF was estimated by the biplane method of Simpson discs. With the help of the speckle-tracking (ST) technique, the indicator of left ventricular longitudinal global systolic strain (LGSS) was evaluated, to determine which video loops were recorded from three standard apical accesses: four-chamber, two-chamber and three-chamber positions, using the sixteen segmental model of left ventricle according to Lang R. [19]. Circumferential global systolic strain (CGSS) and radial global systolic strain (RGSS) were also assessed, for which determination was made by recording video loops along the short axis of the left ventricle at the level of the papillary muscles [24]. While calculating the average deformation and deformation rates of six segments were taken - one segment each of each left ventricular wall in the middle section [15, 24]. The analysis of deformation indicators was carried out using the Wall Motion Tracking software package. The results of ST Echocardiography are presented in the form of absolute indicators.

Cardiac magnetic resonance (CMR) imaging with the use of gadovist as a contrast agent was performed in the department of radiodiagnostics of the State institution "National Scientific Center "The M. D. Strazhesko Institute of Cardiology, Clinical and Regenerative Medicine of the National Academy of Medical Sciences of Ukraine". The Toshiba Vantage titan HSR 1.5 Tesla device (Japan) was used. Images were evaluated in 3 modes along the short and long axis of the heart: before the introduction of a contrast agent (T2 Black blood FSat mode) to detect the area of edema in the myocardium; within 3-5 min. after administration (T1 early contrast) to detect hyperemia in the zone of inflammatory lesions and the mode of T1 delayed enhancement after 10-15 min. from the introduction of a contrast solution to detect fibrotic/necrotic changes [7, 12]. To estimate the number of segments of the left ventricle affected by inflammatory or fibrotic/necrotic changes contemporary model of the 17-segment structure of the left ventricle was used [12]. Figure 1 shows an example of active inflammatory damage of myocardium as a result of diffuse myocarditis, which was accompanied by pronounced morphofunctional disorders: significant dilatation, eccentric remodeling, and severe systolic dysfunction of the heart.

Statistical processing of the received data was carried out using the software package of SPSS Advanced Statistics 27.0 license program number L-CZAA-BT2KCD (USA). The calculated quantitative indicators are given as the mean value and standard deviation of the mean (M ± m), the

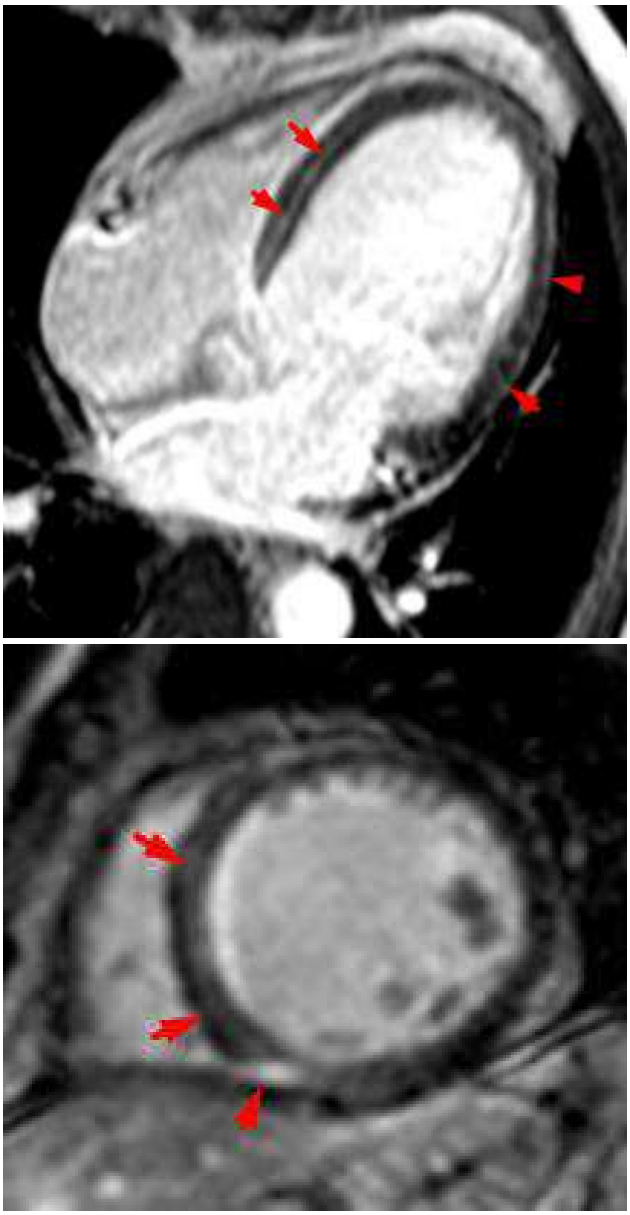

Fig. 1. Cardiac magnetic resonance imaging of a patient with active diffuse myocarditis.
Note: the arrows indicate the zones of subepicardial, intra- and transmural accumulation of gadolinium in the lateral wall of the left ventricle and the interventricular septum, which indicates the damage of the myocardium by an inflammatory and fibrotic/necrotic process (Data of SI "NSC "The M. D. Strazhesko Institute of Cardiology, Clinical and Regenerative Medicine NAMS of Ukraine").

Student's t-test was used to compare the average indicators in all groups. For all types of analysis, the critical level of statistical significance was $p<0.05$. Limit values of indicators that served as predictors of the presence of certain clinical characteristics and confidence intervals were determined based on the Student's test using binary logistic regression. ROC analysis was used to assess the quality of binary classification. Mathematical models were built using discriminant analysis.

Results

The study of immune status indicators during dynamic observation of patients with myocarditis allowed to establish that the highest activity of immunopathological reactions was observed in the 1st month from the onset of the disease in the acute stage. This was confirmed by the highest levels of pro-inflammatory cytokines, a high content of cardiac-specific autoantibodies, in particular to cardiac myosin and β_1-adrenoceptor, which was observed on the background of high expression activity of type 2 and 4 TLRs (table 1). After 6 and 12 months, there was a gradual decrease in the content of pro-inflammatory cytokines and an increase in the concentration of anti-inflammatory IL-10, which was combined with a decrease in the content of cardio-specific autoantibodies and a decrease in the activity of TLR expression.

When studying the structural and functional state of the heart with the help of echocardiography with speckle-tracking technique and the results of CMR with contrast, it was established that the most pronounced violation of the contractility of the left ventricle was noted in the first month after the onset of myocarditis (Table 2). After 6 months of observation, a gradual improvement of the left ventricular contractile capacity was determined, which was evidenced by a significant increase in the value of left ventricular EF, longitudinal and circumferential global systolic strain. Positive dynamics were maintained and after 12 months of follow-up, it was also characterized by reverse remodeling of the left ventricle, which was evidenced by a significant decrease in the left ventricular EDVi. Improvement of the contractile capacity and reverse remodeling of the left ventricle was observed on the background of a decrease in the volume of the inflammatory lesion - according to CMR, the number of segments of the left ventricle with the presence of inflammatory changes significantly decreased after 6 months, and after 12 months their number was 2.3 times less than in the first month from the onset of the disease. After 12 months we also observed the reduction of left ventricular segments number in which delayed enhancement was present, that became a sign of regression of myocardial fibrotic/necrotic changes.

According to the results of 24-hour ECG monitoring, a decrease in the average number of ventricular extrasystoles was established from 3.640±0.412 % in the 1st month to 2.217± 0.312 and 1.714±0.269 after 6 and 12 months, respectively ($p<0.01$). The frequency of NSVT paroxysms detection decreased from 27.50 % at the onset of the disease to 17.50 and 12.50 %, respectively, after 6 and 12 months of observation.

After 12 months of observation, the frequency of cardiovascular events was analyzed and it was established that two patients died (2.50 %), one patient (1.25 %) developed a cerebral circulation disorder due to cerebral vessel thromboembolism of cardiac origin, and 15 patients (18.75 %) required hospitalization due to decompensation of heart failure. It should be noted that the cases of planned hospitalization for routine examinations and correction of therapy, which is provided by the Standards of the All-Ukrainian association of cardiologists of Ukraine for patients with myocarditis, were not classified as cardiovascular events.

On the basis of 12-month follow-up period, we assessed the impact of the studied indicators on the development of cardiovascular events, which included cases of cardiac death, development of a stroke, and the need for hospitalization due to decompensation of heart failure. For this purpose, a search for independent predictors of the development of cardiovascular events in patients with acute myocarditis was conducted based on statistical analysis using the binary logistic regression method. The most significant in this aspect were the following indicators determined in the first month from the onset of the disease: value of left ventricular EF $\leq$30 %, value of LGSS $\leq$7.0 %, the presence of unstable ventricular tachycardia paroxysms, inflammatory changes affecting $\geq$6 segments of the left ventricle, the presence of delayed enhancement (fibrotic /necrotic changes) in $\geq$5 segments of the left ventricle (Table 3).

Next, we constructed a ROC curve reflecting the relationship between the development of cardiovascular

Table 1. Comparative characteristics of indicators of immune status at different times from the onset of myocarditis.

Indicators	Value of indicator (M±m)			
	1st month	After 6 months	After 12 months	Referent values
IL-1b, pg/ml	6.213±0.432	4.201±0.408*	3.121±0.415**	0 - 3
IL-6, pg/ml	14.29±1.32	12.22±0.92	7.184±0.822**	0 - 10
TNF-a, pg/ml	17.20±1.11	9.284±0.803*	7.249±0.805*	0 - 6
IL-10, pg/ml	12.13±1.10	24.12±2.28**	34.25±3.08**	0 - 31
Antibodies to CM, OPU	5.123±0.571	3.445±0.343**	1.993±0.251**	Not detected
Antibodies to b_1-AR, OPU	2.071±0.212	1.828±0.174	0.834±0.142**	Not detected
TLR2, AFI	9.304±1.012	7.923±0.932	6.502±0.837*	0 - 3
TLR4, AFI	12.92±1.43	9.730±1.329*	5.307±0.791**	0 - 3

Note: difference in indicators is significant compared to those in the 1st month from myocarditis onset: * - $p< 0.05$; ** - $p<0.01$.

Table 2. Results of echocardiography and cardiac magnetic resonance during dynamic observation of patients with myocarditis.

Indicators	Value of indicator (M±m)		
	1st month	After 6 months	After 12 months
EF of left ventricle, %	33.13±2.24	39.60±2.33*	43.80±2.66**
EDVi of left ventricle, ml/m^2	105.7±7.2	92.62±6.70	85.96±5.94**
LGSS, %	8.213±0.736	11.71±0.88*	13.12±0.84**
CGSS, %	8.993±0.754	11.74±0.87*	12.45±0.98*
RGSS, %	15.37±1.73	18,86±2,08	22.54±2.66*
Amount of left ventricular segments with inflammatory lesions	6.641±0.630	4,240±0,511*	2.882±0.340**
Amount of left ventricular segments with late gadolinium enhancement	4.755±0.437	4.237±0.414	3.544±0.510*

Note: difference in indicators is significant compared to those in the 1st month from myocarditis onset: * - p< 0.05; ** - p<0.01.

Table 3. The role of pathologic changes detected in the first month from the onset of myocarditis in relation to the development of cardiovascular events during 12 months of observation.

Pathologic changes detected in the first month from the onset of myocarditis	Odds ratio (OR)
EF of the left ventricle ≤30 %	2.021 (CI 1.710-2.322; p=0.021)
LGSS ≤7.0 %	1.794 (CI 1.590-2.034; p=0.032)
Presence of NSVT	2.152 (CI 1.851-2.602; p=0.018)
Presence of inflammatory changes affecting ≥6 segments of left ventricle	1.663 (CI 1.452-1.939; p=0.041)
Presence of delayed enhancement in ≥5 segments of left ventricle	1.712 (CI 1.401-1.993; p=0.029)

Note: CI - confidence interval.

events during the 12-month observation period and the simultaneous presence of all the above-mentioned pathological changes (see Table 3) at the onset of myocarditis (Fig. 2).

Therefore, we can state that independent predictors of the development of cardiovascular events within 12 months from the onset of myocarditis with reduced left ventricular EF are the simultaneous presence in the first month from the onset of the disease of a complex of the following pathological changes: left ventricular EF ≤30 %; value of LGSS ≤7.0 %; presence of NSVT paroxysms; presence of inflammatory changes in ≥6 segments of the left ventricle; presence of delayed enhancement in ≥5 segments of the left ventricle.

The further step was the creation of a mathematical model for predicting the long-term persistence of heart failure, which was based on the most informative immunological markers and morphofunctional indicators. The mathematical model was built using discriminant analysis. The model included indicators with the highest odds ratio (OR) values for persistence of II or higher heart failure functional class and the lowest p values, which were obtained in the 1st month from the onset of the disease. Discriminant function covers 92.50 % of cases; statistics Wilks' Lambda=0.539; F=4.181 at p=0.021. This model, in addition to immunological and echocardiographic indicators, included the results of CMR characterizing the number of segments of the left ventricle affected by inflammatory and/or fibrotic/necrotic changes. The model is based on two equations, with the help of which already in the first month from the onset of myocarditis it is possible to estimate the percentage probability of one or another variant of the disease course: Y_1 - for the presence of II or higher functional class of heart failure after 12 months, Y_0 - for the presence of functional class I of heart failure or its absence after 12 months:

Y_1=3.021 x IL-1β + 9.247 x CA to CM + 15.40 x CA to β_1-AR + 3.105 x TLR2 + 4.653 x TLR4 - 0.422 x EF of left ventricle - 1.489 x LGSS - 1.414 x CGSS + 0.170 x EDVi of left ventricle +17.32 in presence of ≥6 SIL + 14.92 in presence of ≥5 SDE - 66.54;

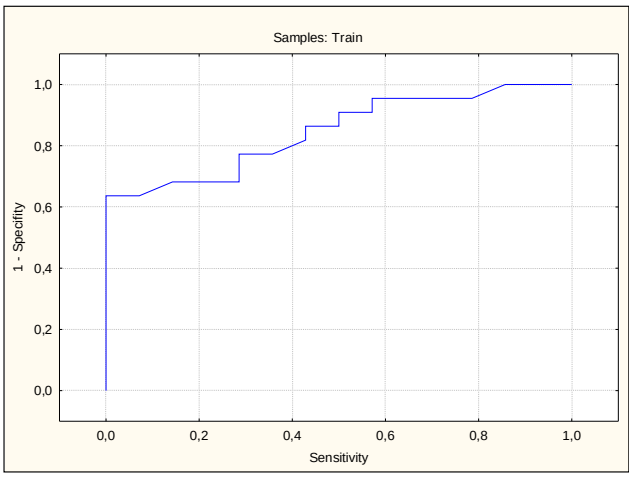

Fig. 2. ROC curve showing the relationship between the simultaneous presence of a complex of pathologic changes and the development of cardiovascular events in patients with acute myocarditis during a 12-month observation period.
Note: area under the curve=0.842; confidence interval - 0.751-0.953; p=0.022.

Y_0=2.236 x IL-1β + 9.447 x CA to CM + 16.01 x CA to β_1-AR + 3.039 x TLR2 + 4.553 x TLR4 - 0.515 x EF of left ventricle - 1.528 x LGSS - 1.322 x CGSS + 0.161 x EDVi of left ventricle +16.53 in presence of ≥6 SIL + 15.94 in presence of ≥5 SDE - 53.20;

Note: CA - cardiospecific antibodies, SIL - segments with inflammatory lesions, SDE - segments with delayed enhancement.

The probability of having II or higher functional class of heart failure after 12 months is estimated by the formula: $Y_1/(Y_1+Y_0)$ x 100 %.

The probability of having functional class I of heart failure or its absence after 12 months is estimated by the formula: $Y_1/(Y_1+Y_0)$ x 100 %.

The sensitivity of the model for predicting the persistence of heart failure is 84.20 %, the specificity is 78.94 %. Positive predictive value - 82.49 %, negative predictive value - 75.92 %. The practical significance of this model is obvious, since with its help, already in the first month from the debut of myocarditis with reduced EF of the left ventricle, the further course of the disease can be predicted with high reliability and the prospects of regression of heart failure clinical symptoms after 12 months can be estimated on the early stage of the disease.

Discussion

According to the world's leading experts on the problems of diagnosis and treatment of myocarditis, the in-depth study of the morphofunctional state of the heart, taking into account its changes in dynamics, nowadays might be the main approach to predicting the clinical course of the disease, preventing the development of complications and choosing the optimal tactics of drug therapy [11, 18, 29]. The results of dynamic monitoring of patients with severe myocarditis, obtained in our study, indicate a gradual recovery of the contractility of the heart after 6 and 12 months of treatment, which occurs on the background of left ventricular dilation decrease and attenuation in the activity of the inflammatory process. A gradual decrease in the concentration of pro-inflammatory cytokines, the content of cardiac-specific antibodies and the expression of type 2 and 4 TLRs after 6 and 12 months had a clear association with a reduction of left ventricular segments number affected by inflammatory changes according to CMR data. A decrease in the activity of the inflammatory process and the volume of the inflammatory lesion of the left ventricle during dynamic observation was accompanied by an improvement in the morphofunctional state and contractility of the left ventricle, and the most informative indicators characterizing this process were the values of longitudinal and circumferential systolic strain. The high informativeness and prognostic value of the LGSS in patients with myocarditis and its comparability with the results of CMR was also proven in several foreign studies [9, 15, 28]. In our study, in addition, an associative relationship was shown between the improvement of the contractile capacity, the reduction of left ventricular dilatation and the reduction of the number of segments affected by inflammatory changes on CMR not only with the value of LGSS, but also with the values of CGSS and RGSS, although the value of the latter increased significantly only after 12 months of observation.

In patients with non-coronary heart diseases, in particular with myocarditis, a high prognostic value has been proven today regarding the future development of cardiovascular events, sudden cardiac death and long-term persistence of heart failure in the presence of delayed contrast on CMR, reduced EF and significant left ventricular dilatation [1, 10, 14, 17, 21]. In addition, a significant role in the development of cardiovascular events has been proven for ventricular rhythm disorders, in particular paroxysms of non-sustained and sustained ventricular tachycardia, which develop in patients with myocarditis both on the background of the influence of stress factors and as a result of morphofunctional changes in the myocardium of inflammatory and fibrotic origin [8, 13, 26, 27]. In the mathematical model created based on the results of our research and according to the data of ROC analysis, in addition to the above indicators, results of speckle tracking echocardiography, in particular LGSS and CGSS, as also immunological biomarkers - IL-1β, CA to CM and β1-AR, demonstrated a high prognostic value, as well as TLR type 2 and type 4 expression activity. Evidence of the prognostic value of active TLR type 4 expression in patients with myocarditis regarding the outcome of the disease and response to immunosuppressive therapy was also obtained by a team of Italian authors led by Chimenti C. [5]. In our study, using statistic analysis it was possible to combine a complex of laboratory and instrumental indicators characterizing the morphofunctional state of the heart, the determination of which already at the onset of myocarditis makes it realistic to assess the risk of cardiovascular events development and calculate the probability of long-term persistence of heart failure.

Nevertheless, the problem of diagnosing and predicting the clinical course of myocarditis, as well as preventing the development of complications remains one of the most difficult for both Ukrainian and foreign cardiology [3, 12, 17, 23]. Currently, the issue of creating recommendations and unified clinical guidelines for the diagnosis and treatment of myocarditis is acute, because this disease remains almost the only common nosology for which, given the complicacy of the problem, no appropriate recommendations have been created by the European Society of Cardiology and the American Heart Association. Taking into account the complexity of the problem, it is obvious that there is a need for prospective investigations devoted to the study of morphofunctional heart state in patients with myocarditis, which should include laboratory tests, a wide range of imaging methods and endomyocardial biopsy. A possible way to solve this problem is to conduct multicenter randomized clinical trials dedicated to improving approaches to diagnosis, prognosis, and treatment of myocarditis,

because contemporary approaches to the problem of myocarditis are based mostly on the results of single-center studies with a small number of patients.

Conclusions

1. According to the results of dynamic monitoring of patients with myocarditis, it was established that the onset of the disease is characterized by a pronounced activation of immunopathological reactions with a significant increase in the concentration of proinflammatory cytokines, cardiospecific autoantibodies on the background of active expression of Toll-like receptors of the 2nd and 4th types, which causes involvement in the inflammatory process of a significant number of segments of the left ventricle and is accompanied by a violation of its morphofunctional state with dilatation, significant impairment of contractility and development of ventricular arrhythmias. After 6 and 12 months of observation, on the background of a decrease in the activity of immunopathological reactions, there is a gradual restoration of the systolic function of the left ventricle, an early marker of which is an increase in the indicators of its longitudinal and circumferential global strain.

2. A set of instrumental indicators determined within the 1st month from the onset of myocarditis, which can serve as predictors of cardiovascular events during the next 12 months, was established: left ventricular ejection fraction $\leq$30 %; index of longitudinal global systolic strain $\leq$7.0 %; the presence of paroxysms of non-sustained ventricular tachycardia; the presence of inflammatory changes in $\geq$6 segments and delayed enhancement in $\geq$5 segments of the left ventricle. A mathematical model has been created, with the help of which within the first month from the onset of myocarditis it is possible to predict the adverse course of the disease with long-term (at least 12 months) persistence of heart failure.

References

[1] Al-Khatib, S. M., Stevenson, W. G., Ackerman, M. J., Bryant, W. J., Callans, D. J., Curtis, A. B., … & Page, R. L. (2018). AHA/ACC/HRS guideline for management of patients with ventricular arrhythmias and the prevention of sudden cardiac death: a report of the American College of Cardiology/American Heart Association Task force on clinical practice guidelines and the heart rhythm society. *Circulation,* 138, e272-e391. doi: 10.1161/CIR.0000000000000549

[2] Ammirati, E., & Moslehi, J. J. (2023). Diagnosis and treatment of acute myocarditis: a review. *JAMA,* 329(13), 1098-1113. doi: 10.1001/jama.2023.3371

[3] Ammirati, E., Frigerio, M., Adler, E. D., Basso, C., Birnie, D. H., Brambatti, M., ... & Camici, P. G. (2020). Management of acute myocarditis and chronic inflammatory cardiomyopathy: an expert consensus document. *Circulation: Heart Failure,* 13(11), e007405. doi: 10.1161/CIRCHEARTFAILURE.120.007405

[4] Caforio, A. L., Pankuweit, S., Arbustini, E., Basso, C., Gimeno-Blanes, J., Felix, S. B., ... & Elliott, P. M. (2013). Current state of knowledge on aetiology, diagnosis, management, and therapy of myocarditis: a position statement of the European Society of Cardiology Working Group on Myocardial and Pericardial Diseases. *European heart journal,* 34(33), 2636-2648. doi: 10.1093/eurheartj/eht210

[5] Chimenti, C., Verardo, R., Scopelliti, F., Grande, C., Petrosillo, N., Piselli, P., ... & Frustaci, A. (2017). Myocardial expression of toll-like receptor 4 predicts the response to immunosuppressive therapy in patients with virus-negative chronic inflammatory cardiomyopathy. *European Journal of Heart Failure,* 19(7), 915-925. doi: 10.1002/ejhf.796

[6] Davis, M. G., Bobba, A., Chourasia, P., Gangu, K., Shuja, H., Dandachi, D., ... & Sheikh, A. B. (2022). COVID-19 associated myocarditis clinical outcomes among hospitalized patients in the United States: a propensity matched analysis of national inpatient sample. *Viruses,* 14(12), 2791. doi: 10.3390/v14122791

[7] Ferreira, V. M., Schulz-Menger, J., Holmvang, G., Kramer, C. M., Carbone, I., Sechtem, U., ... & Friedrich, M. G. (2018). Cardiovascular magnetic resonance in nonischemic myocardial inflammation: expert recommendations. *Journal of the American College of Cardiology*, 72(24), 3158-3176. doi: 10.1016/j.jacc.2018.09.072

[8] Gao, X., Peng, L., Zeng, Q., & Wu, Z. K. (2009). Autonomic Nervous Function and Arrhythmias in Patients with Acute Viral Myocarditis during a 6-Month Follow-Up Period. *Cardiology,* 113, 66-71. doi: 10.1159/000167794

[9] Goody, P. R., Zimmer, S., Öztürk, C., Zimmer, A., Kreuz, J., Becher, M. U., ... & Tiyerili, V. (2022). 3D-speckle-tracking echocardiography correlates with cardiovascular magnetic resonance imaging diagnosis of acute myocarditis-An observational study. I*JC Heart & Vasculature,* 41, 101081. doi: 10.1016/j.ijcha.2022.101081

[10] Gräni, C., Eichhorn, C., Biére, L., Murthy, V. L., Agarwal, V., Kaneko, K., ... & Kwong, R. Y. (2017). Prognostic value of cardiac magnetic resonance tissue characterization in risk stratifying patients with suspected myocarditis. *Journal of the American College of Cardiology*, 70(16), 1964-1976. doi: 10.1016/j.jacc.2017.08.050

[11] Grossman, S. M., Pravda, N. S., Orvin, K., Hamdan, A., Vaturi, M., Bengal, T., … & Weissler-Snir, A. (2021). Characterization and long-term outcomes of patients with myocarditis: A retrospective observational study. *Advances in Interventional Cardiology,* 17, 60-67. doi: 10.5114/aic.2021.104770

[12] Hundley, W. G., Bluemke, D. A., Finn, J. P., Flamm, S. D., Fogel, M. A., ... & Woodard, P. K. - Writing Committee Members (2010). ACCF/ACR/AHA/NASCI/SCMR 2010 expert consensus document on cardiovascular magnetic resonance: a report of the American College of Cardiology Foundation Task Force on Expert Consensus Documents. *Circulation*, 121(22), 2462-2508. doi: 10.1161/CIR.0b013e3181d44a8f

[13] Jeong, S., Ahn, K. O., Shin, S. D., Song, K. J., Kim, J. Y., & Lee, E. J. (2018). Association of recent major psychological stress with cardiac arrest: a case-control study. *American Journal of Emergency Medicine,* 36, 100-104. doi: 10.1016/j.ajem.2017.07.039

[14] Jiang, L., Zuo, H., Liu, J., Wang, J., Zhang, K., Zhang, C., … & Wang, H. (2023). The pattern of late gadolinium enhancement by cardiac MRI in fulminant myocarditis and its prognostic implication: A two-year follow-up study. *Frontiers in Cardiovascular Medicine,* 10, 1144469. doi: 10.3389/fcvm.2023.1144469

[15] Kasner, M., Sinning, D., Escher, F., Lassner, D., Kühl, U., Schultheiss, H. P., & Tschöpe, C. (2013). The utility of speckle

tracking imaging in the diagnostic of acute myocarditis, as proven by endomyocardial biopsy. *International journal of cardiology,* 168(3), 3023-3024. doi: 10.1016/j.ijcard.2013.04.016

[16] Kovalenko, V. M., Lutay, M. I., Sirenko, Yu. M., & Sychov, O. S. (2023). *Серцево-судинні захворювання: класифікація, стандарти діагностики та лікування. 6-те вид., перероб. і доповн. [Cardiovascular diseases: classification, standards of diagnosis and treatment. 6th edition revised and suppl.].* Київ: Четверта хвиля=Kyiv: Fourth wave. ISBN 978-966-529-358-3

[17] Kuruvilla, S., Adenaw, N., Katwal, A. B., Lipinski, M. J., Kramer, C. M., & Salerno, M. (2014). Late gadolinium enhancement on cardiac magnetic resonance predicts adverse cardiovascular outcomes in nonischemic cardiomyopathy: a systematic review and meta-analysis. *Circulation: Cardiovascular Imaging*, 7(2), 250-258. doi: 10.1161/CIRCIMAGING.113.001144

[18] Lampejo, T., Durkin, S. M., Bhatt, N., & Guttmann, O. (2021). Acute myocarditis: aetiology, diagnosis and management. *Clinical Medicine,* 21(5), e505-e510. doi: 10.7861/clinmed.2021-0121

[19] Lang, R. M., Badano, L. P., Mor-Avi, V., Afilalo, J., Armstrong, A., Ernande, L., ... & Voigt, J. U. (2015). Recommendations for cardiac chamber quantification by echocardiography in adults: an update from the American Society of Echocardiography and the European Association of Cardiovascular Imaging. *European Heart Journal-Cardiovascular Imaging,* 16(3), 233-271. doi: 10.1016/j.echo.2014.10.003

[20] Lasica, R., Djukanovich, L., Savic, L., Krljanac, G., Zdravkovich, M., …& Ristic, A. (2023). Update on Myocarditis: From Etiology and Clinical Picture to Modern Diagnostics and Methods of Treatment. *Diagnostics,* 13(19), 3073. doi: 10.3390/diagnostics13193073

[21] Lynge, T. H., Nielsen, T. S., Gregers Winkel, B., Tfelt-Hansen, J., & Banner, J. (2019). Sudden cardiac death caused by myocarditis in persons aged 1-49 years: a nationwide study of 14 294 deaths in Denmark. *Forensic Sciences Research,* 4, 247-256. doi: 10.1080/20961790.2019.159535

[22] Mahrholdt, H., & Greulich, S. (2017). Prognosis in myocarditis: better late than (n) ever!. *Journal of the American College of Cardiology*, 70(16), 1988-1990. doi: 10.1016/j.jacc.2017.08.062

[23] McDonagh, T. A., Metra, M., Adamo, M., Gardner, R. S., Baumbach, A., Böhm, M., ... & Kathrine Skibelund, A. (2021). 2021 ESC Guidelines for the diagnosis and treatment of acute and chronic heart failure: Developed by the Task Force for the diagnosis and treatment of acute and chronic heart failure of the European Society of Cardiology (ESC) With the special contribution of the Heart Failure Association (HFA) of the ESC. *European Heart Journal,* 42(36), 3599-3726. doi: 10.1093/eurheartj/ehab368

[24] Mitchell, C., Rahko, P. S., Blauwet, L. A., Canaday, B., Finstuen, J. A., Foster, M. C., … & Velazquez, E. J. (2018). Guidelines for Performing a Comprehensive Transthoracic Echocardiographic Examination in Adults: Recommendations from the American Society of Echocardiography. *Journal of the American Society of Echocardiography,* 32(1), 1-64. doi: 10.1016/j.echo.2018.06.004

[25] Pannucci, P., Jefferson, S. R., Hampshire, J., Cooper, S. L., Hill, S. J., & Woolard, J. (2023). COVID-19-induced myocarditis: Pathophysiological roles of ACE2 and toll-like receptors. *International Journal of Molecular Sciences,* 24(6), 5374. doi: 10.3390/ijms24065374

[26] Peretto, G., Sala, S., Rizzo, S., De Luca, G., Campochiaro, C., Sartorelli, S., ... & Della Bella, P. (2019). *Arrhythmias in myocarditis: state of the art. Heart rhythm,* 16(5), 793-801. doi: 10.1016/j.hrthm.2018.11.024

[27] Peretto, G., Sala, S., Rizzo, S., Palmisano, A., Esposito, A., De Cobelli, F., ... & Della Bella, P. (2020). Ventricular arrhythmias in myocarditis: characterization and relationships with myocardial inflammation. *Journal of the American College of Cardiology,* 75(9), 1046-1057. doi: 10.1016/j.jacc.2020.01.036

[28] Polte, C. L., Bobbio, E., Bollano, E., Bergh, N., Polte, C., Himmelmann, J., … & Gao, S. A. (2022). Cardiovascular Magnetic Resonance in Myocarditis. *Diagnostics*, 12, 399. doi: 10.3390/diagnostics12020399

[29] Sozzi, F. B., Gherbesi, E., Faggiano, A., Gnan, E., Maruccio, A., Schiavone, M., ... & Carugo, S. (2022). Viral myocarditis: classification, diagnosis, and clinical implications. *Frontiers in Cardiovascular Medicine,* 9, 908663. doi: 10.3389/fcvm.2022.908663

[30] Tschöpe, C., Ammirati, E., Bozkurt, B., Caforio, A. L., Cooper, L. T., Felix, S. B., ... & Van Linthout, S. (2021). Myocarditis and inflammatory cardiomyopathy: current evidence and future directions. *Nature Reviews Cardiology,* 18(3), 169-193. doi: 10.1038/s41569-020-00435-x

[31] Younis, A., Matetzky, S., Mulla, W., Masalha, E., Afel, Y., Chernomordik, F., … & Beigel, R. (2020). Epidemiology characteristics and outcome of patients with clinically diagnosed acute myocarditis. *American Journal of Medicine,* 133, 492-499. doi: 10.1016/j.amjmed.2019.10.015

ДІАГНОСТИЧНІ ТА ПРОГНОСТИЧНІ МАРКЕРИ ПОРУШЕННЯ МОРФОФУНКЦІОНАЛЬНОГО СТАНУ СЕРЦЯ ТА ДОВГОТРИВАЛОЇ ПЕРСИСТЕНЦІЇ СЕРЦЕВОЇ НЕДОСТАТНОСТІ У ХВОРИХ З МІОКАРДИТОМ

Чернюк С. В., Марченко К. С.

Проблема міокардиту в останні роки набула особливої актуальності, тому пошук нових діагностичних і прогностичних маркерів несприятливого перебігу захворювання є доцільним для своєчасного призначення оптимальної медикаментозної терапії, посилення режимних заходів та адекватного моніторингу клінічного стану хворого. Мета дослідження: встановити лабораторні та інструментальні маркери порушення морфофункціонального стану серця та розробити математичну модель для раннього прогнозування довготривалої персистенції серцевої недостатності у хворих з міокардитом. Обстежили 80 хворих на гострий міокардит з тяжким перебігом та зниженою фракцією викиду лівого шлуночка (≤40 %). Оцінку лабораторно-інструментальних показників проводили в перший місяць від моменту появи симптомів, через 6 та 12 місяців спостереження. Усім пацієнтам здійснювали імунологічне дослідження, 24-годинний моніторинг ЕКГ, ехокардіографію зі спекл-трекінг та магнітно-резонансну томографію серця. Через 12 місяців спостереження оцінювали частоту серцево-судинних подій. Статистична обробка включала t-критерій Стьюдента для порівняння середніх значень, бінарну логістичну регресію, а також ROC та дискримінантний аналізи. Встановлено групу морфофункціональних інструментальних показників, визначених протягом першого місяця від початку міокардиту, котрі можуть слугувати предикторами серцево-судинних подій впродовж наступних 12 місяців: фракція викиду лівого шлуночка ≤30 %; показник поздовжньої глобальної деформації ≤7,0 %; наявність пароксизмів нестійкої шлуночкової тахікардії; наявність запальних змін у ≥6 сегментах та відстроченого

контрастування у ≥5 сегментах лівого шлуночка. Створено математичну модель, за допомогою якої впродовж першого місяця від дебюту міокардиту можна прогнозувати несприятливий перебіг захворювання з тривалою (не менше 12 місяців) персистенцією серцевої недостатності.
Ключові слова: *міокардит, діагностика, прогнозування, морфофункціональний стан серця, імунний статус, ехокардіографія, магнітно-резонансна томографія серця.*

Author's contribution

Cherniuk S. V. - conceptualization of the study, formal analysis and verification of data, writing of the original draft and editing of the article.

Marchenko K. S. - creating a database, statistical processing and formal data analysis, writing an original project.

DOI: 10.31393/morphology-journal-2024-30(1)-03 Reports of Morphology, Vol. 30, №1, Pages 25-32

ISSN 1818-1295 eISSN 2616-6194

REPORTS OF MORPHOLOGY

Official Journal of the Scientific Society of Anatomists, Histologists, Embryologists and Topographic Anatomists of Ukraine

journal homepage: https://morphology-journal.com

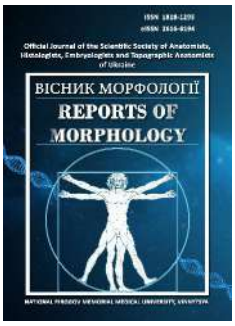

Structural changes of pancreatic components under the conditions of long-time exposure to opioid in the experiment

Popyk P. M.

Danylo Halytsky Lviv National Medical University, Lviv, Ukraine

ARTICLE INFO

Received: 23 November 2023

Accepted: 08 January 2024

UDC: 611.37.018.72:615.212.7].08

CORRESPONDING AUTHOR

e-mail: p.m.popyk@gmail.com

Popyk P. M.

CONFLICT OF INTEREST

The authors have no conflicts of interest to declare.

FUNDING

The author received no financial support for this research.

DATA SHARING

Data are available upon reasonable request to corresponding author.

Use of narcotic drugs in clinical practice for the purpose of obtaining analgesic and anti-inflammatory effects requires a comprehensive morphological study of the peculiarities of structural arrangement of organs under the conditions of exposure to opioids. The aim of our study was to establish the peculiarities of restructuring of the structural components of the pancreas under the conditions of long-time exposure to opioids in the experiment. The study included 24 adult laboratory white male rats. The test animals were divided into 2 groups, the experimental and control ones. The experimental animals were daily administered narcotic analgesic nalbuphine intramuscularly (once a day in the same interval) for four weeks, and the control animals were administered saline solution. The following research methods were used: bloodstream injection followed by translucence of sections of the pancreas and their photographing, morphometry of the vessels of the pancreatic hemomicrocirculatory bed, histological, histochemical studies and electron microscopy of the pancreas, blood biochemistry test; statistical processing of the study results using a software package. After four weeks of opioid exposure, lesion of the pancreatic parenchyma microstructure was observed, manifested by swelling and infiltration by lymphocytes and macrophages of the pancreatic connective tissue stroma, disorganization of the exo- and endocrine parts of the parenchyma, deep destructive changes in the excretory ducts, as well as in the vessels of the hemo- and lympho-microcirculatory bed of the pancreas. At the ultrastructural level, deep dystrophic changes of exo- and endocrinocytes of the pancreas were identified, in particular, loss of regular shape, karyopyknosis and karyorrhexis of the nuclei, swelling and clearing of cytoplasm, development of microcystic degeneration of cells, loosening and disorganization of the basement membrane, which can result in impairment of exocrine function of the pancreas and complication of the process of secretory granules excretion into the lumen of the intercalated ducts. A significant decrease, compared to the control group, in the diameter of arterioles, density of exchange vessels network, as well as increase in the diameter of venules, the indicator of trophic activity of the tissue, are the evidence of destructive changes in the hemomicrocirculatory bed of the pancreas under the effects of nalbuphine. Significant changes in blood biochemistry parameters (alanine aminotransferase, aspartate aminotransferase) after a four-week administration of nalbuphine are illustrative of the process of pancreatic tissue destruction. Therefore, four-week administration of opioid leads to profound changes in the micro- and ultrastructure of the pancreas, vessels of its hemomicrocirculatory bed, and blood biochemistry parameters in experimental white rats.

Keywords: *pancreas, structural changes, opioid, experiment.*

Introduction

The problem of structural changes of organs and systems under the influence of opioids is relevant and important, since the use of narcotic substances is considered in the world not only as a social problem, but also as a general medical problem [14, 26, 30]. The widespread use of narcotic agents in clinical practice with the aim of obtaining analgesic and anti-inflammatory effects requires a complex morphological study of the peculiarities

of the structural organization of organs under the conditions of exposure to opioids [5, 7, 9, 18, 22].

It is possible to predict the negative effect of drugs on the pancreas, but only a few works have been devoted to the study of the structural organization of the pancreas under conditions of harmful effects [29]. In chronic drug intoxication, along with damage to other vital organs and systems [23, 24], the pancreas, which is an important part of the digestive and endocrine systems, is also involved in the pathological process. The pancreas plays a key role in the body's metabolic processes and is particularly sensitive to exo- and endopathogenic factors [6, 25].

The development of pharmacotherapy with narcotic substances requires the development of measures to prevent and correct side effects and complications caused by them, including from the pancreas, which is sensitive to drug effects due to the peculiarities of its structure and function [10]. Morphological reconstruction of the pancreas undoubtedly plays an important role in the pathogenesis of a number of gastroenterological diseases [8, 21]. There remain a number of unsolved questions regarding the problems of structural changes of the pancreas during the use of narcotic agents, as well as the successful selection of the most effective methods of treatment of gastroenterological pathology caused by the influence of opioids. This especially concerns the macro-, micro-, and ultrastructure of the pancreas under the influence of opioids, there are no data on the qualitative and quantitative changes in the angioarchitectonics of the pancreas when using narcotic drugs.

The above-mentioned led to the conduct of a study with the *aim* of establishing the peculiarities of the restructuring of the structural components of the pancreas under the conditions of long-term exposure to opioids in the experiment.

Material and methods

The studies were performed on 24 sexually mature white male rats with an initial weight of 160-180 g, aged 3 months. Experimental animals are divided into 2 groups - experimental and control. The experimental animals were administered intramuscularly the narcotic analgesic nalbuphine daily (once a day at the same time interval) for 4 weeks, and the control animals were administered a saline solution. Nalbuphine was administered intramuscularly according to the following scheme: 1st week - 8 mg/kg, 2nd week - 15 mg/kg, 3rd week - 20 mg/kg, 4th week - 25 mg/kg. The research material is represented by preparations of the pancreas of white rats with an injected vascular bed, histological preparations and ultramicroscopic sections of the pancreas, as well as blood samples of experimental animals. All animals were kept in the conditions of the vivarium of the Danylo Halytsky Lviv National Medical University. The experiments were carried out in accordance with the provisions of the European Convention on the Protection of Vertebrate Animals Used for Experimental and Other Scientific Purposes (Strasbourg, 1986), Council of Europe Directive 86/609/EEC (1986) (protocol No. 5 of the meeting of the commission on the ethics of scientific research, experimental of developments and scientific works of Danylo Halytsky Lviv National Medical University from June 22, 2020).

The following research methods were used in the performance of the work: injection of the vascular bed of the rat pancreas with a carcass-gelatin injection mass, followed by illumination of the pancreas sections in glycerol and alcohol and their photography under the MBY-1 microscope, morphometry of the blood vessels of the hemomicrocirculatory bed of the pancreas, histological , histochemical and electron microscopic examination of the pancreas, biochemical blood examination, statistical processing of the research results.

Histological sections (5-7 μm thick) were made using a sled microtome, the sections were stained with hematoxylin and eosin. For the histochemical study of the pancreas, the PAS reaction according to McManus was used. The preparations were studied and photographed at magnifications of the microscope: x400, x1000. The "AverMedia" computer system was used to photograph micropreparations.

To carry out a morphometric analysis of the angioarchitectonics of the pancreas of a white rat, measurements were made of the diameter of arterioles, capillaries and venules, the density of the network of exchange vessels (namely, capillaries), which was determined by counting the number of vessels per unit area (the area of the field of view of the microscope was chosen as the unit of area), the indicator of trophic tissue activity, or diffusion radius (the distance between two adjacent vessels, divided in half). The preparations were studied on a MBI-1 light microscope at magnifications of the microscope: x120 (objective x8, eyepiece x15); x400 (objective x40, eyepiece x10) and x800 (objective x40, eyepiece x20).

Ultrathin sections of the pancreas were prepared on a UZHTP-3 ultramicrotome using glass knives. Ribbons of sections of silver or delicate citrine color were selected for the study. Sections were contrasted first in a 2% solution of uranyl acetate, and then in lead citrate. Studying and photographing the structures of the pancreas was carried out with the help of a UEMV-100 K microscope at an accelerating voltage of 75 kV and magnifications on the microscope screen of x4000 - x8000.

Standard laboratory methods were used to conduct a biochemical study of blood, determining: the activity of transaminases in blood serum by the Reitman-Frankel dinitrophenylhydrazine method; α-amylase - by the aminoclastic method with a stable starch substrate (Karavey's method); glucose - by the glucose oxidase method ("Filicit"-Diagnostics kit).

The statistical analysis of the research results was

carried out on a computer using the "InStat" application program package for statistical processing of data from medical, biological and epidemiological studies.

Results

After 4 weeks of administration of nalbuphine to experimental animals, the phenomenon of destructuring of the angiographic topography of the pancreas was revealed on pancreas preparations with injected vascular beds. The clear arrangement of the vessels of the hemomicrocirculatory channel is lost (Fig. 1).

In the duodenal part of the pancreas, obliteration of capillaries, hemorrhages, uneven diameter of vessels, rarefaction of the vascular network, tortuousness of preserved vessels are observed in some places (Fig. 2). The diameter of the detected capillaries is 6.002±0.020 μm (control - 6.409±0.210 μm), the density of the network of exchange vessels is 100.0±10.0 (control - 134.0±16.0), the indicator of tissue trophic activity is 34.42±0.86 μm (control - 24.21±0.64 μm).

A reliable expansion of the capillaries of the perilobular network of the biliary part of the pancreas up to 6.230± 0.392 μm (control - 4.264±0.442 μm), a decrease in the density of the network of exchange vessels - 96.00±4.00 (control - 128.0±6.0), an increase in the index of trophic activity of the tissue - 24.23±1.62 μm (control - 27.60±0.41 μm). The venular component of the hemomicrocirculatory channel of the pancreas is also expanded.

In the gastro-splenic part of the pancreas, there is expansion of venules, twisting and unevenness of the caliber of arterioles, deformation of capillaries. The diameter of capillaries is 6.232±0.112 μm (control - 6.410±0.211 μm), the density of the network of exchange vessels is 96.50±4.00 (control - 120.0±8.0), the index of trophic activity of the tissue is 23.53±0.44 μm (control - 28.10±0.82 μm).

The capillary component of the vascular glomeruli of the pancreatic islets is partially destroyed. The diameter of preserved capillaries of vascular glomeruli of pancreatic islets increases to 8.492±0.372 μm ($p<0.05$).

After 4 weeks of the experiment, destructive changes in the microstructure of the pancreas were revealed. The cells of interstitial ducts are thinned, mostly lose their shape, the basement membrane is thickened. Capsules of pancreatic islets are intermittent, loose, swollen, capillaries between insulocytes are dilated, hyperemic. The epithelium of the intralobular and interlobular ducts is thinned, protrusions of the epithelium into the lumen of the ducts are revealed, in the lumen there are single desquamated structures, stagnation of secretion, the own connective tissue plate of the ducts is thickened and swollen (Fig. 3). The shape of most of the acini has changed, their basement membrane is swollen, loose, sometimes stratified, there is an expansion of the zymogenous and a narrowing of the homogeneous zones of exocrinocytes of the pancreas (Fig. 4).

After 4 weeks of nalbuphine administration, morphological changes characteristic of micro- and

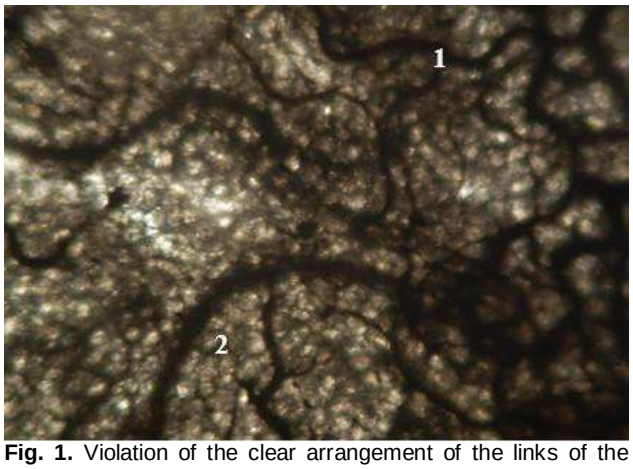

Fig. 1. Violation of the clear arrangement of the links of the hemomicrocirculatory bed of a white rat pancreas after 4 weeks of nalbuphine administration. Photomicrograph. 1 - intralobular arteriole; 2 - capillary. Injection of blood vessels with mascara-gelatin mass. x160.

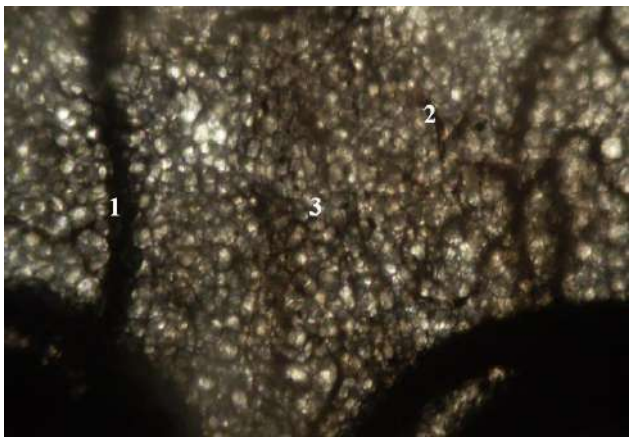

Fig. 2. Capillary obliteration, non-uniformity of vessel diameter in white rat pancreas after 4 weeks of nalbuphine administration. Photomicrograph. 1 - interlobular arteriole; 2 - intralobular arteriole; 3 - capillary. Injection of blood vessels with mascara-gelatin mass. x160.

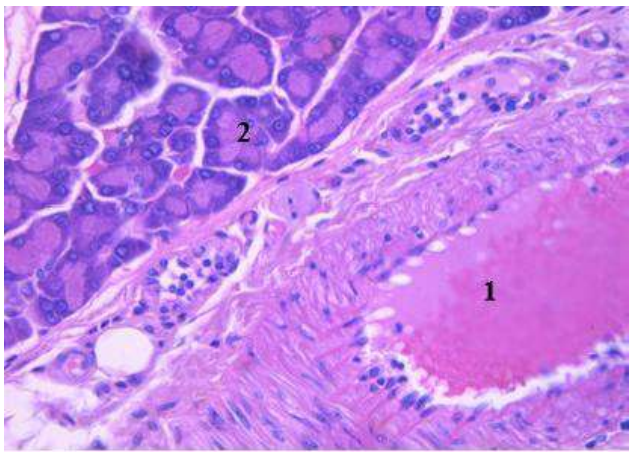

Fig. 3. Pancreas of a white rat after 4 weeks of nalbuphine administration. Photomicrograph. 1 - pancreatic acinus; 2 - stagnation of secretion in the interlobular duct. Staining with hematoxylin and eosin. x400.

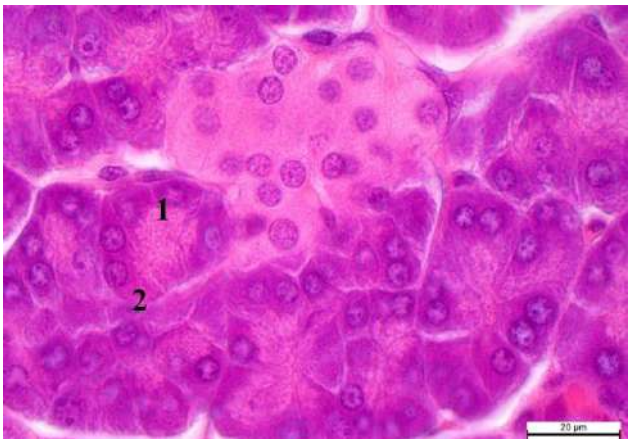

Fig. 4. Pancreas of a white rat after 4 weeks of nalbuphine administration. Photomicrograph. 1 - narrowing of the zymogenic zone of pancreatic exocrinocytes; 2 - expansion of the homogeneous zone of exocrinocytes of the pancreas. Staining with hematoxylin and eosin. x800.

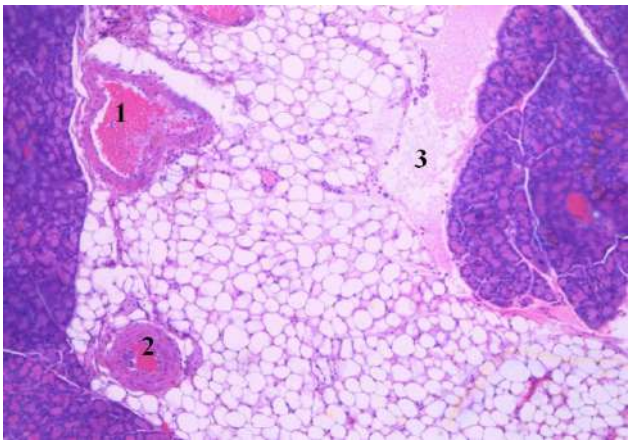

Fig. 5. Rat pancreas after 4 weeks of nalbuphine administration. Photomicrograph. 1 - full blood in a vein of medium diameter; 2 - smooth muscle hyperplasia in an organ artery; 3 - lympho- and leukostasis in the lymphatic vessel. Staining with hematoxylin and eosin. x120.

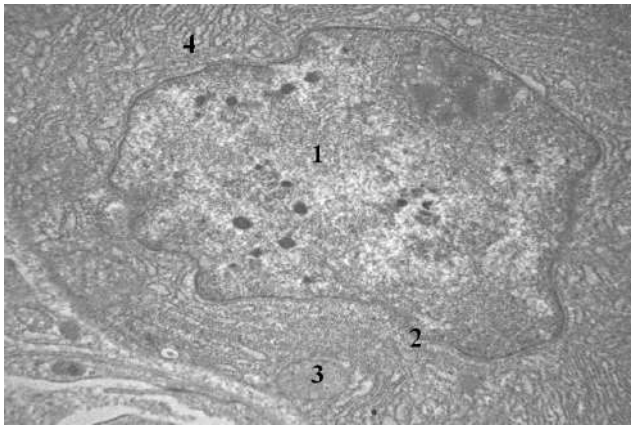

Fig. 6. Irregularly shaped nucleus, intussusception of the nuclear envelope, dilated tubules of the granular endoplasmic reticulum of a white rat exocrinocyte after 4 weeks of nalbuphine administration. Electronogram. 1 - nucleus; 2 - nuclear envelope; 3 - mitochondrion; 4 - granular endoplasmic reticulum. x8000.

macroangiopathy occur, hyalinosis of arterioles, small inflammatory infiltrates represented by macrophages and lymphocytes are revealed. The walls of the links of the hemomicrocirculatory channel of the pancreas are thickened, eosinophilic. Microaneurysms of arterioles, hyperemia of capillaries are revealed. In medium-sized veins there is full blood, in the wall of organ arteries smooth muscle hyperplasia is observed, in lymphatic vessels there is lymphostasis and leukostasis (Fig. 5). In capillaries, erythrocytes are placed in several rows, often in the form of a coin column, stick together (stasis). In addition to erythrocytes, neutrophilic granulocytes and lymphocytes are visualized in the blood vessels, and a marginal position of neutrophilic granulocytes is observed. In the lumen of the capillaries - segmented neutrophilic granulocytes. Sometimes there are isolated hemorrhages in the loose fibrous connective tissue of the interstitium or in the lumen of the excretory ducts, which are located near the hyperemic vessels.

After 4 weeks of administration of nalbuphine, the

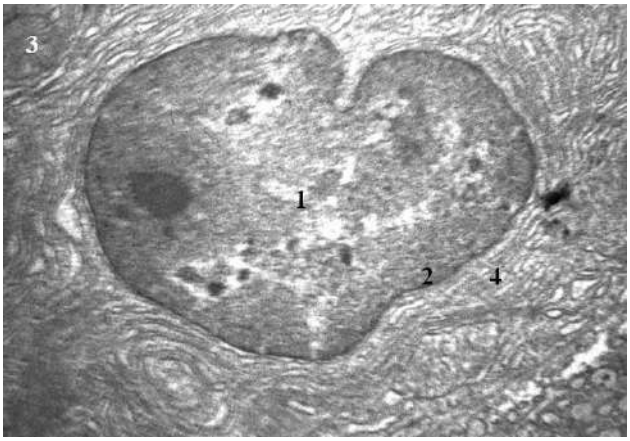

Fig. 7. Karyopyknosis in the B-endocrinocyte of the white rat pancreas after 4 weeks of nalbuphine administration. Electronogram. 1 - nucleus; 2 - nuclear envelope; 3 - mitochondria; 4 - granular endoplasmic reticulum. x8000.

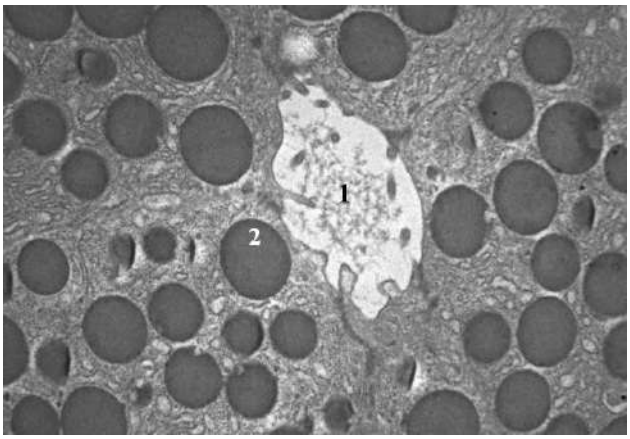

Fig. 8. Secretion-filled pancreatic duct of a white rat after 4 weeks of nalbuphine administration. Electronogram. 1 - intercalated duct; 2 - secretory granule. x4000.

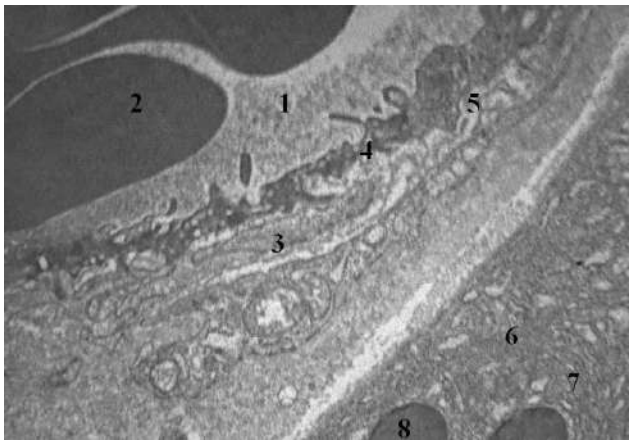

Fig. 9. Disorganized subendothelial layer of white rat pancreatic arteriole after 4 weeks of nalbuphine administration. Electronogram. 1 - lumen of an arteriole; 2 - erythrocyte; 3 - myocyte; 4 - arteriole walls; 5 - basement membrane; 6 - pancreatic exocrinocyte; 7 - granular endoplasmic reticulum; 8 - secretory granule. x4000.

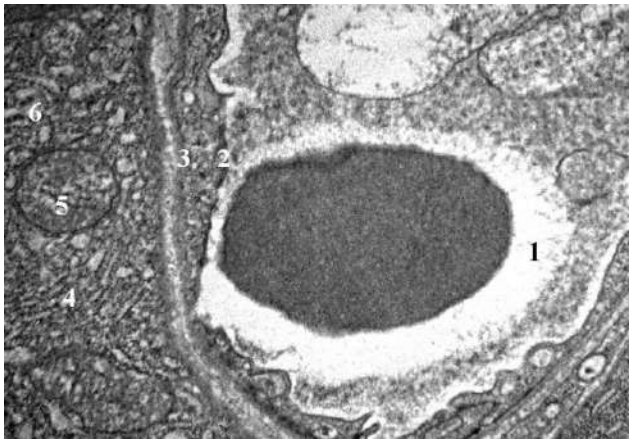

Fig. 10. Dilated fenestrae in the capillary wall of the white rat pancreas after 4 weeks of nalbuphine administration. Electronogram. 1 - capillary lumen; 2 - endotheliocyte; 3 - basement membrane; 4 - the basal part of the B-endocrinocyte of the pancreas; 5 - mitochondrion; 6 - Golgi complex. x4000.

plasmalemma of some exocrinocytes of the pancreas of experimental animals is destroyed, desquamation of the cytoplasm in the interstitium is observed, vacuoles and lipid inclusions are found in the cytoplasm of many cells, the nuclei are enlarged, irregular in shape, the nuclear envelope has uneven contours, forms numerous intussusceptions, heterochromatin is located on the periphery, many compact electron-dense small blocks of heterochromatin (Fig. 6). Mitochondria are swollen, the membranes of some mitochondria are destroyed, discontinuous, cristae are destructured, the matrix is electron transparent. Tubules of agranular and granular endoplasmic reticulum are expanded. In some acinocytes, the number of ribosomes concentrated on the membranes of the endoplasmic reticulum increases, which indicates the development of compensatory processes.

During this period of the experiment, the cytoplasm of some endocrinocytes contains small structureless areas with low electron density, the nuclei are in a state of karyopyknosis (Fig. 7).

Intercalated and intralobular ducts have an uneven lumen, filled with secretion (Fig. 8).

The lumens of arterioles are filled with irregularly shaped erythrocytes, their walls are destructured, myocytes are thinned, the basal membrane is loose, endothelial cells protrude into the vessel lumen, the subendothelial layer is disorganized (Fig. 9). Significant paravasal edema was found around the microvessels.

Capillaries are dilated, filled with deformed erythrocytes and erythrocytes in various stages of hemolysis, the fenestrae are dilated (Fig. 10). The electron density of capillary endotheliocytes is reduced, pinocytotic vesicles are found near the basal surface of the endotheliocyte cytolemma, some endotheliocytes protrude significantly, and sometimes exfoliate into the lumen of the vessel, as a result of which the basement membrane of the hemocapillary is exposed in some places. The basement membrane mostly retains its integrity, but in some places it is expanded, loosened, fibrous and thickened, its outline is unclear. In the nuclei of pericytes, chromatin is marginally located, mitochondrial cristae are expanded and fragmented.

On the basis of a biochemical study of the blood of a white rat under the conditions of long-term exposure to nalbuphine, the indicators of the activity of transaminases, α-amylase, and glucose in the blood serum were determined. The content of the above indicators in the blood of a control white rat and under the experimental influence of nalbuphine is presented in Table 1.

Discussion

Administering nalbuphine to rats for 4 weeks leads to the development of pathological changes that are characteristic of vascular sclerosis, transendothelial transport disorders, disturbances in the coagulation and fibrinolytic systems, circulatory hypoxia, the development of pericapillary edema and the growth of connective tissue in the interstitium of the pancreas, which is characteristic of pancreatic fibrosis.

Table 1. Indicators of activity of alanine aminotransferase (ALT), aspartate aminotransferase (AST), α-amylase, glucose in blood serum.

Indicator	ALT (mol/h.l)	AST (mol/h.l)	a-amylase (g/h.l)	glucose (mmol/l)
Control	0.882±0.022	1.174±0.062	20.70±0.24	6.211±0.414
After 4 weeks of nalbuphine administration	1.922±0.040*	2.120±0.044*	20.60±0.28	6.133±0.140

Notes: * - probable difference in biochemical blood parameters of control and experimental white rats ($p<0.05$).

[1]. Our results allow us to state that long-term opioid administration leads to the development of productive vasculitis with obliteration of the lumen of arterioles, blood separation, leukostasis, and leukodiapedesis in the venous component of the bloodstream, which is a sign of inflammation. The above confirms the opinion of researchers regarding the primary development of angiopathy in opioid abuse, which, in turn, causes destructive changes in organs [11, 12, 19, 27]. The pancreas is particularly sensitive to a lack of blood supply and this leads to a deep restructuring of the exo- and endocrine part of the pancreas [13, 17]. A four-week exposure to an opioid lead to the loss of the correct shape of exo- and endocrinocytes, karyopyknosis and karyorrhexis, swelling and lightening of the cytoplasm, the development of microcystic degeneration of cells, which can lead to a violation of the endo- and exocrine function of the pancreas and difficulty in the process of removing secretory granules into the lumen of the interstitial ducts. Similar changes in the structural components of the pancreas were observed by researchers in other pathological conditions of this organ [2, 3, 15, 16].

The conducted statistical analysis of the indicators of the activity of alanine aminotransferase, aspartate aminotransferase, α-amylase and glucose in the blood serum of a white rat makes it possible to make an objective comparative assessment of the main studied biochemical parameters of the blood of experimental and control groups of animals in accordance with the research objectives. Alanine aminotransferase is an endogenous enzyme from the group of transferases, a subgroup of aminotransferases, synthesized intracellularly, mainly by liver cells, but also found in pancreatic cells. The degree of increase in alanine aminotransferase activity indicates the severity of the cytolytic syndrome [28]. A significant increase in the activity of alanine aminotransferase in the blood serum of a white rat after 4 weeks of nalbuphine administration indicates the toxic effect of this drug, which apparently damages or destroys cells, including those of the pancreas. Aspartate aminotransferase is found in the tissues of the pancreas. Since a significant increase in aspartate aminotransferase was established after a 4-week administration of nalbuphine to white rats, damage to the pancreatic tissue can be assumed [4, 20].

The novelty of the research results obtained by us consists in the establishment of morphological changes in the structural components of the pancreas of laboratory white rats under conditions of four-week exposure to the opioid nalbuphine at the level of light and electron microscopy. The relationship between the depth of changes in the structural organization of the hemomicrocirculatory bed of the pancreas under the conditions of nalbuphine administration and the reorganization of exo- and endocrinocytes of the pancreas is proven by reliable changes in morphometric indicators and biochemical indicators of the blood of experimental animals.

The results of the work are of practical importance for morphologists, gastroenterologists and surgeons, as they can serve as a morphological basis for the development of new methods of diagnosis, prevention and treatment of pancreatic pathology in patients forced to use opioids for a long time, as well as in drug addicts.

Further research into the possibilities of correction of micro- and ultrastructural changes of the pancreas under the conditions of exposure to opioids is promising. The obtained results of the study of the structural features of the pancreas under the experimental influence of an opioid are fundamental data that researchers can rely on when studying the problems of experimental and clinical medicine.

Conclusions

1. A decrease, compared to the control, in the diameter of arterioles, the density of the network of exchange vessels, as well as an increase in the diameter of venules and the indicator of tissue trophic activity indicate destructive changes in the hemomicrocirculatory bed of the pancreas under the influence of nalbuphine, when the capillary component is destroyed, arterioles are sharply twisted, and their lumen is uneven, venules are expanded and deformed.

2. Violations of the microstructure of the pancreatic parenchyma and its blood stream after 4 weeks of nalbuphine administration are manifested by swelling and infiltration by lymphocytes and macrophages of the connective tissue stroma of the pancreas, disorganization of the exo- and endocrine parts of the parenchyma, deep destructive changes in the excretory ducts, as well as blood and lymph microcirculatory vessels pancreas.

3. Significant changes in biochemical blood parameters (alanine aminotransferase, aspartate aminotransferase) after 4-week administration of nalbuphine confirm the process of pancreatic tissue destruction.

4. A four-week exposure to an opioid lead to deep dystrophic changes in exocrinocytes and endocrinocytes of the pancreas, in particular, loss of the correct shape, karyopyknosis and karyorrhexis of the nuclei, swelling and lightening of the cytoplasm, the development of microcystic degeneration of cells, which can lead to a violation of the exocrine function of the pancreas and difficulty in the process of excretion of secretory granules into the lumen of interstitial ducts.

References

[1] An, J., Jiang, T., Qi, L., & Xie, K. (2023). Acinar Cells and the Development of Pancreatic Fibrosis. *Cytokine & Growth Factor Reviews,* 71-72, 40-53. doi: 10.1016/j.cytogfr.2023.05.003

[2] Arvanitakis, M., Ockenga, J., Bezmarevic, M., Gianotti, L., Krznarić, Ž., Lobo, D. N., ... & Bischoff, S. C. (2020). ESPEN guideline on clinical nutrition in acute and chronic pancreatitis. *Clinical Nutrition,* 39(3), 612-631. doi: 10.1016/j.clnu.2020.01.004

[3] Baron, T. H., DiMaio, C. J., Wang, A. Y., & Morgan, K. A. (2020). American Gastroenterological Association clinical practice update: management of pancreatic necrosis. *Gastroenterology,* 158(1), 67-75. doi: 10.1053/j.gastro.2019.07.064

[4] Biczo, G., Vegh, E. T., Shalbueva, N., Mareninova, O. A., Elperin, J., Lotshaw, E., ... & Gukovskaya, A. S. (2018). Mitochondrial dysfunction, through impaired autophagy, leads to endoplasmic reticulum stress, deregulated lipid metabolism, and pancreatitis in animal models. *Gastroenterology,* 154(3), 689-703. doi: 10.1053/j.gastro.2017.10.012

[5] Che, T., & Roth, B. L. (2023). Molecular basis of opioid receptor signaling. *Cell,* 186(24), 5203-5219. doi: 10.1016/j.cell.2023.10.029

[6] Crockett, S. D., Wani, S., Gardner, T. B., Falck-Ytter, Y., Barkun, A. N., Crockett, S., ... & Weinberg, D. (2018). American Gastroenterological Association Institute guideline on initial management of acute pancreatitis. *Gastroenterology,* 154(4), 1096-1101. doi: 10.1053/j.gastro.2018.01.032

[7] Davis, M. P., Fernandez, C., & McPherson, M. L. (2018). Does nalbuphine have a niche in managing pain? *Journal of Opioid Management,* 14(2), 143-151. doi: 10.5055/jom.2018.0441

[8] NICE guideline NG104. (2018). Pancreatitis. www.nice.org.uk/guidance/NG104/chapter/recommendations

[9] He, J., Zhang, L., Tao, T., Wen, X., Chen, D., Zheng, X., ... & Wang, H. (2023). Nalbuphine reduces the incidence of emergence agitation in children undergoing Adenotonsillectomy: A prospective, randomized, double-blind, multicenter study. *Journal of Clinical Anesthesia*, 85, 111044. doi: 10.1016/j.jclinane.2022.111044

[10] Henry, B. M., Skinningsrud, B., Saganiak, K., Pekala, P. A., Walocha, J. A., & Tomaszewski, K. A. (2019). Development of the human pancreas and its vasculature-an integrated review covering anatomical, embryological, histological, and molecular aspects. *Annals of Anatomy-Anatomischer Anzeiger,* 221, 115-124. doi: 10.1016/j.aanat.2018.09.008

[11] Hirnyak, I. I. (2018). Структурна організація жовчних проток за умов патології [Structural organization of bile ducts under pathological conditions]. *Український журнал медицини, біології та спорту - Ukrainian Journal of Medicine, Biology and Sports, 4*(326), 9-20.

[12] Ivankiv, Y. (2019). Structural organization of the links of hemomicrocircular channel of the rats uterus under the conditions of 6-week long administration of Nalbuphine. Proceeding of the Shevchenko Scientific Society. *Medical Sciences,* 55(1), 111-117. doi: 10.25040/ntsh2019.01.01

[13] Jansson, L., & Carlsson, P. O. (2011). Pancreatic blood flow with special emphasis on blood perfusion of the islets of Langerhans. *Comprehensive Physiology,* 9(2), 799-837. doi: 10.1002/cphy.c160050

[14] Jenkins, W. D., Bolinski, R., Bresett, J., Van Ham, B., Fletcher, S., Walters, S., ... & Ouellet, L. (2021). COVID-19 During the opioid epidemic-exacerbation of stigma and vulnerabilities. *The Journal of Rural Health*, 37(1), 172. doi: 10.1111/jrh.12442

[15] Leppäniemi, A., Tolonen, M., Tarasconi, A., Segovia-Lohse, H., Gamberini, E., Kirkpatrick, A. W., ... & Catena, F. (2019). 2019 WSES guidelines for the management of severe acute pancreatitis. *World Journal of Emergency Surgery,* 14(1), 1-20. doi: 10.1186/s13017-019-0247-0

[16] Liao, W. C., Tu, T. C., Lee, K. C., Tseng, J. H., Chen, M. J., Sun, C. K., ... & Lee, C. L. (2020). Taiwanese consensus recommendations for acute pancreatitis. *Journal of the Formosan Medical Association,* 119(9), 1343-1352. doi: 10.1016/j.jfma.2019.07.019

[17] Lv, Y., Wei, Q., Yuan, X., Sun, J., Zhang, J., Qi, L., ... & Li, L. (2021). Two sides of the pancreas: exocrine insufficiency is correlated with endocrine dysfunction in type 2 diabetes. *Clinica Chimica Acta,* 523, 81-86. doi: 10.1016/j.cca.2021.09.008

[18] Mykhalevych, M. M. (2019). Морфологічні зміни органів за впливу опіоїдів [Morphological changes of organs under the influence of opioids]. *Клінічна анатомія та оперативна хірургія - Clinical Anatomy and Operative Surgery*, 18(4), 133-145.

[19] Ozdemir, D., Allain, F., Kieffer, B. L., & Darcq, E. (2023). Advances in the characterization of negative affect caused by acute and protracted opioid withdrawal using animal models. *Neuropharmacology,* 109524. doi: 10.1016/j.neuropharm.2023.109524

[20] Porter, K. K., Zaheer, A., Kamel, I. R., Horowitz, J. M., Arif-Tiwari, H., Bartel, T. B., ... & Carucci, L. R. (2019). ACR Appropriateness Criteria® acute pancreatitis. *Journal of the American College of Radiology,* 16(11), S316-S330. doi: 10.1016/j.jacr.2019.05.017

[21] Quesada, R., Simón, C., Radosevic, A., Poves, I., Grande, L., & Burdio, F. (2019). Morphological changes of the pancreas after pancreaticoduodenectomy. *Scientific reports,* 9(1), 14517. doi: 10.1038/s41598-019-51173-1

[22] Stein, C. (2018). New concepts in opioid analgesia. *Expert Opinion on Investigational Drugs,* 27(10), 765-775. doi: 10.1080/13543784.2018.1516204

[23] Symivska, R. R. (2018). Макро-, мікро- та ультраструктурна організація тристулкового та двостулкового клапанів серця білого щура [Macro-, micro- and ultrastructural organization of the tricuspid and bicuspid heart valves of the white rat]. *Клінічна анатомія та оперативна хірургія - Clinical Anatomy and Operative Surgery,* 17(4), 24-29. doi: 10.24061/1727-0847.17.4.2018.4

[24] Symivska, R. R. (2019). Гістологічні зміни тристулкового клапана серця при тривалому введенні опіоїду в експерименті [Histological changes of the tricuspid heart valve during long-term opioid administration in the experiment]. *Український журнал медицини, біології та спорту - Ukrainian Journal of Medicine, Biology and Sports*, 6(22), 92-98. doi: 10.26693/jmbs04.06.092

[25] Tian, X., Pi, Y. P., Liu, X. L., Chen, H., & Chen, W. Q. (2018). Supplemented use of pre-, pro-, and synbiotics in severe acute pancreatitis: an updated systematic review and meta-analysis of 13 randomized controlled trials. *Frontiers in pharmacology*, 9, 690. doi: 10.3389/fphar.2018.00690

[26] Volkow, N. D., Jones, E. B., Einstein, E. B., & Wargo, E. M. (2019). Prevention and treatment of opioid misuse and addiction: a review. *JAMA Psychiatry,* 76(2), 208-216. doi: 10.1001/jamapsychiatry.2018.3126

[27] Wang, C., Sun, S., Jiao, J., Yu, X., & Huang, S. (2022). Effects of nalbuphine on the cardiotoxicity of ropivacaine in rats. *Fundamental & Clinical Pharmacology,* 36(5), 811-817. doi: 10.1111/fcp.12778

[28] Wild, S. L., & Tosh, D. (2021). Molecular mechanisms of transcription factor mediated cell reprogramming: Conversion of liver to pancreas. *Biochemical Society Transactions,* 49(2), 579-590. doi: 10.1042/BST20200219

[29] Wu, B. U., Butler, R. K., & Chen, W. (2019). Factors associated with opioid use in patients hospitalized for acute pancreatitis. *JAMA Network Open,* 2(4), e191827-e191827. doi: 10.1001/jamanetworkopen.2019.1827

[30] Xiao, J., Wang, W., & Dan, J. (2023). Nalbuphine Suppresses Leukemia Stem Cells and Acts Synergistically with Chemotherapy Drugs via Inhibiting Ras/Raf/Mek/Erk Pathway. *Anti-Cancer Agents in Medicinal Chemistry (Formerly Current Medicinal Chemistry-Anti-Cancer Agents),* 23(8), 922-928. doi: 10.2174/18715206236 66221213120258

СТРУКТУРНІ ЗМІНИ КОМПОНЕНТІВ ПІДШЛУНКОВОЇ ЗАЛОЗИ ЗА УМОВ ТРИВАЛОГО ВПЛИВУ ОПІОЇДУ В ЕКСПЕРИМЕНТІ

Попик П. М.

Застосування наркотичних середників у клінічній практиці з метою отримання знеболювального та протизапального ефектів вимагає комплексного морфологічного дослідження особливостей структурної організації органів за умов впливу опіоїдів. Метою нашого дослідження було встановлення особливостей перебудови структурних компонентів підшлункової залози за умов тривалого впливу опіоїду в експерименті. Дослідження виконано на 24 статевозрілих лабораторних білих щурах-самцях. Піддослідних тварин розподілили на 2 групи - експериментальну та контрольну. Експериментальним тваринам впродовж 4 тижнів щоденно (1 раз на добу в однаковий проміжок часу) вводили внутрішньом'язово наркотичний анальгетик налбуфін, а контрольним тваринам - фізіологічний розчин. Застосовані наступні методи дослідження: ін'єкція судинного русла з наступним просвітленням зрізів підшлункової залози та їх фотографуванням, морфометрія судин гемомікроциркуляторного русла підшлункової залози, гістологічне, гістохімічне та електронно-мікроскопічне дослідження підшлункової залози, біохімічне дослідження крові, статистичне опрацювання результатів дослідження за допомогою пакета прикладних комп'ютерних програм. Через 4 тижні впливу опіоїду спостерігали порушення мікроструктури паренхіми підшлункової залози, що проявлялося набряком та інфільтрацією лімфоцитами і макрофагами сполучнотканинної строми підшлункової залози, дезорганізацією екзо- та ендокринних частин паренхіми, глибокими деструктивними змінами вивідних проток, а також судин гемо- та лімфомікроциркуляторного русла підшлункової залози. На ультраструктурному рівні виявляли глибокі дистрофічні зміни екзо- та ендокриноцитів підшлункової залози, зокрема, втрату правильної форми, каріопікноз та каріорексис ядер, набряк та просвітлення цитоплазми, розвиток мікрокістозної дегенерації клітин, розпушення та дезорганізацію базальної мембрани, що може призводити до порушення екзокринної функції підшлункової залози та затруднення процесу виведення секреторних гранул у просвіт вставних проток. Достовірне зменшення, порівняно з контролем, діаметра артеріол, щільності сітки обмінних судин, а також збільшення діаметра венул й показника трофічної активності тканини свідчать про деструктивні зміни гемомікроциркуляторного русла підшлункової залози під впливом налбуфіну. Достовірні зміни біохімічних показників крові (аланінамінотрансферази, аспартатамінотрансферази) після 4-тижневого введення налбуфіну підтверджують процес руйнування тканини підшлункової залози. Таким чином, 4-тижневе введення опіоїду призводить до глибоких змін мікро- та ультраструктури підшлункової залози, судин її гемомікроциркуляторного русла, біохімічних показників крові експериментальних білих щурів.

Ключові слова: *підшлункова залоза, структурні зміни, опіоїд, експеримент.*

DOI: 10.31393/morphology-journal-2024-30(1)-04 Reports of Morphology, Vol. 30, №1, Pages 33-39

ISSN 1818-1295 eISSN 2616-6194

REPORTS OF MORPHOLOGY

Official Journal of the Scientific Society of Anatomists, Histologists, Embryologists and Topographic Anatomists of Ukraine

journal homepage: https://morphology-journal.com

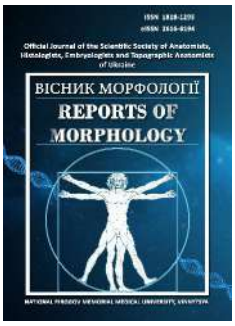

The influence of chronic hyperhomocysteinemia on the structure and immune processes of the spleen in young rats

Dzevulska I. V.[1], Gritsenko A. S.[2], Tymoshenko I. O.[1], Zakalata T. R.[2], Lavrinenko V. Y.[3], Smolko D. G.[2], Gunas I. V.[2]

[1]Bogomolets National Medical University, Kyiv, Ukraine
[2]National Pirogov Memorial Medical University, Vinnytsya, Ukraine
[3]Educational and Scientific Center "Institute of Biology and Medicine", Taras Shevchenko National University of Kyiv, Kyiv, Ukraine

ARTICLE INFO
Received: 07 December 2023
Accepted: 12 January 2024

UDC: 61:615.9/616:616-005/616.4

CORRESPONDING AUTHOR
e-mail: grytsenko.antonina@gmail.com
Gritsenko A. S.

CONFLICT OF INTEREST
The authors have no conflicts of interest to declare.

FUNDING
Not applicable.

DATA SHARING
Data are available upon reasonable request to corresponding author.

Homocysteine is a sulfur-containing amino acid that is an intermediate product of methionine metabolism. Entering the body with products of animal origin, methionine undergoes a number of biochemical transformations. Hyperhomocysteinemia has a negative effect on the body, causing damage to all organs and systems and leading to disruption of homeostasis. The study aims to study the characteristics of changes in the structure and immune processes of the spleen of young rats with chronic hyperhomocysteinemia. Experiments were performed on 22 white male rats. The animals were divided into control and experimental groups (11 individuals in each group) during the experiment. Chronic hyperhomocysteinemia was achieved by administering D, L-thiolactone homocysteine hydrochloride to experimental group animals at a dose of 200 mg/kg of body weight intragastrically in a 1 % starch gel solution once a day for eight weeks. After the end of the experimental simulation of chronic hyperhomocysteinemia, the animals were removed from the experiment by anaesthetising by decapitation and using thiopental anaesthesia. Histological preparations were studied using an SEO SCAN light microscope. Experimental modelling of chronic hyperhomocysteinemia in young rats was not accompanied by significant morphological changes in the stroma and red pulp of the spleen. T-cell periarterial sheaths and B-cell nodules in animals from the experimental group underwent changes. B-cell proliferation leads to growth within the white pulp, expansion of the marginal zones, which become more blurred and infiltration of these cells into the red pulp. Evaluation of the red pulp in the spleen of young rats from the experimental group showed a particular expansion in the venous sinuses, which may be a sign of reaction to the influence of homocysteine and slight swelling of these vessels. The number of T-cells in young animals in the periarterial cuffs is slightly reduced, which can be explained by the increasing activity of macrophages. However, T-cells also infiltrated the red pulp. Such penetration of white blood cells into the red pulp is accompanied by the expansion and "washing out" of the marginal zones of lymph nodes. Thus, the increased homocysteine level significantly potentiated proliferation and partially inhibited apoptosis in T-lymphocytes but did not directly affect dormant T-cells.

Keywords: *homocysteine, spleen, lymphocytes, macrophages, rats.*

Introduction

Homocysteine is a sulfur-containing amino acid that is an intermediate product of methionine metabolism. Entering the body with products of animal origin, methionine undergoes some biochemical transformations. Normally, homocysteine is utilised in the body in remethylation, transsulfation, and desulfation reactions [25]. The transsulfonation pathway begins by condensing two molecules of homocysteine and serine, forming cystathionine. This reaction is catalysed by the pyridoxal phosphate-dependent enzyme cystathionine-β-synthase [29]. Subsequently, cysteine, ammonia and α-ketobutyrate are formed from cystathionine under the influence of cystathionine-γ-lyase. During remethylation processes, methionine is resynthesised from homocysteine with the

help of cobalamin-dependent methionine synthase. There is also another path of remethylation involving the enzyme betaine-homocysteine-S-methyltransferase. Both enzymes are cytosolic and characterised as zinc-dependent methyltransferases. Methionine synthase is present in all body tissues and uses N-5-methyltetrahydrofolate as a metal group. Betaine-homocysteine-S-methyltransferase uses an endogenous derivative of choline-betaine and is present to a greater extent in the liver, adrenal cortex, brain tissue, skeletal muscles, and placenta. When utilising homocysteine by desulfation, it turns into hydrogen sulfide [18].

In blood plasma, homocysteine is present in four forms: homocysteine bound to proteins, the disulfide form of homocysteine, free homocysteine, and the thiol form of homocysteine [31]. According to most authors, its normal level in the body is within 5-15 μmol/l. It has been established that homocysteine concentration varies with age and gender [16, 17]. Compared to children, its content is 2 times higher in adults. During life, the level of homocysteine in the blood increases, correlating with the concentration of vitamin B12 and folate. Normally, it is important for the body, as it maintains the essential amino acid methionine content constantly [26, 27]. However, a significant increase in its concentration has some negative effects [12, 19]. Hyperhomocysteinemia is diagnosed when the homocysteine content is above 15 μmol/l. Scientists distinguish its following degrees: mild, in which homocysteine ranges between 15-30 μmol/l, moderate - 30-100 μmol/l, severe - 100 μmol/l and more [33].

Genetic causes of hyperhomocysteinemia are relatively rare but cause the development of severe pathologies and even death in childhood. Congenital defects of the methylenetetrahydrofolate reductase, cystathionine-β-synthase and methionine synthase genes are studied. Mutations of methylenetetrahydrofolate reductase are the most studied. Those associated with replacing one nucleotide in the gene encoding this enzyme (C677T and A1298 C) are more common. In the first case, valine is replaced by alanine, which leads to the synthesis of a thermolabile enzyme characterised by a decrease in its activity in heterozygotes and homozygotes by 35-50 % and 70 %, respectively. Another defect causes glutamate substitution for alanine in the C-terminal regulatory domain of methylenetetrahydrofolate reductase and is accompanied by moderate hyperhomocysteinemia. Mutations of cystathionine-β-synthase are characterised by a significant increase in the concentration of homocysteine in the blood plasma, in some cases by 80%, and the appearance of homocysteineuria, which is a missense mutation and deletion of alleles. A mutation of the A2756G gene encoding methionine synthase is also known, accompanied by decreased enzyme activity and moderate hyperhomocysteinemia [2].

Experimental studies on animals made it possible to establish the main causes of homocysteine toxicity in the body [22, 28]. To date, scientists have singled out the main ones, namely: homocysteine activation of oxidative stress and endoplasmic reticulum stress, disruption of gene expression, protein homocysteine, stimulation of the production of inflammatory mediators and fibrosis [4, 11, 30].

Hyperhomocysteinemia has a negative effect on the body, causing damage to all organs and systems and leading to a violation of homeostasis due to the impossibility of maintaining their functions at the proper level [21]. The scientific community is actively studying the role of homocysteine in the pathogenesis of numerous diseases [14, 23, 24]. However, in the domestic literature, there is only insignificant data on its influence on the structure and functions of immune defence organs.

The study aims to study the characteristics of changes in the structure and immune processes of the spleen of young rats with chronic hyperhomocysteinemia.

Materials and methods

Modelling of chronic hyperhomocysteinemia was carried out through experimental studies on laboratory rats in compliance with international recommendations on the performance of medical and biological research using animals by the "General Principles of Work on Animals" approved by the 1st National Congress on Bioethics (Kyiv, Ukraine, 2001) and agreed with the provisions "European Convention for the Protection of Vertebrate Animals Used for Experimental and Other Scientific Purposes" (Strasbourg, France, 1986) [7]. Bioethics Committee of National Pirogov Memorial Medical University confirmed that the work complied with ethical principles (protocol No. 3 from 17.10.2019).

Experiments were performed on 22 white male rats obtained from the vivarium of the National Pirogov Memorial Medical University, Vinnytsya. Rats were kept under normal laboratory conditions with a 12-hour day/night regime; water and balanced pelleted feed were received ad libitum by established norms.

The animals were divided into control and experimental groups (11 individuals in each group) during the experiment. Chronic hyperhomocysteinemia was achieved by administering D, L-thiolactone homocysteine hydrochloride (Acros Organics, Italy) to animals of the experimental group at a dose of 200 mg/kg of body weight intragastrically in a 1 % solution of starch gel (1 ml/100 g of rat weight) once a day for 8 weeks. After the end of the experimental simulation of chronic hyperhomocysteinemia, the animals were removed from the experiment by decapitation and using thiopental anaesthesia (thiopental sodium 100 mg/kg).

For microscopic examination, pieces of spleen were taken from prematurely weighed animals of all groups. The selected samples were fixed in a 10 % formalin solution. The next stage was the dehydration of samples in alcohols of increasing concentration and pouring them into paraffin blocks. Sections with a thickness of 3 μm were

made from paraffin blocks and stained with hematoxylin and eosin [10]. Histological preparations were studied using an SEO SCAN light microscope and photo-documented by a Vision CCD Camera with a system of image output from histological preparations.

Results

When assessing the state of the spleen of rats subjected to the simulation of chronic persistent hyperhomocysteinemia, we focused our attention primarily on the elements of the white pulp of this hematopoietic organ because exactly lymphocytes are most sensitive to high levels of homocysteine. In turn, substances that fight free radicals reduce the proliferation of lymphocytes caused by hyperhomocysteinemia.

The stroma of the spleen of young animals from the experimental group did not undergo significant changes - the dense connective tissue of the capsule and trabeculae does not show signs of stratification or morphological changes in cells, the nuclei of single fibroblasts are spread between wavy eosinophilic collagen fibres (Fig. 1 A). This group's spleen's blood vessels also show no signs of pathological changes. We can observe the nuclei of smooth myocytes and endothelial cells without pathology (Fig. 1 B).

In the experimental groups, changes are most likely localised within the white pulp. T-lymphocytes, located in the sheath around the central arteries, practically do not show changes in morphology. However, the cells do not form such dense dark clusters, which is probably explained by the presence of a greater number of macrophages, which, on the one hand, destroy damaged and defective cells, reducing the number of their populations, on the other hand, have a lower nuclear-cytoplasmic ratio and therefore form a lighter overall background of the periarterial sheath (see Fig. 1 B, Fig. 1 C, D).

Elevated levels of homocysteine and related compounds

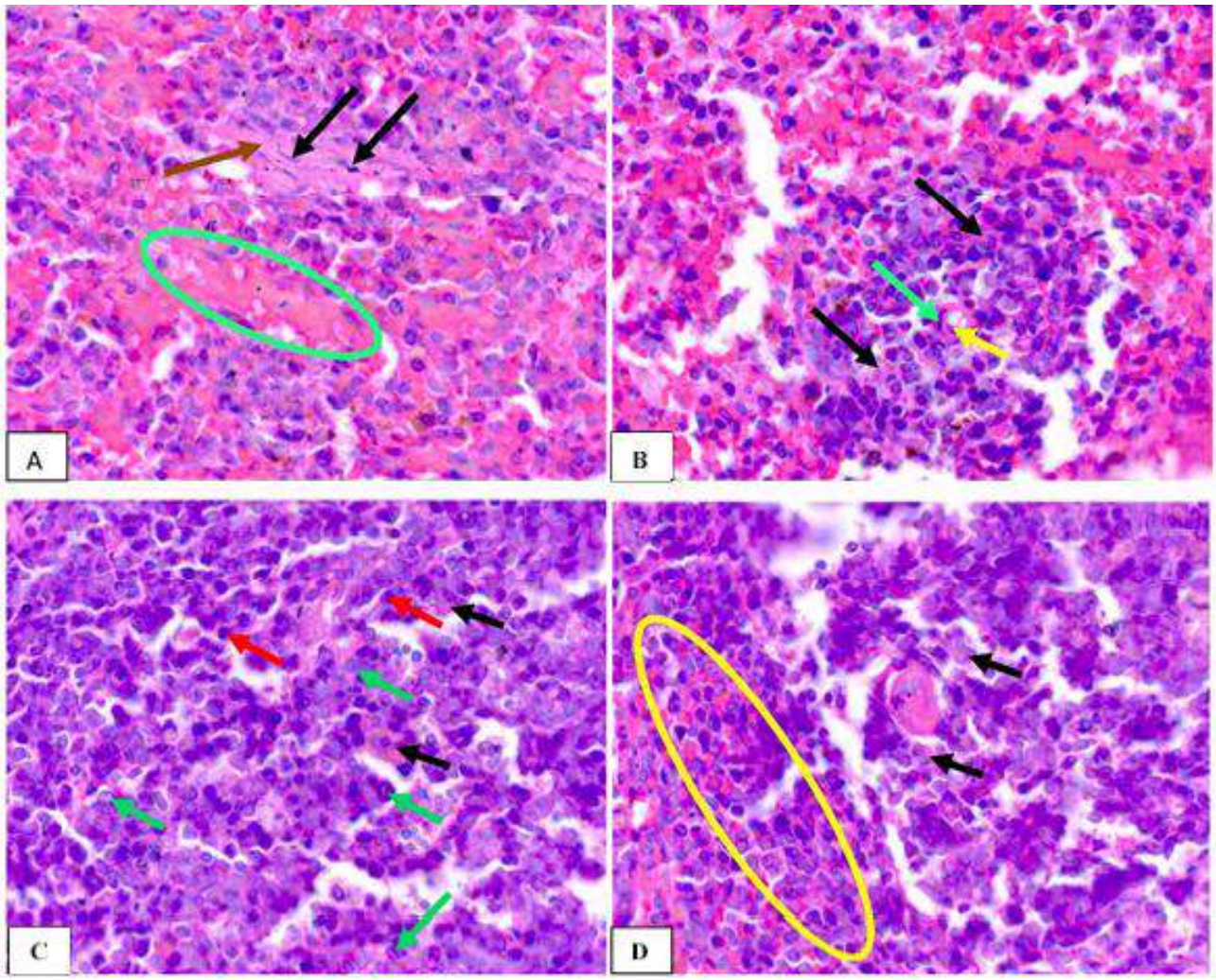

Fig. 1. Stroma and parenchyma of the spleen of young rats of the experimental group. **A**: nuclei of fibroblasts (black arrows), collagen fibres of the capsule (brown arrow), venous sinus (green oval); **B**: nucleus of a smooth myocyte (green arrow), endotheliocyte nucleus (yellow arrow); **C**: B-lymphocytes (red arrows), plasma cells (green arrows); **D**: marginal zone (yellow oval); B, C, D: macrophages (black arrows). Staining with hematoxylin and eosin. x1000.

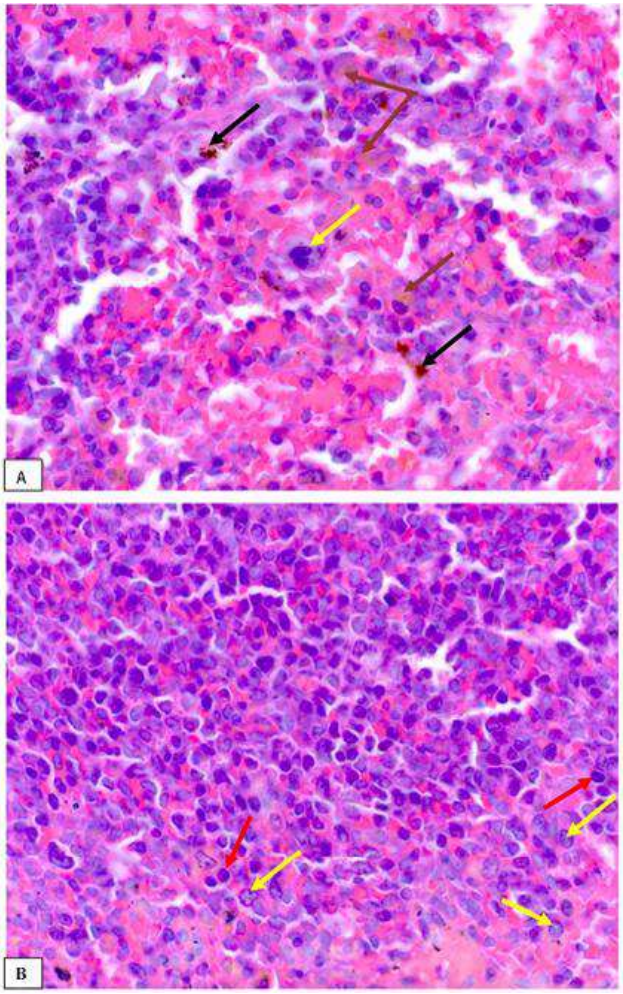

Fig. 2. Red and white pulp of young rats with chronic hyperhomocysteinemia. **A**: megakaryocyte (yellow arrow), macrophages with hemosiderin (black arrows), macrophages with lipofuscin (brown arrows); **B**: infiltration of plasma cells into the red pulp (yellow arrows), lymphocytes (red arrows). Staining with hematoxylin and eosin. x1000.

such as cysteine and glutathione significantly potentiated proliferation and partially inhibited apoptosis in T-lymphocytes but didn't directly affect latent T-cells.

B-lymphocytes and their derivatives (plasma cells), in turn, increase in number, which can be judged by the density of the location of these cells in the lymphoid nodes of the spleen of experimental animals (see Fig. 1 C). Numerous proliferating B-lymphoblasts are accompanied by macrophages, which carry out antigen-dependent B-cell differentiation before transforming into plasma cells. Plasma cells are fairly easily differentiated by their rounded or oval shape and a large amount of dark blue cytoplasm with a pale perinuclear region corresponding to the Golgi apparatus. These cells have a round, eccentrically located nucleus with heterochromatin arranged in a dial (wheel spokes).

The assessment of the state of red pulp in the spleen of young experimental rats showed a certain expansion in the venous sinuses, which may be a sign of reaction to external influences in the slight swelling of these vessels (see Fig. 1 A). In the red pulp of young animals, the hematopoietic processes continue, so detecting megakaryocytes among erythrocytes is not a deviation from the norm (Fig. 2 A). These cells, as known, are the precursors of platelets and, reaching large sizes, later disintegrate into single blood platelets.

Also very interesting is the presence in both white and red pulp macrophages of not only dark brown inclusions of hemosiderin, which is a physiological consequence of the breakdown of erythrocytes phagocytosed by them, but also lipofuscin (see Fig. 2 A). It is known that lipofuscin is the pigment inclusion which characterises the intensity of lipid oxidation processes in the spleen, which most likely leads to an increase in the concentration of free oxygen radicals in this organ and is typical for chronic hyperhomocysteinemia.

As already mentioned, when assessing the condition of the spleen under the influence of chronic hyperhomocysteinemia, it is necessary to pay attention to the lymphocytic component, not only of the white but also of the red pulp. It is interesting to note the infiltration of these cells into the red pulp, which is a characteristic sign of their proliferation in response to oxidative stress (Fig. 2 B). The number of small cells with dark nuclei (T-lymphocytes) and plasma cells, which can be recognised by the characteristic pattern of heterochromatin in the nucleus, indicates an increase in the percentage of lymphocytes in the red pulp in response to stimulation of chronic hyperhomocysteinemia in animals. Such penetration of white blood cells into the red pulp is accompanied by expansion and "blurring" of the marginal zones of lymph nodes, which are not as clearly defined as in the control group (see Fig. 1 D).

Discussion

Thus, homocysteine can disrupt the functioning of individual parts of the immune system through the death of cells or their excessive hyperstimulation, which in turn leads to exhaustion of the system as a whole. However, to this day, there is no data on changes in the structure of hematopoietic organs and immune protection, mainly the spleen, under conditions of hyperhomocysteinemia.

Experiments on rats proved that lymphocytes express NMDA receptors on their surface, capable of interacting with homocysteine. Under its influence, the amount of ROS and the content of Ca2+ and ATP in cells increases. In addition, hyperhomocysteinemia stimulates the production of IFN-γ and TNF-α by lymphocytes, involving protein kinase, NADPH-oxidase and NO-synthase. The consequence of such exposure is the death of lymphocytes by apoptosis. Constant stimulation of immune system cells under these conditions leads to its exhaustion [5, 20].

According to the literature, homocysteine interacts with inotropic glutamate receptors activated by NMDA. Activation of these receptors leads to an increase in the entry of Ca2+ ions into the cell and an increase in the level of reactive

oxygen species, activation of the lipid peroxidation processes and apoptosis of lymphocytes. It should be noted that the blockade of NMDA receptors of T cells with homocysteine inhibits mRNA synthesis and increases the secretion of INF-γ, TNF-α, and IL-10. Its single administration is accompanied by a pronounced decrease in T-lymphocytes and their subpopulations [15]. According to the authors, this is due to an increase in the expression of adhesion molecules to both endotheliocytes and lymphocytes, which ensures the adhesion of lymphocytes to the vascular wall and, thereby, a reduction in the pool of circulating lymphocytes. Some may be eliminated due to the activation of NMDA receptors with the subsequent development of apoptosis. However, under conditions of chronic hyperhomocysteinemia in animals, on the contrary, an increase in the number of T-lymphocytes at the expense of T-cytotoxic ones was registered. When homocysteine is administered 1 time per day for a week in animals, apparently, adaptation mechanisms are activated, which allows the inactivation of aminothiol as a xenobiotic. High doses of homocysteine damage the tissue structures of the spleen, which is accompanied by the development of autoimmune reactions, evidenced by a sharp increase in the concentration of all cytokines and especially IL-17A [1, 9].

Reviews of the literature show that, in many cases, pathologies associated with the accumulation of homocysteine are accompanied by a malfunction of the immune system. On the other hand, intensive immunocompetent cell proliferation can lead to homocysteine accumulation. For example, sources report that a Th1-type immune response promotes the development of B cells and may be a major determinant of the progression of disorders associated with hyperhomocysteinemia. Other studies also demonstrate that reactive oxygen species formed due to autooxidation of homocysteine participate in the induction of B-lymphocyte proliferation [6].

The study of the effect of homocysteine on lymphocytes in patients with coronary heart disease showed that Fas-receptors of T-helpers and their ligand CD178 were activated in the culture of peripheral blood cells during its growth. An early marker of apoptosis was the expression of APO 2.7. Subsequently, negatively charged phospholipids, mainly phosphatidylserine, appeared on the cell membrane. At the same time, the concentration of Bcl-2, which normally protects cells from apoptosis, decreased, leading to their death [13, 32].

In the model of folate-induced hyperhomocysteinemia, the instability of the genomic DNA of the rat spleen was revealed, which is expressed by a decrease in elastic viscosity and molecular weight, as well as an increase in its availability for hydrolysis by DNAse I and EcoRI restriction enzyme [19].

It is known that homocysteine can be involved in the metabolic processes of cell mitochondria, increasing the production of reactive oxygen species and the level of Ca2+ ions, which leads to disorders of tissue respiration and an increase in the membrane potential of organelles. Being involved in the mitochondrial metabolism of T-lymphocytes causes their reprogramming. The specified changes in T-cells trigger the mechanisms of endoplasmic reticulum stress development, which in the spleen is manifested by an increase in their markers - p-eIF2α, p-PERK, IRE-1α, XBP-1 [8].

D. Zhang and others. [33] proved that severe hyperhomocysteinemia causes inflammatory differentiation of monocytes in the red bone marrow and increases blood plasma levels of TNF-α, IL-6, and production of superoxide anion, IFN-γ. The author notes that similar processes under these conditions are also observed in primary splenocytes of rats, and the cause is the activation of oxidative stress by homocysteine.

B. Cai and others. [3] demonstrated in their experimental studies that elevated levels of homocysteine cause apoptosis of red bone marrow stem cells by activating JNK1 (N-terminal kinase of the myogen-activated protein kinase family).

In the literature, there are also references to the fact that homocysteine significantly increases B-lymphocyte proliferation in the spleen. Researchers associate the cause of this phenomenon with the activation of protein kinase C and nuclear factor kappa B (NF-KB) [34, 35].

Conclusions

1. Experimental modelling of chronic hyperhomocysteinemia in young rats was not accompanied by significant morphological changes in the stroma and red pulp of the spleen.

2. T-cell periarterial sheaths and B-cell nodules in animals from the experimental group underwent changes. B-cell proliferation leads to growth within the white pulp, expansion of the marginal zones, which become more blurred and infiltration of these cells into the red pulp.

3. The number of T-cells in young animals in the periarterial sheaths is slightly reduced, which can be explained by the increasing activity of macrophages. However, T-cells also infiltrated into the red pulp.

References

[1] Abe, I., Shirato, K., Hashizume, Y., Mitsuhashi, R., Kobayashi, F., Shiono, C., … & Imaizumi, R. (2013). Folate-deficiency induced cell-specific changes in the distribution of lymphocytes and granulocytes in rats. *Environ. Health Prev. Med.,* 18(1), 78-84. doi: 10.1007/s12199-012-0286-6

[2] An, H., Fan, C. Q., Duan, J. G., Ren, Y., Dong, K., Zhang, Q., … & Huang, X. Q. (2018). Severe Hyperhomocysteinemia with Two Novel Mutations of c.154T > C and c.4576G > A in Cystathionine Beta-Synthase Gene. *Chin. Med. J. (*Engl), 131(19), 2368-2370. doi: 10.4103/0366-6999.241801

[3] Cai, B., Li, X., Wang, Y., Liu, Y., Yang, F., Chen, H., … & Lu, Y. (2013). Apoptosis of bone marrow mesenchymal stem cells caused by homocysteine via activating JNK signal. *PLoS ONE,* 8(5), e63561. doi: 10.1371/journal.pone.0063561

[4] Cheng, Z., Jiang, X., Fang, P., Kishore, R., & Kevil, C. (2015). Hyperhomocysteinemia Potentiated the Impairment of Hydrogen Sulfide-Induced Endothelium-Derived Hyperpolarization-Mediated Vascular Relaxation in Diabetic Db/db Mice. *Circ. Res.,* 117(1), 272-276. doi: 10.1161/res.117.suppl_1.272

[5] Deep, S. N., Mitra, S., Rajagopal, S., Paul, S., & Poddar, R. (2019). GluN2A-NMDA receptor-mediated sustained Ca2+ influx leads to homocysteine-induced neuronal cell death. *J. Biol. Chem.,* 294(29), 11154-11165. doi: 10.1074/jbc.RA119.008820

[6] Deng, J., L, S., Liu, H., Liu, B., Jiang, C., Xu, Q., … & Wang, X. (2017). Homocysteine Activates B Cells via Regulating PKM2-Dependent Metabolic Reprogramming. *J. Immunol.,* 198(1), 170-183. doi: 10.4049/jimmunol.1600613

[7] Dobrelia, N. V., Boitsova, L. V. & Danova, I. V. (2015). Правова база для проведення етичної експертизи доклінічних досліджень лікарських засобів з використанням лабораторних тварин [Legal basis for ethical examination of preclinical studies of drugs using laboratory animals]. *Фармакологія та лікарська токсикологія - Pharmacology and drug toxicology,* (2), 95-100.

[8] Feng, J., Lu, S., Ding, Y., Zheng, M., & Wang, X. (2016). Homocysteine activates T cells by enhancing endoplasmic reticulum-mitochondria coupling and increasing mitochondria respiration. *Protein Cell,* 7(6), 391-402. doi: 10.1007/s13238-016-0245-x

[9] Gao, X., Li, J., & Chen, M. (2018). Effect of Homocysteine on the Differentiation of CD4+ T Cells into Th17 Cells. *Dig. Dis. Sci.,* 63(12), 3339-3347. doi: 10.1007/s10620-018-5177-2

[10] Horalskyi, L. P., Khomych, V. T., & Kononskyi, O. I. (2011). *Основи гістологічної техніки і морфофункціональні методи досліджень у нормі та при патології [Fundamentals of histological technique and morphofunctional research methods in normal and pathology].* Житомир, Полісся - Zhytomyr: Polissya.

[11] Jakubowski, H. (2019). Homocysteine Modification in Protein Structure / Function and Human Disease. *Physiol. Rev.,* 99(1), 555-604. doi: 10.1152/physrev.00003.2018

[12] Kim, J., Kim, H., Roh, H., & Kwon, Y. (2018). Causes of hyperhomocysteinemia and its pathological significance. *Arch. Pharm. Res.,* 41(4), 372-383. doi: 10.1007/s12272-018-1016-4

[13] Li, T., Chen, Y., Li, J., Yang, X., Zhang, H., Qin, X., … & Mo, Z. (2015). Serum Homocysteine Concentration Is Significantly Associated with Inflammatory/Immune Factors. *PLoS One,* 10(9): e0138099. doi: 10.1371/journal.pone.0138099

[14] Lu, S., Deng, J., Liu, H., Liu, B., Yang, J., Miao, Y., … & Feng, J. (2018). PKM2-dependent metabolic reprogramming in CD4+ T cells is crucial for hyperhomocysteinemia-accelerated atherosclerosis. *J. Mol. Med.* (Berl)., 96(6), 585-600. doi: 10.1007/s00109-018-1645-6

[15] McCully, K. S. (2019). Chemical Pathology of Homocysteine VII. Cholesterol, Thioretinaco Ozonide, Mitochondrial Dysfunction, and Prevention of Mortality. *Ann. Clin. Lab. Sci.,* 49(4), 425-438. PMID: 31471331

[16] Pentyuk, O. O., Lutsyuk, M. B., Andrushko, I. I., & Postovitenko, K. P. (2003). Метаболізм гомоцистеїну та його роль у патології [Homocysteine metabolism and its role in pathology]. *Український біохімічний журнал - The Ukrainian Biochemical Journal,* 1, 5-17.

[17] Pentyuk, O. O., Lutsyuk, M. B., Postovitenko, K. P., Artemchuk, M. A., Asachova, O. S., & Pryzymirska, T. V. (2004). Гіпергомоцистеїнемія: моделювання та вплив на стан судинної системи в експерименті [Hyperhomocysteinemia: experimental modeling and influence on vascular system state]. *Досягнення біології та медицини - Achievments of Biology and Medicine*, 1(3), 35-38.

[18] Perez-Miguelsauz, J., Vallecillo, N., Carrido, F., Reytor, E., Perez-Sala, D., & Pajares, M. A. (2017). Betaine homocesteine S-methyltransferase emerges as a new player of the nuclear methionine cycle. *Biochim. Biophys. Acta Mol. Cell Res.,* 1864(7), 1165-1182. doi: 10.1016/j.bbamcr.2017.03.004

[19] Pizzolo, F., Blom, H. J., Choi, S. W., Girelli, D., Guarini, P., Martinelli, N., … & Friso, S. (2011). Folic acid effects on s-adenosylmethionine, s-adenosylhomocysteine, and DNA methylation in patients with intermediate hyperhomocysteinemia. *J. Am. Coll. Nutr.,* 30(1), 11-18. doi: 10.1080/07315724.2011.10719939

[20] Poddar, R., Chen, A., Winter, L., Rajagopal, S., & Paul, S. (2017). Role of AMPA receptors in homocysteine-NMDA receptor-induced crosstalk between ERK and p38 MAPK. *J. Neurochem,* 142(4), 560-573. doi: 10.1111/jnc.14078

[21] Raksha, N., Halenova, T., Vovk, T., Kharchenko, O., Savchuk, O., Samborska, I., … & Maievskyi, O. (2021). Protein-peptide composition in the lungs of rats with hyperhomocysteinemia. *J. of Biological Research,* 94(2), 9858. doi: 10.4081/jbr.2021.9858

[22] Sakowicz-Burkiewicz, M., & Pawelczyk, T. (2014). Recent advances in understanding the relationship between adenosine metabolism and the function of T and B lymphocytes in diabetes. *J. Physiol. Pharmacol.*, 62(5), 505-512. PMID: 22204797

[23] Samborska, I. A. (2020). Changes in the histostructure of the lungs of old rats under conditions of persistent hyperhomocysteinemia. *Biomedical and Biosocial Anthropology*, 41, 41-45. doi: 10.31393/bba41-2020-07

[24] Samborska, I., Kovalchuk, O., Fagoonee, S., Falalyeyeva, T., & Maievskyi, O. (2020). The Role of Hyperhomocysteinemia in the Development of Changes in the Lungs. *Reviews on Recent Clinical Trials,* 15(1), 48-59. doi: 10.2174/1574887114666191114152235

[25] Silla, Y., Varshney, S., Ray, A., Basak, T., Zinelly, A., Sabaresh, V., … & Sengupta, S. (2019). Hydrolysis of homocysteine thiolactone results in the formation of protein-cys-S-S-homocysteinylation. *Proteins*, 87(8), 625-634. doi: 10.1002/prot.25681

[26] Skovierova, H., Vidomanova, E., Mahmood, S., Sopkova, J., Drgova, A., Cervenova, T., … & Lehotsky, J. (2016). The molecular and cellular effect of homocysteine metabolism imbalance on human health. *Int. J. Mol. Sci.,* 17(10), 1733. doi: 10.3390/ijms17101733

[27] Sorensen, J. T., Gaustadnes, M., Stabler, S. P., Allen, R. H., Mudd, S. H., & Hvas, A. M. (2016). Molecular and biochemical investigations of patients with intermediate or severe hyperhomocysteinemia. *Mol. Genet. Metab.,* 117(3), 344-350. doi: 10.1016/j.ymgme.2015.12.010

[28] Tripathi, M., Zhang, C. W., Singh, B. K., Sinha, R. A., Moe, K. T., DeSilva, D. F., … & Yen, P. M. (2016). Hyperhomocysteinemia causes ER stress and impaired autophagy that is reversed by vitamin B supplementation. *Cell Death and Disease,* 7(12), 1-14. doi: 10.1038/cddis.2016.374

[29] Wang, H., Sun, Q., Zhou, Y., Zhang, H., Luo, C., Xu, J., … & Wang, W. (2017). Nitration-mediated deficiency of cystathione β-synthase activity accelerates the progression of hyperhomocysteinemia. *Free Radical Biology and Medicine,* 113, 519-529. doi: 10.1016/j.freeradbiomed.2017.10.389

[30] Wang, N., Tang, H., Wang, X., Wang, W., & Feng, J. (2017). Homocysteine upregulates interleukin-17A expression via NSun2-mediated RNA methylation in T lymphocytes. Biochem. Biophys. *Res. Commun.*, 493(1), 94-99. doi: 10.1016/j.bbrc.2017.09.069

[31] Yang, A., Jiao, Y., Yang, S., Deng, M., Yang, X., Mao, C., ... & Jiang, Y. (2018). Homocysyeine activates autophagy by inhibition of CFTR expression via interaction between DNA methylation and H3K27me3 in mouse liver. *Cell Death and Disease,* 9(2), 169. doi: 10.1038/s41419-017-0216-z

[32] Zaric, B. L., Obradovic, M., Bajic, V., Haidara, M. A., Jovanovic, M., & Isenovic, E. R. (2019). Homocysteine and Hyperhomocysteinemia. *Curr. Med. Chem.,* 29(16), 2948-2961. doi: 10.2174/0929867325666180313105949

[33] Zhang, D., Fang, P., Jiang, X., Nelson, J., Moore, J. K., Kruger, W. D., ... & Wang, H. (2012). Severe hyperhomocysteinemia promotes bone marrow-derived and resident inflammatory monocyte differentiation and atherosclerosis in LDLr/CBS-deficient mice. *Circ. Res.,* 111(1), 37-49. doi: 10.1161/CIRCRESAHA.112.269472

[34] Zhang, J., Liu, T. T., Zhang, W., Li, Y., Niu, X. Y., Fang, Y. L., ... & Li, C. X. (2016). Hyperhomocysteinemia Is Associated with Vitamin B12 Deficiency: A Cross-Sectional Study in a Rural, Elderly Population of Shanxi China. *J. Nutr. Health Aging,* 20(6), 594-601. doi: 10.1007/s12603-015-0650-5

[35] Zhang, Q., Li, Q., Chen, Y., Huang, X., Yang, I. H., Cao, L., ... & Tan, H. (2012). Homocysteine-impaired angiogenesis is associated with VEGF/VEGFR inhibition. *Front Biosc.,* 4(7), 2525-2535. doi: 10.2741/e563

ВПЛИВ ХРОНІЧНОЇ ГІПЕРГОМОЦИСТЕЇНЕМІЇ НА СТРУКТУРУ ТА ІМУННІ ПРОЦЕСИ СЕЛЕЗІНКИ МОЛОДИХ ЩУРІВ

Дзевульська І. В., Гриценко А. С., Тимошенко І. О., Закалата Т. Р., Лавриненко В. Є., Смолко Д. Г., Гунас І. В.

Гомоцистеїн - сірковмісна амінокислота, що є проміжним продуктом обміну метіоніну. Потрапляючи до організму з продуктами тваринного походження, метіонін піддається низці біохімічних перетворень. Гіпергомоцистеїнемія чинить негативний вплив на організм, зумовлюючи ураження всіх органів та систем і призводить до порушення гомеостазу. Метою дослідження є вивчення особливостей змін структури та імунних процесів селезінки молодих щурів при хронічній гіпергомоцистеїнемії. Досліди виконано на 22 білих щурах-самцях. Під час експерименту тварин розподілили на контрольну і дослідну групи (по 11 особин в кожній групі). Хронічну гіпергомоцистеїнемію досягали введенням D,L-тіолактон гомоцистеїну гідрохлориду тваринам дослідної групи в дозі 200 мг/кг маси тіла внутрішньошлунково на 1 % розчині крохмального гелю 1 раз на добу впродовж 8 тижнів. Після закінчення термінів експериментального моделювання хронічної гіпергомоцистеїнемії, тварин виводили з експерименту, знеживлюючи методом декапітації та використанням тіопенталового наркозу. Гістологічні препарати вивчали за допомогою світлового мікроскопа SEO SCAN. Експериментальне моделювання хронічної гіпергомоцистеїнемії у молодих щурів не супроводжувалось відчутними морфологічними зрушеннями строми та червоної пульпи селезінки. Т-клітинні периартеріальні піхви і В-клітинні вузлики у тварин з експериментальної групи зазнавали змін. Проліферація В-клітин призводить до розростань в межах білої пульпи, розширення маргінальних зон, що стають більш розмитими, та інфільтрації цих клітин у червону пульпу. Оцінка стану червоної пульпи у селезінці молодих щурів експериментальної групи показала певне розширення у венозних синусах, що може бути ознакою реакції на вплив гомоцистеїну і незначного набрякання цих судин. Чисельність Т-клітин у молодих тварин в периартеріальних муфтах дещо знижується, що можна пояснити зростаючою активністю макрофагів. Тим не менш, Т-клітини також інфільтрували у червону пульпу. Подібне проникнення білих клітин крові у червону пульпу супроводжується розширенням і "розмиванням" маргінальних зон лімфатичних вузликів. Таким чином, підвищений рівень гомоцистеїну значно потенціював проліферацію і частково інгібував апоптоз у Т-лімфоцитах, але не мав прямого впливу на сплячі Т-клітини.

Ключові слова: *гомоцистеїн, селезінка, лімфоцити, макрофаги, щури.*

Author's contribution

Dzevulska I. V. - conceptualization, review writing and editing.
Gritsenko A. S. - research, methodology and writing of the original draft, formal analysis and validation.
Tymoshenko I. O. - software, resources.
Zakalata T. R. - review writing and editing.
Lavrinenko V. Y. - project administration.
Smolko D. G. - software, resources.
Gunas I. V. - conceptualization.

DOI: 10.31393/morphology-journal-2024-30(1)-05 Reports of Morphology, Vol. 30, №1, Pages 40-46

ISSN 1818-1295 eISSN 2616-6194

REPORTS OF MORPHOLOGY

Official Journal of the Scientific Society of Anatomists, Histologists, Embryologists and Topographic Anatomists of Ukraine

journal homepage: https://morphology-journal.com

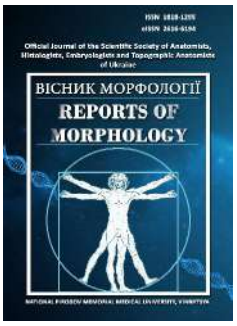

Histopathological changes in the spleen of rats exposed to N,N-dimethylhydrazine with the following protective input of Au/Ag/Fe

Kramar S. B., Soroka Yu. V., Nebesna Z. M., Korda M. M., Lisnychuk N. Ye.

I. Horbachevsky Ternopil National Medical University, Ternopil, Ukraine

ARTICLE INFO

Received: 24 November 2023

Accepted: 16 January 2024

UDC: 616.411-091.8:616.345-006.6:616-08:546.57/.59/.72-022.532]-092.9

CORRESPONDING AUTHOR

e-mail: kramarsb@tdmu.edu.ua

Kramar S. B.

CONFLICT OF INTEREST

The authors have no conflicts of interest to declare.

FUNDING

This investigation is a part of the research project, which was funded by the Ministry of Health of Ukraine (Grant number 0119U002307).

DATA SHARING

Data are available upon reasonable request to corresponding author.

Colon cancer is one of the leading causes of cancer-related deaths worldwide. Despite the growing number of studies on nanoparticles of different metals, there is still a lack of reliable information about their ability to work together as a composition and their antitumor effects. It has been established that the regulation of genes encoding proteins of the Bcl-2 family changes in cancer. Bcl-2 family proteins can be a potential target in cancer diagnosis and have a prognostic value in treating cancer with chemotherapeutic drugs. The tumor microenvironment includes myeloid suppressor cells, tumor-associated neutrophils, and tumor-associated macrophages that promote cancer progression and are derived from splenic hematopoietic stem cells and progenitor cells. The work aimed to ascertain histological changes and expression of Bcl-2 family proteins in the spleen of rats with N,N-dimethylhydrazine-induced carcinogenesis followed by the protective administration of Au/Ag/Fe nanometal composition. The study was conducted on 72 outbred white male rats. Colon adenocarcinoma was modelled by N,N-dimethylhydrazine hydrochloride administration for 30 weeks. Animals received an aqueous dispersion of Au/Ag/Fe nanoparticles intragastrically once a day for 21 days at a dose of 0.842 mg Ag/0.0526 mg Fe/1.625 μg Au per 1 kg of rat body weight. Paraffin sections of the spleen were stained with hematoxylin and eosin. For immunohistochemical analysis, sections were stained with rabbit monoclonal antibodies to Bcl-2. Under conditions of 30-week exposure to N,N-dimethylhydrazine hydrochloride, blood circulation disorders, stasis, thrombosis, reduction in the size of white pulp lymphatic nodules and loss of their zonation were histologically proved in the rat's spleen. The development of sclerotic processes in the organ was noted. It was indicated that using metal nanoparticles under N,N-dimethylhydrazine hydrochloride-induced colon carcinogenesis leads to less evidenced morphological manifestations of structural changes in the spleen. Immunohistochemically, the expression of Bcl-2 protein in the white pulp of the spleen of animals subjected to correction was lower than in animals without the corrective effect of the composition of nanoparticle metals. Administration of the Au/Ag/Fe metal nanoparticle composition to intact white rats does not cause pathological changes in the spleen morphology. The structural components of the red and white pulp match the typical histological structure of the organ.

Keywords: *spleen, colorectal cancer, N,N-dimethylhydrazine hydrochloride, Bcl-2, histopathological changes.*

Introduction

Colon cancer is one of the leading causes of cancer-related deaths worldwide [9, 15, 19, 27]. In the United States, this figure is 10 % of all cancer deaths annually [9], and in Ukraine - 13.2 % among men and 15.3 % among women [29]. According to recent studies, various mechanisms contribute to the progression of colorectal cancer, including mutations in the cell cycle, apoptotic pathways, angiogenesis, invasion and metastasis, and the ability of tumor cells to avoid the immune response [3, 15, 27, 28].

Bcl-2 family proteins perform various critical functions during the body development and functioning [3, 14]. In accordance with numerous studies, it has been demonstrated that in cancer, the regulation of genes that encode proteins of the Bcl-2 family changes [11, 21]. Their overexpression inhibits cell death caused by various biological stimuli, particularly if such a stimulus is an

antitumor cytotoxic drug. In account of this Bcl-2 family proteins can be a potential target in cancer diagnosis and have a prognostic value in treating cancer with chemotherapeutic drugs [3, 11, 21].

Spleen is the largest peripheral organ of hematopoiesis and the immune system [4, 2, 16]. L. M. Sun et al. [24] described that people with splenectomies have a higher risk of developing cancer, especially of non-traumatic origin. Animal studies displayed that the role of splenectomy in the progression of non-small cell lung cancer depended on the time of splenectomy [28]. The tumor microenvironment includes myeloid suppressor cells, tumor-associated neutrophils, and tumor-associated macrophages that promote cancer progression and are generated from splenic hematopoietic stem cells and progenitor cells [13]. The study deVisser K. E., Eichten A. та Coussens L. M. [8] showed that splenectomy can reduce the percentage of myeloid suppressor cells and inhibit the growth of hepatocellular carcinoma. However, there is still no consensus on the role of the spleen in cancer progression.

Many factors cause obstacles to the development of effective cancer treatment. In particular, one of the main problems is the effective delivery of drugs to the tumor and the insufficient selectivity of chemotherapy for tumor cells [6, 30]. Advances in nanotechnology have led to the development of various nanomaterials for therapeutic and diagnostic purposes [1, 6]. There are already more than eight hundred different products made based on nanotechnology. Among them are polymer micelles, liposomes, inorganic nanoparticles, etc. These nanomaterials have many unique advantages over traditional anticancer treatments [1, 5]. One of the first nanoparticles known for a long time are nanometals and nanoclusters formed by them, in particular nanoparticles of iron, gold and silver [18, 23, 26]. Despite the growing number of studies on nanoparticles of different metals, there is still no reliable information on their ability to work together as a composition.

Therefore, *our work aimed* to investigate the histological changes and expression of Bcl-2 family proteins in the spleen of rats with N,N-dimethylhydrazine-induced colon adenocarcinoma followed by protective administration of Au/Ag/Fe nanometals.

Material and methods

Animals

The research was accomplished on 72 white outbred male rats with a body weight 190±5 g. The animals had been retained in standard conditions of vivarium. Body weights and survival had been supervised all through. Experimental animals had unfastened access to drinking water and basal food regimen ad libitum. All manipulations with animals throughout this experiment have been conformed according to internationally accepted requirements and accredited by the Bioethical Committee of Ternopil National Medical University (protocol № 75, 01.11.2023). All experiments were carried out in accordance with the requirements of the "European Convention for the Protection of Vertebrate Animals Used for Experimental and Different Medical Functions" [7].

This investigation is a part of the research project "Immunogenetics of malignant growth: the influence of Bcl-2 gene expression on the state of anti-tumor immunity and under the corrective influence of nanomaterials", which was funded by the Ministry of Health of Ukraine (Grant number 0119U002307), and is also a fragment of the initiative research "Morphological and metabolic aspects of carcinogenesis" (№ 0123U100070).

Colorectal cancer model

N,N-dimethylhydrazine-induced (DMH-induced) colon adenocarcinoma was modelled by introducing N,N-dimethylhydrazine hydrochloride (Sigma-Aldrich Chemie, Japan, series D161802) dissolved in an isotonic sodium chloride solution. The chemical carcinogen was administered subcutaneously into the interscapular area once per week for a duration of 30 weeks, with a single dose of 7.2 mg/kg of body weight (primarily based on the active substance). Animals in the control group received 0.1 ml of physiological saline following the same frequency and procedure. At 30 weeks of N,N-dimethylhydrazine hydrochloride administration, colon adenocarcinoma in situ was histologically diagnosed in all rats.

Nanoparticle's dosage and administration

In this study, the composition of spherical silver (d=30 nm), gold (d=30 nm) and iron (d=40 nm) nanoparticles with a concentration per 1 ml: 1.6 mg Ag; 0.1 mg Fe; 3.088 μg Au was used. Silver nanoparticles' initial water dispersion was synthesized by the tannin (tannic acid) reduction of silver nitrate ($AgNO_3$) in the presence of potassium carbonate (K_2CO_3). The synthesis of gold nanoparticles was performed via reduction of the tetra chloroauric (III) acid ($HAuCl_4 \times 3H_2O$) ($\geq$99.9 % trace metals basis, Sigma-Aldrich) by sodium citrate tribasic dehydrate in the presence of potassium carbonate. Iron nanoparticles were synthesized via reduction of iron (III) chloride by sodium borohydride ($NaBH_4$). The nanoparticle Au/Ag/Fe composition for this research was acquired by the mechanical mixing of the silver, gold and iron nanoparticle water dispersions. Metal nanoparticles used to receive the experimental mixture, as well as the obtained composition, was characterized as safe according to the criteria of cytotoxicity (MTT-test), genotoxicity (comet assay), mutagenicity (Allium-test) and immunotoxicity under in vitro tests [22].

Animals received nanoparticle Au/Ag/Fe water dispersion intragastrically once a day for 21 days at a dose of 0.842 mg Ag/0.0526 mg Fe/1.625 μg Au per 1 kg of rat body weight. The initial nanoparticle Au/Ag/Fe mixture was diluted with sterile distilled water at a ratio of 1:10 before the intragastric administration.

Histological and immunohistochemical study

Splenic tissue was collected from animals and fixed

overnight in 10 % neutral buffered formalin (Biognost, Croatia). The tissue was processed in a histoprocessor LOGOSone (Milestone, Italy). For histological analysis, spleen paraffin sections (5 μm thickness) were made with manual rotary microtome AMR 400 (Amos Scientific, Australia), stained with Hematoxylin and Eosin (H&E) (Biognost, Croatia), and analyzed with a light microscope Nikon Eclipse Ci (Nikon, Japan), and fixing photos with a digital camera Sigeta M3CMOS 14000.

Immunohistochemical analysis was performed on thin formalin paraffin-embedded sections of the rat spleen. The sections were stained with a rabbit monoclonal antibody against Bcl-2 (Cat. № ab32124). Bcl-2 detection was accomplished using a Mouse/Rabiit PolyVue Plus HRP/ DAB Detection System (Diagnostic Biosystems). The sections were then counterstained with Hematoxylin M (Biognost, Croatia) and mounted under coverslips.

Results

Histological studies of the spleen after 30 weeks of exposure to N,N-dimethylhydrazine established destructive and degenerative changes in it. Disorders of blood circulation in the organ with uneven blood supply of red and white pulp was detected. In some fields of view, vessels were found without blood-formed elements; in others, they were filled with erythrocytes, indicating stasis and, in some places, thrombosis. Microscopically, macrophages with accumulation of hemosiderin in the cytoplasm were noted. During this observation period, the reduction of lymphatic nodules and the loss of their zonality are pronounced. The lumen of the central artery is narrowed, and its wall is thickened. In the red pulp's stroma, the thickening of trabeculae, growth of the population of fibroblastic cells and, consenquently collagen formation were noticed. A particularly noticeable location of the concentration of the fibrous component was the perivascular spaces around arteries and capillaries. These changes indicate sclerotic processes in the organ (Fig. 1).

Immunohistochemical study of Bcl-2 expression in the rat's spleen with DMH-induced colorectal cancer at the 30th week of the experiment revealed an intense positive reaction in the cytoplasm of cells of the spleen's white and red pulp. The development of chronic neoplastic endotoxemic syndrome and destructive-degenerative changes in vascular beds and lymphatic nodules are accompanied by an increase in the number of Bcl-2 cells in the red and white spleen pulp, which indicates a malfunction of the organ, and that can significantly affect both the progression of the tumour process and its subsequent correction.

The use of the Ag/Au/Fe nanometals composition showed a positive effect on the histological structure of the spleen components and the expression of the Bcl-2 in the organ.

At the microscopic level, it was found that the use of nanometals Ag/Au/Fe in DMH-induced carcinogenesis lead to the less pronounced morphological manifestations of

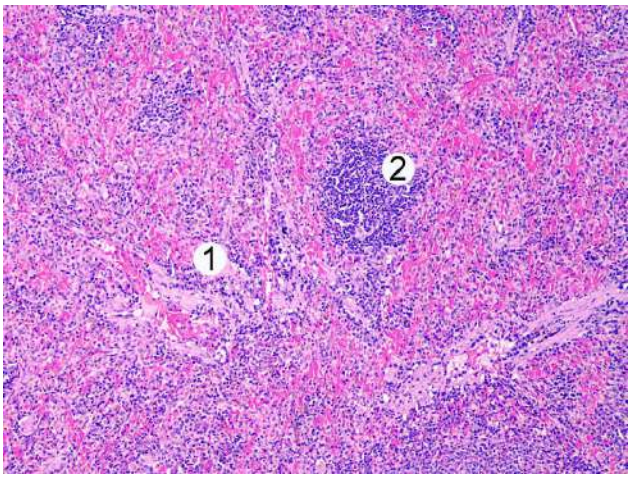

Fig. 1. The structure of the red and white pulp of the spleen after 30 weeks of the experiment. Sclerosis of red pulp (1) and delimphatization of lymphatic nodules (2) of the white pulp. Hematoxylin and eosin staining. Ocular magnification x10, objective x10.

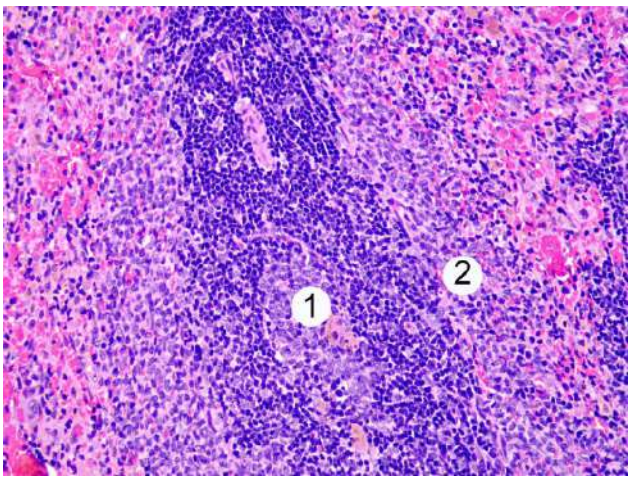

Fig. 2. Structural changes of the rats' spleen under N,N-dimethylhydrazine hydrochloride intoxication and Ag/Au/Fe nanometals composition administration. Lymphatic nodules with hemosiderophages (1) and enlarged marginal zone (2). Hematoxylin and eosin staining. Ocular magnification x10, objective x20.

structural changes in the spleen compared with the N,N-dimethylhydrazine-only group. Lymphatic nodules of the white pulp contained an enlarged germinal center, represented by lymphoblasts with normochromic nuclei. Hemosiderophages were observed in some places, which may indicate the presence of hemorrhages in this area in the previous stages of the experiment. Lymphocytes in the periarterial pulp were compact and their nuclei were hyperchromic. The number of lymphocytes and macrophages in the marginal areas and periarteriolar lymphoid sheaths was moderate. The mantle and marginal areas were expanded. The latter often came into contact with neighboring follicles. At the same time, the manifestations of hemodynamic disorders persisted, namely the plethora of red pulp sinusoids (Fig. 2).

Under the conditions of nanoparticle administration, a moderately pronounced (++) positive reaction against Bcl-2 in the cytoplasm of cells of germinal centers and marginal zones of lymphatic nodules of white pulp and a pronounced (+++) cytoplasmic reaction in red pulp cells were detected immunohistochemically (Fig. 3).

To assess the biosafety of the composition of nanometals, we examined their effect on the histological state of the spleen of unaffected animals. Manifestations of the pathological changes in the organ were not detected. The structure of the red and white pulp corresponded to the normal histological structure of the organ (Fig. 4).

Immunohistochemical examination against Bcl-2 of the spleens of unaffected animals injected with nanoparticles revealed a moderately expressed (++) positive reaction in the cytoplasm of the cells of the germinal centers of lymphatic nodules of the white pulp and a pronounced (+++) cytoplasmic reaction in their marginal zones in the cells of the red pulp (Fig. 5).

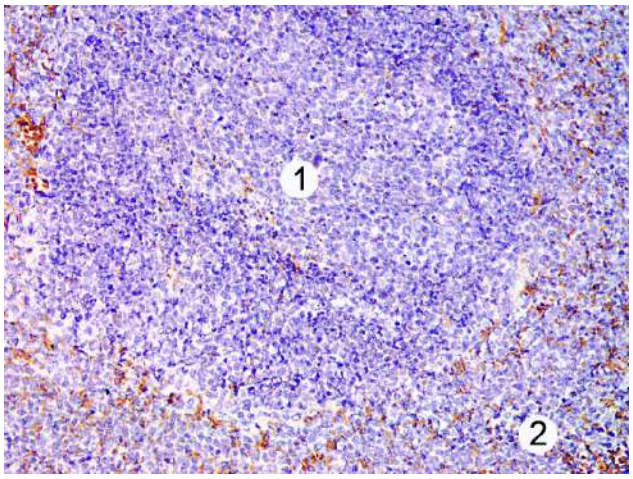

Fig. 3. Immunohistochemical staining against Bcl-2 in the rats' spleen under N,N-dimethylhydrazine hydrochloride intoxication and Ag/Au/Fe nanoparticles administration. Lymphatic nodules (1) with moderate expression of Bcl-2 and red pulp (2) with strong expression of Bcl-2. Ocular magnification x10, objective x20.

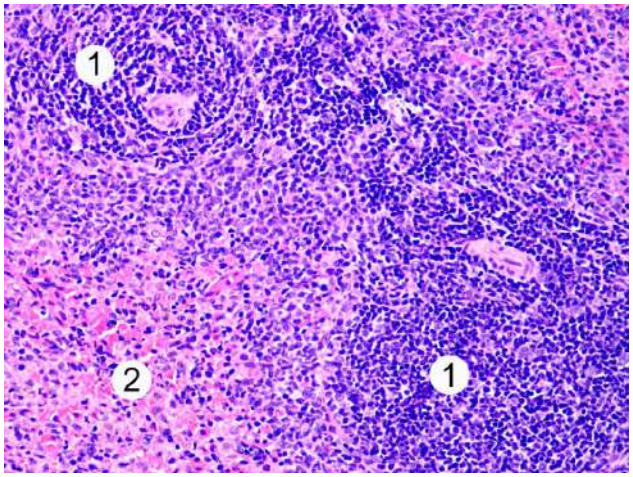

Fig. 4. The structure of the red and white pulp of the spleen, day 21 of Ag/Au/Fe nanoparticles administration. Lymphatic nodules with a dense arrangement of cells (1). Moderately blood-filled sinusoids of the red pulp (2). Hematoxylin and eosin staining. Ocular magnification x10, objective x20.

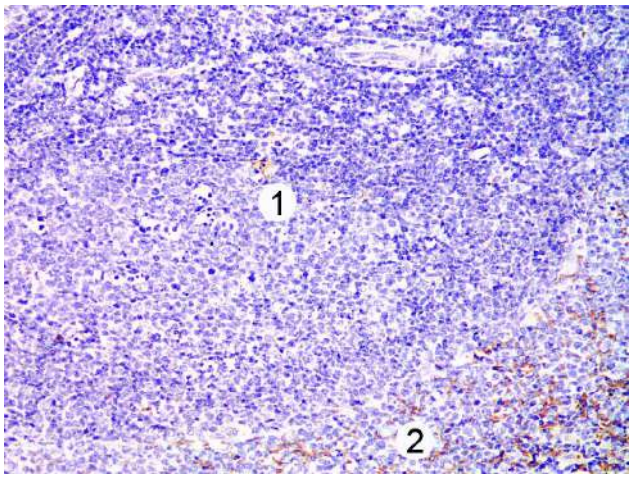

Fig. 5. Immunohistochemical staining against Bcl-2 in the spleen of unaffected rats after Ag/Au/Fe nanoparticles administration. Moderate Bcl-2 expression in lymphatic nodules (1) and strong Bcl-2 expression in red pulp (2). Ocular magnification x10, objective x20.

Discussion

Our research aims to elucidate histopathological changes and detection of Bcl-2 expression in the rat's spleen during DMH-induced oncogenesis and the corrective effect of Ag/Au/Fe nanometal compositions. The spleen is the largest secondary lymphoid organ that performs essential immune functions and participates in the formation of cells that create the tumor microenvironment [2, 4, 16, 24]. That is why the study of changes in the structure of this organ during carcinogenesis can have significant prognostic and immunotherapeutic value. The red pulp of the spleen is a depot of blood, particularly erythrocytes and platelets, as well as a depot of iron. Blood is filtered in the red pulp of the spleen, and in fetal and newborn rodents, it is the site of hematopoiesis [2, 4, 16]. It can be assumed that under the conditions of its destruction, there will be a decrease in the elimination of cellular debris and the ageing of erythrocytes, increasing general intoxication. The white pulp of the spleen, which surrounds the central arteries, includes a quarter of the body's lymphocytes and stimulates the immune response to antigens [4, 13, 28].

The results of microscopic studies after 30 weeks of N,N-dimethylhydrazine hydrochloride administration proved the presence of destructive-degenerative changes in the spleen with the phenomena of sclerosing of the organ and delymphatization of the white pulp. These data are consistent with the results of research by Caprezo N. O. et al. [12], observed the appearance of dystrophic zones in the spleen and damage to the nuclear apparatus of its

cells when exposed to N,N-dimethylhydrazine hydrochloride. Research by Svitina H. M. et al. [25] demonstrated a decrease in the proliferative activity of splenocytes under the influence of N,N-dimethylhydrazine hydrochloride. According to the analysis conducted by Li B. et al. [17], the spleen plays a dual role in cancer incidence and progression.

Detection of the expression of Bcl-2 family proteins is important in oncogenesis because anti- and pro-apoptotic mechanisms are among the main ones in cancer progression [11, 14, 21]. An increase in the expression of Bcl-2 by parenchymal cells of the spleen under the influence of N,N-dimethylhydrazine hydrochloride was established. These data are confirmed by other researchers, who testify to their increased expression in various types of cancer [20]. Abnormalities in the expression of anti-apoptotic or pro-apoptotic members of the BCL-2 protein family can promote tumor development and make malignant cells resistant to anticancer therapy [10].

When studying the effect of metal nanoparticles, the main studies are devoted to changes at the cellular level, while morphological data describing changes at the tissue level are generally insufficient [1, 18]. An open problem of nanotoxicology remains a large number of studies using nanoparticles of different sizes, shapes and compositions, the results of which are contradictory, unreliable and unregulated. Currently, the entire aspect of the long-term residence of nanomaterials in the human body remains unexplored [30]. Our choice of components of the Ag/Au/Fe nanocomposite was connected with the already proven effectiveness of each nanometal separately.

Since nanoparticles of Ag/Au/Fe metals have antimicrobial, antifungal, antiviral, catalytic, photocatalytic, and antioxidant properties [18, 23, 26], this allowing us to understand our positive results.

To adequately assess the effect of nanoparticles, a group of unaffected N,N-dimethylhydrazine hydrochloride experimental animals with a 21-day administration of Ag/Au/Fe nanoparticle composite was also selected. Our studies demonstrated the absence of pathological changes in the spleen of white rats of this group.

Conclusions

1. Induced carcinogenesis in the colon causes evident reactive changes in the spleen: remodeling of its structural elements, hemodynamic disorders, sclerosis, deterioration of the white pulp, and increased expression of the Bcl-2 gene by parenchymal cells.

2. The use of the composition of metal nanoparticles contributed to a significant improvement in the histological structure of the spleen: the balance of parenchymal ratios of red and white pulp was restored, as well as the zoning of lymphatic nodules, thrombi in the vessels of the microcirculatory bed were undiscovered. Immunohistochemically confirmed a decrease in the level of Bcl-2 expression by white pulp cells.

References

[1] Alshomer, F., Chaves, C., Serra, T., Ahmed, I., & Kalaskar, D. M. (2017). Micropatterning of nanocomposite polymer scaffolds using sacrificial phosphate glass fibers for tendon tissue engineering applications. *Nanomedicine: Nanotechnology, Biology and Medicine,* 13(3), 1267-1277. doi: 10.1016/j.nano.2017.01.006

[2] Bronte, V., & Pittet, M. J. (2013). The spleen in local and systemic regulation of immunity. *Immunity,* 39(5), 806-818. doi: 10.1016/j.immuni.2013.10.010

[3] Campbell, K. J., & Tait, S. W. (2018). Targeting BCL-2 regulated apoptosis in cancer. *Open Biology,* 8(5), 180002. doi: 10.1098/rsob.180002

[4] Cesta, M. F. (2006). Normal structure, function, and histology of the spleen. *Toxicologic Pathology,* 34(5), 455-465. doi: 10.1080/01926230600867743

[5] Chekman, I. S., Hovorukha, M. O., & Doroshenko, A. M. (2011). Наногенотоксикологія: вплив наночастинок на клітину [Nanogenotoxicology: the effect of nanoparticles on the cell]. *Український медичний часопис - Ukrainian Medical Journal,* 1(81), 30-35.

[6] Cheng, Z., Li, M., Dey, R., & Chen, Y. (2021). Nanomaterials for cancer therapy: current progress and perspectives. *Journal of Hematology & Oncology*, 14(1), 85. doi: 10.1186/s13045-021-01096-0

[7] Council of Europe. (1986). European convention for the protection of vertebrate animals used for experimental and other scientific purposes. Strasbourg. ETS 123.

[8] De Visser, K. E., Eichten, A., & Coussens, L. M. (2006). Paradoxical roles of the immune system during cancer development. *Nature Reviews Cancer,* 6(1), 24-37. doi: 10.1038/nrc1782

[9] Fidelle, M., Yonekura, S., Picard, M., Cogdill, A., Hollebecque, A., Roberti, M. P., & Zitvogel, L. (2020). Resolving the Paradox of Colon Cancer Through the Integration of Genetics, Immunology, and the Microbiota. *Frontiers in Immunology,* 11, 600886. doi: 10.3389/fimmu.2020.600886

[10] Kaloni, D., Diepstraten, S. T., Strasser, A., & Kelly, G. L. (2023). BCL-2 protein family: Attractive targets for cancer therapy. *Apoptosis,* 28(1-2), 20-38. doi: 10.1007/s10495-022-01780-7

[11] Kaloni, D., Diepstraten, S. T., Strasser, A., & Kelly, G. L. (2023). BCL-2 protein family: attractive targets for cancer therapy. *Apoptosis: an International Journal on Programmed Cell Death,* 28(1-2), 20-38. doi: 10.1007/s10495-022-01780-7

[12] Kaprezo, N. O., Hurniak, O. M., & Rybalchenko, V. K. (2011). Вплив похідного малеіміду на селезінку за умов хімічно індукованого раку товстого кишечника у щурів [The effect of a maleimide derivative on the spleen under conditions of chemically induced colon cancer in rats]. *Сучасні проблеми токсикології - Modern problems of toxicology*, 5(55), 88-89.

[13] Kim, J., & Bae, J. S. (2016). Tumor-associated macrophages and neutrophils in tumor microenvironment. *Mediators of Inflammation*, 2016, 6058147. doi: 10.1155/2016/6058147

[14] Kollek, M., Müller, A., Egle, A., & Erlacher, M. (2016). Bcl-2 proteins in development, health, and disease of the hematopoietic system. *The FEBS Journal,* 283(15), 2779-2810. doi: 10.1111/febs.13683

[15] Lee, W. S., Baek, J. H., You, D. H., & Nam, M. J. (2013). Prognostic value of circulating cytokines for stage III colon cancer. *Journal of Surgical Research,* 182(1), 49-54. doi:

10.1016/j.jss.2012.08.051
[16] Lewis, S. M., Williams, A., & Eisenbarth, S. C. (2019). Structure and function of the immune system in the spleen. *Science Immunology,* 4(33), eaau6085. doi: 10.1126/sciimmunol.aau6085
[17] Li, B., Zhang, S., Huang, N., Chen, H., Wang, P., Li, J., ... & Li, Z. (2016). Dynamics of the spleen and its significance in a murine H22 orthotopic hepatoma model. *Experimental Biology and Medicine,* 241(8), 863-872. doi: 10.1177/1535370216638772
[18] Lopez-Chaves, C., Soto-Alvaredo, J., Montes-Bayon, M., Bettmer, J., Llopis, J., & Sanchez-Gonzalez, C. (2018). Gold nanoparticles: distribution, bioaccumulation and toxicity. In vitro and in vivo studies. *Nanomedicine: Nanotechnology, Biology and Medicine,* 14(1), 1-12. doi: 10.1016/j.nano.2017.08.011
[19] Malka, D., Lievre, A., André, T., Taïeb, J., Ducreux, M., & Bibeau, F. (2020). Immune scores in colorectal cancer: Where are we? *European Journal of Cancer,* 140, 105-118. doi: 10.1016/j.ejca.2020.08.024
[20] Meda, B. A., Frost, M., Newell, J., Bohling, S. D., Huebner-Chan, D. R., Perkins, S. L., ... & Elenitoba-Johnson, K. S. (2003). BCL-2 is consistently expressed in hyperplastic marginal zones of the spleen, abdominal lymph nodes, and ileal lymphoid tissue. *The American Journal of Surgical Pathology,* 27(7), 888-894. doi: 10.1097/00000478-200307000-00003
[21] Qian, S., Wei, Z., Yang, W., Huang, J., Yang, Y., & Wang, J. (2022). The role of BCL-2 family proteins in regulating apoptosis and cancer therapy. *Frontiers in Oncology,* 12, 985363. doi: 10.3389/fonc.2022.985363
[22] Ryzhenko, G. F., Dybkova, S. M., Horbatyuk, O. I., Andriyashchuk, V. O., Zhovnir, O. M., Ukhovska, T. M., & Gruzina, T. G. (2017). Скринінг наночастинок металів для біотехнології ветеринарних імунобіологічних засобів [Screening of metal nanoparticles for the biotechnology of veterinary immunobiological agents]. *Ветеринарна біотехнологія - Veterinary Biotechnology,* 30, 206-213.
[23] Soetaert, F., Korangath, P., Serantes, D., Fiering, S., & Ivkov, R. (2020). Cancer therapy with iron oxide nanoparticles: Agents of thermal and immune therapies. *Advanced Drug Delivery Reviews,* 163, 65-83. doi: 10.1016/j.addr.2020.06.025
[24] Sun, L. M., Chen, H. J., Jeng, L. B., Li, T. C., Wu, S. C., & Kao, C. H. (2015). Splenectomy and increased subsequent cancer risk: a nationwide population-based cohort study. *The American Journal of Surgery,* 210(2), 243-251. doi: 10.1016/j.amjsurg.2015.01.017
[25] Svitina, H. M., Kalmykova, O. O., Shelest, D. V., Skachkova, O. V., Harmanchuk, L. V., & Shabliy, V. A. (2016). Клітинна імунна відповідь у щурів з 1,2-диметилгідразин-індукованим раком товстої кишки після трансплантації мультипотентних клітин плаценти [Cellular immune response in rats with 1,2-dimethylhydrazine-induced colon cancer after transplantation of placental multipotent cells]. *Клітинна та органна трансплантологія - Cell and Organ Transplantology,* 4(1), 48-54.
[26] Takáč, P., Michalková, R., Čižmáriková, M., Bedlovičová, Z., Balážová, Ľ., & Takáčová, G. (2023). The Role of Silver Nanoparticles in the Diagnosis and Treatment of Cancer: Are There Any Perspectives for the Future? *Life,* 13(2), 466. doi: 10.3390/life13020466
[27] Testa, U., Pelosi, E., & Castelli, G. (2018). Colorectal cancer: genetic abnormalities, tumor progression, tumor heterogeneity, clonal evolution and tumor-initiating cells. *Medical Sciences* (Basel, Switzerland), 6(2), 31. doi: 10.3390/medsci6020031
[28] Vesely, M. D., Kershaw, M. H., Schreiber, R. D., & Smyth, M. J. (2011). Natural innate and adaptive immunity to cancer. *Annual Review of Immunology,* 29, 235-271. doi: 10.1146/annurev-immunol-031210-101324
[29] Yakovtsova, I. I., Ivahno, I. V., Yakymenko, A. S., Dolgaya, O. V., Danyliuk, S. V., Chertenko, T. M. (2020). Аналіз смертності на колоректальний рак у багатопрофільних лікарнях м. Харків. [Analysis of mortality from colorectal cancer in multidisciplinary hospitals in Kharkiv]. *Клінічна онкологія - Clinical Oncology,* 10(3-4), 39-40. doi: 10.32471/clinicaloncology.2663-466X.39-3.27380
[30] Zhao, H., Ding, R., Zhao, X., Li, Y., Qu, L., Pei, H., ... & Zhang, W. (2017). Graphene-based nanomaterials for drug and/or gene delivery, bioimaging, and tissue engineering. *Drug Discovery Today,* 22(9), 1302-1317. doi: 10.1016/j.drudis.2017.04.002

ГІСТОПАТОЛОГІЧНІ ЗМІНИ В СЕЛЕЗІНЦІ ЩУРІВ, ЯКІ ПІДДАВАЛИСЯ ДІЇ N,N-ДИМЕТИЛГІДРАЗИНУ З НАСТУПНИМ ПРОТЕКТИВНИМ ВВЕДЕННЯМ НАНОМЕТАЛІВ AU/AG/FE

Крамар С. Б., Сорока Ю. В., Небесна З. М., Корда М. М., Лісничук Н. Є.

Рак товстої кишки є однією з основних причин смертності від канцер-асоційованих захворювань в усьому світі. Незважаючи на зростаючу кількість досліджень наночастинок різних металів, досі відсутня достовірна інформація щодо їх можливості працювати разом та їх протипухлинні властивості. Встановлено, що при ракових захворюваннях змінюється регуляція генів, які кодують білки родини Bcl-2. Білки родини Bcl-2 можуть бути потенційною мішенню при діагностиці раку і мати прогностичне значення при його лікуванні хіміотерапевтичними препаратами. Мікрооточення пухлини містить мієлоїдні супресорні клітини, пухлиноасоційовані нейтрофіли та пухлиноасоційовані макрофаги, що сприяють прогресії раку, та утворюються із селезінкових гемопоетичних стовбурових клітин та клітин-попередників. Мета роботи - встановлення гістологічних змін та експресії білків родини Bcl-2 в селезінці щурів при N,N-диметилгідразин-індукованому канцерогенезі з наступним протективним введенням композиції наночастинок металів Au/Ag/Fe. Дослідження проведено на 72 білих безпородних щурах-самцях. Аденокарциному товстої кишки моделювали шляхом введення N,N-диметилгідразину гідрохлориду впродовж 30 тижнів. Тварини отримували водну дисперсію наночастинок металів Au/Ag/Fe внутрішньошлунково 1 раз на добу впродовж 21 дня в дозі 0,842 мг Ag/0,0526 мг Fe/1,625 мкг Au на 1 кг маси тіла щура. Парафінові зрізи селезінки забарвлювали гематоксиліном та еозином. Для імуногістохімічного аналізу зрізи були забарвлені із застосуванням кролячих моноклональних антитіл до Bcl-2. Встановлено, що введення композиції наночастинок металів Au/Ag/Fe інтактним білим щурам не зумовлює порушення морфології селезінки. Структурні компоненти червоної та білої пульпи відповідали нормальній гістологічній будові органу. За умов 30-тижневого впливу N,N-диметилгідразину гідрохлориду у селезінці щурів гістологічно встановлено розлади кровообігу, стази, тромбози, зменшення розмірів лімфатичних вузликів білої пульпи та втрата їх зональності. Відмічено розвиток склеротичних процесів в органі. Мікроскопічно з'ясовано, що застосування наночастинок металів Au/Ag/Fe при N,N-диметилгідразину гідрохлориду індукованому канцерогенезі призводить до менш виражених морфологічних проявів структурних змін селезінки порівняно з групою, яка отримувала лише N,N-диметилгідразин

гідрохлорид. Імуногістохімічно виявлено менш виражену експресію Bcl-2 у білій пульпі селезінки тварин, яким проводили ін'єкцію наночастинок металів Au/Ag/Fe після 30-тижневого випливу N,N-диметилгідразину гідрохлориду, порівняно з тваринами без корегуючого впливу композиції нанометалів.
Ключові слова: *селезінка, колоректальний рак, N,N-диметилгідразину гідрохлорид, Bcl-2, гістопатологічні зміни.*

Author's contribution

Kramar S. B. - data curation, investigation, methodology, visualization, conceptualization, writing - original draft.
Soroka Yu. V. - formal analysis, investigation, writing - review & editing.
Nebesna Z. M. - conceptualization, investigation, visualization, writing - review & editing.
Korda M. M. - conceptualization, project administration, supervision, validation, writing - review & editing.
Lisnychuk N. Ye. - conceptualization, data curation, formal analysis, funding acquisition, methodology, project administration, supervision, validation, writing - review & editing.

DOI: 10.31393/morphology-journal-2024-30(1)-06 Reports of Morphology, Vol. 30, №1, Pages 47-54

ISSN 1818-1295 eISSN 2616-6194

REPORTS OF MORPHOLOGY

Official Journal of the Scientific Society of Anatomists, Histologists, Embryologists and Topographic Anatomists of Ukraine

journal homepage: https://morphology-journal.com

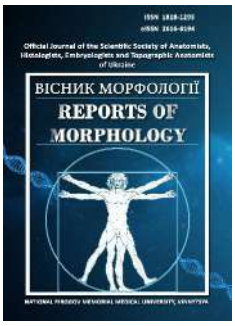

Optimization of the selection of the volume of surgical intervention in cases of pronounced morphological and structural changes of the parenchyma in patients with a high risk of developing pancreatic cancer

Usenko O. Yu.[1], Petrushenko V. V.[2], Sukhodolia S. A.[2], Sukhodolia A. I.[2], Savchuk O. M.[3], Radoga Ia. V.[2], Savchuk I. I.[2]

[1]SI "A. A. Shalimov National Institute of Surgery and Transplantology" NAMS of Ukraine, Kyiv, Ukraine
[2]National Pirogov Memorial Medical University, Vinnytsya, Ukraine
[3]Educational and Scientific Center "Institute of Biology and Medicine" of Taras Shevchenko National University of Kyiv, Kyiv, Ukraine

ARTICLE INFO
Received: 20 December 2023
Accepted: 17 January 2024

UDC: 616.37- 002-007.253-089

CORRESPONDING AUTHOR
e-mail: ssukhodolia@gmail.com
Sukhodolia S. A.

CONFLICT OF INTEREST
The authors have no conflicts of interest to declare.

FUNDING
Not applicable.

DATA SHARING
Data are available upon reasonable request to corresponding author.

Chronic pancreatitis is a common recurrent pathology of the pancreas. The long course of the inflammatory process, accompanied by chronicity, is often attributed to the causes that lead to the development of pancreatic cancer. The aim of the work is to study the morphological changes of the pancreas in rats and the level of of matrix metalloproteinases and tissue inhibitor of metalloproteinases in patients with complicated forms of chronic pancreatitis and a high risk of developing pancreatic cancer in order to optimize the selection of the volume of surgical intervention. A histological study of the pancreas of rats with chronic pancreatitis and chronic pancreatitis on the background of diabetes was carried out. 27 patients operated on during 2020-2022 were examined. In 15 of them, we were unable to clearly and convincingly differentiate of chronic pancreatitis from pancreatic cancer, since quite often the clinical symptoms and diagnostic picture of these diseases are similar. In the remaining 12 patients it was confirmed with all the inherent clinical signs of chronic pancreatitis and ductal hypertension. Matrix metalloproteinases (MMP-1, -2, -3, -8, -9, -10) and tissue inhibitor of metalloproteinases were studied. The obtained results were processed statistically. Morphological changes of the pancreas in rats correspond to high and moderate ductal dysplasia of the PanIN 2 and PanIN 3 class, which are direct predictors of pancreatic adenocarcinoma. In 22 patients moderate and severe exocrine insufficiency was observed, confirmed by a significant decrease in fecal elastase. An intraoperative biopsy of the changed tissue of the pancreas was performed. Among the 15 operated patients of the main group, 9 were diagnosed with diabetes mellitus and changes in MMTs and a peptide pool inherent in malignant tissue. Intraoperatively, after performing a punch biopsy, acinar metaplasia was detected in 3 patients, tissue changes characteristic of PanIN2-PanIN3 in 4 patients, and pancreatic cancer in the head area was confirmed in 3 patients. Changes in the protein profile of the plasma, clinical manifestations, as well as characteristic changes in the pancreas tissue, gave us grounds for performing extended resection interventions. Studying the morphological structure of the pancreas, using as many methods as possible for differential diagnosis between chronic pancreatitis and pancreatic cancer, as well as a comprehensive approach to the patient will allow for the most correct and effective intervention.

Keywords: *pancreas, morphological changes, chronic pancreatitis, fibrosis, pancreatic ductal adenocarcinoma.*

Introduction

Chronic pancreatitis is a common recurrent pathology of the pancreas. The long course of the inflammatory process, accompanied by chronicity, is often attributed to the causes that lead to the development of a pathology with

an extremely unfavorable prognosis - pancreatic cancer. That is why the search for diagnostic criteria that would allow predicting the transition of inflammatory processes in the tissue of the pancreas to hyperproliferative processes and the risk of developing pancreatic cancer is gaining relevance [13].

According to the study results, in pancreatic injury due to KRAS hyperactivity and increased inflammatory signaling with loss of cell-cell and cell-matrix contacts, loss of polarity can induce acinar cells to transdifferentiate to a duct-like phenotype with acinar-ductal metaplasia and initiate further progression to low-grade degree of precancerous lesions [1, 10, 30]. Chronic stimulation and proliferation of the pancreatic duct in response to islets of Langerhans inflammation in type 2 diabetes is associated with an increased risk of pancreatic cancer with concomitant type 2 diabetes [9, 14]. Ductal adenocarcinoma of the pancreas is a type of exocrine cancer and accounts for 95 % of all pancreatic cancers. It is an aggressive malignant tumor, and surgical removal of the tumor is the only possible radical treatment. However, up to 90 % of patients, at the time of clinical manifestation of the disease, have a neglected condition and are surgically incurable [2]. TNF-α expression is increased during the initiation of pancreatic ductal adenocarcinoma, and anti-TNF-α antibodies have shown promising effects in ductal adenocarcinoma in preclinical models by killing tumor cells and reducing desmoplasia and inflammation in the tumor stroma of pancreatic ductal adenocarcinoma [28].

Pancreatic stellate cells (PSCs) can synthesize and secrete acetylcholine and play a role in mediating exocrine secretion from acinar cells. PSCs transform into activated myofibroblast-like cells in response to inflammation. These cells play an important role in the progression of chronic pancreatitis to pancreatic cancer. PSCs respond to proinflammatory cytokines in acute pancreatitis and may progress to chronic pancreatitis with pancreatic damage, fibrosis, diabetes, and metaplasia [22, 31].

Because both diabetes mellitus and chronic pancreatitis are risk factors for pancreatic ductal adenocarcinoma, their combination may particularly raise concerns about progression and malignancy to pancreatic ductal adenocarcinoma. [26]. In a population-based cohort study in Taiwan, the risk of malignancy and development of pancreatic ductal adenocarcinoma was significantly increased in participants with existing diabetes and chronic pancreatitis (hazard ratio 33.5) [19]. Separate research databases also showed an increased, but slightly more modest, hazard ratio (4.7-12.1) for pancreatic ductal adenocarcinoma in individuals with unclassified diabetes and a history of chronic pancreatitis [21].

In other studies, subgroups of participants with newly diagnosed diabetes showed an even higher prevalence of pancreatic ductal adenocarcinoma (5.2-13.6 %). Thus, while long-standing diabetes moderately increases the risk of pancreatic ductal adenocarcinoma, adult-onset diabetes is a marker of possible pre-existing, but preclinical, pancreatic ductal adenocarcinoma. [11, 24].

The aim of the work is to study the morphological changes of the pancreas in rats and the level of of matrix metalloproteinases and tissue inhibitor of metalloproteinases in patients with complicated forms of chronic pancreatitis and a high risk of developing pancreatic cancer in order to optimize the selection of the volume of surgical intervention.

Materials and methods

The study included 27 patients, the average age of which was 56 years (39-77 years). In 15 of them (55 %), despite a thorough preoperative examination, it was impossible to clearly and convincingly differentiate chronic pancreatitis from pancreatic cancer, because the clinical symptoms and diagnostic picture of these diseases are similar. In the remaining 12 (45 %) patients, the diagnosis of chronic pancreatitis was confirmed by all inherent clinical signs and existing ductal hypertension.

The patients who were included in the study cohort had a complicated medical history at the time of the beginning of the diagnostic and treatment process. They were repeatedly treated for acute and exacerbation of chronic pancreatitis after dieting, as well as alcohol abuse and smoking. In 22 (83 %) patients (13 men - 60 %, 9 women - 40 %) moderate and severe exocrine insufficiency was observed, confirmed by a significant decrease in fecal elastase, manifested by indigestion, weight loss, and weakness. In some cases, we observed sarcopenia, which did not allow patients to live without external assistance.

First-onset diabetes in adulthood was diagnosed in 9 (33.5 %) of 27 patients. In medical literature, it is interpreted as type 3 diabetes. This means, the majority of the group has endo- and exocrine insufficiency, which is a characteristic of a decompensated, fibrotic pancreas. According to the results of research by various authors [4, 11, 24], diabetes that occurs suddenly in adulthood in patients with pancreatic pathology is one of the predictors of the development of cancer of this organ.

According to the decision of the bioethical commission of the National Pirogov Memorial Medical University, Vinnytsia, Ukraine (protocol No. 15 dated 26.09.2021), the conducted research fully met the ethical and moral and legal requirements of the current provisions of the Ministry of Health of Ukraine and the Helsinki Declaration of the World Medical Association on the principles of conducting scientific medical research with human participation.

We conducted studies of matrix metalloproteinases (MMP-1, -2, -3, -8, -9, -10) and tissue inhibitor of metalloproteinases (TIMP) in the plasma of patients and obtained changes that directly correlate with the results of our experimental study, which we presented in our previous works.

An experimental study was conducted, in which 50 non-linear white adult male rats weighing 200.0±10.0 g were used. When working with laboratory animals, international recommendations on conducting medical and biological

research using animals were followed in accordance with the "General principles of work on animals", approved by the 1st National Congress on Bioethics (Kyiv, Ukraine, 2001) and agreed with the provisions of the "European Convention for the Protection of Vertebrates" animals used for experimental and other scientific purposes" (Strasbourg, France, 1986). Experimental work with rats was carried out in the vivarium of Taras Shevchenko Kyiv National University. Work with animals was regulated by the rules for conducting experimental work with experimental animals, which were approved by the bioethical commission of Educational and Scientific Centre "Institute of Biology and Medicine" at Taras Shevchenko National University of Kyiv.

Chronic pancreatitis was induced by intraperitoneal injection of cerulein (Sigma, St. Louis, MO, USA) diluted in saline (5.0 μg/kg) five times a day at one-hour intervals. Control rats received equal volumes of 0.9 % NaCl administered intraperitoneally. Injections were carried out for five consecutive days. After the last day of cerulein injection, the rats were kept under standard conditions, without restriction in access to water, for the next 9 days. The development of pancreatitis was confirmed by a high level of amylase in blood serum, as well as by the study of pathogistological changes in the pancreas` parenchyma of the rats under experiment. On the 14th day from the beginning of the experiment, half of the animals from the chronic pancreatitis group were randomly selected and diabetes was induced in them. Diabetes mellitus was induced in rats after a 16-hour fast with a single intraperitoneal injection of streptozotocin (STZ; Sigma, USA) at a dose (65.0 mg/kg) dissolved in 0.5 ml of freshly prepared 0.01 M citrate buffer (pH 4.5). Other animals from the chronic pancreatitis group and all control rats received an equal volume of placebo. The diagnosis of diabetes was confirmed on the basis of a high blood glucose concentration (above 15 mmol/l). Animals were removed from the experiment on the 134th day after the beginning of cerulein administration.

Statistical processing of the obtained results was carried out using the methods of variational statistics using the computer program Excel (Microsoft corporation, USA).

Results

Histological examination of the changed tissue of the pancreas of experimental groups of animals established pathological changes in the group of chronic pancreatitis (Fig. 1) and chronic pancreatitis+diabetes (Fig. 2). In the group of chronic pancreatitis, changes in the pancreas are characterized by the presence of fibrosis in all animals of this group. In most cases, growth of fibrous tissue with polymorphic cellular inflammatory infiltration was observed. In half of the animals with experimental chronic pancreatitis, the interlobular excretory duct wall fibrosis with the formation of glands in the fibrous tissue of the duct was detected. Proliferation of the glandular epithelium with dysplasia also developed. The changes described are classified as PanIN 1.

The pancreas of rats in the chronic pancreatitis + diabetes group had more pronounced changes (Fig. 3). Adherence to ductal dysplasia (see Fig. 3, Fig. 4) was also observed with pronounced acinar metaplasia (Fig. 5). The formation of glands in the fibrous tissue of the duct, the proliferation of glandular epithelium with pronounced dysplasia, the appearance of papillary and cribriform structures corresponding to high and moderate ductal dysplasia of the PanIN 2 and PanIN 3 class - these changes are direct predictors of pancreatic adenocarcinoma. The development of PanIN is a route to pancreatic cancer and directly to ductal adenocarcinoma.

Significant differences in the content of individual forms of MMP in the blood plasma and in the pancreatic tissue of patients with chronic pancreatitis compared to the control group were established. The greatest changes were found in the pathologically changed tissue of the pancreas. The

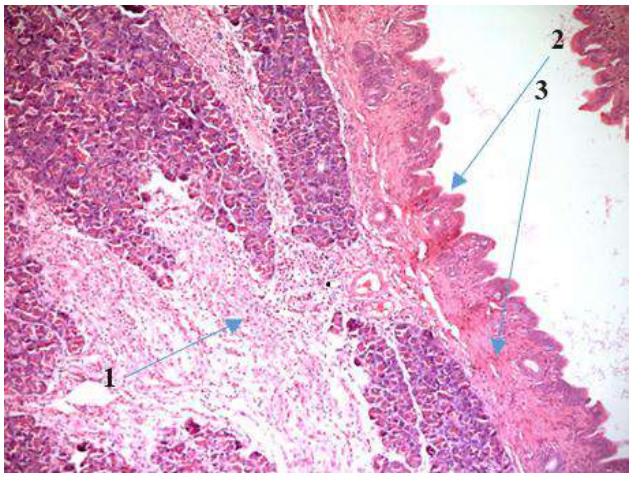

Fig. 1. Morphological changes of pancreatic tissue in conditions of chronic pancreatitis. Growth of fibrous tissue (1) with polymorphic cellular inflammatory infiltration (2, 3). Hematoxylin-eosin staining, x100.

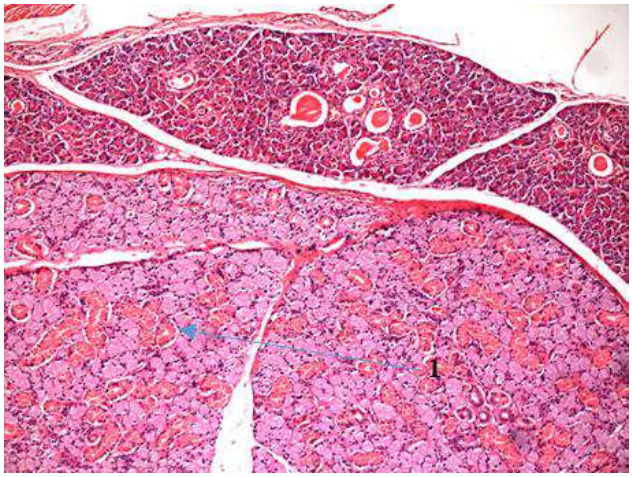

Fig. 2. Morphological changes of pancreatic tissue in conditions of chronic pancreatitis in combination with diabetes. Fibrous tissue growth (1) associated with ductal dysplasia. Hematoxylin-eosin staining, x100.

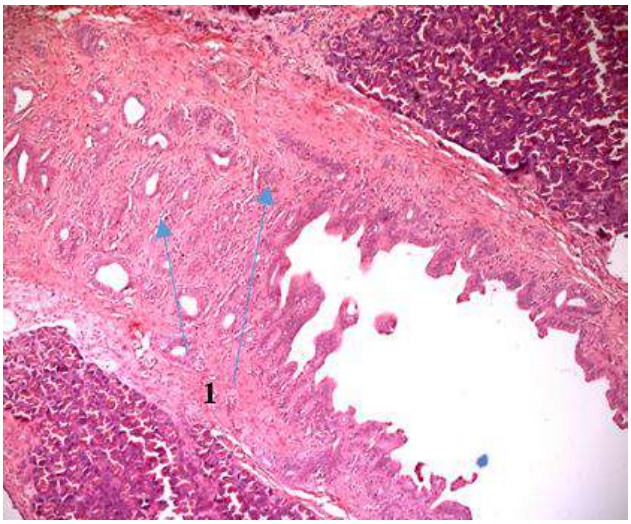

Fig. 3. Morphological changes of pancreatic tissue in conditions of chronic pancreatitis in combination with diabetes. The formation of glands in the fibrous tissue of the duct, the proliferation of the epithelium with its dysplasia and the formation of papillary structures. PanIN 2-3 (1). Staining with hematoxylin-eosin x100.

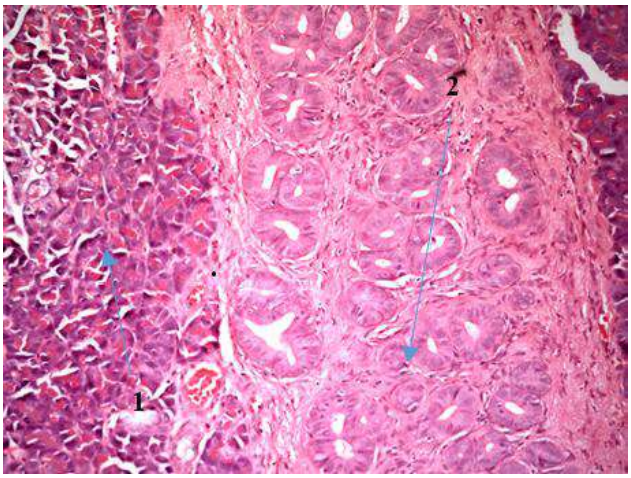

Fig. 4. Morphological changes of pancreatic tissue in conditions of chronic pancreatitis in combination with diabetes. Proliferation of glandular epithelium with severe dysplasia (1), formation of papillary (2), cribrose structures. PanIN 3. Hematoxylin-eosin staining, x400.

increase in the concentration of MMP in the blood plasma of patients with chronic pancreatitis was maximal for the collagenases MMP-1 and MMP-8 and amounted to 80 %, $p<0.05$, further decreasing in the following series: MMP-2 (50 %, $p<0.05$), MMP-3 (42 %, $p<0.05$), MMP-10 (40 %, $p<0.05$). A compensatory increase in the content of TIMP in the systemic circulation was established under conditions of chronic pancreatitis (by 67 %, $p<0.05$). In contrast to chronic pancreatitis, in the presence of pancreatic cancer, the plasma levels of all studied parameters did not reliably differ from those of the control group, probably due to the local involvement of the studied enzymes in the processes of tumorigenesis - precisely at the tissue level, in the place of their secretion, and not in the systemic circulation

These assumptions are consistent with the results obtained by us, when studying the content of MMP and TIMP in pancreatic tissue, according to which the levels of all investigated indicators of patients with both chronic pancreatitis and pancreatic cancer were significantly higher than those in the control group. In chronic pancreatitis, the maximum increase in content was also found for MMP-1 collagenase (3.2 times, $p<0.05$); the levels of other MMPs increased as follows (MMP-8 - by 2.7 times, $p<0.05$; MMP-9 and MMP-10 - by 2.3 times, $p<0.05$; MMP-3 - by 83 %, $p<0.05$; MMP-2 - by 66 % $p<0.05$), and the content of TIMP increased 2.6 times ($p<0.05$). The content of MMP in pancreatic tissue under cancer conditions exceeded the corresponding levels of the control group: gelatinase MMP-9 - 3.3 times ($p<0.05$), stromelysin MMP-10 - 3.1 times ($p<0.05$) and collagenase MMP-8 and MMP-1 - 2.9 times ($p<0.05$), MMP-3 - 2.7 times ($p<0.05$) and MMP-2 - 2.3 times ($p<0.05$). The content of TIMR exceeded the similar indicator of the control group by 3.1 times. At the same time, the levels of MMP-2, -3, -9, -10 and TIMP in the pancreatic tissue of patients with pancreatic cancer were higher than the levels of the corresponding indicators for the group of patients with chronic pancreatitis - by 39 %, 48 %, 43 %, 34 %, 19 %, respectively, $p<0.05$.

The data we obtained regarding the increase in the levels of MMP in the pancreatic tissue of patients with chronic pancreatitis and pancreatic cancer is consistent with the currently available literature data, which indicate the active role of these enzymes in the remodeling of the extracellular matrix, which in the case of chronic pancreatitis contributes to the development of pancreatic fibrosis. and in the presence of pancreatic cancer, it facilitates invasion, angiogenesis and metastasis.

Taking into account the changes in the protein profile of the plasma and pancreatic tissue, total proteolytic activity,

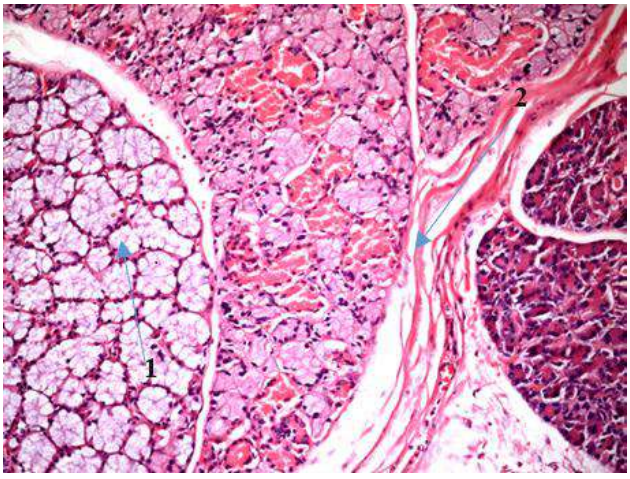

Fig. 5. Morphological changes of pancreatic tissue in conditions of chronic pancreatitis in combination with diabetes. Pronounced acinar metaplasia (1). The appearance of papillary and cribriform structures corresponding to high and moderate ductal dysplasia of the PanIN 2 and PanIN 3 class (2). Hematoxylin-eosin staining. x400.

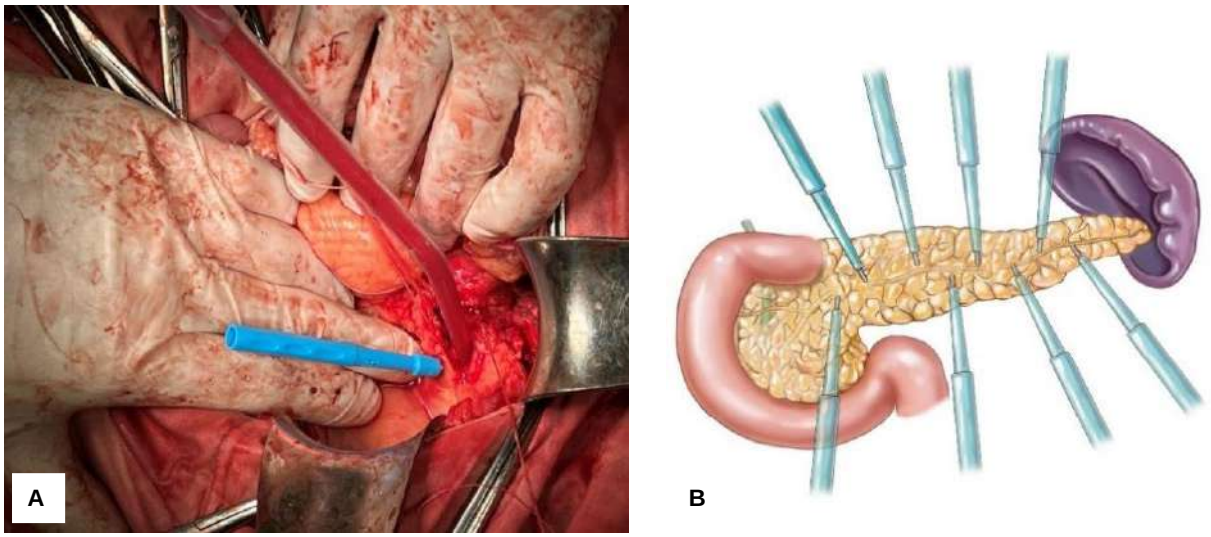

Fig. 6. Multiple punch biopsy of the pancreas. A - intraoperative removal of the pancreas, B - scheme of puncture biopsy.

MMP and serine proteinase activity in the pancreas in the experiment, as well as studying the changes in the blood plasma in the preoperative period of patients at risk, we focused on intraoperative biopsy and diagnosis.

Usually, the surgeon performs the biopsy in the most convenient place for the doctor and the safest place for the patient to ensure the prevention of possible complications (bleeding, acute postoperative pancreatitis, pancreatic fistula). Therefore, from the diagnostic point of view of, the effectiveness of this biopsy and its result are often questionable and ineffective. The possibility of performing a draining operation and forming an anastomosis on already malignantly regenerated tissue is not excluded. Therefore, we improved this method, and the uniqueness and novelty were confirmed by obtaining a certificate of copyright registration. In the case of complicated chronic pancreatitis during surgery, a biopsy is taken with a punch pen along the entire length of the Wirsung duct along its upper and lower edges of the dissection in a chequerwise manner along the entire length of the gland. Thus, during the study, a safe and complete collection of material takes place (Fig. 6).

In the same patients, we implemented scraping from the duct in the proximal and distal directions, which is effective, considering that 95 % of malignant tumors of the pancreas are ductal adenocarcinoma (Figs. 7, 8).

There were no complications of punch biopsy. Patients with fibrotic tissue were included in the study; accordingly, it was safe to obtain a biopsy with a diameter of 2 mm, and the development of postoperative pancreatitis was not established.

Among 15 (55 %) operated patients of the main group, 9 (60 %) were diagnosed with diabetes with changes in MMP and peptide pool, which was characteristic of malignant tissue. Intraoperatively, after performing a punch biopsy, 3 (33 %) were diagnosed with acinar metaplasia, 4 (44 %) had tissue changes characteristic of PanIN 2-PanIN 3, and 2 (23 %) were intraoperatively confirmed to have pancreatic cancer localized in its head. Changes in the protein profile of the plasma, which we determined at the preoperative stage, as well as characteristic changes in the tissue of the pancreas, provided the basis for performing extended resection interventions. Therefore, 5 (30 %)

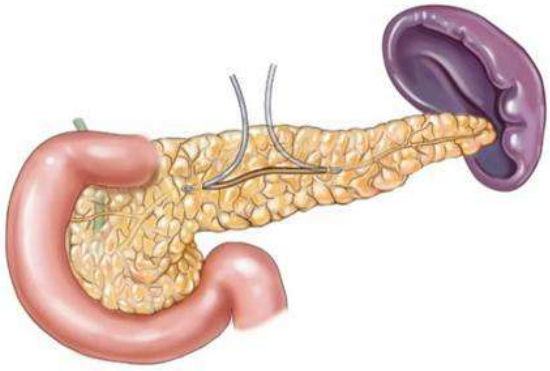

Fig. 7. Schematic representation of the scraping site of the altered pancreatic duct.

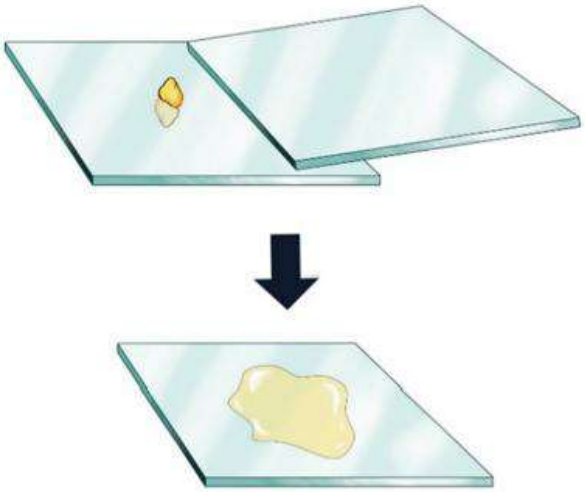

Fig. 8. Cytological express study.

Whipple operations and 6 (40 %) left-sided distal resections were performed. In the remaining four (30 %) patients with complicated chronic pancreatitis, ductal hypertension, pain syndrome, but without suspicion of malignancy, drainage surgery was performed.

Discussion

According to the latest and most up-to-date data from Global Cancer Statistics 2020, pancreatic cancer is a fatal disease characterized by a poor response to treatment and a poor prognosis. A more than 2.5-fold increase in the global annual number of cases has been reported over the past three decades. There were approximately 495,773 and 441,000 newly identified cases of pancreatic cancer worldwide in 2020 and 2017, respectively, compared with 196,000 subjects in 1990. Worldwide, pancreatic cancer has been identified as the leading cause of cancer-related deaths [3, 17, 29]. Therefore, taking into account the social aspects, the relatively low 5-year survival of patients, the study of this problem becomes more relevant every year [7, 20, 25, 27].

In our studies, we obtained similar results to Gao L. with co-authors [8] and Hart P. A. with co-authors [9] confirming the dependence and relationship between chronic pancreatitis and diabetes in an experiment, which where is manifested by more active inflammation and contributes to tumor development.

In a meta-analysis, Ben Q. and co-authors [4] reported a relative risk of pancreatic cancer of 5.4 (95 % CI 3.5-8.3), which is associated with a duration of diabetes of less than 1 year and a moderate risk of its occurrence in about 1.5 times after 5 years of its course. A population-based study conducted in Rochester, Minnesota, USA, found that approximately 1 % of participants with new-onset diabetes aged 50 years or older had diabetes secondary to pancreatic cancer. It is early and comprehensive diagnosis, according to Caban M. and Malecka-Wojciesko E., as well as screening of the disease in the general population and directly in high-risk groups with the use of various biomarkers of pancreatic cancer, that will allow to diagnose the pathology before the appearance of distant metastases and apply radical surgical intervention [5].

Y. Miyashita and co-authors in a long-term cohort study in Japan state that the metabolic syndrome is closely related to the incidence of pancreatic cancer. In 2005, they recruited approximately 4.6 million Japanese subjects and followed these subjects for over 10 years. Metabolic syndrome has been confirmed to be associated with pancreatic cancer. They also demonstrated an association between pre-metabolic syndrome and pancreatic cancer [23].

Patients with chronic fibrotic changes of the pancreas in the background or in combination with diabetes have a significantly higher risk of malignancy of the process and the development of accompanying complications inherent in this disease. The main focus of our research was to concentrate on the intraoperative diagnosis of complicated chronic pancreatitis and to confirm or deny the development of pancreatic cancer. To do this, we performed an intraoperative multiple poly-punch biopsy and scraping of the Wirsung duct with express (intraoperative) diagnosis and determination of further tactics of surgical intervention. We received a certificate of copyright registration for these methods: "Methodology of intraoperative biopsy of the pancreas" No. 115178 and "Methodology of intraoperative multiple biopsies of the pancreas" No. 114856, respectively. The methods are simple, affordable and were the reason for the change in the surgical correction of pancreatic pathology in the direction of increasing the resection volume, which ensured and guaranteed receiving a more radical treatment.

The patients included in the study had pronounced fibrotic changes in the tissue, which were provoked by the activation of pancreatic stellate cells in the early stages of the disease. Pronounced pain syndrome was characteristic of patients with ductal hypertension, which develops under conditions of progression of chronic pancreatitis. According to the latest International consensus recommendations on surgical treatment and timing of intervention in complicated chronic pancreatitis [15] for 2020, there is drainage or combined (drainage + resection) surgery to eliminate ductal hypertension, as well as altered parenchyma, which is the pacemaker of pain, and in suspicion of malignancy of the process. In order to achieve the maximum effect, today we lean towards early surgical interventions. Such operations include Puestow-Gillesby procedure, Frey procedure, Beger procedure, left-distal resection of the pancreas. These operations have long been known and are effective as palliative and symptomatic care for patients with chronic pancreatitis and ductal hypertension. Whipple surgery is indicated for patients with an enlarged head of the pancreas and existing Groove pancreatitis [6, 12, 16, 18].

Thus, thanks to a careful morphological study, the application of as many methods of differential diagnosis between chronic pancreatitis and pancreatic cancer as possible, it is possible to perform the most correct and effective surgical intervention.

Conclusion

1. It has been confirmed that the morphological changes of the pancreatic tissue in rats with chronic pancreatitis in combination with diabetes, corresponding to the development of PanIN, are direct predictors of pancreatic adenocarcinoma. The effectiveness of multiple intraoperative biopsies of the pancreas for the verification of malignant tissue of the pancreas, as well as the high risk of developing pancreatic cancer in complicated and clinically manifest forms of chronic pancreatitis, has been proven.

2. The effectiveness of multiple intraoperative biopsies of the pancreas for the verification of malignant tissue of the pancreas, as well as the high risk of developing pancreatic cancer in complicated and clinically manifest

forms of chronic pancreatitis, has been proven.

3. Using all the described methods of pre- and intraoperative diagnostics, it was possible to optimize the choice of the volume of surgical intervention in complicated forms of chronic pancreatitis in patients with a high risk of developing pancreatic cancer. The obtained results improved the quality and extent of the surgical interventions performed.

References

[1] Algül, H., Treiber, M., Lesina, M., Nakhai, H., Saur, D., Geisler, F., … & Schmid, R. M. (2007). Pancreas-specific RelA/p65 truncation increases susceptibility of acini to inflammation-associated cell death following cerulein pancreatitis. *J. Clin. Invest.*, 117(6), 1490-1501. doi: 10.1172/JCI29882

[2] Amin, K., Khan, H., Hearld, L. R., Chu, D. I., Prete, V., Mehari, K. R., Heslin, M. J., & Fonseca, A. L. (2023). Association between Rural Residence and Processes of Care in Pancreatic Cancer Treatment. *Journal of Gastrointestinal Surgery: Official Journal of the Society for Surgery of the Alimentary Tract*, 27(10), 2155-2165. doi: 10.1007/s11605-023-05764-z

[3] Ansari, D., Tingstedt, B., Andersson, B., Holmquist, F., Sturesson, C., Williamsson, C., … & Andersson, R. (2016). Pancreatic cancer: yesterday, today and tomorrow. *Future Oncology,* 12(16), 1929-1946. doi: 10.2217/fon-2016-0010

[4] Ben, Q., Xu, M., Ning, X., Liu, J., Hong, S., Huang, W., … & Li, Z. (2011). Diabetes mellitus and risk of pancreatic cancer: A meta-analysis of cohort studies. *Eur. J. Cancer,* 47(13), 1928-1937. doi: 10.1016/j.ejca.2011.03.003

[5] Caban, M., & Malecka-Wojciesko, E. (2023). Gaps and Opportunities in the Diagnosis and Treatment of Pancreatic Cancer. *Cancers,* 15(23), 5577. doi: 10.3390/cancers15235577

[6] Committee of the Korean clinical practice guideline for pancreatic cancer and National Cancer Center, Korea (2021). Korean clinical practice guideline for pancreatic cancer 2021: A summary of evidence-based, multi-disciplinary diagnostic and therapeutic approaches. *Pancreatology,* 21(7), 1326-1341. doi: 10.1016/j.pan.2021.05.004

[7] Gallegos, J. M., Taylor, A., Vardell, V., & Silberstein, P. T. (2023). Socioeconomic Factors Associated With a Late-Stage Pancreatic Cancer Diagnosis: An Analysis of the National Cancer Database. *Cureus,* 15(3), e35857. doi: 10.7759/cureus.35857

[8] Gao, L., Lu, G. T., Lu, Y. Y., Xiao, W. M., Mao, W. J., Tong, Z. H., … Li, W. Q. (2018). Diabetes aggravates acute pancreatitis possibly via activation of NLRP3 inflammasome in db/db mice. *Am. J. Transl. Res.,* 10(7), 2015-2025. PMID: 30093939

[9] Hart, P. A., Bellin, M. D., Andersen, D. K., Bradley, D., Cruz-Monserrate, Z., Forsmark, C. E., … & Chari, S. T. (2016). Consortium for the Study of Chronic Pancreatitis, Diabetes, and Pancreatic Cancer (CPDPC). Type 3c (pancreatogenic) diabetes mellitus secondary to chronic pancreatitis and pancreatic cancer. *Lancet Gastroenterol Hepatol.,* 1(3), 226-237. doi: 10.1016/S2468-1253(16)30106-6

[10] Hessmann, E., Zhang, J. S., Chen, N. M., Hasselluhn, M., Liou, G. Y., Storz, P., … & Koenig, A. (2016). NFATc4 Regulates Sox9 Gene Expression in Acinar Cell Plasticity and Pancreatic Cancer Initiation. *Stem Cells Int.,* 2016, 5272498. doi: 10.1155/2016/5272498

[11] Illés, D., Terzin, V., Holzinger, G,. Kosár, K., Róka, R., Zsóri, G. …& Czakó, L. (2016). New-onset type 2 diabetes mellitus - A high-risk group suitable for the screening of pancreatic cancer? *Pancreatology,* 16(2), 266-271. doi: 10.1016/j.pan.2015.12.005

[12] Jablońska, B., & Mrowiec, S. (2023). Pancreatectomy and Pancreatic Surgery. *Life*, 13(6), 1400. doi: 10.3390/life13061400

[13] Kandikattu, H. K., Venkateshaiah, S. U., & Mishra, A. (2020). Chronic Pancreatitis and the Development of Pancreatic Cancer. *Endocr. Metab. Immune Disord. Drug Targets*, 20(8), 1182-1210. doi: 10.2174/1871530320666200423095700

[14] Ke, T. M., Lophatananon, A., & Muir, K. R. (2022). Risk Factors Associated with Pancreatic Cancer in the UK Biobank Cohort. *Cancers,* 14(20), 4991. doi: 10.3390/cancers14204991

[15] Kempeneers, M. A., Issa, Y., Ali, U. A., Baron, R. D., Besselink, M. G., Büchler, M., … & Boermeester, M. A. (2020). Working group for the International (IAP - APA - JPS - EPC) Consensus Guidelines for Chronic Pancreatitis. International consensus guidelines for surgery and the timing of intervention in chronic pancreatitis. *Pancreatology,* 20(2), 149-157. doi: 10.1016/j.pan.2019.12.005

[16] Kim, H. S., Hong, T. H., You, Y. K., Park, J. S., & Yoon, D. S. (2021). Radical antegrade modular pancreatosplenectomy (RAMPS) versus conventional distal pancreatectomy for left-sided pancreatic cancer: findings of a multicenter, retrospective, propensity score matching study. Surgery *Today,* 51(11), 1775-1786. doi: 10.1007/s00595-021-02280-y

[17] Klein, A. P. (2021). Pancreatic cancer epidemiology: understanding the role of lifestyle and inherited risk factors. Nature reviews. *Gastroenterology & Hepatology,* 18(7), 493-502. doi: 10.1038/s41575-021-00457-x

[18] Lee, S. E., Han, S. S., Kang, C. M., Kwon, W., Paik, K. Y., Song, K. B., … & Kim, S. W. (2022). Korean Surgical Practice Guideline for Pancreatic Cancer 2022: A summary of evidence-based surgical approaches. Annals of Hepatobiliary Pancreat. *Surgery,* 26(1), 1-16. doi: 10.14701/ahbps.22-009

[19] Liao, K. F., Lai, S. W., Li, C.I., & Chen, W. C. (2012). Diabetes mellitus correlates with increased risk of pancreatic cancer: a population-based cohort study in Taiwan. *J. Gastroenterol. Hepatol.,* 27(4):709-13. doi: 10.1111/j.1440-1746.2011.06938.x

[20] Lucas, A. L., & Kastrinos, F. (2019). Screening for Pancreatic Cancer. JAMA, 322(5), 407-408. doi: 10.1001/jama.2019.9690

[21] Lundberg, R., Beilman, G. J., Dunn, T. B., Pruett, T. L., Freeman, M. L., Ptacek, P. E., ... & Bellin, M. D. (2016). Early alterations in glycemic control and pancreatic endocrine function in non-diabetic patients with chronic pancreatitis. *Pancreas,* 45(4), 565. doi: 10.1097/MPA.0000000000000491

[22] Midha, S., Chawla, S., & Garg, P. K. (2016). Modifiable and non-modifiable risk factors for pancreatic cancer: A review. *Cancer Lett.,* 381(1), 269-277. doi: 10.1016/j.canlet.2016.07.022

[23] Miyashita, Y., Hitsumoto, T., Fukuda, H., Kim, J., Ito, S., Kimoto, N., … & Kitakaze, M. (2023). Metabolic syndrome is linked to the incidence of pancreatic cancer. *eClinicalMedicine*, 67, 102353. doi: 10.1016/j.eclinm.2023.102353

[24] Ogawa, Y., Tanaka, M., Inoue, K., Yamaguchi, K., Chijiiwa, K., Mizumoto, K., … & Nakamura, Y. (2002). A prospective pancreatographic study of the prevalence of pancreatic carcinoma in patients with diabetes mellitus. *Cancer,* 94(9), 2344-2349. doi: 10.1002/cncr.10493

[25] Poulson, M. R., Papageorge, M. V., LaRaja, A. S., Kenzik, K. M., & Sachs, T. E. (2023). Socioeconomic Mediation of Racial Segregation in Pancreatic Cancer Treatment and Outcome

Disparities. *Annals of surgery,* 278(2), 246-252. doi: 10.1097/SLA.0000000000005543
[26] Roy, A., Sahoo, J., Kamalanathan, S., Naik, D., Mohan, P., & Kalayarasan, R. (2021). Diabetes and pancreatic cancer: Exploring the two-way traffic. *World J. Gastroenterol.,* 27(30), 4939-4962. doi: 10.3748/wjg.v27.i30.4939
[27] Saad, A. M., Gad, M. M., Al-Husseini, M. J., AlKhayat, M. A., Rachid, A., Alfaar, A. S., & Hamoda, H. M. (2019). Suicidal death within a year of a cancer diagnosis: A population-based study. *Cancer,* 125(6), 972-979. doi: 10.1002/cncr.31876
[28] Singhi, A. D., Koay, E. J., Chari, S. T., & Maitra, A. (2019). Early Detection of Pancreatic Cancer: Opportunities and Challenges. *Gastroenterology,* 156(7), 2024-2040. doi: 10.1053/j.gastro.2019.01.259
[29] Sung, H., Ferlay, J., Siegel, R. L., Laversanne, M., Soerjomataram, I., Jemal, A., & Bray, F. (2021). Global Cancer Statistics 2020: GLOBOCAN Estimates of Incidence and Mortality Worldwide for 36 Cancers in 185 Countries. *CA: A Cancer Journal for Clinicians,* 71(3), 209-249. doi: 10.3322/caac.21660
[30] Williams, J. A. (2010). Regulation of acinar cell function in the pancreas. *Curr. Opin. Gastroenterol.*, 26(5), 478-483. doi: 10.1097/MOG.0b013e32833d11c6
[31] Zhao, Z., & Liu, W. (2020). Pancreatic Cancer: A Review of Risk Factors, Diagnosis, and Treatment. *Technology in Cancer Research & Treatment*, 19. doi: 10.1177/1533033820962117

ОПТИМІЗАЦІЯ ВИБОРУ ОБ'ЄМУ ОПЕРАТИВНОГО ВТРУЧАННЯ ПРИ ВИРАЖЕНИХ МОРФОЛОГІЧНИХ ТА СТРУКТУРНИХ ЗМІНАХ ПАРЕНХІМИ У ПАЦІЄНТІВ З ВИСОКИМ РИЗИКОМ РОЗВИТКУ РАКУ ПІДШЛУНКОВОЇ ЗАЛОЗИ

Усенко О. Ю., Петрушенко В. В., Суходоля С. А., Суходоля А. І., Савчук О. М., Радьога Я. В., Савчук І. І.

Хронічний панкреатит є поширеною рецидивною патологією підшлункової залози. Тривалий перебіг запального процесу, що супроводжується хронізацією, призводить до розвитку раку підшлункової залози. Мета роботи - вивчити морфологічні зміни підшлункової залози у щурів та рівень матриксних металопротеїназ і тканинного інгібітора металопротеїназ у пацієнтів з ускладненими формами хронічного панкреатиту та високим ризиком розвитку раку підшлункової залози для оптимізації вибору об'єму оперативного втручання. Проведено гістологічне дослідження підшлункової залози щурів із хронічним панкреатитом та хронічним панкреатитом на фоні цукрового діабету. Обстежено 27 пацієнтів, прооперованих впродовж 2020-2022 рр. З них у 15 чітко та переконливо віддиференціювати хронічний панкреатит від раку підшлункової залози ми не змогли, тому що досить часто клінічні симптоми та діагностична картина цих захворювань практично однакова. У решти 12 пацієнтів хронічний панкреатит був підтверджений усіма притаманними клінічними ознаками та наявною протоковою гіпертензією. Проведено дослідження матриксних металопротеїназ (MMP-1, -2, -3, -8, -9, -10) та тканинного інгібітора металопротеїназ. Отримані результати були оброблені статистично. Морфологічні зміни підшлункової залози у щурів відповідають високій і помірній дисплазії протоки класу PanIN 2 і PanIN 3, що є прямими предикторами аденокарциноми підшлункової залози. У 22 пацієнтів встановлена екзокринна недостатність середнього та важкого ступенів, підтверджена значним зниженням фекальної еластази. Була проведена інтраопераційна біопсія зміненої тканини підшлункової залози. Серед 15 прооперованих пацієнтів основної групи у 9 діагностували цукровий діабет, зміну MMTs та пептидного пулу, що притаманно малігнізованій тканині. Інтраопераційно після проведення панч-біопсії у 3 пацієнтів виявлено ацинарну метаплазію, у 4 - зміни у тканині, характерні для PanIN2-PanIN3, у 3 - інтраопераційно підтверджений рак підшлункової залози у ділянці головки. Зміни у білковому профілі плазми, клінічні прояви, а також характерні зміни у тканині підшлункової залози давали підстави для виконання розширених резекційних втручань. Вивчення морфологічної структури підшлункової залози, застосування якомога більше методів для диференційної діагностики між хронічним панкреатитом та раком підшлункової залози, а також комплексний підхід до пацієнта дозволить виконати найбільш правильне та ефективне втручання.

Ключові слова: *підшлункова залоза, морфологічні зміни, хронічний панкреатит, фіброз, протокова аденокарцинома підшлункової залози.*

Author's contribution

Usenko O. Yu. - conceptualization of research.
Petrushenko V. V. - formal data analysis and verification.
Sukhodolia A. I. - research conceptualization, article editing.
Sukhodolia S. A. - writing an original project and creating a database, statistical processing and formal data analysis.
Savchuk O. M. - database creation, formal analysis and data validation.
Radoga Ia. V. - software, resourses.
Savchuk I. I. - statistical data processing and article editing.

DOI: 10.31393/morphology-journal-2024-30(1)-07 Reports of Morphology, Vol. 30, №1, Pages 55-60

ISSN 1818-1295 eISSN 2616-6194

REPORTS OF MORPHOLOGY

Official Journal of the Scientific Society of Anatomists, Histologists, Embryologists and Topographic Anatomists of Ukraine

journal homepage: https://morphology-journal.com

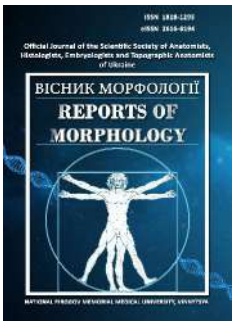

Changes of rat's brain vesseles after air shock wave exposure

Kozlova Yu. V., Kozlov S. V., Maslak H. S., Bondarenko O. O., Dunaev O. V., Oberemok M. H.
Dnipro State Medical University, Dnipro, Ukraine

ARTICLE INFO
Received: 12 December 2023
Accepted: 22 January 2024

UDC: 616.831-001:623.565:616.13/.14]-018-091.8-092.9

CORRESPONDING AUTHOR
e-mail: kozlova_yuv@ukr.net
Kozlova Yu. V.

CONFLICT OF INTEREST
The authors have no conflicts of interest to declare.

FUNDING
Not applicable.

DATA SHARING
Data are available upon reasonable request to corresponding author.

Mild blast-induced traumatic brain injury is common among the military, resulting in cognitive impairment, reduced socialization, which leads to disability and, as a result, a deterioration in the quality of life. It is considered that blood-brain barrier disruption and microvascular dysfunction are the key to this type of injury. The purpose of study was to study changes in brain vessels after air shock wave exposure. The study was carried out on 48 mature male Wistar rats, which were randomly divided into 2 groups: an experimental group, in which animals were subjected to inhalation anesthesia using halothane and exposed to a shock wave with an overpressure of 26.4±3.6 kPa, and a Sham group. After simulation of injury on days 1st, 3rd, 7th, 14th, and 21st, the rats were euthanized and the brain was removed and after all subjected to standard histological procedures and stained with hematoxylin and eosin. For immunohistochemical studies, as primary antibodies were used eNOS. The finished preparations were examined by light microscopy and photographed. Disorders of the cerebral vessels in experimental rats were detected from day 1st of the posttraumatic period. It was found that the blast wave led to vascular rupture, as well as increased vascular permeability with diapedesis of red blood cells and cerebral edema for up to 21st days. Focal violations of the vascular wall integrity in cortical and hippocampal hemocapillaries, venular link of the submembrane vessels; changes in the morphology of the metabolic vessels endothelium; uneven blood filling of the brain vessels were of major importance. These changes indicate that increased eNOS expression leads to dilation of cerebral vessels, which is a compensatory mechanism in response to injury to improve cerebral blood circulation. However, eNOS is not involved in vasodilation, which we observed up to 21st day post-trauma.

Key words: *blood-brain barrier, explosion, trauma, brain, blood vessels.*

Introduction

In the context of military operations, terrorist attacks or man-made disasters, the number of injuries caused by explosions is increasing [18, 22]. Depending on many factors, including the body position and distance from the explosion, different organs injuries occur with varying degrees of severity. The most sensitive to the blast wave are lungs, eardrum and brain [7]. Mild blast-induced traumatic brain injury is a common phenomenon among military, leading to cognitive impairment, reduced socialization and disability, as well as a deterioration in quality of life [9]. Therefore, in order to improve medical and social assistance to the victims of the explosion, it is necessary to find out the mechanisms of brain damage.

Despite the fact that the exact pathophysiological mechanisms of blast injuries are not yet fully understood, it is known that the blast wave is the main pathogenic factor in such injuries [11]. Numerous studies show that when a blast wave hits the head, part of the energy is reflected from the skull bones, and the part that passes through the tissues extremely excites the phonon continuum, which leads to brain cells damage at the subcellular level [24]. After the primary injury, a wide range of pathobiochemical reactions of secondary alteration are triggered, including the release of pro- and inflammatory mediators, the development of oxidative stress, etc. [19, 32]. Many histopathological studies clearly indicate a blood-brain barrier disorder [14]. Is considered that blood-brain barrier disruption and microvascular dysfunction are key factors in the course of blast-induced traumatic brain injury and further development of neurodegeneration [5, 30]. However, studies of these changes pathogenesis are multidirectional, which does not provide a holistic picture and requires further research on this issue. A well-known factor in the regulation of cerebral blood vessels is eNOS,

the increase or decrease of which lead to vascular tone and permeability changes [10]. Lots of studies on eNOS in cerebrovascular disorders have shown that eNOS deficiency leads to dysregulation of systemic blood pressure and a decrease of the blood-brain barrier protective function [6, 25]. While the increase in eNOS content performs a protective function by improving the removal of toxic substances and excess fluid from the brain [1].

The purpose of the study is to investigate changes in brain vessels after exposure by an air shock wave.

Materials and methods

The work was carried out as the framework of the planned initiative research topic of the Pathological Anatomy, Forensic Medicine and Pathological Physiology Department of Dnipro State Medical University "Mechanisms of changes formation in the central nervous system after exposure to extreme factors", state registration number 0120U105394.

The study was carried out on 48 sexually mature male Wistar rats weighing 220-270 g, aged 6-7 months. The animals were kept in standard conditions and on a standard diet at the vivarium of the Dnipro State Medical University. All studies were conducted in accordance with modern international requirements and standards for the humane treatment of animals (Council of Europe Convention of 18.03.1986 (Strasbourg), the 1975 Helsinki Declaration, revised and supplemented in 2000, Law of Ukraine, February 21, 2006 No. 3447-IV), as evidenced by an extract from the meeting of the Biomedical Ethics Commission of Dnipro State Medical University minutes No. 3, November 2, 2021.

The selected rats were randomly divided into two groups: group I - experimental (n=24), animals of which were subjected to inhalation anesthesia with halothane (Halothan Hoechst AG, Germany), fixed in a horizontal position on the abdomen with the head to the muzzle cut at a distance of 5 cm and simulated blast brain injury by generating a shock wave with an overpressure of 26.4± 3.6 kPa on a self-made device (Ukraine patent № 146858). The overpressure was measured using an electronic manometer BIT02B-10B (AEP transducers, Italy). And group II - sham (n=24). After simulation of mild blast-induced traumatic brain injury on 1st, 3rd, 7th, 14th, and 21st days, rats were euthanized with a lethal dose of halothane, and then brains were removed. Subsequently, the material was fixed in a 10 % formalin solution (pH 7.4) for at least 24 hours at room temperature [27]. The infiltration process was performed on a Microm STP-120 histoprocessor (Thermo Fisher Scientific, Germany). The samples were dehydrated in increasing concentrations of isopropanol (70 %, 80 %, 95 %, and in three steps in 100 % for 90 min per step 1). After that, the tissues were embedded in paraffin blocks using a HistoStar embedding station (Thermo Fisher Scientific, USA). Serial sections of no more than 4 μm thickness were obtained from the blocks using a Thermo HM 355S microtome (Thermo Fisher Scientific, Germany). Sections of each tissue sample were used for general histological tissues staining with hematoxylin and eosin [27].

For immunohistochemical study, 4 μm thick sections were applied to Superfrost adhesive slides (Thermo, Germany), then they were deparaffinized with xylene and dehydrated. The activity of endogenous peroxidase was blocked with a 3 % solution of hydrogen peroxide in 70 % methanol for 20 min at room temperature.

Then the sections were washed in three steps with sodium phosphate buffer followed by heat-induced antigen retrieval (HIAR) by heating in a water bath in citrate buffer with pH 6.0 or tris-EDTA buffer with pH 9.0 (20 minutes after reaching a temperature of 98°C) with symmetrical arrangement of slides in the cuvette with the addition of 2 ml of Triton-X100 detergent (Sigma, Germany) per 200 ml of buffer [27].

After washing in three steps with sodium phosphate buffer, the slides were placed on a moistened plate and incubated with a 1 % blocking serum solution (normal goat serum) in 1 % BSA (bovine serum albumin) for 20 minutes. Antibodies to endothelial NO synthase, eNOS (clone M221, dilution 1:400, Abcam, UK) were used as primary antibodies.

Sections were incubated with primary antibodies in a humid chamber at 40 0C overnight. Visualization was performed using the Master Polymer Plus Detection System reagent kit (Master Diagnostica, Spain), which was completed by the reaction of DAB chromogen with hydrogen peroxide in the presence of horseradish peroxidase with the formation of a brown color at the sites of binding of diagnostic antibodies to test markers [27]. For the nuclei background staining, sections were additionally stained with Gill's hematoxylin for 30 seconds. Then they were dehydrated in increasing concentrations of alcohol, cleared in xylene, and placed in the final medium under a coverslip.

Microscopy of histological specimens was performed using an Axio Imager 2 microscope (Zeiss, Germany) at x100 and x200 magnification.

Results

Brain cells have a high level of metabolic processes [17], which requires adequate arterial blood supply and venous outflow (Fig. 1).

The cerebral vessels network is strictly regulate the penetration of substances from the vessels into the brain and ensures the outflow of metabolic products [9]. Disorders of cerebral vessels, the wall of which is a component of the blood-brain barrier, were observed in experimental rats throughout the study period starting from 1st day (Fig. 2).

Among the changes that occurred in the brain vessels after exposure to an air shock wave during the posttraumatic period, the leading role was played by focal violations of the vascular wall integrity in cortical and hippocampal hemocapillaries, the venular link of the subcortical vessels;

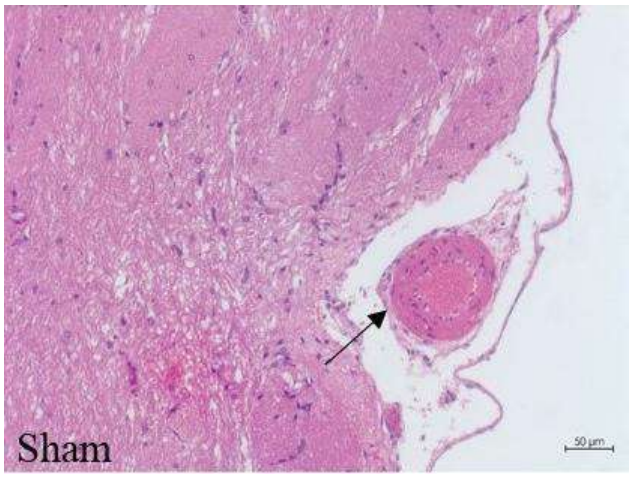

Fig. 1. Cross histological section of the subclavian subpial artery of the sham rat brain. The arrow points to the cerebral vessel. Staining: hematoxylin and eosin, magnification x200.

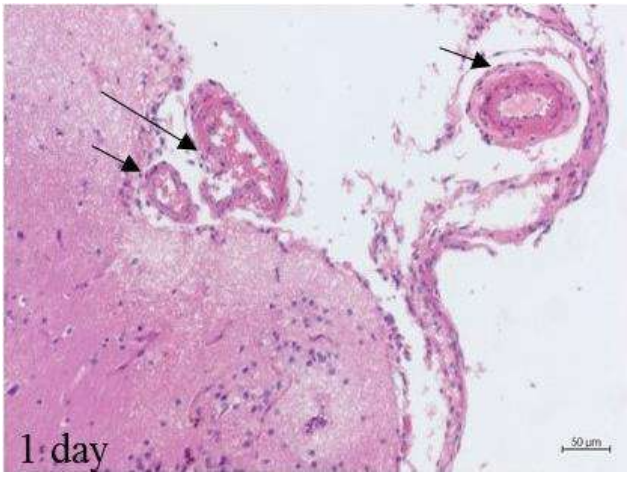

Fig. 2. Subpial vessels of the experimental rat brain (1st day). The arrow points to the cerebral vessels that underwent changes due to the blast wave. Venule wall rupture. Staining: hematoxylin and eosin, magnification x200.

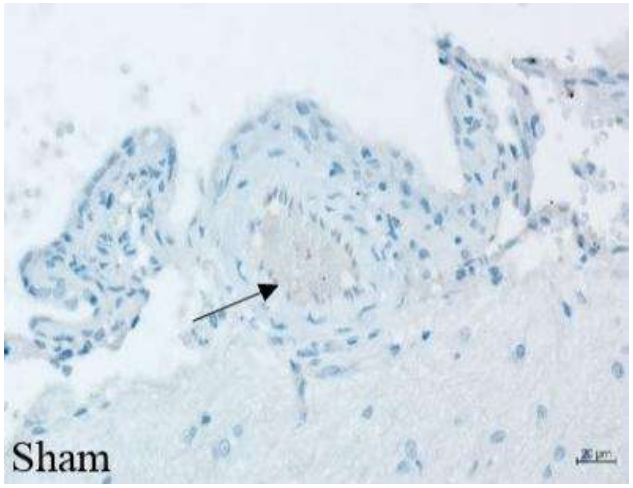

Fig. 3. Expression of eNOS in brain vessels of sham rats. The arrow indicates a brain vessel with low eNOS expression. Magnification x200.

changes in the morphology of the metabolic vessels endothelium; and uneven blood filling of the brain vessels. Violation of the vessel wall integrity was accompanied by the appearance of diapedesis and small-focal hemorrhages, neutrophil release and formation of perivascular infiltrates of polymorphonuclear cells on 1st day (see Fig. 2) and persisted up to 7th day in the group of experimental animals. By the end of the third week of the experiment, we recorded uneven blood filling of the microcirculatory system vessels on histological preparations of the brain, which was due to impaired hemocapillary patency due to endothelial cell edema and impaired rheological properties of blood with the formation of stasis and aggregation of blood cells. Also, the patency of the hemocapillary bed was affected by perivascular edema, which increased in the first week of the posttraumatic period.

Due to the observed impairment of blood-brain barrier permeability, vascular wall integrity, and regional blood

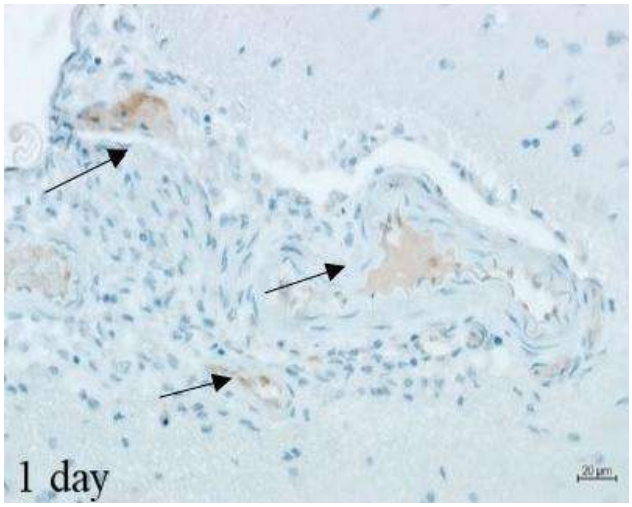

Fig. 4. Expression of eNOS in the brain vessels of the experimental group rats on 1st day of the posttraumatic period. Arrow indicates brain vessels with moderate eNOS expression. Magnification x200.

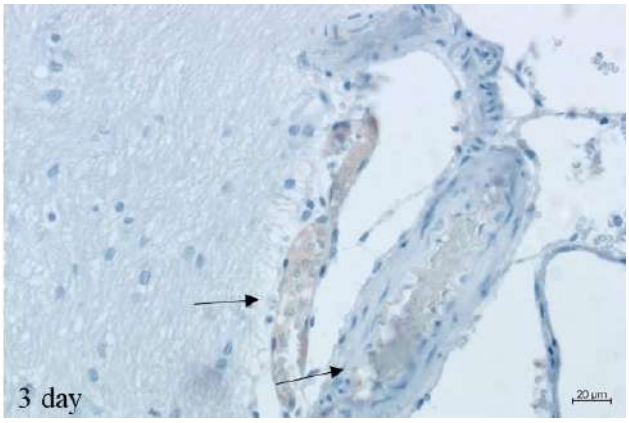

Fig. 5. Expression of eNOS in the brain vessels of the experimental group rats on 3rd day of the posttraumatic period. The arrow indicates the brain vessels with eNOS expression. Magnification x200.

supply in rats with mild blast-induced traumatic brain injury, it was decided to investigate the degree of eNOS expression as the hypoxia and ischemia marker.

A slight expression of eNOS was detected in the samples of the sham group rats (Fig. 3).

Comparison of the results of immunohistochemical detection of eNOS in the brain vessels showed the presence of this enzyme expression in the endothelium of the brain vessels of experimental rats on 1st day (Fig. 4) and 3rd day (Fig. 5).

The shape of the vessels, in the endothelial cells of which we noted the expression of eNOS, was corrugated, and some vessels were paretic dilated or collapsed (see Figs. 4, 5).

In the dynamics of the further course of the posttraumatic period, the degree of eNOS expression in the brain vessels of the experimental group rats did not differ from that of the sham group.

Discussion

The studied and established consequences of mild blast-induced traumatic brain injury in the acute period are disruption of the blood-brain barrier, which leads to energy and metabolic changes, as well as cerebral edema [3]. Most scientists thought that these changes underlie the cognitive functions of the brain and the subsequent development of neurodegeneration [18]. In the case of mild blast-induced traumatic brain injury, which was simulated using our own device, we found vascular wall disorders with diapedesis hemorrhages, the nonruptured vessels wall edema, and cerebral edema resulting from blood-brain barrier dysfunction. Such changes in blood-brain barrier vessels are associated with direct compressive shock wave loading and indirect cavitation, which together lead to overstretching and detachment of endothelial cell membranes [30].

We also found the brain itself diffuse damage, which causes an inflammatory process involving neutrophils. Comparing our results with previous studies which are showing an existing systemic cytokine response to mild blast-induced traumatic brain injury, we think that an active inflammatory response is unfolding [21, 23, 27]. All of these changes, both individually and in combination, require the launch of compensatory mechanisms to maintain the brain functional activity [13]. However, the mechanisms of both blood-brain barrier dysfunction and recovery have not been thoroughly investigated. Thus, there is a need for their in-depth study.

Vascular tone ensures adequate blood supply of the brain, the regulation of which is complex and clearly controlled by the nervous and humoral systems. Among the numerous regulatory systems, it is important to understand the function of the endothelium, which affects the tone of the brain vessels both chemically and through interaction with neurons. This complex allows not only to regulate vascular tone, but also to control the permeability of the blood-brain barrier [2, 16].

Among the chemical factors involved in the regulation of cerebral vascular tone, eNOS is known to be involved in brain protection during various acute cerebrovascular disorders, including traumatic brain injuries of various genesis [8]. Endothelial nitric oxide synthase is a membrane-binding enzyme and the main source of NO, which is a secondary messenger of guanylyl cyclase-related receptor activation in the central nervous system and is involved in autoregulation of cerebral blood flow and regulation of neuronal plasticity [15].

Many literature sources have shown that increased eNOS activity is a protective mechanism that is realized in response to, at least, the synthesis of pro- and inflammatory cytokines, the development of oxidative stress [24, 26, 30]. After all, NO, which is an autocrine and paracrine signaling factor, leads to dilatation of the brain arterial vessels and also has antithrombotic effects. These properties help to improve the brain blood supply [28, 31]. However, there is evidence to suggest a negative effect of increased eNOS activity. Nevertheless, eNOS promotes vasodilation and increased permeability, which leads to the entry of pro- and inflammatory mediators into the brain, which increases inflammation itself [20].

We consider that eNOS activation occurs when blood-brain barrier vessels are disrupted and it is one of the compensatory mechanisms in response to primary and secondary damage, in particular, to the development of oxidative stress. It is known that mild blast-induced traumatic brain injury leads to mitochondria primary damage and, as a result, free radicals are formed. Subsequently, due to blood-brain barrier damage, hypoxia occurs, which also contributes to free radicals formation. Taken together, oxidative stress itself leads to endothelial dysfunction and eNOS activation [20]. After all, NO is known to have antioxidant properties due to its ability to reduce the formation of superoxide anion by activating superoxide dismutase [12]. However, as our study showed, this occurs only on 1st and 3rd days after simulation of mild blast-induced traumatic brain injury. Next, obviously, in the pathogenesis of vascular wall dilation involve other mechanisms that need to be further investigated.

Conclusions

1. As a result of the blast wave exposure disorders of the cerebral vessels were detected.

2. An increase in eNOS expression in the cerebral vessels of rats with mild blast-induced traumatic brain injury on 1st and 3rd days of the posttraumatic period was found in comparison with sham rats.

3. These changes indicate that increased eNOS expression leads to cerebral vasodilation, which is a compensatory mechanism in trauma response to improve cerebral circulation. However, eNOS is not involved in vasodilation, which we observed up to 21st days post-trauma.

References

[1] An, L., Shen, Y., Chopp, M., Zacharek, A., Venkat, P., Chen, Z., … & Chen, J. (2021). Deficiency of endothelial nitric oxide synthase (enos) exacerbates brain damage and cognitive deficit in a mouse model of vascular dementia. *Aging Dis.,* 12(3), 732-746. doi: 10.14336/AD.2020.0523

[2] Ashby, J. W., & Mack, J. J. (2021). Endothelial control of cerebral blood flow. *Am. J. Pathol.,* 191(11), 1906-1916. doi: 10.1016/j.ajpath.2021.02.023

[3] Badaut, J., Ajao, D. O., Sorensen, D. W., Fukuda, A. M., & Pellerin, L. (2015). Caveolin expression changes in the neurovascular unit after juvenile traumatic brain injury: signs of blood-brain barrier healing? *Neuroscience,* 285, 215-216. doi: 10.1016/j.neuroscience.2014.10.035

[4] Boyko, M., Gruenbaum, B. F., Frank, D., Natanel, D., Negev, S., Azab, A. N., … & Zlotnik, A. (2023). The integrity of the blood-brain barrier as a critical factor for regulating glutamate levels in traumatic brain injury. *Int. J. Mol. Sci.*, 24(6), 5897. doi: 10.3390/ijms24065897

[5] Bulnes, S., Argandoña, E. G., Bengoetxea, H., Leis, O., Ortuzar, N., & Lafuente, J. V. (2010). The role of eNOS in vascular permeability in ENU-induced gliomas. *Acta Neurochir.* Suppl., 106, 277-282. doi: 10.1007/978-3-211-98811-4_52

[6] Chen, X., Chen, L., Lin, G., Wang, Z., Kodali, M. C., Li, M., … & Liao, F. F. (2022). White matter damage as a consequence of vascular dysfunction in a spontaneous mouse model of chronic mild chronic hypoperfusion with eNOS deficiency. *Mol. Psychiatry,* 27(11), 4754-4769. doi: 10.1038/s41380-022-01701-9

[7] Denny, J. W., Dickinson, A. S., & Langdon, G. S. (2021). Defining blast loading 'zones of relevance' for primary blast injury research: a consensus of injury criteria for idealised explosive scenarios. *Med. Eng. Phys.*, 93, 83-92. doi: 10.1016/j.medengphy.2021.05.014

[8] Hafez, S., Khan, M. B., Awad, M. E., Wagner, J. D., & Hess, D. C. (2020). Short-term acute exercise preconditioning reduces neurovascular injury after stroke through induced eNOS activation. *Transl. Stroke Res.*, 11(4), 851-860. doi: 10.1007/s12975-019-00767-y

[9] Howlett, J. R., Nelson, L. D., & Stein, M. B. (2022). Mental health consequences of traumatic brain injury. *Biol. Psychiatry,* 91(5), 413-420. doi: 10.1016/j.biopsych.2021.09.024

[10] Huang, L., Cheng, F., Zhang, X., Zielonka, J., Nystoriak, M. A., Xiang, W., … & Wang, R. A. (2023). Nitric oxide synthase and reduced arterial tone contribute to arteriovenous malformation. *Sci. Adv.,* 21(9), eade7280. doi: 10.1126/sciadv.ade7280

[11] Iacono, D., Murphy, E. K., Stimpson, C. D., Leonessa, F., & Perl, D. P. (2023). Double blast wave primary effect on synaptic, glymphatic, myelin, neuronal and neurovascular markers. *Brain Sci.,* 13(2), 286. doi: 10.3390/brainsci13020286

[12] Janaszak-Jasiecka, A., Ploska, A., Wierońska, J. M., Dobrucki, L. W., & Kalinowski, L. (2023). Endothelial dysfunction due to eNOS uncoupling: molecular mechanisms as potential therapeutic targets. *Cell Mol. Biol. Lett.,* 28(1), 21. doi: 10.1186/s11658-023-00423-2

[13] Kadry, H., Noorani, B., & Cucullo, L. (2020). A blood-brain barrier overview on structure, function, impairment, and biomarkers of integrity. *Fluids Barriers CNS*, 17(1), 69. doi: 10.1186/s12987-020-00230-3

[14] Kawoos, U., Abutarboush, R., Gu, M., Chen, Y., Statz, J. K., Goodrich, S. Y., & Ahlers, S. T. (2021). Blast-induced temporal alterations in blood-brain barrier properties in a rodent model. *Sci. Rep.,* 11(1), 5906. doi: 10.1038/s41598-021-84730-8

[15] Langen, U. H., Ayloo, S., & Gu, C. (2019). Development and cell biology of the blood-brain barrier. *Ann. Rev. Cell. Dev. Biol.,* 35, 591-613. doi: 10.1146/annurev-cellbio-100617-062608

[16] Lansdell, T. A., Chambers, L. C., & Dorrance, A. M. (2022). Endothelial cells and the cerebral circulation. *Compr. Physiol.,* 12(3), 3449-3508. doi: 10.1002/cphy.c210015

[17] Liao, F. F., Lin, G., Chen, X., Chen, L., Zheng, W., Raghow, R., … & Tan, X. L. (2021). Endothelial nitric oxide synthase-deficient mice: a model of spontaneous cerebral small-vessel disease. *Am. J. Pathol.*, 191(11), 1932-1945. doi: 10.1016/j.ajpath.2021.02.022

[18] Liu, M., Zhang, C., Liu, W., Luo, P., Zhang, L., Wang, Y., … & Fei, Z. (2015). A novel rat model of blast-induced traumatic brain injury simulating different damage degree: implications for morphological, neurological, and biomarker changes. *Front. Cell Neurosci.*, 9, 168. doi: 10.3389/fncel.2015.00168

[19] Ma, J., Xiao, W., Wang, J., Wu, J., Ren, J., Hou, J., … & Yu, B. (2016). Propofol inhibits NLRP3 inflammasome and attenuates blast-induced traumatic brain injury in rats. Inflammation, 39(6), 2094-2103. doi: 10.1007/s10753-016-0446-8

[20] Nakayama, K., & Hasegawa, H. (2022). Blood vessels as a key mediator for ethanol toxicity: implication for neuronal damage. *Life* (Basel), 12(11), 1882. doi: 10.3390/life12111882

[21] Norris, C., Weatherbee, J., Murphy, S. F., & VandeVord, P. J. (2024). Quantifying acute changes in neurometabolism following blast-induced traumatic brain injury. *Neurosci. Res.,* 198, 47-56. doi: 10.1016/j.neures.2023.06.008

[22] Ratliff, W. A., Mervis, R. F., Citron, B. A., Schwartz, B., Rubovitch, V., Schreiber, S., & Pick, C. G. (2020). Effect of mild blast-induced TBI on dendritic architecture of the cortex and hippocampus in the mouse. *Sci. Rep.,* 10(1), 2206. doi: 10.1038/s41598-020-59252-4

[23] Rusiecki, J., Levin, L. I., Wang, L., Byrne, C., Krishnamurthy, J., Chen, L., … & French, L. M. (2020). Blast traumatic brain injury and serum inflammatory cytokines: a repeated measures case-control study among U.S. military service members. *J. Neuroinflammation,* 17(1), 1-12. doi: 10.1186/s12974-019-1624-z

[24] Rutter, B., Song, H., DePalma, R. G., Hubler, G., Cui, J., Gu, Z., & Johnson, C. E. (2021). Shock wave physics as related to primary non-impact blast-induced traumatic brain injury. *Mil. Med.,* 186(Suppl 1), 601-609. doi: 10.1093/milmed/usaa290

[25] Schmitt, R., Qayum, S., Pliss, A., Kuzmin, A. N., Muthaiah, V. P. K., Kaliyappan, K., … & Mahajan, S. D. (2023). Mitochondrial dysfunction and apoptosis in brain microvascular endothelial cells following blast traumatic brain injury. *Cell Mol. Neurobiol.,* 43(7), 3639-3651. doi: 10.1007/s10571-023-01372-2

[26] Shen, Y., Dong, Z., Fan, F., Li, K., Zhu, S., Dai, R., … & Fu, Y. (2023). Targeting cytokine-like protein FAM3D lowers blood pressure in hypertension. *Cell Rep. Med.,* 4(6), 101072. doi: 10.1016/j.xcrm.2023.101072

[27] Suvarna, K. S., Layton, C., & Bancroft, J. D. (2018). *Bancroft's theory and practice of histological techniques*. Elsevier health sciences. doi: 10.1016/C2015-0-00143-5

[28] Szyller, J., Kozakiewicz, M., Siermontowski, P., & Kaczerska, D. (2022). Oxidative stress, HSP70/HSP90 and eNOS/iNOS serum levels in professional divers during hyperbaric exposition. *Antioxidants* (Basel), 11(5), 1008. doi: 10.3390/antiox11051008

[29] Tran, N., Garcia, T., Aniqa, M., Ali, S., Ally, A., & Nauli, S. M. (2022). Endothelial nitric oxide synthase (eNOS) and the cardiovascular system: in physiology and in disease states. *Am. J. Biomed. Sci. Res.*, 15(2), 153-177. PMID: 35072089

[30] Wei, T., Zhou, M., Gu, L., Zhou, Y., & Li, M. (2022). How shockwaves open tight junctions of blood-brain barrier: comparison of three biomechanical effects. *J. Phys. Chem. B.,* 126(27), 5094-5102. doi: 10.1021/acs.jpcb.2c02903

[31] Zhang, D., Jin, C., Han, T., Chen, J., Ali Raza, M., Li, B., … & Yan, H. (2023). Sinomenine promotes flap survival by upregulating eNOS and eNOS-mediated autophagy via PI3K/AKT pathway. *Int. Immunopharmacol.,* 116, 109752. doi: 10.1016/j.intimp.2023.109752

[32] Zhou, Y., Tian, M., Wang, H. D., Gao, C. C., Zhu, L., Lin, Y. X., … & Ding, K. (2019). Activation of the Nrf2-ARE signal pathway after blast induced traumatic brain injury in mice. *Int. J. Neurosci.,* 129(8), 801-807. doi: 10.1080/00207454.2019.1569652

ЗМІНИ СУДИН ГОЛОВНОГО МОЗКУ ЩУРІВ ПІСЛЯ ДІЇ ПОВІТРЯНОЇ УДАРНОЇ ХВИЛІ

Козлова Ю. В., Козлов С. В., Маслак Г. С., Бондаренко О. О., Дунаєв О. В., Оберемок М. Г.

Поширеною серед військових є легка вибухо-індукована травма головного мозку, наслідками якої є когнітивні порушення та зниження соціалізації людини, що призводить до втрати працездатності і, в результаті, до погіршення якості життя. Вважається, що саме порушення гематоенцефалічного бар'єру та мікросудинна дисфункція є ключовими у перебігу даного виду травми. Метою роботи стало вивчення змін в судинах головного мозку після впливу повітряної ударної хвилі. Дослідження проведено на 48 статевозрілих щурах самцях лінії Wistar, які випадковим чином були розділені на 2 групи: експериментальну (тварин піддавали інгаляційній анестезії із застосуванням галотану та впливу ударної хвилі з надлишковим тиском 26,4±3,6 кПа) і контрольну. Після відтворення травми на 1, 3, 7, 14 та 21 добу щурів піддавали евтаназії з наступним вилученням головного мозку, котрий у подальшому піддавали стандартним гістологічним процедурам. Гістологічні зрізи забарвлювали гематоксиліном та еозином. Для імуногістохімічного дослідження у якості первинних використовували антитіла до eNOS. Готові препарати досліджували за допомогою світлової мікроскопії та фіксували фотоапаратом. Виявлено порушення судин головного мозку у щурів експериментальної групи з 1 доби посттравматичного періоду. Встановлено, що вибухова хвиля призвела до розриву судин, а також підвищення судинної проникності з діапедезною екстравазацією еритроцитів і набряком головного мозку до 21 доби. Провідне значення мали фокальні порушення цілісності судинної стінки в кортикальних та гіпокампальних гемокапілярах, у венулярній ланці підоболонкових судин; зміни морфології ендотелію обмінних судин; нерівномірне кровонаповнення судин мозку. Порівняння отриманих результатів імуногістохімічного визначення eNOS в судинах головного мозку показало наявність експресії цього ензима в ендотелії судин головного мозку експериментальних щурів у 1 та 3 добу. Таким чином, встановлені нами зміни свідчать про те, що підвищення експресії eNOS призводить до розширення судин головного мозку, що є компенсаторним механізмом у відповідь на травму для покращення кровообігу головного мозку. Проте eNOS не бере участь у розширенні судин, яке ми спостерігали до 21 доби посттравматичного періоду.

Ключові слова: *гематоенцефалічний бар'єр, вибух, травма, головний мозок, кровоносні судини.*

Author's contribution:

Kozlova Yu. V. - conceptualization, providing equipment for the experiment, supervision.
Kozlov S. V. - data visualization, conducting an experiment, methodology and writing an original draft.
Maslak H. S. - project administration.
Bondarenko O. O. - formal analysis and verification, review writing and editing.
Dunaev O. V. - software for morphometric research, histological analysis.
Oberemok M. H. - resources.

DOI: 10.31393/morphology-journal-2024-30(1)-08 Reports of Morphology, Vol. 30, №1, Pages 61-67

ISSN 1818-1295 eISSN 2616-6194

REPORTS OF MORPHOLOGY

Official Journal of the Scientific Society of Anatomists, Histologists, Embryologists and Topographic Anatomists of Ukraine

journal homepage: https://morphology-journal.com

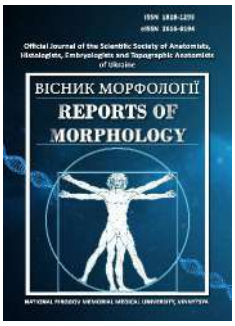

Localized osteophytic changes in the thoracic vertebra: an osteological and cadaveric study

Afroze Mookane K. H., Sangeeta M., Varalakshmi K. L., Anusha R., Jesima Preethi A.
MVJ Medical College & Research Hospital, Bangalore, India

ARTICLE INFO
Received: 18 December 2023
Accepted: 08 February 2024

UDC: 616.711.5:616-091.1:001

CORRESPONDING AUTHOR
e-mail: drafroze.homoeo@gmail.com
Afroze Mookane K. H.

CONFLICT OF INTEREST
The authors have no conflicts of interest to declare.

FUNDING
Not applicable.

DATA SHARING
Data are available upon reasonable request to corresponding author.

Vertebral spinal osteophytes remain an urgent problem for clinicians of various specialties due to the fact that they can cause problems with food consumption, breathing, and sometimes cause compression of blood vessels and spinal cord. Clinical presentations encompass pain, often radiating, reduced function, stiffness, tenderness in the joints, limited movement, nerve compression, and bone pressing against tissues. Vertebral osteophytes are frequently observed in cadaveric anatomy and skeletal remains. Many instances go untreated or undetected. Several cross-sectional and prospective studies have been conducted and published concerning the cervical and lumbar spine. The current study was carried out to observe the incidence of osteophytes in the thoracic vertebrae and to document their frequency of distribution and prevalence. To study the frequency of distribution of thoracic osteophytes was reviewed in 25 cadavers (over a period of 5 years) & 188 dry thoracic vertebras (T1-T12) of south Indian population of unknown age & sex at the Department of Anatomy, MVJ MC& RH, Bangalore. The study meticulously enumerates the positions of osteophytes across different thoracic levels, aiming to investigate and understand their recurrence patterns. Incidence was expressed in terms of frequency and percentage. Incidence of osteophytes was documented in 6 cadavers and 33 dry bones which accounts for 24 % and 17.6 % respectively. Out of these, majority of them were recognized on to right side than on left side of the vertebras. The frequency of osteophytes was most commonly seen at mid thoracic level (T4-T8) followed by T9, T10 and T2. The data we received allow us to form an idea not only about the prevalence of vertebral spinal osteophytes in general, but also about the specific features of their location. Knowledge regarding the thoracic osteophytes is further required for detailed study along with dry bones. A comparative analysis of the prevalence of vertebral spinal osteophytes among people of different specialties, different ethnicities and age groups is important in further research, which will complement the obtained results.

Key words: *osteophytes, thoracic vertebrae, degeneration of disc, dry bones, cadaveric study.*

Introduction

Osteophytes are the lumps that are formed on bones either in spine or around joint, developed by the degeneration of the bony surfaces and are also called as bone spurs or bone lumps. Osteoarthritis-induced joint damage is the primary cause of bone spurs further includes vertebral stenosis, degenerative disc changes [14]. Osteophytes are developed where excessive pressure is produced [4, 28]. Presence of osteophytes are mostly seen in places such as: Foot, especially the heel (calcaneal spurs) [1], Hand or finger [6], Hip & Knee [11], Shoulder [9], Neck, and Spine [2]. According to research, the occurrence of osteophytes increases with age [23] and are common along the right lateral side of thoracic vertebral levels T4-T10 [15, 25]. Vertebral osteophytes are thought to be a common finding in cadaveric anatomy and dry bones. However, they are also frequently reported as common radiological findings [17]. A large number of cases are neither cured nor identified. Clinical manifestations include pain (radiating pain), loss of function, stiffness, joint tenderness, movement restriction, nerve compression, bone crushing against the tissues.

An extensive review of literature on osteophytes has yielded limited findings. It was observed that there is a scarcity of cadaveric studies on osteophytes, and the

majority of previous clinical investigations have primarily concentrated on the cervical [7, 8] and lumbar vertebrae [3]. We examined thoracic vertebrae in order to analyse osteophytes on both wet (cadaveric) and dry (osteological) specimens. Aim of the current study was to determine the frequency of occurrence and distribution of osteophytes along the thoracic vertebrae, as well as potential side effects affecting the surrounding structures of the posterior mediastinum.

The aim - to observe the incidence of osteophytes in the thoracic vertebrae and to document their frequency of distribution and prevalence.

Materials and methods

Protocol of the Ethics Commission

This study was approved by the Institutional ethics committee of MVJMC & RH (dated December 7, 2023). This study was based on the National Ethical guidelines for biomedical and health research complied by ICMR Bioethics unit, Bangalore, India.

The study was conducted in Department of Anatomy of MVJ MC& RH, Bangalore. 25 cadaveric vertebral columns and 188 dry thoracic vertebrae were used to study the incidence of osteophytes.

Cadaveric analysis

Following the removal of lung and heart, posterior mediastinum structures were dissected and the posterior thoracic vertebral column was exposed. Osteophytes were studied for their position and vertebrate levels. Cadavers with all deformities such Kyphosis, Scoliosis were excluded.

Osteological analysis

188 dry thoracic vertebras (T1-T12) of south Indian population of unknown age & sex from the Department of Anatomy, MVJ MC& RH were procured. The location (vertebral levels) and the position (anterior/lateral) of osteophytes were observed. Vertebras with sign of trauma were excluded from the study.

Statistical analysis

The data observed from this morphometric study was entered and analyzed using Microsoft excel version 2019. Incidence was expressed in terms of frequency and percentage.

Results

Cadaveric Findings. In the present study, we found osteophytes in six thoracic vertebra (24 %) out of 25 Cadaveric vertebral columns analyzed. Osteophytes were identified at anterior and lateral aspect of vertebral column. It was noted that majority of the osteophytes occurred mostly on right side of vertebral bodies than on to the left. Also observed that osteophytes were most commonly seen in mid thoracic level (T4-T8), followed by T9, T10 and T2 (Fig. 1, 2). Table 1 shows the frequency of position of osteophytes with vertebral levels.

Osteological Findings. Out of 188 thoracic vertebrae studied, 33 (17.5 %) of them showed the presence of

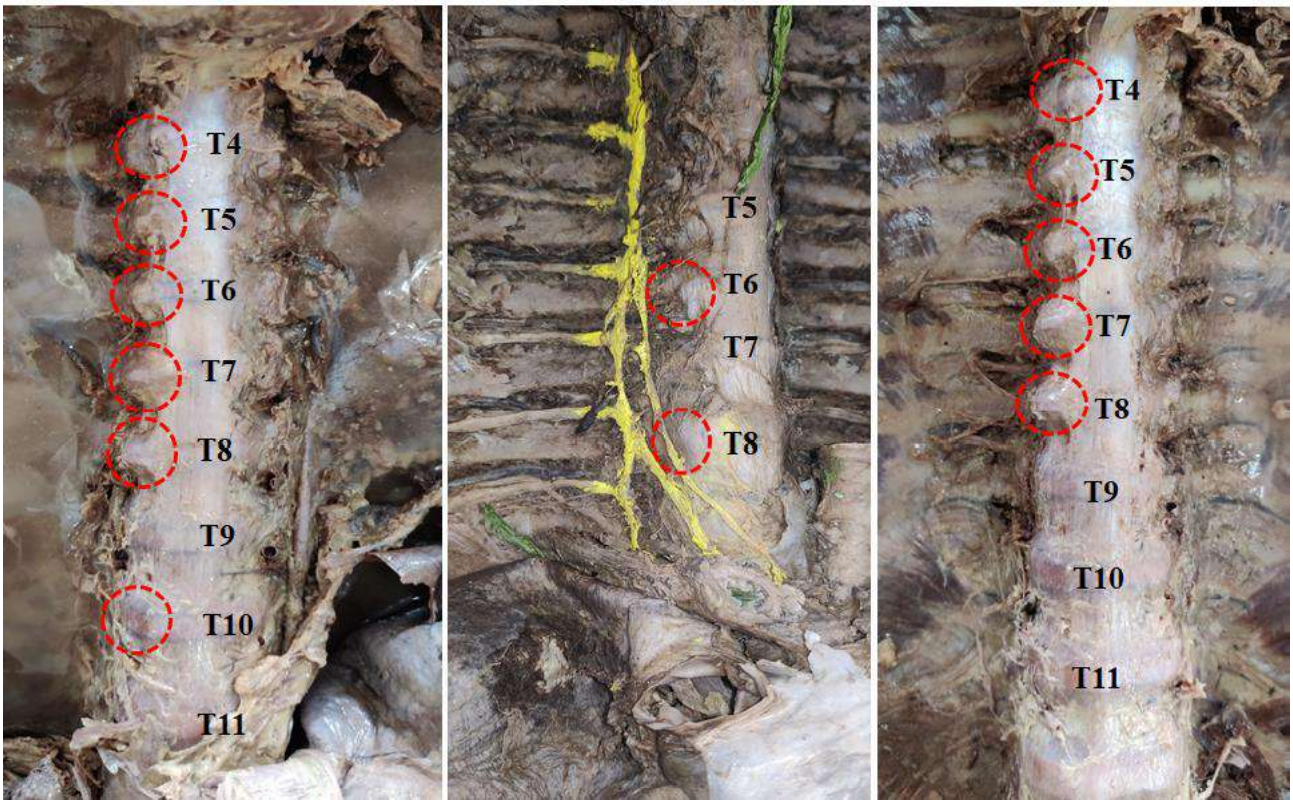

Fig. 1. Position of osteophytes in different vertebral levels (marked with red circles).

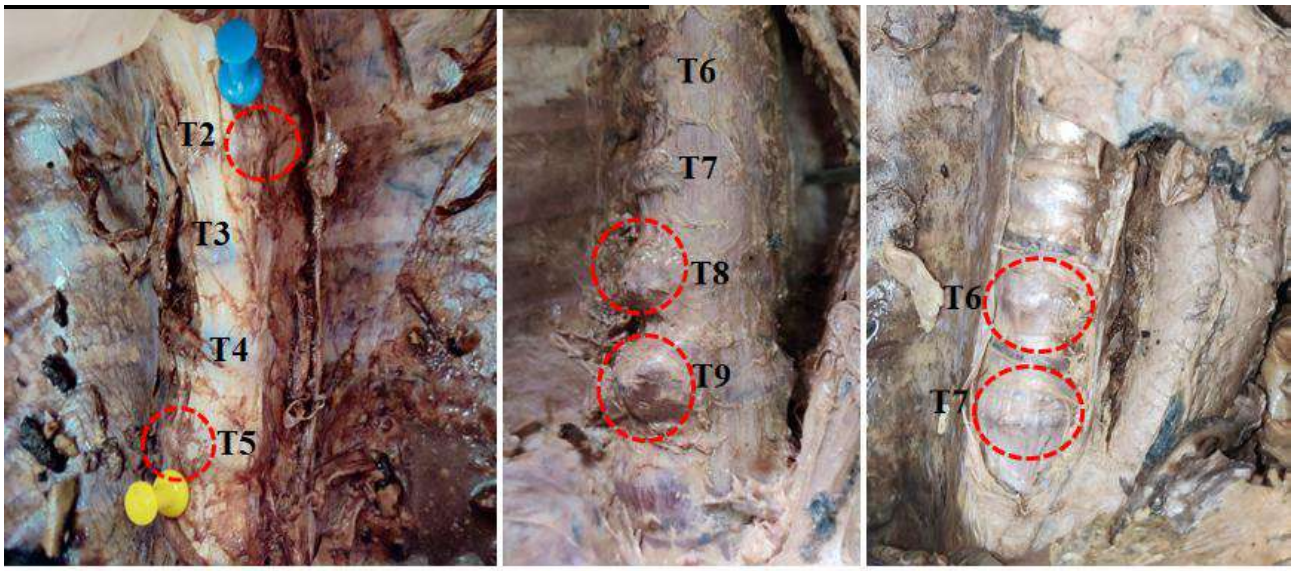

Fig. 2. Position of osteophytes in different vertebral levels (marked with red circles).

Table 1. Distribution of osteophytes in the cadaveric thoracic vertebra.

Specimen	Total no. of Osteophytes	Position	Vertebral level
1	2	Left, Lateral side of the vertebral body Right, Lateral side of the vertebral body	T2 T5
2	2	Right, Lateral side of the vertebral body Right, Lateral side of the vertebral body	T8 T9
3	2	Anterior side of the vertebral body Anterior side of the vertebral body	T6 T7
4	6	Right, Lateral side of vertical body Right, Lateral side of vertical body	T4-T8 T10
5	2	Right, Lateral side of vertical body Right, Lateral side of vertical body	T6 T8
6	5	Right, Lateral side of vertical body	T4-T8

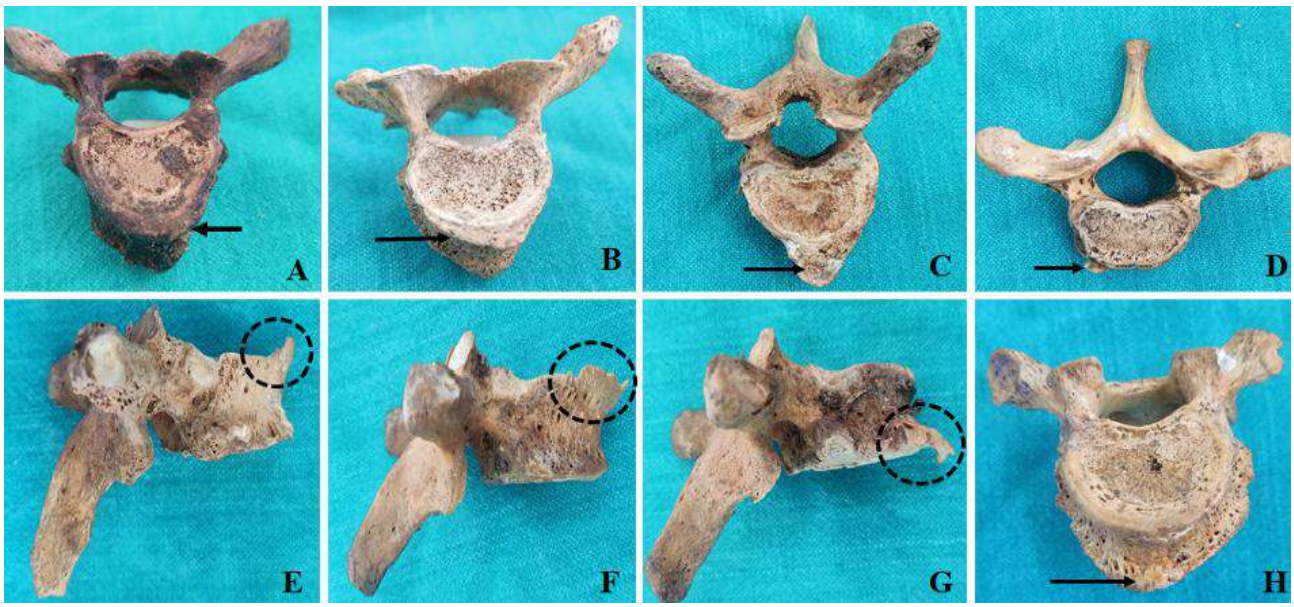

Fig. 3. Incidence of different position of osteophytes (marked with black circles and arrows). A-D: Anterior; E, F: Anterior Upper border; G, H: Anterior Lower border.

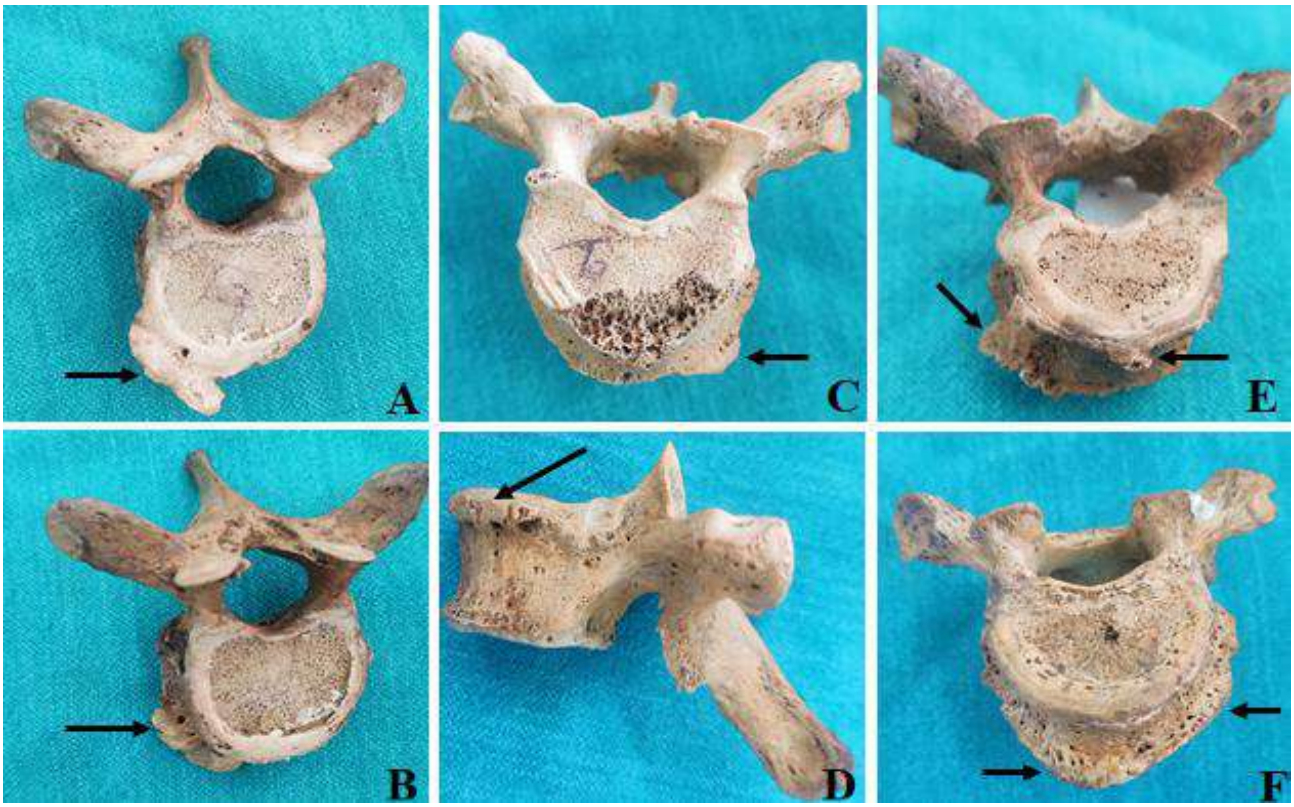

Fig. 4. Incidence of different position of osteophytes (marked with black circles and arrows). A: Right Lateral Upper border; B: Right Lateral lower border; C: Left Lateral Lower border; D: Left Lateral Upper border; E: Anterior & Right Lateral; F: Anterior &Left Lateral.

Table 2. Incidence of different position of osteophytes in dry vertebra.

Position		Total number of osteophytes (n=188)	Incidence
Anterior	Upper Border	15	7.9 %
	Lower Border	12	6.3 %
Lateral	Right	2	1.06 %
	Left	2	1.06 %
Combined	Anterior & Right Lateral	1	0.53 %
	Anterior & Left Lateral	1	0.53 %

osteophytes. Osteophytes were observed at anterior and lateral aspect of the thoracic vertebrate. High incidence of osteophytes were observed along the upper border followed by lower border of vertebra, combination of anterior and right / left laterality osteophytes were also observed (Fig. 3, 4).

Discussion

Osteophytes are bone spurs formed due to degeneration of bone surfaces. Vertebral column is more prone for occurrence of osteophytes. In the current study, cadaveric vertebral columns were examined alongside dry bones to determine the frequency and prevalence of osteophytes in relation to position, whereas previous studies have used Magnetic resonance imaging (MRI), computerized tomography (CT) and X-rays to estimate the prevalence of osteophytes. Vertebral stenosis, degenerative disc changes, and arthritis are the etiological factors predisposing to the occurrence of osteophytes [24, 25]. Few studies indicate that increase in age is also a predisposing factor [23].

N. Kumar et al. [14] used 50 cadaveric vertebral columns and recorded the highest incidence of osteophytes in lower thoracic levels T10-T11. Z. Klaasen et al. [13], observed maximum osteophytes at T9-T10 level. H. Nathan [15] also quoted highest incidence around T10 in the right side and T11 & T12 on the left side. Anterior osteophytes were more commonly observed. He further proposed an anatomical classification to grade the osteophytes which can be used for all levels of vertebral column. Grade 0 signifies absence of osteophytes, Grade1-points of isolated hyperostosis, Grade 2-Horizontal protrusion of osteophytes from body of vertebra, Grade 3 end of osteophytes curving to intervertebral disc, grade 4 signifying real bony bridge between two vertebra. T. Valasek et al. [25] also observed commonest location of osteophytes at T7-9 segments. He also studied the correlation between the grade of osteophyte with age and BMI and observed no correlation between the two.

A study conducted by Kim D. K. et al. [12] on 87 Joseon skeletons involving cervical, thoracic and Lumbar

vertebras. They documented that the higher incidence of osteophtyes were observed in the C5, T9, T10, and L4. They also added that mean osteophytic value was found significantly higher in thoracic vertebra when compared to cervical and lumbar osteophytes. In present study, we found out the highest frequency at T4-T8 levels along the right lateral side of vertebral body.

S. R. Pye et al. [19] postulated that decreased disc space could be a causative factor resulting in formation of osteophyte. Degeneration of intervertebral disc or pressure on vertebral end plates can also lead to formation of osteophytes [19, 21]. Macnab's theory indicates that osteophytes are formed as a result of instability between adjacent vertebral bodies [27]. Clinical features such as decreased flexibility of joint, stiffness and numbness, pain are usually associated with presence of osteophytes.

J. Jankowsky et al. [10] reported a case of 39 year old man presenting with history of chronic pain in the lower ribs on the right side initially, later involving thoracic spine and upper abdomen. CT scan revealed the presence of massive osteophyte on the anterolateral aspect of T8-9 vertebra compressing the greater splanchnic nerve. Surgical removal of osteophyte was done to relieve symptoms.

A. A. Padur et al. [17] observed that osteophytes may compress the aorta or inferior vena cava causing ischemia or perforation. The current study found out the incidence of anterior and right lateral osteophytes in great numbers than posterior osteophytes. Anterior osteophytes can present as dysphagia [20], focal pulmonary fibrosis, and obstructive pneumonia due to pressure effects on bronchus [5, 18, 29]. Osteophyte-induced nerve root compression may present as back and leg pain [17]. It may co exist with abdominal aortic calcification. The least frequency of osteophyte presence was seen on left lateral and posterior aspect of thoracic vertebrae. Posterior lumbar osteophytes may present as lumbar stenosis

N. Kumar et al. [14] studied the microscopic anatomy of osteophytes encountered in routine dissection and found a layer of hyaline cartilage capping the trabecular bone indicating endochondral ossification and concluded that osteophytes develop through the process of endochondral ossification.

The pathogenesis of osteophytes starts with degeneration of disc, nucleus pulposus. As the disc loses height there's redistribution of stress which increases stress to surrounding structures causing capsular synovitis and cartilage thinning. Further facet degeneration occurs eventually resulting in formation of osteophytes. Due to this there is less room for nerve, causing compression [16]. Synovial mesenchymal stem cells were considered as the cellular source of osteophyte precursors, developed osteophytes consists of fibroblasts, mesenchymal pre-chondrocytes, maturing chondrocytes, hypertrophic chondrocytes and osteoblasts. TGF?and Fibroblast growth factor play a major role to initiate chondrogenesis in osteophytes [26].

Even a normal vertebrate may develop osteophytes by excessive pressure as in labor work or strenuous exercise. With respect to age, the intervertebral disc is intact in young age, able to distribute load uniformly along the vertebral end plates and absorbs shocks effectively. Therefore, osteophytes develop when degeneration of disc starts as age progress [15]. Vertebral osteophytes are formed as compensatory mechanism for lack of nucleus pulposus to maintain the stability and flexibility to bear the load [28]. The size and position of thoracic osteophytes varies from each other at each level. Occurrence of thoracic osteophytes increases along with the age [12, 23].

MRI scan is used to find out any pathology associated which causes osteophyte formation, CT is used to diagnose any bone tumors, or muscle disorders. By presence of osteophyte on CT, size and location can be determined for further study. Simonovich et al. based on CT readings as observed the number of osteophytes on each side of the thoracic vertebrae [22].

Study of osteophyte is important to radiologists as they may be confused with anterior mediastinal mass in X Ray Anthropologists use them to estimate for age at death. The clinical importance must be known by the anatomist, radiologist, clinicians so as to cure with efficient treatment.

By and large further research needs to be carried out to explore the developmental basis and pathophysiology and molecular mechanisms involved in the formation of osteophytes.

Conclusion

1. In the present study, the highest frequency and prevalence were observed at thoracic vertebrae T4-T8 levels which was 24 % of cadaveric findings and 17.6 % of osteological findings irrespective of age and sex. Therefore, occurrence of osteophytes is due to degenerative disc changes of vertebral column.

2. Clinical features depend on the site where osteophytes are located.

Acknowledgement:

We sincerely acknowledge the generous contributions of body donors to the Department's teaching and research resource material.

References

[1] Afroze, M. K. H., Bharat, S., Jayagopal, C., & Ramesh, P. (2018). Radiological classification and prevalence of plantar spur and their relationship with plantar fasciitis. *International Journal of Orthopaedics,* 4(2), 147-150. doi: 10.22271/ortho.2018.v4.i2c.21

[2] Al-Jafari, M., Tapanjeh, S. A., Al-Azzawi, H., Eid, S. A., Baidoun, H. J., Abu-Jeyyab, M., ... & Sarhan, M. (2023). Cervical Spine Osteophyte: A Case Report of an Unusual Presentation. *Cureus,* 15(9), e44762. doi: 10.7759/cureus.44762

[3] Al-Rawahi, M., Luo, J., Pollintine, P., Dolan, P., & Adams, M. A.

(2011). Mechanical function of vertebral body osteophytes, as revealed by experiments on cadaveric spines. *Spine*, 36(10), 770-777. doi: 10.1097/BRS.0b013e3181df1a70

[4] Amabile, A. H., Shea, J. R., Desai, V., Hoglund, L. T., Elcock, J. N., Lombardo, A., & Schiffino, M. C. (2020). A Case of Thoracic Spondylosis Deformans and Multilevel Instrumented Spinal Fusion in an 84-Year-Old Male. *Case Reports in Orthopedics,* 2020, 8435816. doi: 10.1155/2020/8435816

[5] Balbay, E. G. (2015). Bronchiolectasis due to giant thoracic vertebral osteophytes. *The Spine Journal,* 15, e29. doi: 10.1016/j.spinee.2015.07.430

[6] Crisco, J. J., Morton, A. M., Moore, D. C., Kahan, L. G., Ladd, A. L., & Weiss, A. P. (2019). Osteophyte growth in early thumb carpometacarpal osteoarthritis. *Osteoarthritis and cartilage,* 27(9), 1315-1323. doi: 10.1016/j.joca.2019.05.008

[7] Ezra, D., Hershkovitz, I., Salame, K., Alperovitch-Najenson, D., & Slon, V. (2019). Osteophytes in the cervical vertebral bodies (C3-C7) - demographical perspectives. *The Anatomical Record,* 302(2), 226-231. doi: 10.1002/ar.23901

[8] Guvencer, M., Naderi, S., Men, S., Sayhan, S., & Tetik, S. (2016). Morphometric evaluation of the uncinate process and its importance in surgical approaches to the cervical spine: a cadaveric study. *Singapore medical journal*, 57(10), 570. doi: 10.11622/smedj.2015193

[9] Hirose, T., Nakagawa, S., Sato, S., Tachibana, Y., & Mae, T. (2019). Computed Tomography Features of Glenoid Osteophytes in Traumatic Anterior Shoulder Instability: Comparison Between Younger and Older Patients. *Orthopaedic Journal of Sports Medicine,* 7(5), 2325967119846908. doi: 10.1177/2325967119846908

[10] Jankowski, J., Pawelczyk, A., & Radek, M. (2022). Thoracic osteophyte as a cause of symptomatic greater splanchnic nerve compression. Case report. *Neurochirurgie*, 68(2), 232-234. doi: 10.1016/j.neuchi.2021.02.017

[11] Katz, J. N., Arant, K. R., & Loeser, R. F. (2021). Diagnosis and treatment of hip and knee osteoarthritis: a review. *Jama*, 325(6), 568-578. doi: 10.1001/jama.2020.22171

[12] Kim, D. K., Kim, M. J., Kim, Y. S., Oh, C. S., & Shin, D. H. (2012). Vertebral osteophyte of pre-modern Korean skeletons from Joseon tombs. *Anatomy & Cell Biology,* 45(4), 274-281. doi: 10.5115/acb.2012.45.4.274

[13] Klaassen, Z., Tubbs, R. S., Apaydin, N., Hage, R., Jordan, R., & Loukas, M. (2011). Vertebral spinal osteophytes. *Anatomical science international,* 86, 1-9. doi: 10.1007/s12565-010-0080-8

[14] Kumar, N., Aithal, A., Bishnu, A., Nayak, S., & KG, M. R. (2017). Morphometric and Histological Analysis of 'Spondylosis Deformans' of Thoracic Region in South-Indian Cadaveric Spines. *Journal of Krishna Institute of Medical Sciences* (JKIMSU), 6(3), 94-102.

[15] Nathan, H. (1962). Osteophytes of the vertebral column: an anatomical study of their development according to age, race, and sex with considerations as to their etiology and significance. *JBJS,* 44(2), 243-268. doi: 10.2106/00004623-196244020-00003

[16] Ögrenci, A. (2018). Bone Protrusion That We Should be Aware of: Foraminal Osteophytes; Classification and Surgical Results. Haseki Tip Bulteni, 56(4), 299. doi: 10.4274/haseki.4310

[17] Padur, A. A., Kumar, N., Shanthakumar, S. R., & Bishnu, A. (2017). Morphometric and Histological Study of Osteophytes in Human Cadaveric Lumbar Vertebrae. J Clin of Diagn Res. 11(10), AC05-AC07. doi: 10.7860/JCDR/2017/29594/10734

[18] Psathakis, K., Skouras, V., Chatzivassiloglou, F., & Tsintiris, K. (2013). Osteophytes may be a rare cause of recurrent pleural effusions. Monaldi Archives for Chest Disease, 79(2), 87-89. doi: 10.4081/monaldi.2013.97

[19] Pye, S. R., Reid, D. M., Lunt, M., Adams, J. E., Silman, A. J., & O'Neill, T. W. (2007). Lumbar disc degeneration: association between osteophytes, end-plate sclerosis and disc space narrowing. Annals of the rheumatic diseases, 66(3), 330-333. doi: 10.1136/ard.2006.052522

[20] Rana, S. S., Bhasin, D. K., Rao, C., Gupta, R., Nagi, B., & Singh, K. (2012). Thoracic spine osteophyte causing dysphagia. Endoscopy, 44(S 02), E19-E20. doi: 10.1055/s-0031-1291501

[21] Rustenburg, C. M., Emanuel, K. S., Peeters, M., Lems, W. F., Vergroesen, P. P. A., & Smit, T. H. (2018). Osteoarthritis and intervertebral disc degeneration: Quite different, quite similar. JOR spine, 1(4), e1033. doi: 10.1002/jsp2.1033

[22] Simonovich, A., Naveh, Y., & Kalichman, L. (2021). Pattern of thoracic osteophytes development and the association between calcification of the aorta and thoracic osteophytes: CT study. *Clinical Anatomy,* 34(7), 1009-1015. doi: 10.1002/ca.23699

[23] Snodgrass, J. J. (2004). Sex differences and aging of the vertebral column. *Journal of forensic sciences,* 49(3), 458-463. doi: 10.1520/JFS2003198

[24] Steinmetz, M. P., Berven, S. H., & Benzel, E. C. (Eds.). (2021). *Benzel's Spine Surgery: Techniques, Complication Avoidance, and Management*. Elsevier Health Sciences.

[25] Valasek, T., Vago, E., Danielisz, Z. S., Babka, M., & Kovacs, E. (2020). Anatomical changes of the thoracic vertebrae in asymptomatic individuals-A cross-sectional study. *Developments in Health Sciences,* 3(2), 33-38. doi: 10.1556/2066.2020.00007

[26] Van Der Kraan, P. M., & Van Den Berg, W. B. (2007). Osteophytes: relevance and biology. *Osteoarthritis and cartilage,* 15(3), 237-244. doi: 10.1016/j.joca.2006.11.006

[27] Wagnac, E., Aubin, C. E., Chaumoitre, K., Mac-Thiong, J. M., Menard, A. L., Petit, Y., ... & Arnoux, P. J. (2017). Substantial vertebral body osteophytes protect against severe vertebral fractures in compression. *Plos one,* 12(10), e0186779. doi: 10.1371/journal.pone.0186779

[28] Wong, S. H. J., Chiu, K. Y., & Yan, C. H. (2016). Osteophytes. *Journal of orthopaedic surgery,* 24(3), 403-410. doi: 10.1177/1602400327

[29] Yoshida, R., Katsube, T., Yoshizako, T., & Kitagaki, H. (2015). Focal pulmonary interstitial opacities adjacent to the thoracic spine osteophytes among the cases with right-sided aortic arch. *SpringerPlus,* 4, 1-4. doi: 10.1186/s40064-015-1212-3

ЛОКАЛІЗОВАНІ ОСТЕОФІТНІ ЗМІНИ ГРУДНОГО ХРЕБЦЯ: ОСТЕОЛОГІЧНЕ ТА ТРУПНЕ ДОСЛІДЖЕННЯ

Afroze Mookane K. H., Sangeeta M., Varalakshmi K. L., Anusha R., Jesima Preethi A.

Остеофіти хребта залишаються актуальною проблемою для клініцистів різних спеціальностей у зв'язку з тим, що вони можуть викликати проблеми з прийомом їжі, диханням, а, іноді, й спричиняти компресію кровоносних судин і спинного мозку. Клінічні прояви включають біль, часто іррадіюючий, зниження функціональних можливостей, скутість, болючість у суглобах, обмеження рухів, стиснення нервів та тиск кістки на оточуючі тканини. Остеофіти хребців часто спостерігаються під час дослідження трупного матеріалу та скелетованих залишків. Багато випадків даної патології не виявляється або не лікується. Було проведено та опубліковано декілька поперечних та проспективних досліджень щодо шийного та поперекового

відділів хребта. Поточне дослідження було проведено з метою спостереження за поширеністю остеофітів у грудних хребцях і документування їх частоти поширення. На кафедрі анатомії, MVJ MC& RH, Бангалор з метою вивчення частоти поширення грудних остеофітів було оглянуто 25 трупів (протягом 5 років) і 188 грудних хребців без м'яких тканин (T1-T12) жителів південної Індії невідомого віку та статі. У роботі ретельно вивчили положення остеофітів на різних рівнях грудної клітки з метою дослідження та розуміння моделей їх рецидивів. Захворюваність виражали у вигляді частоти та відсотків. Задокументовано наявність остеофітів у 6 трупів і 33 препаратах кісток, що становить 24 % і 17,6 % відповідно. Остеофіти частіше виявлялися з правого боку хребців, ніж з лівого. Остеофіти найчастіше спостерігалися на рівні середини грудної клітки (T4-T8), за якою слідують T9, T10 і T2. Отримані дані дозволяють скласти уявлення не тільки про поширеність остеофітів хребта в цілому, а й про особливості їх розташування. Для детального вивчення препаратів кісток необхідні знання про грудні остеофіти. Порівняльний аналіз поширеності остеофітів хребта серед людей різних спеціальностей, різних етнічних та вікових груп є важливим у подальших дослідженнях, які доповнять отримані результати.
Ключові слова: *остеофіти, грудні хребці, дегенерація диска, сухі кістки, дослідження трупа.*

Author's contribution:

Afroze Mookane K. H. - conceptualization and design, review writing and editing, methodology and writing of the original draft, final approval.

Sangeeta M. - writing of the original draft, critical review, final approval.

Varalakshmi K. L. - analysis and interpretation of data, final approval.

Anusha R. - data collection, analysis and interpretation of data, review writing and editing.

Jesima Preethi A. - data collection, analysis and interpretation of data.

DOI: 10.31393/morphology-journal-2024-30(1)-09 Reports of Morphology, Vol. 30, №1, Pages 68-75

ISSN 1818-1295 eISSN 2616-6194

REPORTS OF MORPHOLOGY

Official Journal of the Scientific Society of Anatomists, Histologists, Embryologists and Topographic Anatomists of Ukraine

journal homepage: https://morphology-journal.com

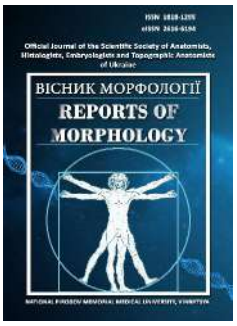

Effect of quercetin administration on electron microscopic changes in testicular interstitial endocrinocytes during long-term central blockade of luteinising hormone in rats

Stetsuk Ye. V., Shepitko V. I., Pronina O. M., Zaporozhets T. M., Boruta N. V., Vilkhova O. V., Lysachenko O. D., Pelypenko L. B., Voloshyna O. V., Levchenko O. A.

Poltava State Medical University, Poltava, Ukraine

ARTICLE INFO

Received: 26 December 2023

Accepted: 12 February 2024

UDC: 616.682-018.1-02:615.357]-076.4:615.356]-092.9

CORRESPONDING AUTHOR

e-mail: stetsuk78@gmail.com

Stetsuk Ye. V.

CONFLICT OF INTEREST

The authors have no conflicts of interest to declare.

FUNDING

Not applicable.

DATA SHARING

Data are available upon reasonable request to corresponding author.

Quercetin is a flavonoid with potential health benefits and it may help prevent cardiovascular diseases, reduce the risk of degenerative brain processes and cancer, and has antioxidant properties that neutralise free radicals. Substances in this group also have antioxidant properties, which help the body protect itself from the harmful effects of free radicals by neutralising these unstable molecules. Research indicates that the impact of free radicals on cell structure is associated with the development of chronic diseases such as diabetes, cancer, and cardiovascular pathologies. The aim of the study was to investigate the effect of quercetin administration on electron microscopic changes in the interstitial endocrinocytes of the testes under long-term central blockade of the synthesis of luteinising hormone by tryptorelin. The experiment involved 35 sexually mature male white rats. They were divided into two groups: the control group (I) received saline, while group II received subcutaneous injections of tryptorelin at a dose of 0.3 mg of active ingredient per kg of rat body weight to induce experimental central deprivation of luteinising hormone synthesis and additionally, quercetin was administered three times a day by gastric tube in terms of body weight. The study has demonstrated that the administration of tryptorelin results in structural and functional changes in the connective tissue components of rat testes. Specifically, there are quantitative and qualitative disorders in the population of interstitial endocrine cells, as well as electron microscopic changes at the subcellular level. Various pathological changes and abnormalities in the functional activity of the internal components of the cell were detected on days 270 and 365 of the experiment. The frequency, number, and size of Reinke crystals in relation to the cell volume correlated with changes in cells and increased at later stages of the study. A similar correlation with testosterone levels has not been found in the literature, which leads us to classify Reinke crystals as the result of degenerative processes in the cell. Thus, additional administration of quercetin reduces the adverse effect of tryptorelin and delays the onset of changes in the structure of interstitial endocrinocytes from day 180 to later observation periods.

Keywords: *testes, electron microscopy, rats, interstitial endocrinocytes, luteinising hormone, quercetin, tryptorelin.*

Introduction

Quercetin is a flavonoid commonly found in fruits, vegetables, and seeds [25]. Flavonoids can help prevent cardiovascular diseases, reduce the risk of degenerative brain processes and cancer [4, 38]. These substances have antioxidant properties that help the body protect itself from the damaging effects of free radicals by binding and neutralising these unstable molecules [20]. Research has shown that the destructive effects of free radicals are linked to the development of several chronic diseases, such as diabetes, cancer and cardiovascular disease [13].

The distribution of quercetin was investigated in rats and pigs, revealing that it is primarily concentrated in the lungs, colon, kidneys, and liver. Metabolites of this substance were also detected in lower levels in the brain.

If the flavonoid is only obtained from the diet, it is found in the nanomolar range in the plasma, but the concentration can be increased to the low micromolar range by supplementation with aglycones or glycosides [25].

Tryptorelin is a synthetic analogue of gonadotropin-releasing hormone (GnRH) [3, 19, 22, 26-28]. It suppresses receptor expression in the pituitary gland without affecting the functioning of the pituitary-testicular complex as a whole. Deprivation of luteinising hormone synthesis in rats leads to the development of oxidative stress in their internal organs [5, 7, 31, 32]. Nitric oxide production during central inhibition of luteinising hormone synthesis undergoes complex changes. Initially, there is a decrease in NO synthase-dependent nitric oxide production [1, 34] on days 30 and 90, but later there is hyperproduction of nitric oxide from NO synthases in the heart [13, 17].

Quercetin, a flavonoid, serves as a substrate for the synthesis of NO. It reduces the activation and adhesion of white blood cells and thrombocytes to the vascular endothelium, inhibits the synthesis of the adhesion proteins VCAM-1 and MCP-1, and prevents the formation and development of atherosclerotic plaque. Quercetin inhibits the synthesis of endothelin-1, a potent vasoconstrictor that stimulates the proliferation and migration of smooth muscle cells in the vascular wall [20]. According to reference [20], the substance exhibits antioxidant, antiplatelet, antiradical, and membrane-stabilising properties. It also prevents an increase in calcium levels in cells, has an angioprotective effect, inhibits protein kinase, and has a pronounced cytoprotective (endothelioprotective) activity. Quercetin can directly affect the pathophysiological processes associated with endothelial dysfunction as an endothelial protective agent. This is evidenced by a decrease in individual markers, leading to improved vasomotor reactions, better control of major blood pressure parameters, and an overall improved prognosis for patients [38].

Quercetin is a modulator of several enzymes involved in phospholipid degradation, such as phospholipases, phosphogenases and cyclooxygenase. These enzymes affect free radical processes and are responsible for the biosynthesis of nitric oxide and proteinases in cells. The inhibitory effect of quercetin on membranotropic enzymes, especially on 5-lipoxygenase, affects the inhibition of the synthesis of leukotrienes LTC4 and LTB4 [20]. In addition, quercetin increases the level of nitric oxide in endothelial cells in a dose-dependent manner, which explains its cardioprotective effect in ischemic and reperfusion myocardial damage [13]. Quercetin has antioxidant and immunomodulatory properties. It reduces the production of cytotoxic superoxide anion, normalises the activation of lymphocyte subpopulations, and reduces the level of their activation. By inhibiting the production of anti-inflammatory cytokines IL-1β and IL-8, it helps to reduce the volume of necrotic myocardium and enhance reparative processes [6]. The protective action mechanism is also linked to preventing an increase in platelet intracellular calcium concentration and aggregation activation, while simultaneously inhibiting thrombogenesis. The drug restores regional blood circulation and microcirculation without significantly altering vascular tone, thereby increasing microvessel reactivity. Quercetin normalises cerebral haemodynamics in ischaemic lesions and reduces the cerebral blood flow asymmetry ratio in ischaemic stroke [38]. The mechanisms of action of quercetin can be used experimentally to correct the pathological effects on testicular interstitial endocrinocytes. This has been demonstrated in our study.

The aim of the study was to investigate the effect of quercetin administration on electron microscopic changes in the interstitial endocrinocytes of the testes under long-term central blockade of the synthesis of luteinising hormone by tryptorelin.

Materials and methods

The study was carried out on 35 sexually mature male white rats, which were randomly divided into two groups: control (10 animals) and experimental (25 animals). The control rats were injected with saline. The experiment lasted for 365 days. To model central withdrawal of luteinising hormone synthesis, animals in the experimental group were administered a solution of tryptorelin at a rate of 0.3 mg active ingredient per kg animal weight [12, 21]. In addition, quercetin was administered orally three times a day using a gastric tube, taking into account the body weight of the animals.

The animals were kept under standard conditions at the vivarium of Poltava State Medical University. The investigation is a part of the research project "Experimental and morphological study of the effect of cryopreserved preparations of cord blood and embryofetoplacental complex (EFPC), dipherelin, ethanol and 1 % methacrylic acid ester on the morphological and functional state of a number of internal organs" (state registration number 0119U102925). The animals were euthanised in accordance with the provisions of the European Convention for the Protection of Vertebrate Animals Used for Experimental and Other Scientific Purposes (Strasbourg, 1986), as well as the General Ethical Principles for Animal Experiments adopted by the First National Congress on Bioethics (Kyiv, 2001). The animals were withdrawn from the experiment on days 30, 90, 180, 270 and 365 by an overdose of ether anaesthesia. The study was approved and confirmed by the Bioethics Committee of Poltava State Medical University (protocol No. 195 - 24.06.2021).

For electron microscopic studies [11], the organ fragments were fixed in a 2.5 % glutaraldehyde solution, fixed in a 1 % osmium tetraoxide solution in phosphate buffer (pH 7.2-7.4), dehydrated in alcohols and propylene oxide, and poured into a mixture of epoxy resins with araldite. Ultrathin sections were prepared on a ZKB-3 ultramicrotome (Sweden) and grids were made. The sections were contrasted first in a 1 % uranyl acetate

solution in methanol and then with lead citrate according to Reynolds. The preparations were examined on a PEM-125 K electron microscope (serial number 38-76, TU 25-07-871-70), accelerating voltage 50-75 kW.

Morphometric quantitative analysis was conducted using Microsoft Office Excel and its Real Statistics 2019 extension, following generally accepted statistical methods.

Results

At the 1-month follow-up, electron microscopic photographs were studied in the experimental group. It was observed that the testicular connective tissue reacted asynchronously and underwent various changes in the structure of interstitial endocrinocytes at the cellular and subcellular levels. The population of interstitial endocrinocytes in the studied animals showed significant quantitative changes, with a variety of cell shapes ranging from round to polygonal. A few spinous and spindle-shaped cells were also observed (Fig. 1).

The cell size was 16.33±2.34 μm. In addition, cells up to 18 μm in diameter were observed due to the number and size of intracellular lipid granules. The cell nuclei were round or ellipsoidal, with euchromatin evenly distributed throughout the entire area. The content of parietal heterochromatin varied. The analysis of the entire population of endocrinocytes on day 30 revealed three distinct cell types based on their degree of development and differentiation, as determined by chromatin distribution and the number and quality of lipophilic granules in the cytoplasm. A functionally active state was observed in the majority of cells (65-70 % of the population). The cells were arranged in groups of 3-5, primarily located near capillaries. Single macrophages and stromal cells (fibroblastic cells) were found in close proximity.

The nuclei reflected the shape of the cell and were either rounded or elliptical, with 1-2 nucleoli. Depending on the cell activity, the amount of hetero- and euchromatin varied, with a predominance of heterochromatin. The nuclear envelope appeared clear and contained a large number of pores. The cytoplasm revealed the endoplasmic reticulum, formed by numerous branching tubes filled with a thin fibrous substance; many ribosomes were present on the membranes, and individual ribosomes were also found in the cytoplasm of the cells.

The mitochondria were clearly visible, numerous and varied in shape. The matrix was dense, with tubular and mixed-type cristae rarely visible. Various cytolemma protrusions were observed on the cell surface, and contacts between cell processes and blood and lymphatic capillaries were frequently detected. The endocrinocytes were found to be connected to each other by desmosomes and gap junctions. Additionally, curvatures of the biological membrane were detected in some areas. The lipophilic granules in the cytoplasm varied in size, shape, and density.

On the 90th day, the experimental group exhibited connective tissue membrane swelling and an increase in macrophage count, with parietal macrophages predominating over paravascular ones. The number of endocrinocytes decreased. Cell nuclei remained normal in size and shape (Fig. 2).

Minor destructive changes in the ultrastructural organization of the lamellar cytoplasmic Golgi complex were detected in the structure of interstitial endocrinocytes. The content of lysosomes in the cytoplasm of endocrinocytes was low, and lipid granules were large in size and present in each cell. Cells with a large number of lipid inclusions and small electron-dense hormonal granules in the cytoplasm are observed in some cases. A characteristic feature of these cells is the presence of numerous mitochondria with cristae immersed in a matrix of moderate electron density. The mitochondria of interstitial cells were of medium size, with an osmiophilic matrix and a small number of cristae. The cytoplasm of the cells was cleared, contained very few free ribosomes and polysomes,

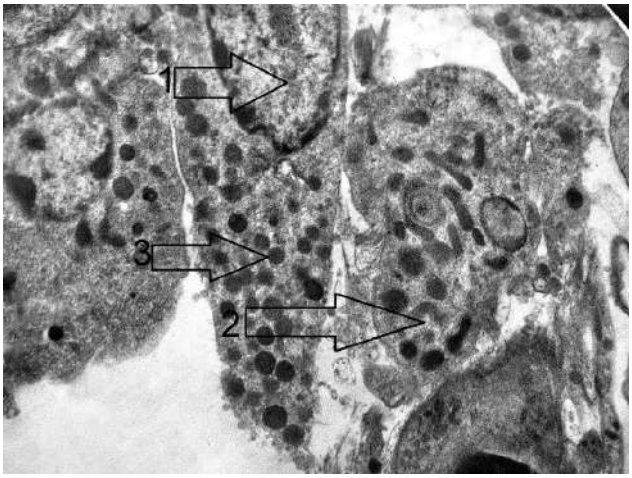

Fig. 1. Interstitial endocrinocytes of the testicular connective tissue on the 30th day of observation. 1 - endocrinocyte nucleus, 2 - endocrinocyte cytoplasm, 3 - inclusions. Magnification x12 000.

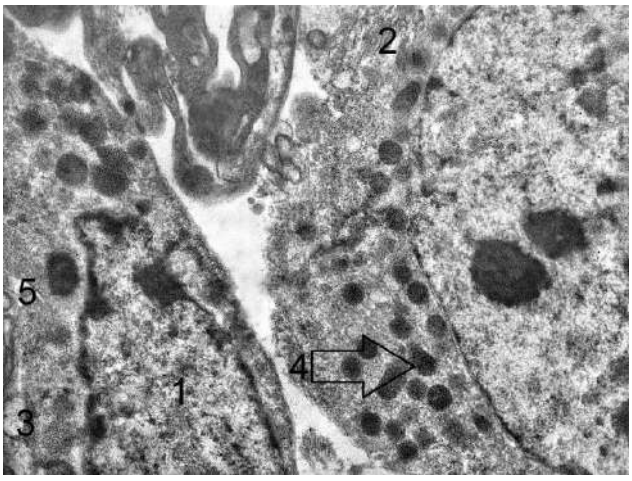

Fig. 2. Interstitial endocrinocytes of the testicular stroma on the 90th day of observation. 1 - endocrinocyte nucleus, 2 - Golgi complex, 3 - mitochondria, 4 - inclusions, 5 - endoplasmic reticulum. Magnification x12 000.

compared to the control group of animals and the previous observation period. The cytoplasmic membrane matched the structure of the elementary membrane.

On the 180th day of observation, there are signs of connective tissue edema, the number of macrophages is increased, and fibroblasts are sporadic. The number of endocrinocytes is reduced. Cell groups are still being determined, but the number of such groups is significantly reduced compared to the previous observation periods. In the interstitial space, there are cells in both the stages of destruction and dystrophy. Some cells appear unchanged. The nuclei of the cells vary in shape and size, with reduced density due to euchromatin. Heterochromatin is adjacent to the inner membrane of the nucleolemma in small depths. Most cells do not have nuclei. The cytoplasm is clear with a small amount of lipid inclusions. The endoplasmic reticulum shows signs of disruption. Lysosomes are single, clear and small. Single, few mitochondria are present in the cytoplasm. They are variable in size and shape, but mostly rounded, the matrix is not seen, cristae are not visualised. The outer membrane is blurred and loose. Intercellular contacts are mostly absent. Cell remnants are found in the interstitial space (Fig. 3).

When we examined the electron micrographs of the experimental group of animals on day 270, the interstitial space between the convoluted tubules was enlarged and the number of hormone-producing cells was significantly reduced. The cells were mostly solitary. The number of blood vessels is increased, and macrophages are observed in large numbers near them. The endocrinocytes are small, elongated, with acidophilic cytoplasm, vacuolated at the periphery, and no smooth endoplasmic reticulum is seen. The nuclei are elongated and occupy most of the cell. Nuclei are present in some of the cells but not in all of them. The caryolemma is indistinct, and the number of pores is small. Fragmented nuclei with dense chromatin are sometimes observed. Mitochondria are single and rounded. In certain cells, the smooth membranes of the Golgi complex were randomly oriented and surrounded by large, electron-transparent vacuoles, lipid inclusions, and secretory granules. The cytoplasmic membrane was indistinct. A significant number of cells had a fragmented smooth endoplasmic reticulum (Fig. 4).

On Day 360, there was an increase in connective tissue layers due to fibroblastic cells. The number and quality of blood vessels increased several times compared to previous periods of the experiment. In addition, the interstitial endocrinocytes were observed to be small in size and to be solitary. In certain locations, there were regions where these cells were entirely absent. If there were pairs of cells, they were not connected to each other. The cell membrane lacked clear boundaries, and there were no cell junctions. Isolated lipid granules were seen in the cytoplasm, and the endoplasmic reticulum and Golgi complex were poorly developed. The nuclei show light-optical alterations, and may be absent or in the process of

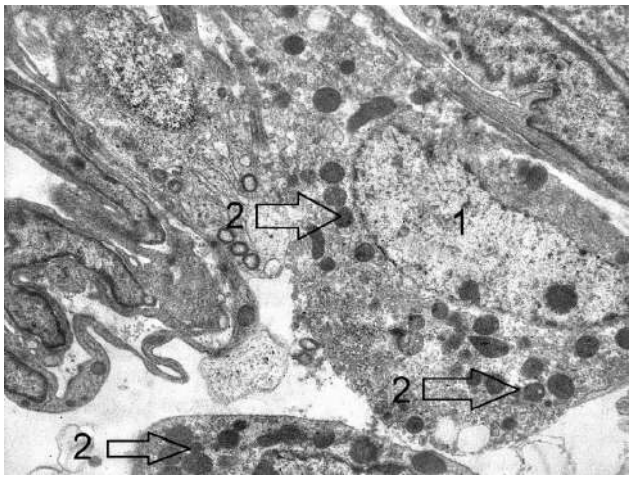

Fig. 3. Lipid inclusions of the endocrinocyte in the testicular stroma on the 180th day of observation. 1 - endocrinocyte nucleus, 2 - inclusions. Magnification x12 000.

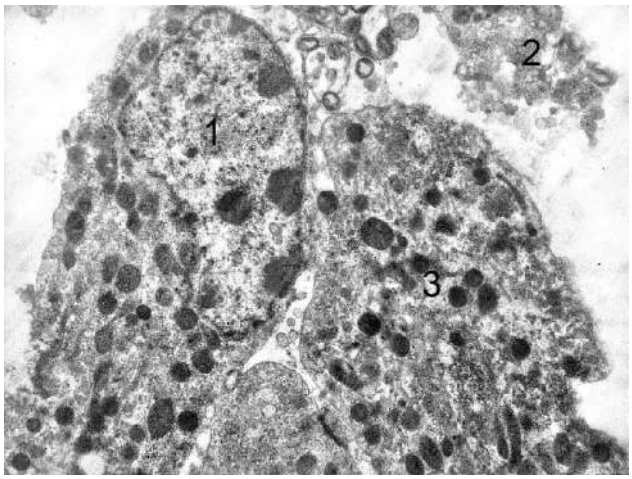

Fig. 4. Testicular stromal endocrinocyte on the 270th day of observation. 1 - endocrinocyte nucleus, 2 - part of the cytoplasm outside the cell, 3 - lipid inclusions. Magnifications x12 000.

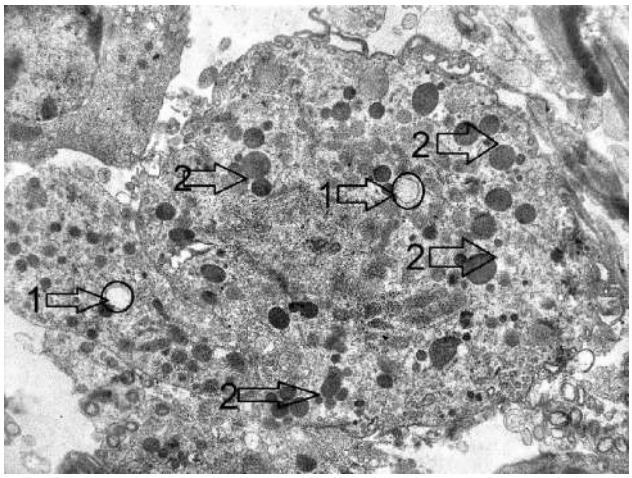

Fig. 5. Testicular stromal endocrinocyte on day 360 of observation. 1 - intracellular Reinke crystals, 2 - inclusions. Magnification x12 000.

destruction. Nucleoli are not present. Mitochondria are single and rounded, with no detected cristae. Reinke's crystals are present in the cytoplasm. The cell membrane is unclear (see Fig. 5).

Discussion

The article discusses the structural characteristics of testicular interstitial endocrinocytes under long-term (365 days) blockade of luteinising hormone synthesis by tryptorelin, as a result of the effect on the hypothalamic-pituitary-testicular system. The presented results of the study of the structure, differentiation and regulation of interstitial endocrinocytes in the rat testis prove that in rats, as in humans, we have recognised two different populations of these cells, namely, fetal and functional interstitial endocrinocytes, which were actually detected only at the early stages of the experiment. The ultrastructure, lifespan, ability to synthesise androgens, and regulatory mechanisms of these two populations' cells are quite different [15, 29].

The observed differences in the morphological parameters of endocrine cells under tryptorelin administration at different follow-up periods clearly confirm that tryptorelin is capable of inducing oxidative stress [8, 30, 34], which is manifested by increasing destructive alterations in the ultrastructural organisation of these cells. Various pathological changes and abnormalities were observed in the functional activity of the internal components of the cell. The analysis of the structure of interstitial endocrinocytes revealed that the population of these cells consists of round, oval or polygonal cells of medium size with well-developed cytoplasm and average, sometimes large nuclei. These are mature, specialised cells that have acquired the ability to synthesise androgens through determination and differentiation. The younger, less differentiated cells are small and spindle-shaped, sharing some structural features with fibroblasts. They are likely to maintain the constancy of cell composition in this population. Literature data [9, 29, 36] and our results confirm that no mitotic activity is detected in the pubertal population of endocrinocytes [10, 35]. Changes in mitochondrial structure and a decrease in cell cytoplasm volume, observed in the early stages of the tryptorelin experiment, suggest that steroid hormone synthesis, initiated at the endoplasmic reticulum, is completed in these organelles. Mitochondria in close contact with elements of the endoplasmic reticulum is a common cellular pattern. The diverse range of lipid inclusions found in the cytoplasm of interstitial endocrinocytes in various mammals can be attributed to several factors. It has been reported [37] that animals with non-seasonal reproduction typically have fewer lipid inclusions in the cytoplasm of endocrinocytes. In animals with seasonal reproduction, the cytoplasm of such cells almost always contains many lipid droplets of different electron densities surrounded by a membrane. This information is confirmed by our data [19]. A large amount of secretory product in a cell can indicate either a delay in the secretory process at the stage of secretion or high functional activity. The presence of well-developed agranular endoplasmic reticulum, numerous mitochondria, and frequent contact between mitochondria and smooth endoplasmic reticulum vesicles and lipid droplets are indicative of the latter. Counting the number of mitochondria and considering the peculiarities of their structure can significantly contribute to the analysis of morphological equivalents of steroidogenesis. Steroid-producing cells are identified by the presence of tubulovesicular cristae in their mitochondria. This feature is one of the indicators of active steroidogenesis. Additionally, pigment inclusions may be present in the cytoplasm of interstitial testicular endocrinocytes. A high content of pigment inclusions in the cytoplasm of interstitial endocrinocytes was not detected in the rats we studied at all stages of the experiment. The abundance of Reinke crystals, their number and the size of the crystals in relation to the cell volume correlate with changes in the cells and increase at later stages of the experiment [14, 31], which is confirmed by information from the literature. A similar correlation with testosterone levels has not been found in the literature, which allows us to consider Reinke crystals as a product of degenerative processes in the cell [16], which may also be indirectly evidenced by an increase in their number in testicular biopsies of men with cryptorchidism [19]. Therefore, the presence of these crystals in the interstitial cells and in the pericellular space after tryptorelin administration in our experiment is an indication of the cessation of androgen synthesis in these cells and of degenerative changes in the cells.

The population of rat endocrinocytes is a stable type of cell population. This is evidenced by the fact that no mitoses were detected in the interstitial endocrinocytes of the testes in any of the mature rats studied. Resident macrophages are important for the differentiation and function of interstitial endocrinocytes [22, 23]. The apoptosis of these cells in the late stages of the experiment contributes to the regulation of the number and quality of these cells, which can be induced by cytotoxins [2]. The characteristics of the ageing of these cells in rats are likely to be species specific. It is known [32] that 11-beta-hydroxysteroid dehydrogenase protects testosterone synthesis in interstitial endocrinocytes of stressed rats. In the cytoplasm of endocrinocytes of experimental animals on the 365th day of observation, hexagonal prisms with clearly defined edges and corners, formations in the form of a "wasp's nest" - Reinke crystals (layers arising from the disintegration of smooth endoplasmic reticulum membranes) are sometimes detected. The stability of the population is therefore ensured by a dynamic equilibrium between the processes taking place in these structures. In our experiment, we used quercetin as a drug to correct the oxidative stress of the testicular interstitial space caused by tryptorelin, which has both antioxidant and immunomodulatory properties, reducing the production of cytotoxic superoxide anion, which we believe normalises the structure of the endoplasmic

reticulum and mitochondria of a subpopulation of these cells.

Our results provide a theoretical basis for the development of methods to correct disorders of the generative and endocrine function of the testes in the pathological effects of a central dyshormonal state on the body: in the case of disorders of the hypothalamic-pituitary-testicular system. The data on the functional morphology of the testes during the stages of adaptation to changes in endocrine and immune function of the testes extend the existing knowledge of the causes of spermatogenesis and its regulation.

Conclusions

1. Tryptorelin administration induces structural and functional abnormalities in the connective tissue components of the rat testis, characterised by quantitative and qualitative changes in the population of interstitial endocrine cells, as evidenced by electron microscopic alterations at the level of subcellular structures.

2. The additional administration of quercetin reduces the negative effect of tryptorelin and delays the appearance of disturbances in the structure of interstitial endocrinocytes from day 180 to later observation periods.

References

[1] Abarikwu, S. O., Adesiyan, A. C., Oyeloja, T. O., Oyeyemi, M. O., & Farombi, E. O. (2010). Changes in sperm characteristics and induction of oxidative stress in the testis and epididymis of experimental rats by a herbicide, atrazine. *Archives of environmental contamination and toxicology*, 58, 874-882. doi: 10.1007/s00244-009-9371-2

[2] Abdelhameed, R. F., Ali, A. I., Elhady, S. S., Abo Mansour, H. E., Mehanna, E. T., Mosaad, S. M., ... & Eltahawy, N. A. (2022). Marrubium alysson L. Ameliorated Methotrexate-Induced Testicular Damage in Mice through Regulation of Apoptosis and miRNA-29a Expression: LC-MS/MS Metabolic Profiling. *Plants,* 11(17), 2309. doi: 10.3390/plants11172309.

[3] Abdelzaher, W. Y., Abdel-Hafez, S. M. N., Rofaeil, R. R., Ali, A. H. S. A., Hegazy, A., & Bahaa, H. A. (2021). The protective effect of fenofibrate, triptorelin, and their combination against premature ovarian failure in rats. *Naunyn-Schmiedeberg's archives of pharmacology,* 394(1), 137-149. doi: 10.1007/s00210-020-01975-2

[4] Amevor, F. K., Cui, Z., Ning, Z., Shu, G., Du, X., Jin, N., ... & Zhao, X. (2022). Dietary quercetin and vitamin E supplementation modulates the reproductive performance and antioxidant capacity of aged male breeder chickens. *Poultry science,* 101(6), 101851. doi: 10.1016/j.psj.2022.101851

[5] Aborode, A. T., Pustake, M., Awuah, W. A., Alwerdani, M., Shah, P., Yarlagadda, R., ... & Alexiou, A. (2022). Targeting Oxidative Stress Mechanisms to Treat Alzheimer's and Parkinson's Disease: A Critical Review. *Oxidative medicine and cellular longevity,* 2022, 7934442. doi: 10.1155/2022/7934442

[6] Akbari, F., Azadbakht, M., Gaurav, A., Azimi, F., Mahdizadeh, Z., Vahedi, L., ... & Eghbali, M. (2022). Evaluation of the Therapeutic Effect of the Traditional Herbal Medicine Atrifil and Oshagh Gum on Testosterone-Induced Benign Prostatic Hyperplasia in Wistar Rats. *Advances in urology,* 2022, 5742431. doi: 10.1155/2022/5742431

[7] Akimov, O. Ye., Mykytenko, A. O., & Kostenko, V. O., (2023). Nitric oxide cycle activity in rat biceps femoris muscle under conditions of bacterial lipopolysaccharide influence, experimental metabolic syndrome and their combination. *Ukrainian Biochemical Journal,* 95(4), 24-34. doi: 10.15407/ubj95.04.024

[8] Akimov, O. Y., & Kostenko, V. O. (2016). Functioning of nitric oxide cycle in gastric mucosa of rats under excessive combined intake of sodium nitrate and fluoride. Ukrainian biochemical journal, 88(6), 70-75. doi: 10.15407/ubj88.06.070

[9] Almeida, S., Rato, L., Sousa, M., Alves, M. G., & Oliveira, P. F. (2017). Fertility and Sperm Quality in the Aging Male. Current pharmaceutical design, 23(30), 4429-4437. doi: 10.2174/1381612823666170503150313

[10] Atallah, A., Mhaouty-Kodja, S., & Grange-Messent, V. (2017). Chronic depletion of gonadal testosterone leads to blood-brain barrier dysfunction and inflammation in male mice. Journal of cerebral blood flow and metabolism: official journal of the International Society of Cerebral Blood Flow and Metabolism, 37(9), 3161-3175. doi: 10.1177/0271678X16683961

[11] Bahriy, M. M., Dibrova, V. A., Popadynets, O. H., & Hryshchuk, M. I. (2016). *Методики морфологічних досліджень [Metodyky morfolohichnykh doslidzhen]*. Вінниця: Нова книга=Vinnytsya: Nova knyha.

[12] Botté, M. C., Lerrant, Y., Lozach, A., Bérault, A., Counis, R., & Kottler, M. L. (1999). LH down-regulates gonadotropin-releasing hormone (GnRH) receptor, but not GnRH, mRNA levels in the rat testis. *The Journal of endocrinology,* 162(3), 409-415. doi: 10.1677/joe.0.1620409

[13] Chekalina, N. I. (2017). Resveratrol has a positive effect on parameters of central hemodynamics and myocardial ischemia in patients with stable coronary heart disease. *Wiadomosci lekarskie* (Warsaw, Poland: 1960), 70(2 pt 2), 286-291. PMID: 29059644

[14] Chung, J. Y., Brown, S., Chen, H., Liu, J., Papadopoulos, V., & Zirkin, B. (2020). Effects of pharmacologically induced Leydig cell testosterone production on intratesticular testosterone and spermatogenesis. *Biology of reproduction*, 102(2), 489-498. doi: 10.1093/biolre/ioz174

[15] Garza, S., & Papadopoulos, V. (2023). Testosterone recovery therapy targeting dysfunctional Leydig cells. *Andrology,* 11(5), 816-825. doi: 10.1111/andr.13304

[16] Garza, S., Chen, L., Galano, M., Cheung, G., Sottas, C., Li, L., ... & Papadopoulos, V. (2022). Mitochondrial dynamics, Leydig cell function, and age-related testosterone deficiency. *FASEB journal: official publication of the Federation of American Societies for Experimental Biology*, 36(12), e22637. doi: 10.1096/fj.202201026R

[17] Giordano, G., Mastrantoni, L., & Colloca, G. F. (2023). Myocardial bridge in a patient with castration-resistant metastatic prostate cancer treated with enzalutamide. *Journal of oncology pharmacy practice: official publication of the International Society of Oncology Pharmacy Practitioners*, 29(7), 1754-1756. doi: 10.1177/10781552231180599

[18] Han, S., Luo, J., Xu, S., Zhao, L., Yao, C., Xu, J., ... & Li, P. (2022). Low-Intensity Pulsed Ultrasound Alleviates Human Testicular Leydig Cell Senescence In Vitro. *International journal of molecular sciences,* 24(1), 418. doi: 10.3390/ijms24010418

[19] Hotta, Y., Kataoka, T., & Kimura, K. (2019). Testosterone Deficiency and Endothelial Dysfunction: Nitric Oxide, Asymmetric Dimethylarginine, and Endothelial Progenitor Cells. *Sexual medicine reviews,* 7(4), 661-668. doi: 10.1016/

j.sxmr.2019.02.005
[20] Kostenko, V., Akimov, O., Gutnik, O., Kostenko, H., Kostenko, V., Romantseva, T., … & Taran, O. (2023). Modulation of redox-sensitive transcription factors with polyphenols as pathogenetically grounded approach in therapy of systemic inflammatory response. *Heliyon,* 9(5), e15551. doi: 10.1016/j.heliyon.2023.e15551
[21] Liu, F. H., Yang, D. Z., Wang, Y. F., Liang, X. P., Peng, W. M., Cao, C. A., … & Guo, Z. M. (2007). Making of the animal model with sterilized testes. *Zhonghua nan ke xue = National journal of andrology,* 13(2), 125-129. PMID: 17345767
[22] Merseburger, A. S., & Hupe, M. C. (2016). An Update on Triptorelin: Current Thinking on Androgen Deprivation Therapy for Prostate Cancer. *Advances in therapy,* 33(7), 1072-1093. doi: 10.1007/s12325-016-0351-4
[23] Wang, M., Yang, Y., Cansever, D., Wang, Y., Kantores, C., Messiaen, S., … & Bhushan, S. (2021). Two populations of self-maintaining monocyte-independent macrophages exist in adult epididymis and testis. *Proceedings of the National Academy of Sciences of the United States of America*, 118(1), e2013686117. doi: 10.1073/pnas.2013686117
[24] Mossadegh-Keller, N., & Sieweke, M. H. (2018). Testicular macrophages: Guardians of fertility. *Cellular immunology,* 330, 120-125. doi: 10.1016/j.cellimm.2018.03.009
[25] Opryshko, V., Prokhach, A., Akimov, O., Riabushko, M., Kostenko, H., Kostenko, V., … & Kostenko, V. (2024). Desmodium styracifolium: Botanical and ethnopharmacological insights, phytochemical investigations, and prospects in pharmacology and pharmacotherapy. *Heliyon,* 10(3), e25058. doi: 10.1016/j.heliyon.2024.e25058
[26] Rawla P. (2019). Epidemiology of Prostate Cancer. *World journal of oncology,* 10(2), 63-89. doi: 10.14740/wjon1191
[27] Rice, M. A., Malhotra, S. V., & Stoyanova, T. (2019). Second-Generation Antiandrogens: From Discovery to Standard of Care in Castration Resistant Prostate Cancer. *Frontiers in oncology*, 9, 801. doi: 10.3389/fonc.2019.00801
[28] Scovell, J. M., & Khera, M. (2018). Testosterone Replacement Therapy Versus Clomiphene Citrate in the Young Hypogonadal Male. *European urology focus,* 4(3), 321-323. doi: 10.1016/j.euf.2018.07.033
[29] Swelum, A. A., Saadeldin, I. M., Zaher, H. A., Alsharifi, S. A. M., & Alowaimer, A. N. (2017). Effect of sexual excitation on testosterone and nitric oxide levels of water buffalo bulls (Bubalus bubalis) with different categories of sexual behavior and their correlation with each other. *Animal reproduction science,* 181, 151-158. doi: 10.1016/j.anireprosci.2017.04.003
[30] Tarasenko, L. M., Neporada, K. S., & Klusha, V. (2002). Stress-protective effect of glutapyrone belonging to a new type of amino acid-containing 1,4-dihydropyridines on periodontal tissues and stomach in rats with different resistance to stress. *Bulletin of experimental biology and medicine,* 133(4), 369-371. doi: 10.1023/a:1016250121896
[31] Tas, M., Oner, G., Ulug, P., Yavuz, A., & Ozcelik, B. (2019). Evaluation of protective effects of GnRH agonist or antagonist on ovarian reserve with anti-M?llerian hormone and histological analysis in a rat model using cisplatin. *Archives of medical science: AMS,* 19(2), 448-451. doi: 10.5114/aoms.2019.87540
[32] Teoli, J., Mallet, D., Renault, L., Gay, C. L., Labrune, E., Bretones, P., … & Plotton, I. (2023). Case Report: Longitudinal follow-up and testicular sperm extraction in a patient with a pathogenic NR5A1 (SF-1) frameshift variant: p.(Phe70Serfs*5). *Frontiers in endocrinology,* 14, 1171822. doi: 10.3389/fendo.2023.1171822
[33] Yelins'ka, A. M., Akimov, O. Y., & Kostenko, V. O. (2019). Role of AP-1 transcriptional factor in development of oxidative and nitrosative stress in periodontal tissues during systemic inflammatory response. *Ukrainian biochemical journal,* 91(1), 80-85. doi: 10.15407/ubj91.01.080
[34] Zhao, Y., Liu, X., Qu, Y., Wang, L., Geng, D., Chen, W., … & Lv, P. (2019). The roles of p38 MAPK® COX2 and NF-kB® COX2 signal pathways in age-related testosterone reduction. *Scientific reports,* 9(1), 10556. doi: 10.1038/s41598-019-46794-5
[35] Zhang, Y., Zhang, C., Li, Z., Zeng, C., Xue, Z., Li, E., … & Guo, B. (2022). New 8-prenylated quercetin glycosides from the flowers of Epimedium acuminatum and their testosterone production-promoting activities. *Frontiers in chemistry,* 10, 1014110. doi: 10.3389/fchem.2022.1014110
[36] Zhao, Y., Liu, H., Yang, Y., Huang, W., & Chao, L. (2022). The effect and mechanism of Grim 19 on mouse sperm quality and testosterone synthesis. *Reproduction* (Cambridge, England), 163(6), 365-377. doi: 10.1530/REP-21-0385
[37] Zirkin, B. R., & Papadopoulos, V. (2018). Leydig cells: formation, function, and regulation. *Biology of reproduction,* 99(1), 101-111. doi: 10.1093/biolre/ioy059
[38] Zullkiflee, N., Taha, H., & Usman, A. (2022). Propolis: Its Role and Efficacy in Human Health and Diseases. *Molecules* (Basel, Switzerland), 27(18), 6120. doi: 10.3390/molecules27186120

ВПЛИВ ВВЕДЕННЯ КВЕРЦЕТИНУ НА ЕЛЕКТРОННО-МІКРОСКОПІЧНІ ЗМІНИ ІНТЕРСТИЦІЙНИХ ЕНДОКРИНОЦИТІВ ЯЄЧОК ПРИ ДОВГОТРИВАЛОМУ ЦЕНТРАЛЬНОМУ БЛОКУВАННІ ЛЮТЕЇНІЗУЮЧОГО ГОРМОНУ У ЩУРІВ

Стецук Є. В., Шепітько В. І., Проніна О. М., Запорожець Т. М., Борута Н. В., Вільхова О. В., Лисаченко О. Д., Пелипенко Л. Б., Волошина О. В., Левченко О. А.

Кверцетин - це поширений флавоноїд, який допомагає уникнути розвитку хвороб серцево-судинної системи, знижує ризик виникнення дегенеративних процесів у головному мозку та онкологічних захворювань. Речовини цієї групи мають антиоксидантні властивості, допомагають організму захиститися від агресивного впливу вільних радикалів, нейтралізуючи ці нестабільні молекули. Проведені дослідження показують, що інтенсивний вплив вільних радикалів на структуру клітин корелює з розвитком низки хронічних захворювань, серед яких цукровий діабет, рак та серцево-судинні патології. Мета дослідження - з'ясувати вплив введення кверцетину на електронно-мікроскопічні зміни інтерстиційних ендокриноцитів яєчок при довготривалому центральному блокуванні синтезу лютеїнізуючого гормону трипторелін. Експеримент проведений на 35 статевозрілих самцях білих щурів. Щури були розподілені на 2 групи: контрольна група (I) - вводили фізіологічний розчин, II група - тварини з експериментальною центральною депривацією синтезу лютеїнізуючого гормону (підшкірно вводили трипторелін у дозі 0,3 мг діючої речовини на 1 кг маси тіла щура) та паралельно вводили кверцетин три рази на добу за допомогою гастрального зонду у перерахунку на вагу тіла тварин. Проведене дослідження показало, що введення трипторелін призводить до структурно-функціональних змін у будові сполучнотканинних компонентів яєчок щурів. Це проявляється кількісно-якісними порушеннями в популяції інтерстиційних ендокринних клітин та електронно-мікроскопічними змінами на рівні субклітинних структур. На 270 та 365 день експерименту виявлені патологічні зміни в структурі інтерстиційних ендокриноцитів яєчок та функціональної активності внутрішніх компонентів клітин.

Встановлено, що частота знаходження кристалів Рейнке, їх кількість і розмір по відношенню до об'єму клітини корелює зі змінами в клітинах і збільшується на більш пізніх термінах дослідження. Відомостей щодо аналогічної кореляції з рівнем тестостерону в літературі виявлено не було, що дозволяє позначити кристали Рейнке, як продукт дегенеративних процесів у клітині. Таким чином, додаткове введення кверцетину зменшує негативний вплив трипторелін і відтерміновує виникнення змін у структурі інтерстиційних ендокриноцитів зі 180-ї доби на більш пізні часові проміжки спостереження.
Ключові слова: *яєчка, електронна мікроскопія, щури, інтерстиційні ендокриноцити, лютеїнізуючий гормон, кверцетин, трипторелін.*

Author's contribution

Stetsuk Ye. V. - work concept and design, data collection and analysis, writing the article.
Shepitko V. I. - work concept and design.
Pronina O. M. - final approval of the article.
Zaporozhets T. M. - critical review, final approval of the article.
Boruta N. V. - responsibility for statistical analysis.
Vilkhova O. V. - data collection and analysis.
Lysachenko O. D. - data collection and analysis.
Pelypenko L. B. - work concept and design, data collection and analysis.
Voloshyna O. V. - writing the article.
Levchenko O. A. - data collection and analysis, responsibility for statistical analysis.

DOI: 10.31393/morphology-journal-2024-30(1)-10 Reports of Morphology, Vol. 30, №1, Pages 76-83

ISSN 1818-1295 eISSN 2616-6194

REPORTS OF MORPHOLOGY

Official Journal of the Scientific Society of Anatomists, Histologists, Embryologists and Topographic Anatomists of Ukraine

journal homepage: https://morphology-journal.com

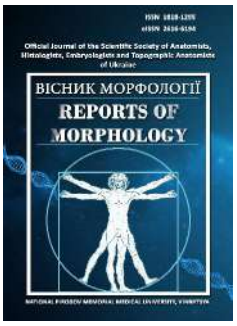

Analytical and quantitative assessment of the structural components of the adrenal glands of rats under the conditions of exposure to the venom of vipers Vipera berus berus and Vipera berus nikolskii

Niyazmetov T. S.[1], Samborska I. A.[2], Butska L. V.[3], Kasianenko D. M.[4], Ocheretna O. L.[4], Halahan Yu. V.[4], Fik V. B.[5]

[1]Bogomolets National Medical University, Kyiv, Ukraine
[2]National University of Ukraine on Physical Education and Sport, Kyiv, Ukraine
[3]Educational and Scientific Center "Institute of Biology and Medicine", Taras Shevchenko National University of Kyiv, Kyiv, Ukraine
[4]National Pirogov Memorial Medical University, Vinnytsya, Ukraine
[5]Danylo Halytsky Lviv National Medical University, Lviv, Ukraine

ARTICLE INFO
Received: 04 January 2024
Accepted: 14 February 2024

UDC: 61:612.4:615.9.616.4:616-09

CORRESPONDING AUTHOR
e-mail: samborska1990@gmail.com
Samborska I. A.

CONFLICT OF INTEREST
The authors have no conflicts of interest to declare.

FUNDING
Not applicable.

DATA SHARING
Data are available upon reasonable request to corresponding author.

Snakebite envenoming is a common but neglected public health problem worldwide, especially in tropical countries. Annual mortality as a result of snakebites exceeds 138,000. It is believed that this problem is underestimated, and in many countries, individual cases of bites are not subject to proper fixation. The purpose of the study is the analytical and quantitative assessment of the structural components of the rats' adrenal glands under exposure to the venom of Vipers Vipera berus berus and Vipera berus nikolskii. Experimental studies were carried out on white, non-linear male rats. Vipera berus berus and Vipera berus nikolskii viper venom were obtained from V. N. Karazin Kharkiv National University. The freeze-dried native venom was stored at -20 °C and dissolved in saline immediately before the experiment. The animals were divided into three groups (control and 2 experimental groups) of 10 individuals each. Experimental rats were injected intraperitoneally in a physiological solution with a semi-lethal dose (LD50) (1.576 mg/g^{-1}) of Vipera berus berus and Vipera berus nikolskii venoms. Animals of the control group were injected intraperitoneally with only a physiological solution. Rats were removed from the experiment 24 hours after exposure to the poison and anesthetised by cervical dislocation. Statistical analysis of the area of the microcirculatory channel and the nuclear-cytoplasmic index was performed using Fiji: ImageJ program and processed in Excel. Administration of the venom of the vipers Vipera berus berus and Vipera berus nikolskii to rats was accompanied by a significant increase in the area of the microcirculatory bed relative to the control group (2.9 times for Vipera berus berus and 6.5 times for Vipera berus nikolskii). Exposure to Vipera berus berus viper venom was associated with a significant decrease in the nuclear-cytoplasmic index in rats of the experimental group compared to the control group (13 % and 42 %, respectively), which is evidence of a decrease in the area of the nuclei of endocrinocytes of the adrenal cortex. This indicator in rats under the administration of Vipera berus nikolskii venom was even lower and amounted to 12 %. According to the statistical analysis of the quantitative assessment of the state of the cortical substance of the adrenal glands, it is worth noting the similar effect of the poisons of both types of snakes at the cellular level. At the same time, at the tissue level, the effect of Vipera berus nikolskii venom is more pronounced than that of Vipera berus berus - this is evidenced by the higher degree of disruption of the structure of the hemomicrocirculatory channel in the adrenal cortex of animals from the group that was affected by this venom. It led to an increase in the area of vessels due to their expansion and ruptures of their walls and haemorrhages into the surrounding parenchyma and stroma.

Keywords: *vipers, poison, nuclear-cytoplasmic index, microcirculatory channel, rats.*

Introduction

Envenomation from the bites of snakes and other venomous animals, including scorpions, is a common but neglected public health problem worldwide, especially in tropical countries [23, 29]. Annual mortality from snake bites exceeds 138,000, and mortality from scorpion bites reaches 1.5 million cases [9, 12, 13]. It is believed that this problem is underestimated, and in many countries, individual cases of bites are not subject to proper fixation [15, 39]. In India, about 58,000 people die each year from complications caused by snake and in particular viper venom [33].

It is known that the toxins of snakes and vipers are a complex mixture of proteins, peptides, low molecular weight substances, and salts in the water environment [10, 19]. Usually, venom causes a neurotoxic effect, local destruction of soft tissues in the places of its inoculation, or a vasohemotoxic effect [24, 31]. These data correlate with the mechanism of action of scorpion venoms, in which the severity of envenomation is closely related to the neurotoxic effects of the venom (excitation of neurons and release of catecholamines). However, developing severe systemic disorders may be associated with increased enzymatic activity in tissues, which also activates the inflammatory response [11]. Clinical manifestations are diverse and include local (oedema, tissue necrosis) and systemic [14, 34]. The latter is manifested in the form of neuromuscular paralysis, rhabdomyolysis, hypotension, collapse, and DIC syndrome [37, 38].

In recent years, scientists have reported the development of endocrine and metabolic disorders as a result of pituitary dysfunction, adrenal gland damage, dysglycemia, electrolyte disturbances, and renal tubular acidosis [21, 26, 36].

The endocrine system, which has a wide range of hormonal influences on various organs and systems, plays an extremely important role in the emergence of body reactions to stimuli [5, 8]. At the same time, not individual hormones but the overall endocrine balance, which is formed in a state of stress and tension, determines the nature and strength of compensatory-adaptive and protective processes for adaptation and resistance of the organism [28, 27].

Adrenal glands occupy an important place in the endocrine regulation of the human body's vital processes in a changing environment. It is a well-known fact that the adrenal glands participate in the mechanisms of adaptation of an individual to stress of exo- or endogenous origin [18, 35]. Their role has also been established in regulating water-mineral balance and the synthesis of biomolecules (proteins, fats, carbohydrates). It should be noted that in response to the action of a stressor, the adrenal glands ensure adaptation and the development of compensatory and adaptive changes in organs and systems [20, 30]. The formation of these mechanisms is possible mainly due to the influence of epinephrine and glucocorticoids, the level of which is a determining factor for the degree of expressiveness of the body's reaction and the development of morphological changes in organs [7, 16].

Considering the above facts, studying the qualitative and quantitative composition of the adrenal glands and cellular components of rats under *Vipera berus* berus and *Vipera berus* nikolskii venom is an urgent task.

The research aims to analyse and quantitatively assess the structural components of the adrenal glands of rats under exposure to the venom of *Vipera berus* berus and *Vipera berus* nikolskii.

Materials and methods

Experimental studies were carried out on white, non-linear male rats. For preliminary acclimatisation, the animals were kept for 7 days in the animal facility of Taras Shevchenko National University of Kyiv, and later - in laboratory conditions with compliance with temperature and light regimes [3]. Rats received standard chow and water ad libitum. All experiments were conducted in accordance with the National Institutes of Health Guidelines for the care and use of laboratory animals and the European Council Directive of 24 November 1986 for the Care and Use of Laboratory Animals (86/609/EEC). The research was approved and confirmed by the Bioethics Commission of the NSC "Institute of Biology and Medicine" of the Taras Shevchenko National University of Kyiv (protocol No. 2, dated August 19, 2021).

Vipera berus berus and *Vipera berus nikolskii* venom were obtained from the V. N. Karazin Kharkiv National University. The lyophilised crude venom was stored at - 20 °C and dissolved in a saline solution immediately before the experiment.

The animals were divided into a control and 2 experimental groups of 10 individuals each. Experimental rats were injected intraperitoneally with a semi-lethal dose (LD50) (1.576 mg/g^{-1}) of *Vipera berus berus* and *Vipera berus nikolskii* venom in saline solution. Animals in the control group were injected intraperitoneally with only a saline solution. Rats were removed from the experiment 24 hours after exposure to the venom and anesthetised by cervical dislocation.

The statistical analysis of rat adrenal gland parameters evaluated two continuous variables: the microcirculatory bed's area in these glands' stroma and the nuclear-cytoplasmic index of hormone-producing cells in their parenchyma. These parameters were determined for one control group and two experimental groups, in which rats were exposed to the venom of two vipers - *Vipera berus berus* and *Vipera berus nikolskii*. All measurements were made using the Fiji: ImageJ program and processed in Excel.

In order to estimate the share of the adrenal glands occupied on the sections by elements of the microcirculatory channel, we measured the area of the corresponding vessels in 8 sections of the adrenal glands of animals from the control and two experimental groups (four animals from each group). Next, we calculated the sum of these areas for each slice. Digital images obtained under a light

microscope at a magnification of x1000 were used for measurements. The section area within which vessels were measured for all groups is 23803 μm^2.

In order to quantitatively assess the general condition of adrenal parenchyma cells, we calculated the nuclear-cytoplasmic ratio in the endocrine cells of the zona glomerulosa and zona fasciculata of the cortex.

The nuclear-cytoplasmic index was calculated in 40 cells on 4 sections from four animals from each group. Measurements were performed on digital images obtained from a light microscope at x1000 magnification.

Since when checking the measurements of the control and both experimental groups for normality of distribution, the graphs did not correspond to the Gaussian curve, the non-parametric Mann-Whitney test was used to determine the reliability of the differences between the groups [17].

Results

When analysing the total area of the microcirculatory channel of the cortex, which is occupied by small vessels on the sections of the adrenal glands, a significant increase of this index was found in the group with the injection of Vipera berus berus venom compared to the control group (Table 1). If in the control group, this index is 445.3 μm^2 (first quartile 318 μm^2; third quartile 512 μm^2), then for the corresponding experimental group, it is 1298 μm^2 (first quartile 915 μm^2; third quartile 1615 μm^2).

This expansion of the microcirculatory bed is quite logical and is related to several factors. First, venom damages the walls of blood vessels as it is transported with the blood. Formal blood elements are affected, particularly erythrocytes, which aggregate and clog vessels. Snake venom primarily affects proteins, including blood plasma proteins, coagulating them and thus disrupting the structure and viscosity of blood. In addition, the arrival of a foreign factor to the tissues and its spread there provokes the development of inflammatory reactions, accompanied by swelling of the tissues, expansion of blood vessels and increased permeability.

It is worth noting the insignificant standard deviation for both groups, which indicates the regularity of the processes of vessel expansion, which is equally inherent to all elements of the microcirculatory channel (Fig. 1). It can be assumed that the venom of Vipera berus berus damages the microcirculatory processes in the adrenal gland, which leads to a violation of its morphology and functioning and, ultimately, to necrosis. Because we assessed the adrenal glands 24 hours after venom administration, the tissue changes are not radical, and the vascular damage will likely worsen over time.

The assessment of the condition of the vessels of the microcirculatory bed in the group with the introduction of *Vipera berus nikolskii* venom showed a significant increase in the area of the microcirculatory bed of the animals compared to the control group (Fig. 1). Here, this indicator is 2916 μm^2 (first quartile 1533 μm^2; third quartile 3884 μm^2).

Table 1. The average value of the microcirculatory channel area of the adrenal glands in the control and experimental groups (M±σ).

Group	The average value of the area, mm^2	The presence of a reliable difference with the control group
Control group	445.3±226.5	-
Group with an injection of Vipera berus berus venom	1298±608	Present*
Group with an injection of Vipera berus nikolskii venom	2916±1655	Present*

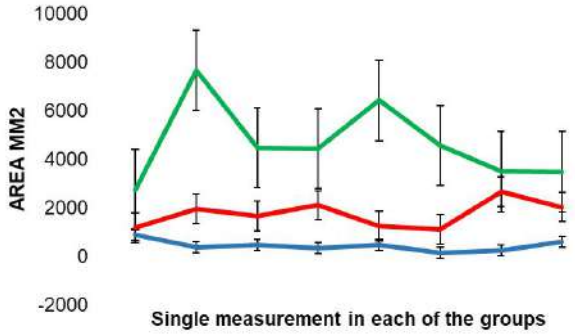

Fig. 1. Individual indexes of the area of the microcirculatory bed of animals of the control and experimental groups with standard deviation. Green colour - control group; red colour - the group with the injection of *Vipera berus berus* venom; blue colour - the group with the introduction of *Vipera berus nikolskii* venom; I - standard deviation.

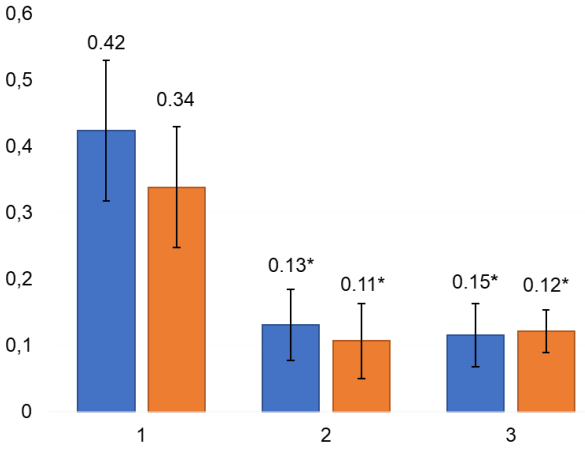

Fig. 2. The average value of the nuclear-cytoplasmic index in the adrenal cortex cells in the control group, the group with the injection of *Vipera berus berus* venom and *Vipera berus nikolskii* venom. 1 - control group; 2 - a group with an injection of *Vipera berus berus* venom; 3 - a group with an injection of *Vipera berus nikolskii* venom; blue columns - zona glomerulosa; orange columns - zona fasciculata; * - the difference from the control group is significant at $p \leq 0.05$.

The vessels of the adrenal cortex increase in size due to swelling and disruption of their content. The lumens of capillaries and venules expand due to the accumulation of aggregated erythrocytes and blood plasma clots in them. Similar processes are observed under the action of *Vipera berus berus* venom. Although we did not find a reliable

Table 2. Nuclear-cytoplasmic index of endocrinocytes of the adrenal cortex in control and experimental groups.

Group	Control group		The group with injection of *Vipera berus berus* venom		The group with injection of *Vipera berus nikolskii* venom	
Zone	Glomerulosa	Fasciculata	Glomerulosa	Fasciculata	Glomerulosa	Fasciculata
1	0.23	0.48	0.12	0.21	0.14	0.08
2	0.33	0.27	0.2 1	0.23	0.23	0.14
3	0.56	0.43	0.09	0.23	0.15	0.11
4	0.68	0.28	0.15	0.23	0.09	0.07
5	0.50	0.43	0.08	0.18	0.13	0.11
6	0.36	0.37	0.10	0.16	0.09	0.08
7	0.34	0.48	0.18	0.10	0.15	0.14
8	0.47	0.37	0.16	0.10	0.14	0.15
9	0.34	0.42	0.17	0.19	0.12	0.16
10	0.31	0.42	0.11	0.21	0.09	0.18
11	0.35	0.23	0.26	0.10	0.07	0.14
12	0.42	0.28	0.09	0.13	0.09	0.15
13	0.63	0.29	0.19	0.07	0.10	0.15
14	0.26	0.21	0.20	0.11	0.06	0.14
15	0.46	0.28	0.11	0.08	0.08	0.11
16	0.55	0.21	0.19	0.05	0.03	0.14
17	0.43	0.22	0.17	0.07	0.10	0.13
18	0.41	0.50	0.10	0.06	0.07	0.12
19	0.39	0.42	0.22	0.08	0.13	0.08
20	0.49	0.21	0.24	0.06	0.13	0.18
21	0.53	0.42	0.12	0.07	0.11	0.14
22	0.23	0.29	0.09	0.12	0.17	0.12
23	0.39	0.33	0.05	0.07	0.14	0.12
24	0.34	0.30	0.07	0.08	0.10	0.12
25	0.38	0.27	0.10	0.09	0.09	0.11
26	0.27	0.23	0.09	0.09	0.08	0.19
27	0.48	0.24	0.15	0.12	0.06	0.15
28	0.56	0.43	0.12	0.07	0.11	0.13
29	0.31	0.36	0.09	0.09	0.11	0.07
30	0.41	0.32	0.043	0.12	0.09	0.16
31	0.43	0.26	0.20	0.05	0.08	0.14
32	0.44	0.25	0.12	0.07	0.07	0.10
33	0.38	0.33	0.12	0.05	0.12	0.14
34	0.48	0.38	0.08	0.10	0.13	0.13
35	0.43	0.51	0.13	0.08	0.11	0.08
36	0.52	0.32	0.14	0.09	0.22	0.08
37	0.58	0.29	0.04	0.05	0.10	0.11
38	0.45	0.35	0.09	0.06	0.12	0.09
39	0.44	0.53	0.17	0.06	0.26	0.08
40	0.35	0.34	0.08	0.08	0.20	0.05

difference between the two experimental groups, the larger value of the average area of blood vessels in the group exposed to the Vipera berus nikolskii venom is worth noting. In addition to the pathological processes that develop as a result of the action of both venoms, the impressive action of the toxins causes the rupture of the wall of small vessels and the release of formal elements and blood plasma from them into the surrounding interstitium and parenchyma.

The value of the nuclear-cytoplasmic index conveniently assesses the influence of toxic substances on the morphology and functioning of cells since this parameter reflects the state of the nucleus, as a participant in protein synthesis, and the cytoplasm, in which most of the processes important for the functioning of the entire tissue and organ take place. In the case of an endocrine gland, the main process in the cytoplasm of parenchyma cells is the synthesis of hormones. Since we focused our attention precisely on the zona glomerulosa and zona fasciculata of the adrenal cortex, we are talking about the synthesis of steroid hormones, so the main part of the cytoplasm is occupied by a smooth endoplasmic reticulum and lipid droplets, which are the source of hormone synthesis.

Indexes of the nuclear-cytoplasmic ratio of zona glomerulosa cells of the adrenal cortex from the control group form a series with a slight standard deviation, indicating the homogeneity of differentiated endocrinocytes morphology (Table 2). This index averages 42 % for the control group (first quartile 35 %; third quartile 49 %), which is explained by the active functioning of these cells - their nuclei are large and bright, the cytoplasm is quite compact (Fig. 2).

In zona glomerulosa of the adrenal cortex of the group injected with *Vipera berus berus* venom, the nuclear-cytoplasmic index deviates significantly from the average value (Table 2) and is significantly lower than this index in the control group (see Fig. 2). The average value of the index in this group is 13 % (first quartile 9 %; third quartile 17 %). Such a low index indicates a decrease in the area of the nucleus, which is probably caused by its pyknosis because karyopyknosis accompanies the early stages of cell necrosis due to the action of external toxic factors. At the same time, the expansion of endoplasmic reticulum cisternae in the cytoplasm of cells leads to its vacuolisation. The expansion of the cisternae is related to the detoxification function of the endoplasmic reticulum in the cell, and the vacuoles increase the total area of the cytoplasm.

Let's talk about the group with the introduction of Vipera berus nikolskii venom. The pathological effect of this venom is manifested in a decrease in the nuclear-cytoplasmic index in zona glomerulosa cells (see Table 2). The average value of this index here is 12 % (first quartile 8 %; third quartile 14 %), which is significantly less than such index in the control group.

The decrease in the nuclear-cytoplasmic index in both experimental groups is proportional (Table 2), indicating that 24 hours after venom injection, their effect on this parameter is equally negative. Vacuolisation of the cytoplasm and condensation of the nucleus leads to a decrease in the functionality of the cells of zona glomerulosa of the adrenal cortex and a violation of normal metabolism.

A comparison of the nuclear-cytoplasmic index of the endocrinocytes of zona fasciculata of the adrenal cortex demonstrates a significant decrease of this index in both experimental groups relative to the control group (see Fig. 2). For the control group, the average value of this index is 34 % (first quartile 28 %; third quartile 42 %). The third of the cell, occupied by the nucleus, indicates the active work of these endocrinocytes in the production of cortisol and other glucocorticoids - the nucleus has a predominance of euchromatin and is quite large, the cytoplasm is enriched with lipid inclusions, which are a source of steroids for the synthesis of these hormones.

In the group with the introduction of *Vipera berus berus* viper venom, a number of indexes of nuclear-cytoplasmic ratio demonstrate its decrease (see Table 2). The average value of this index is 10 % (first quartile 7 %; third quartile 12 %), which is 3 times less than the index of the control group. Such a difference shows not only the vacuolisation of the cytoplasm but also the development of oedema in it, which is a manifestation of necrotic processes in endocrinocytes.

A decrease in the nuclear-cytoplasmic index in the group with the introduction of *Vipera berus nikolskii* venom is similar (see Table 2). Here, this index averages 12 % (first quartile 10 %; third quartile 14 %) and is also significantly different from the control group (see Fig. 2). Such a similarity in this index between the venoms of both vipers indicates that at the cellular level, their action is equally manifested already 24 hours after their entry into the body - probably the energy exchange in the cell is disturbed, which leads to the disorganisation of the work of ion pumps and the subsequent influx water into the cell, due to which its cytoplasm swells. Quantitatively, this is reflected in the nuclear-cytoplasmic index, and functionally, it results in a decrease in the ability of these cells to produce glucocorticoids.

Discussion

Measurement of the microcirculatory bed area was chosen to analyse the effect of viper venom on the adrenal glands because the bloodstream carries toxic substances and, obviously, harms the vessel walls and intravascular elements, such as plasma and formal blood elements. The total area of arterioles, capillaries and venules present in the sections of these endocrine organs can quantitatively characterise such pathological processes as oedema, haemorrhages, dilation of blood vessels during inflammation, etc. To assess the state of the circulatory system in the stroma of the adrenal glands, we chose the adrenal cortex since the predominant type of vessels in the medulla are veins that do not belong to the microcirculatory channel. In addition, studies show that

the main negative effect of venom toxins is on the cortex, not the medulla, so it is more appropriate to analyse the microcirculation there [2].

In order to quantitatively assess the general condition of the adrenal parenchyma cells, we chose to calculate the nuclear-cytoplasmic ratio in the endocrine cells of zona glomerulosa and zona fasciculata because, according to the literature, these two zones are the most vulnerable to the influence of venom toxins. The action of venomous substances on the cell is characterised, on the one hand, by the pyknosis of the nucleus as an early element of the manifestation of necrosis [6]. On the other hand, the cytoplasm is subject to swelling associated with the disruption of the functional activity of mitochondria, which are affected by external factors, in this case, Vipera venom. Karyopyknosis and cytoplasm swelling lead to a decrease in the nuclear-cytoplasmic index.

The results of experimental studies on mice under the administration of Bothrops venezuelensis viper venom showed changes in the qualitative and quantitative composition of the structural components of the adrenal glands. 3 hours after the venom injections, such ultrastructural changes were noted in the animals as the loss of integrity of the endothelial lining of the walls of blood vessels, swelling of mitochondria and disorganisation of their cristae. In the endocrinocytes of the adrenal cortex, the nuclei had indistinct contours with a large amount of heterochromatin and expanded perinuclear spaces [1, 4].

According to Sánchez E. E. and co-authors [22], when the crotamine-like peptide of snake venom of the Crotalidae family affects the cortex of the adrenal glands, zona fasciculata and zona reticularis experience the greatest damage. In the cells of the indicated areas of the adrenal cortex, the expansion of smooth and granular ER was detected during morphological studies, which, according to the researchers, led to a violation of steroid hormone synthesis processes. Vacuolar degeneration, haemorrhages and foci of necrosis were characteristic. In some places, with prolonged exposure to venom toxins, atrophy, nodular hyperplasia and fibroproliferative changes in the cortical substance of the adrenal glands were detected.

The functional activity of the adrenal glands depends on the influence of the central endocrine glands, particularly the pituitary gland. According to the literature, the action of adverse factors, including the viper and snake venom toxins, leads to a violation of the coordinated activity of the pituitary-adrenal system. Experimental studies and data from clinical cases prove the fact that envenomation due to viper bites causes massive haemorrhages in the adrenal and pituitary glands in 36 % and 43 % of cases, respectively. Pathophysiologists are actively studying hemorrhagic necrosis of the pituitary and adrenal glands, but its reliable mechanisms have not yet been elucidated. It was established that the peculiarities of the blood supply of these organs are the cause of the probable extravasation of blood caused by viper toxins. S. Senthilkumaran et al. [27] note that Daboia russelii viper venom contains protein components that have vasculotoxic, hemorrhagic, and proteolytic properties, cause the development of thrombocytopenia, and activate blood coagulation and fibrinolysis factors [21]. The consequence of this is the appearance of consumption coagulopathy and DIC-syndrome. In addition, scientists found a decrease in the blood levels of cortisol, testosterone, ACTH, TTH, and prolactin in the patient's blood, which indicated primary and secondary adrenal insufficiency and damage to the pituitary gland. Attention should be paid to hypotension and circulatory shock, which are the consequences of snake bites and are also associated with disorders of blood supply to vital organs, including the pituitary gland. As a result of a series of autopsies of patients who became victims of snakebites, it was investigated that DIC syndrome is a precursor of haemorrhage or organ necrosis. Some scientists also suggest that dysfunction of the anterior lobe of the pituitary gland may be associated with the formation of autoantibodies. It has been established that acute pituitary insufficiency develops within two weeks with snake and viper bites and is characterised by hypoglycemia and refractory hypotension. Chronic failure can be asymptomatic and characterised by fatigue and weight loss. The researchers note that somatotropocytes (83 %) and gonadotropocytes (50 %) undergo the greatest changes. In the case of the vasotoxic effect of the venom, corticotropocytes are subject to morphological changes (39 %) [25].

Conclusions

1. Administration of *Vipera berus berus* and *Vipera berus nikolskii* venom to rats was accompanied by a significant increase in the area of the microcirculatory bed compared to the control group (in 2.9 times for *Vipera berus berus* and in 6.5 times for *Vipera berus nikolskii*).

2. Exposure to *Vipera berus berus* venom was associated with a significant decrease in the nuclear-cytoplasmic index in rats of the experimental group compared to the control group (13 % and 42 %, respectively), which is evidence of a decrease in the area of the nuclei of endocrinocytes of the adrenal cortex. This index in rats under the conditions of *Vipera berus nikolskii* venom injection was even lower and amounted to 12 %.

3. According to the statistical analysis of the quantitative assessment of the adrenal cortex's state, the similar effect of the venom of both species of vipers at the cellular level is worth noting. At the same time, at the tissue level, the effect of *Vipera berus nikolskii* venom is more pronounced than that of *Vipera berus berus* - this is evidenced by the higher degree of disruption of the structure of the hemomicrocirculatory channel in the adrenal cortex of animals from the group that was affected by this venom. It led not only to an increase in the area of vessels due to their expansion but also to ruptures of their walls and haemorrhages into the surrounding parenchyma and stroma.

References

[1] Alberto-Silva, C., Franzin, C. S., Gilio, J. M., Bonfim, R. S., & Querobino, S. M. (2020). Toxicological effects of bioactive peptide fractions obtained from Bothrops jararaca snake venom on the structure and function of mouse seminiferous epithelium. *J Venom Anim Toxins Incl Trop Dis,* 26, e20200007. doi: 10.1590/1678-9199-JVATITD-2020-0007

[2] Colby, H. D. (1988). Adrenal gland toxicity: chemically induced dysfunction. *International Journal of Toxicology*, 7(1), 45-69. doi: 10.3109/10915818809078702

[3] Dobrelia, N. V., Boitsova, L. V. & Danova, I. V. (2015). Правова база для проведення етичної експертизи доклінічних досліджень лікарських засобів з використанням лабораторних тварин [Legal basis for ethical examination of preclinical studies of drugs using laboratory animals]. *Фармакологія та лікарська токсикологія=Pharmacology and Drug Toxicology,* (2), 95-100.

[4] Echeverria, S., Leiguez, E., Guijas, C., do Nascimento, N. G., Acosta, O., Teixeira, C., … & Rodriguez, J. P. (2018). Evaluation of pro-inflammatory events induced by Bothrops alternatus snake venom. *Chem Biol Interact,* 281, 24-31. doi: 10.1016/j.cbi.2017.12.022

[5] Fernandes, F. H., Bustos-Obregon, E., Matias, R., & Dourado, D. M. (2018). Crotalus durissus sp. rattlesnake venom induces toxic injury in mouse sperm. *Toxicon,* 153, 17-18. doi: 10.1016/j.toxicon.2018.08.006

[6] Finol, H. J., Garcia-Lunardi, E., González, R., Girón, M. E., Uzcátegui, N. L., & Rodriguez-Acosta, A. (2020). Qualitative and Quantitative Study of the Changes in the Ultrastructure of Mammalian Adrenal Cortex Caused by the Venezuelan Tigra Mariposa (Bothrops venezuelensis) Snake Venom. *J Microsc Ultrastruct,* 8(3), 104-114. doi: 10.4103/JMAU.JMAU_49_19

[7] Gilliam, L. L. (2023). Snake Envenomation. *Vet Clin North Am Equine Pract,* 14, S0749-0739(23)00056-1. doi: 10.1016/j.cveq.2023.08.003

[8] Gopalakrishnan, M., Vinod, K. V., Dutta, T. K., Shaha, K. K., Sridhar, M. G., & Saurabh, S. (2018). Exploring circulatory shock and mortality in viper envenomation: a prospective observational study from India. *QJM,* 111(11), 799-806. doi: 10.1093/qjmed/hcy175

[9] Gunas, V., Maievskyi, O., Raksha, N., Vovk, T., Savchuk, O., Shchypanskyi, S., & Gunas, I. (2023). Protein and peptide profiles of rats' organs in scorpion envenomation. *Toxicology Reports,* 10, 615-620. doi: 10.1016/j.toxrep.2023.05.008 PMID: 37234066

[10] Gunas, V., Maievskyi, O., Raksha, N., Vovk, T., Savchuk, O., Shchypanskyi, S., & Gunas, I. (2023). The Activity of Metalloproteases and Serine Proteases in Various Organs after Leiurus macroctenus Envenomation. *Journal of Toxicology,* 2023. Article ID 5262729. doi: 10.1155/2023/5262729

[11] Jayakrishnan, M. P., Geeta, M. G., Krishnakumar, P., Rajesh, T. V., & George, B. (2017). Snake bite mortality in children: beyond bite to needle time. *Arch Dis Child,* 102(5), 445-449. doi: 10.1136/archdischild-2016-311142

[12] Kou, J. Q., Han, R., Xu, Y. L., Ding, X. L., Wang, S. Z., Chen, C. X., … & Qin, Z. H. (2014). Differential effects of Naja naja atra venom on immune activity. *Evid Based Complement Alternat Med,* 2014, 287631. doi: 10.1155/2014/287631

[13] Križaj, I. (2023). Toxinology and Pharmacology of Snake Venoms. *Toxins* (Basel), 15(3), 212. doi: 10.3390/toxins15030212

[14] Longbottom, J., Shearer, F. M., Devine, M., Alcoba, G., Chappuis, F., Weiss, D. J., … & Pigott, D. M. (2018). Vulnerability of snakebite envenoming: a global mapping of hotspots. *Lancet,* 392(10148), 673-684. doi: 10.1016/S0140-6736(18)31224-8

[15] Minghui, R., Malecela, M. N., Cooke, E., & Abela-Ridder, B. (2019). WHO's snakebite envenoming strategy for prevention and control. *Lancet Glob Health,* 7(7), 837-838. doi: 10.1016/S2214-109X(19)30225-6

[16] Mishra, P., Pandey, C. M., Singh, U., Keshri, A., & Sabaretnam, M. (2019). Selection of appropriate statistical methods for data analysis. *Ann Card Anaesth,* 22(3), 297-301. doi: 10.4103/aca.ACA_248_18

[17] Oliveira, A. L., Viegas, M. F., da Silva, S. L., Soares, A. M., Ramos, M. J., & Fernandes, P. A. (2022). The chemistry of snake venom and its medicinal potential. *Nat Rev Chem,* 6(7), 451-469. doi: 10.1038/s41570-022-00393-7

[18] Ongidi, I. H., Abdulsalaam, F. Y., Amuti, T. M., Kaisha, W. O., Awori, K. O., & Pulei, A. N. (2021). Microscopic features of the rat adrenal gland associated with chronic codeine phosphate administration. *Anat Cell Biol,* 54(2), 241-248. doi: 10.5115/acb.20.230

[19] Paolino, G., Di Nicola, M. R., Pontara, A., Didona, D., Moliterni, E., Mercuri, S. R., … & Pampena, R. (2020). Vipera snakebite in Europe: a systematic review of a neglected disease. *J Eur Acad Dermatol Venerol,* 34(10), 2247-2260. doi: 10.1111/jdv.16722

[20] Pucca, M. B., Knudsen, C., S Oliveira, I., Rimbault, C., A Cerni, F., Wen, F. H., … & Monteiro, W. M. (2020). Current knowledge on snake dry bites. *Toxins* (Basel), 12(11), 668. doi: 10.3390/toxins12110668

[21] Sampat, G. H., Hiremath, K., Dodakallanavar, J., Patil, V. S., Harish, D. R., Biradar, P., … & Roy, S. (2023). Unraveling snake venom phospholipase A2: an overview of its structure, pharmacology, and inhibitors. *Pharmacol Rep,* 75(6), 1454-1473. doi: 10.1007/s43440-023-00543-8

[22] Sánchez, E. E., González, R., Lucena, S., Garcia, S., Finol, H. J., Suntravat, M., … & Rodriguez-Acosta, A. (2018). Crotamine-like from Southern Pacific rattlesnake (Crotalus oreganus helleri) venom acts on human leukemia (K-562) cell lines and produces ultrastructural changes on mice adrenal gland. *Ultrastruct Pathol,* 42(2), 116-123. doi: 10.1080/01913123.2017.1422827

[23] Sanhajariya, S., Duffull, S. B., & Isbister, G. K. (2018). Pharmacokinetics of snake venom. *Toxins* (Basel), 10(2), 73. doi: 10.3390/toxins10020073

[24] Saraiva, R. M., Caldas, A. S., Rodriguez, T. T., & Casais-e-Silva, L. L. (2015). Influence of thyroid states on the local effect induced by Bothrops envenoming. *Toxicon*, 102, 25-31. doi: 10.1016/j.toxicon.2015.05.009

[25] Sartim, M. A., Cezarette, G. N., Jacob-Ferreira, A. L., Frantz, F. G., Faccioli, L. H., & Sampaio, S. V. (2017). Disseminated intravascular coagulation caused by moojenactivase, a procoagulant snake venom metalloprotease. *Int J Biol Macromol,* 103, 1077-1086. doi: 10.1016/j.ijbiomac.2017.05.146

[26] Seifert, S. A., Armitage, J. O., & Sanchez, E. E. (2022). Snake Envenomation. *N Engl J Med,* 386(1), 68-78. doi: 10.1056/NEJMra2105228

[27] Senthilkumaran, S., Almeida, J. R., Williams, J., Williams, H. F., Thirumalaikolundusubramanian, P., Patel, K., & Vaiyapuri, S. (2023). Rapid identification of bilateral adrenal and pituitary haemorrhages induced by Russell's viper envenomation results in positive patient outcome. *Toxicon*, 225, 107068. doi: 10.1016/j.toxicon.2023.107068

[28] Shalaby, A. M., Aboregela, A. M., Alabiad, M. A., & El Shaer, D. F. (2020). Tramadol promotes oxidative stress, fibrosis, apoptosis,

ultrastructural and biochemical alterations in the adrenal cortex of adult male rat with possible reversibility after withdrawal. *Microsc Microanal,* 26(3), 509-523. doi: 10.1017/S1431927620001397

[29] Simoes-Silva, R., Alfonso, J., Gomez, A., Holanda, R. J., Sobrinho, J. C., Zaqueo, K. D., … & Soares, A. M. (2018). Snake venom, a natural library of new potential therapeutic molecules: challenges and current perspectives. *Curr Pharm Biotechnol,* 19(4), 308-335. doi: 10.2174/1389201019666180620111025

[30] Spiga, F., & Lightman, S. L. (2015). Dynamics of adrenal glucocorticoid steroidogenesis in health and disease. *Mol Cell Endocrinol,* 408, 227-234. doi: 10.1016/j.mce.2015.02.005

[31] Sunil, K. K., Joseph, J. K., Joseph, S., Varghese, A. M., & Jose, M. P. (2020). Cardiac involvement in vasculotoxic and neurotoxic snakebite - a not so uncommon complication. *J Assoc Physicians India,* 68(11), 39-41. PMID: 33187035

[32] Thakur, R., & Mukherjee, A. (2017). Pathophysiological significance and therapeutic applications of snake venom protease inhibitors. *Toxicon,* 131, 37-47. doi: 10.1016/j.toxicon.2017.03.011

[33] Tseilikman, V., Komelkova, M., Kondashevskaya, M. V., Manukhina, E., Fred Downey, H., Chereshnev, V., … & Ullmann, E. (2021). A rat model of post-traumatic stress syndrome causes phenotype-associated morphological changes and hypofunction of the adrenal gland. *Int J Mol Sci,* 22(24), 13235. doi: 10.3390/ijms222413235

[34] Ullah, A. (2020). Structure-function studies and mechanism of action of snake venom L-amino acid oxidases. *Front Pharmacol,* 11, 110. doi: 10.3389/fphar.2020.00110

[35] Variawa, S., Buitendag, J., Marais, R., Wood, D., & Oosthuizen, G. (2021). Prospective review of cytotoxic snakebite envenomation in a paediatric population. *Toxicon,* 190, 73-78. doi: 10.1016/j.toxicon.2020.12.009

[36] Waiddyanatha, S., Silva, A., Siribaddana, S., & Isbister, G. K. (2019). Long-term effects of snake envenoming. *Toxins* (Basel), 1(4), 193. doi: 10.3390/toxins11040193

[37] Wallig, M. A., Haschek, W. M., & Rousseaux, C. G. (2009). *Fundamentals of Toxicologic Pathology.* 2nd Edition. Hardback ISBN: 9780123704696, eBook ISBN: 9780080919324

[38] Williams, H. F., Layfield, H. J., Vallance, T., Patel, K., Bicknell, A. B., Trim, S. A., … & Vaiyapuri, S. (2019). The urgent need to develop novel strategies for the diagnosis and treatment of snakebites. *Toxins* (Basel), 11(6), 363. doi: 10.3390/toxins11060363

[39] Zaki, S. M., Abdelgawad, F. A., El-Shaarawy, E. A. A., Radwan, R. A. K., & Aboul-Hoda, B. E. (2018). Stress-induced changes in the aged-rat adrenal cortex. Histological and histomorphometric study. *Folia Morphol* (Warsz), 77(4), 629-641. doi: 10.5603/FM.a2018.0035

АНАЛІТИЧНА І КІЛЬКІСНА ОЦІНКА СТРУКТУРНИХ КОМПОНЕНТІВ НАДНИРКОВИХ ЗАЛОЗ ЩУРІВ ЗА УМОВ ВПЛИВУ ОТРУТИ ГАДЮК VIPERA BERUS BERUS ТА VIPERA BERUS NIKOLSKII

Ніязметов Т. С., Самборська І. А., Буцька Л. В., Касьяненко Д. М., Очеретна О. Л., Галаган Ю. В., Фік В. Б.

Отруєння внаслідок укусів змій є частою, але занедбаною проблемою охорони здоров'я в усьому світі та особливо в тропічних країнах. Щорічна смертність, як наслідок зміїних укусів, перевищує 138 000. Вважають, що дана проблема є недооціненою і в багатьох країнах окремі випадки укусів не підлягають належній фіксації. Метою дослідження є аналітична і кількісна оцінка структурних компонентів надниркових залоз щурів за умов впливу отрути гадюк Vipera berus berus та Vipera berus nikolskii. Експериментальні дослідження проводили на білих нелінійних щурах самцях. Отруту гадюк Vipera berus berus та Vipera berus nikolskii отримували з Харківського національного університету імені В. Н. Каразіна. Ліофілізовану нативну отруту зберігали при -20 °С, а потім розчиняли у фізіологічному розчині безпосередньо перед експериментом. Тварин розподіляли на три групи (контрольну і 2 дослідних) по 10 особин у кожній. Дослідним щурам внутрішньоочеревинно вводили напівлетальну дозу (LD50) (1,576 мг/г$^{-1}$) отрути Vipera berus berus або Vipera berus nikolskii на фізіологічному розчині. Тваринам контрольної групи вводили внутрішньоочеревинно лише фізіологічний розчин. Виводили щурів з експерименту через 24 години після впливу отрути, знеживлюючи шляхом цервікальної дислокації. Статистичний аналіз площі мікроциркуляторного русла та ядерно-цитоплазматичного індексу проводили за допомогою програми Fiji: ImageJ та обробляли в Excel. Введення щурам отрути гадюк Vipera berus berus та Vipera berus nikolskii супроводжувалось достовірним збільшенням площі мікроциркуляторного русла відносно групи контролю (в 2,9 рази для Vipera berus berus та в 6,5 разів для Vipera berus nikolskii). Вплив отрути гадюк Vipera berus berus асоціювався зі значним зниженням ядерно-цитоплазматичного індексу у щурів дослідної групи порівняно з групою контролю (13 % та 42 % відповідно), що є свідченням зменшення площі ядер ендокриноцитів кори надниркових залоз. За умови введення щурам отрути гадюк Vipera berus nikolskii цей показник був ще нижчим та становив 12 %. Результати статистичного аналізу кількісної оцінки стану кіркової речовини надниркових залоз показали подібний вплив отрут обох видів змій на клітинному рівні. При цьому на тканинному рівні дія отрути Vipera berus nikolskii проявлялась більш виражено, ніж Vipera berus berus: про це свідчив вищий ступінь порушення структури гемомікроциркуляторного русла у корі надниркових тварин у групі, в котрій використовували цю отруту. Дія отрути Vipera berus nikolskii призводила не лише до підвищення площі судин через їх розширення, але й до розриву їх стінок та крововиливів в оточуючі паренхіму і строму.

Ключові слова: *гадюки, отрута, ядерно-цитоплазматичний індекс, мікроциркуляторне русло, щури.*

Author's contribution

Niyazmetov T. S. - conceptualization, research, writing of the original draft.
Samborska I. A. - research, review writing and editing.
Butska L. V. - project administration.
Kasianenko D. M. - software, methodology.
Ocheretna O. L. - project administration.
Halahan Yu. V. - formal analysis and validation.
Fik V. B. - software, resources.

Signed for print 13.03.2024
Format 60x84/8. Printing offset. Order № 1850. Circulation 100.
Vinnytsia. Printing house “TVORY”, Nemyrivske shose St., 62a,
Vinnytsya, 21034
Phone: 0 (800) 33-00-90, (096) 97-30-934, (093) 89-13-852,
(098) 46-98-043
e-mail: tvory2009@gmail.com
http://www.tvoru.com.ua